8-25-2011 12:00 AM

Vibration Isolation Using In-filled Geofoam Trench Barriers

Ashref Mohamed A. Alzawi, *University of Western Ontario*

Supervisor: M. Hesham El Naggar, *The University of Western Ontario*

A thesis submitted in partial fulfillment of the requirements for the Doctor of Philosophy degree in Civil and Environmental Engineering

VIBRATION ISOLATION USING IN-FILLED GEOFOAM TRENCH BARRIERS

(Spine title: «Vibration Isolation Using In-filled Geofoam Trench Barriers»)

(Thesis format: Monograph)

by

Ashref Alzawi

Graduate Program in Engineering Science

Department of Civil and Environmental Engineering

A thesis submitted in partial fulfillment
of the requirements for the degree of
Doctor of Philosophy

The School of Graduate and Postdoctoral Studies
The University of Western Ontario
London, Ontario, Canada

THE UNIVERSITY OF WESTERN ONTARIO
School of Graduate and Postdoctoral Studies

CERTIFICATE OF EXAMINATION

Supervisor

Dr. M. Hesham El Naggar

Supervisory Committee

Dr. Tim A. Newson

Examiners

Dr. Giovanni Cascante

Dr. Liying Jiang

Dr. Maged A. Youssef,

Dr. Horia Hangan

The thesis by

Ashref Alzawi

entitled:

Vibration Isolation Using In-filled Geofoam Trench Barriers

is accepted in partial fulfillment of the
requirements for the degree of
Doctor of Philosophy

Date

Chair of the Thesis Examination Board

ABSTRACT

A significant amount of numerical and experimental research has been conducted to study the vibration isolation by wave barriers considering open trenches, in-filled concrete or bentonite trenches, sheet-pile walls, and rows of piles. A few studies have investigated the use of expanded polystyrene (EPS) geofoam material as wave barriers, which indicated that in-filled geofoam trenches can be used as effective wave barriers. However, no engineering design method is available to date for the design of such type of wave barriers. This dissertation presents comprehensive experimental and numerical investigations on the use of in-filled geofoam trench barriers to scatter machine foundations vibration, in order to provide some recommendations and design guidelines for their implementation in design.

Two- and three-dimensional time-domain finite element models have been developed utilizing the finite element package ABAQUS. The numerical models have been verified and then used to study the effectiveness of different configurations of in-filled geofoam wave barriers. All the proposed configurations performed well in scattering surface waves. However, the single-continuous wall system was considered to be more economic and practical alternative for wave scattering.

Based on the findings of the preliminary numerical investigations, a full scale field experimental study has been conducted to investigate the performance of in-filled geofoam trenches. An innovative approach to construct geofoam trenches involving hydro-dig technology was utilized. A series of experimental tests have been conducted to evaluate the performance of both open and in-filled geofoam trench barriers considering their geometry and distance from the source of disturbance. The results of the field experimental investigations were analyzed and interpreted to provide recommendations for implementation in design. Experimental results confirmed that in-filled geofoam trench barriers can effectively reduce the transmitted vibrations and its protective effectiveness is comparable to the open trench barrier.

An extensive numerical parametric study was conducted to investigate the behaviour of in-filled geofoam wave barrier under different soil conditions and to point

out the key parameters that dominate the performance of in-filled geofoam trench barriers. The influence of various key parameters on the screening performance were carefully analyzed and discussed. A model using Multiple Linear Regression (MLR) analysis was developed for design purpose. Finally, an artificial neural network (ANN) model has been developed, which aims at extrapolating the parametric study results to predict the in-filled geofoam wave barrier protective effectiveness in different soil profiles with different geometric dimensions.

Keywords: Geofoam material, vibration scattering, active isolation, passive isolation, wave barriers, machine foundations, wave propagation, finite element modeling, non-reflecting boundaries, artificial neural networks, multiple linear regression.

ACKNOWLEDGMENTS

I would like to express my deep appreciation and sincere gratitude to my supervisor, Dr. M. H. El Naggar for his consistent guidance, advice and encouragement and support throughout this work. I am truly thankful for him for giving me this opportunity to work in this research project which expanded my geotechnical knowledge, and for providing many resources for completing this project within this time limit. His experience, suggestions and encouragement were priceless.

I also would like to thank the Libyan Secretariat of High Education for help and financial support throughout this study. Furthermore, I would like to express my appreciation to URETEK Canada for their support. In particular, the help of Mr. Casey Moroschan and Matt McCullough of URETEK Canada is much appreciated.

I would like to thank my colleagues at the Civil and Environmental Engineering Department at the University of Western Ontario for the friendly environment and help. Very special thanks to Dimitar Mihaylov (PhD Candidate) for his help in preparing and conducting the experimental work and for his valuable suggestions. Another special thanks to Mohamed Elkasabgy; (PhD Candidate) for his great assistance during the field testing in Alberta.

Last but not the least, I would like to convey my appreciation to my family members for their support; May Allah bless them all. I would like particularly to extend and express my deepest and sincere gratitude to my beloved wife for her continuous support and encouragement.

DEDICATION

To:

My Father: *"God bless his soul"*

My Mother: *to whom I am indebted*

My Beloved Wife: *Ebtesam*
My Beloved Son: *Mohamed*
My Beloved Daughters: *Mais & Nuha*
who endured my engagement during this work

TABLE OF CONTENTS

LIST OF FIGURES

LIST OF TABLES

CHAPTER ONE

INTRODUCTION

1.1 OVERVIEW

Wave barriers are used to mitigate the level of ground-borne vibrations induced by different sources such as machine foundations, blasting activities and high speed trains, which can cause unfavourable effects. For example, wave barriers can be a suitable alternative when other vibration isolation solutions such as machine base isolation are not technically or economically feasible. Wave barriers are usually used to scatter the ground-borne vibrations for environmental reasons or to protect structures housing sensitive equipment. Unfavourable vibrations may affect the performance of sensitive equipment such as magnetic resonance Imaging (MRI) and printing machines. Moreover, a quiet zone may be needed in a specific operation such as high level laser work. In other cases, high level of ground-borne vibrations near residential areas might lead to some problems varying from disturbing neighbours to structural damage to adjacent buildings. To control the transmitted vibrations and their disturbance, suitable wave barriers can be a successful technique to scatter the generated waves. The geometry, location and composition of the wave barrier influence the isolation performance.

Wave barriers can be established in the form of open trenches, in-filled concrete or bentonite trenches, sheet-pile walls, rows of solid or hollow concrete or steel piles, and

gas-cushion screen system. The effectiveness of these wave barriers depends on the success of choosing the most efficient barrier for each application. For high frequency machine foundations (i.e. produce vibrations with relatively short wavelengths), it may be feasible to construct a shallow open, if the soil stability is not an issue, or install in-filled trenches as wave barriers. On the other hand, for low frequency machine foundations (i.e. larger wavelengths), deeper trenches are needed for effective screening. Therefore, a row of piles or sheet-pile walls may be a suitable choice in such case.

Vibration isolation (also known as vibration screening) is the screening of waves generated from any source of disturbance via the use of wave barriers. Vibration isolation can be classified into two categories according to their proximity to the source of disturbance: active isolation and passive isolation. When the wave barrier is placed close to or surrounding the source of disturbance, it is known as active (near-field) isolation. Figure 1-1-a (after Woods, 1968) presents a sketch of active isolation with an open trench barrier. On the other hand, if the barrier is constructed away from the source of disturbance (i.e. located near the sensitive zone), it is known as passive (far-field) isolation. Figure 1-1-b (after Woods, 1968) shows a schematic diagram of passive isolation by an open trench barrier. For instance, active isolation systems can be effectively used in the case of dynamically loaded foundations (machine foundations, where the barrier needs to be installed close to the foundation) while passive isolation systems are suitable for protecting residential areas against the induced vibration due to the passing of high speed trains.

Ground-borne vibrations originating from traffic activities, such as high speed trains are transient with a significantly low-frequency content; while those emanating

from machine foundations (rotating or reciprocating machines) are steady-state and are described as periodic, low to high-frequency, and low-amplitude excitations. Most of these vibrations propagate in the soil in the form of surface waves and can travel for long distances. A source of disturbance such as a machine foundation located at the ground surface would generate both body waves that radiate in all directions and surface waves in the form of Rayleigh waves (R-waves), which propagate horizontally in a zone close to the free ground surface. The R-waves transmit most of the dynamic energy emitted into the ground (Miller and Pursey, 1954). Also, body waves have a much higher radiation damping compared to R-waves. Therefore, in terms of prominent waves versus the system efficiency: in the case of active vibration and because the barrier is constructed close to the source of disturbance, not only do body waves dominate the system protective efficiency, but body waves also dominate and influence the system behaviour. For passive isolation, the wave field along the ground surface and far from the source of disturbance is determined almost by the R-wave alone.

1.2 NEED FOR RESEARCH

Published literature reveals that a significant amount of numerical and experimental research has been carried out in the past few decades to study the vibration isolation by wave barriers in order to improve the understanding of the vibration isolation phenomenon. Most of this body of research has mainly dealt with the development of numerical methodologies as a tool for analyzing vibration isolation problems, which resulted in comprehensive understanding of the various parameters involved for some

cases such as open trenches, in-filled concrete or bentonite trenches, sheet-pile walls, and rows of solid or hollow concrete or steel piles.

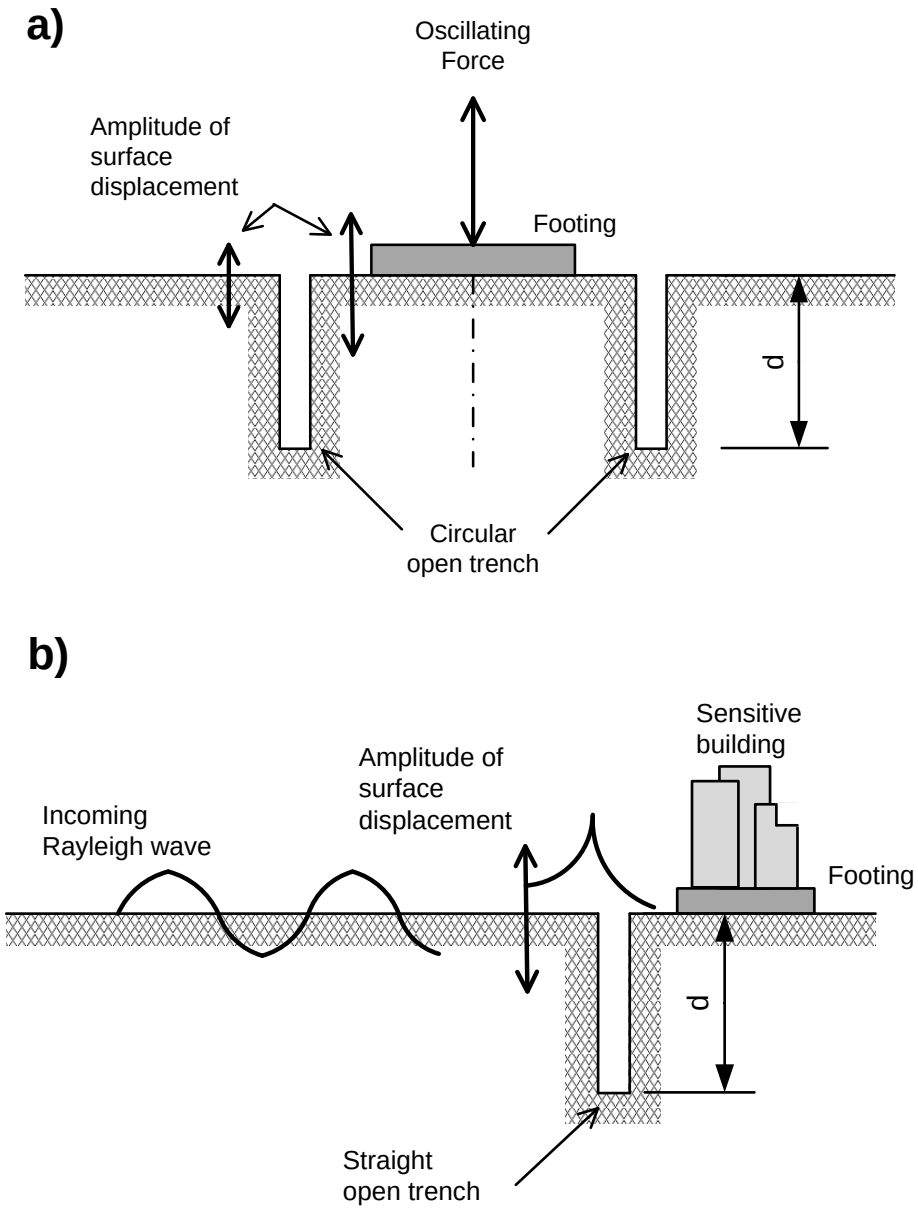

Figure 1- 1: Schematic diagram for vibration isolation systems
a) circular open trench surrounding vibrating footing (active)
b) straight open trench to protect sensitive installations (passive)
(after Woods, 1968)

On the other hand, a few studies have investigated the use of lightweight fill materials such as expanded polystyrene (EPS) geofoam material as wave barriers. These studies indicated that in-filled geofoam trench wave barriers can be used as an effective tool to screen blast-induced ground shocks and traffic activities, and that geofoam polymers can provide an attractive construction material for these barriers. However, no engineering design method based on a solid framework is available to date for the design of such type of wave barriers. Moreover, no information is available on the performance of in-filled geofoam trench barriers in reducing ground-borne vibrations due to machine foundations (i.e. steady state harmonic excitations). Therefore, a proper understanding for the performance of in-filled geofoam trench under steady state excitation needs to be gained, and the key parameters that govern its behaviour need to be explored.

A systematic in-depth numerical and experimental investigation into all the parameters that adequately describe the vibration screening process using geofoam material needs to be done to determine the influence of each parameter precisely. Furthermore, there is a need to examine the constructability of this type of wave barrier and its effectiveness in screening the ground-borne vibrations due to the harmonic excitations. Such a rigorous study can lay the foundation for a design method to determine the screening capability of an in-filled geofoam trench wall type barrier system, which can then be readily used by practicing engineers. It was -therefore- considered appropriate to embark upon this comprehensive study of vibration isolation with the prime objective of better understanding of the in-filled geofoam trench as a wave barrier as well as developing a procedure that could be used in the design process for such type of in-filled trench barriers.

1.3 OBJECTIVES AND SCOPE OF WORK

To address the aforementioned research needs, the fundamental theme of this research is to improve the current level of knowledge on the use of geofoam material as a wave barrier in screening the steady-state machine foundation vibration and evaluating the efficiency of in-filled geofoam trench under layered and half-space soil conditions. This research involves numerical and full-scale experimental investigations. The specific objectives of the research are multi-fold:

- Investigating, experimentally, the performance of in-filled geofoam trenches as a wave barrier under harmonic loading in the vertical direction.

- Evaluating, numerically, the performance of different configurations of the in-filled geofoam trench under harmonic loadings in the vertical direction as active and passive isolation systems.

- Investigating, numerically, the influence of changing some key parameters (geometric dimensions, location, and soil dynamic properties) on the in-filled geofoam trench protective performance.

- Building a numerical model as a quick and easy technique to be used as a preliminarily design tool that is capable of predicting the in-filled geofoam trench protective performance within a wide range of geometrical dimensions and configurations under various soil conditions.

To achieve the above objectives, the scope of this research includes:

- Experimental investigations: conducting a full-scale experimental field tests that represent the problem of vibration isolation by wave barriers in the real field conditions in order to understand the behaviour and the performance of in-filled geofoam trench as a wave barrier under vertical harmonic excitation.

- Evaluating the performance of different configurations: developing two-dimensional and three-dimensional finite element models for the adopted in-filled geofoam trenches configurations utilizing the finite element package, ABAQUS (2007). The calibration process of the models is conducted using three well-documented reference studies. Then conducting a comprehensive parametric study on protective performance of different configurations of the in-filled geofoam trench.

- The influence of variable key parameters: developing a two-dimensional finite element models utilizing the finite element package, ABAQUS (2007). The model is calibrated using the field results considering the layering effect from the first point. Then conducting a comprehensive parametric study by varying the barrier geometric dimensions and the soil parameters independently considering elastic half-space soil conditions.

- Preliminarily design tool: developing an Artificial Neural Network (ANN) model, an emerging computational intelligence-based tool in geotechnical engineering research, as well as a design model based on Multiple Linear Regression analysis

(MLR model) which can predict the in-filled geofoam trenches protective performance based on the numerical database obtained from the previous step.

1.4 STRUCTURE OF THESIS

This thesis has been prepared according to the guidelines of the School of Graduate and Postdoctoral Studies at the University of Western Ontario for a monograph-article format. Substantial parts of these chapters have been either published, accepted, or will be submitted for possible publication in peer-reviewed technical journals and national and international conferences. It comprises 8 chapters, which present comprehensive numerical and experimental investigations on an innovative approach to scatter machine foundations vibration by in-filled trenches (geofoam walls) wave barriers leading to provide some recommendations and design guidelines for implementation in the design procedure for such type of vibration screening systems.

The thesis is organized into eight chapters as follows:

In *chapter one*, the problem of vibration isolation is defined, the need for the present study is described, the objectives, the scope of the present work and the original contributions are listed, and the contents of this thesis are briefly summarized.

Chapter two provides general background information about the problem of vibration isolation by wave barriers in terms of a brief summary about the principles of wave propagation in an elastic half-space medium and listing the different types of machine foundations excitations. In addition, *chapter two* provides the literature survey of the previous work done on vibration isolation by wave barriers followed by a section

about the proposed geofoam material properties. Finally, an introductory section about the artificial neural networks technique is followed.

The finite element method has been used as a numerical tool to simulate the problem of wave propagation in soil medium. The developed two dimensional (2D) and three dimensional (3D) time-domain finite element models for the adopted configurations of in-filled geofoam trench barriers placed at different locations and subjected to vertical harmonic excitations utilizing the finite element package ABAQUS are presented in *chapter three*. The process of numerical models verification using three well-documented reference studies as well as a parametric study on the effectiveness of different configurations of in-filled geofoam trench barriers are also included in *chapter three*.

The field experimental work conducted as part of this study is presented in detail in *chapter four*. This chapter explains the site investigations, testing procedures, and the innovative approach to construct the trench wall. In addition, the protective effectiveness of both open and in-filled geofoam trench barriers and the influence of barrier geometry and location from the source of disturbance as well as the influence of changing the ratio between the barrier depth and its location are discussed in *chapter four*.

Chapter four also presents the experimental verification of the finite element models developed in chapter three. Given the fact that the 2D finite element model has much lower computational cost, the validity of the 2D finite element model results is ensured by comparing with the 3D finite element model results as well as the field results presented in chapter four to demonstrate their utility in conducting an extensive

parametric study to well understand the behaviour of in-filled geofoam trench barriers in different soil conditions.

In *chapter five*, a comprehensive parametric study has been carried out to better understand the factors that influence the performance of in-filled geofoam trench barriers. Therefore, the influence of various key parameters on the screening performance of in-filled geofoam barriers are carefully analyzed and discussed. Then a design model using multiple linear regression (MLR model) is developed for design followed by a worked example.

A basic introduction of the artificial neural networks approach is presented in *chapter six*. Based on the results of the extensive parametric study presented in chapter five, an artificial neural network (ANN) model has been developed in order to predict the in-filled geofoam trench barrier protective effectiveness. The validity and limitations of this model are discussed in *chapter six*. Moreover, a comparison of the developed ANN model and the MLR model predictions for the in-filled geofoam trench protective efficiency as a wave barrier has been carried out followed by discussion of results.

Finally, in *chapter seven*, general conclusions on the effectiveness of using in-filled geofoam trench walls as wave barriers and some design guidelines are presented and prospects for future research are outlined.

1.5 ORIGINAL CONTRIBUTIONS

This research introduces a series of fundamental numerical and experimental investigations related to the vibration isolation by in-filled wave barriers. It explores the influence of the key parameters such as the barrier geometrical dimensions and soil properties as well as the efficiency of using the geofoam material as wave barriers. Moreover, it proposes an innovative and practical approach to construct wave barriers using geofoam material. Specific original contributions of this dissertation include:

1. Evaluating the performance and the efficiency of different configurations of the in-filled geofoam trench as an active and passive isolation system in the form of box-wall, single-continuous wall, double-continuous and double-staggered wall systems. Specifically, it was found that: (i) all the proposed geofoam isolation systems perform well in reducing the surface waves; (ii) the screening effectiveness varies between 38% and 80%; (iii) the double-continuous walls system is the most effective isolation system and its protection effectiveness is not affected by its location from the source of disturbance; (iv) as an active isolation system, both the double-staggered walls system and the double-continuous walls system have the capability to screen the vibration; (v) the double-staggered walls system is an economic solution as an active isolation system since less geofoam material will be used; (vi) the single-continuous wall system and the double-staggered walls system perform almost the same as passive isolation systems; and (vii) the single-continuous wall system is an economic solution as a passive isolation system since less geofoam material will be used.

2. Conducting, for the first time, full-scale field tests on the performance of open and in-filled geofoam trenches as wave barriers in screening the machine foundation vibration induced by harmonic loadings in the vertical direction taking into consideration the layering effect. An innovative approach to construct the open and in-filled geofoam trenches is proposed. More specifically: (i) the field results show that the geofoam barrier can be considered as a practical alternative for wave scattering since the observed protective effectiveness is 68% or higher; (ii) for practical construction purposes, the width of the in-filled geofoam trench of 0.25m is found to be sufficient; (iii) the field results confirmed that the open trench is the ideal solution where the soil stability is not a problem and the observed protective effectiveness is 84% or higher; (iv) the protective effectiveness is influenced by the barriers normalized depth and the barrier's proximity to the source of disturbance; (v) the barriers are found to be generally more effective when the normalized depth is greater than or equal to 0.60 for both open and in-filled geofoam trenches; (vi) the field results show that a deeper trench is required as the ratio x/d (i.e. barrier's proximity to the source of disturbance to depth) increases; and (vii) as the ratio x/d increased, open trench barriers effectiveness decreased while no significant change is observed for in-filled geofoam trench barriers.

3. Identifying the parameters that govern the in-filled geofoam trench performance as a wave barrier through conducting a comprehensive parametric study employing a two-dimensional finite element model. The barrier depth and location are varied independently as well as the soil dynamic properties. Specifically, it

was revealed that: (i) the key parameters are found to be the barrier's depth, barrier's proximity to the source of disturbance, and the shear wave velocity of soil medium; (ii) the soil density, Poisson's ratio, and material damping also have some influence but are less significant; (iii) as the barrier's proximity to the source of disturbance increases, a deeper trench is required to achieve a significant improvement in its effectiveness; (iv) for practical design, the normalized depth should be greater than 1.2 for maximum performance (for both active and passive cases), however, the normalized depth can be as low as 0.8 for normalized distance of 0.4; and (v) in-filled geofoam trench barrier performs more effectively in stiff soils (i.e. with relatively high Vs values) than in soft soils (i.e. with low Vs values).

4. Establishing a comprehensive database on the in-filled geofoam trench performance as a wave barrier under a wide range of geometrical configurations and soil parameters.

5. Utilizing the principles of multiple linear regression in developing a MLR design model which can be considered as a preliminary tool in designing such type of wave barriers in terms of estimating the preliminarily optimum dimensions.

6. Advancing the promising use of artificial neural networks for predicting and estimating protective effectiveness of the in-filled geofoam trench as a wave barrier in reducing the steady state vibration induced by machine foundations and use it as a second preliminary tool in the design procedure for such type of wave barriers.

CHAPTER TWO

LITERATURE REVIEW

This chapter provides general background information about the problem of vibration isolation by wave barriers. It starts with describing the mechanism of wave propagation in an elastic semi-infinite soil medium, including the different types of the generated waves because of ground-borne vibrations by machine foundations. Due to the importance of understanding the wave phenomenon in vicinity of wave barriers, a brief description is presented and followed by listing the different types of machine foundations excitations. In addition, a literature review of the previous work conducted on vibration isolation using wave barriers. Furthermore, the properties of the proposed geofoam material used as wave barrier in this study are provided. Finally, a brief description of the artificial neural networks technique is presented.

2.1 WAVE PROPAGATION IN SEMI-INFINITE SOIL MEDIUM

Elastic waves originate in many ways: from earthquakes, blasting activities, pile driving operations, or vibrating machine foundations. Understanding the propagation mechanism of these elastic waves in a semi-infinite soil medium (i.e. half-space soil) is important when studying the problem of vibration isolation by wave barriers. The energy which causes foundation motion or ground motion is transmitted away from the source into the

soil medium in the form of elastic waves (i.e. seismic waves). The source of these elastic waves could be contained within the half-space or could be situated on the surface. Since most of machinery foundations and building footings are located on or near the surface of the ground, seismic waves generated by surface sources are of primary interest in vibration isolation studies. Furthermore, in such type of wave propagation analysis, it is common to assume that the soil medium can be simulated as homogeneous, isotropic, elastic half-space.

The elastic half-space theory defines two basic types of elastic waves, body waves and surface waves. The characteristics of these two types are well described in the available literature (Lamb (1904); Richart et al. 1970; Kolsky 1953; Ewing et al. 1957; Achenbach 1973; Kramer 1996; Haupt 1977, 1978; Fuyuki and Matsumoto 1980 and others). A brief description of this description is given here.

2.1.1 Body Waves

Two types of body waves can exist in an infinite elastic medium, P-wave (also known as primary or compressional wave) and S-wave (also known as shear wave). P-wave involves no shearing rotation of the body they pass through. This wave type will propagate through the body at a velocity

$$V_p = \sqrt{\frac{\lambda + 2G}{\rho}} = \sqrt{\frac{E(1-\nu)}{(1+\nu)(1-2\nu)\rho}} \qquad (2\text{-}1)$$

where E is the Young's modulus, ρ is the mass density and ν is the Poisson's ratio. The constants G (shear modulus) and λ are called Lame's constants and are given by:

$$G = \frac{E}{2(1+\nu)}, \qquad \text{and} \qquad \lambda = \frac{\nu E}{(1+\nu)(1-2\nu)}$$

The general nature of P-wave motion is illustrated in Figure 2-1. The particle displacements are parallel to the direction of wave propagation.

The second type of body waves is the S-wave, which involves no volume change and propagates through the medium at a velocity

$$V_s = \sqrt{\frac{G}{\rho}} \tag{2-2}$$

The general nature of S-wave motion is illustrated in Figure 2-2. The particle motion is constrained to a plane perpendicular to the direction of wave propagation. Moreover, S-waves are often divided into two perpendicular components or resolved into two perpendicular components: SH- and SV-waves. For SH-waves, the particle motion occurs only in the horizontal plane while it lies in a vertical plane for the case of SV-waves. A given S-wave can be represented as the vector sum of its SH and SV components.

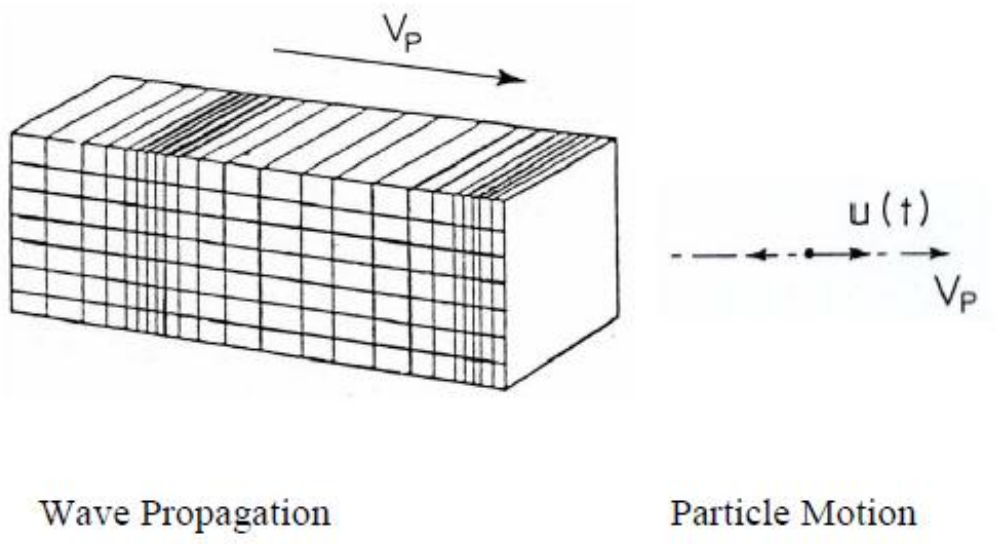

Figure 2- 1: Primary wave (P-wave)

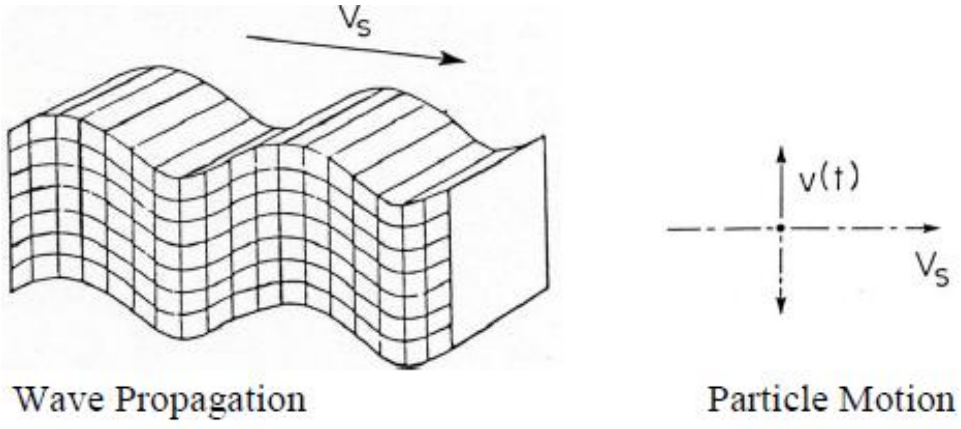

Figure 2- 2: Shear wave (S-wave)

The velocities of P-waves and S-waves depend on the stiffness of the medium with respect to the types of deformation induced by each wave. By comparing Equations 2-1 and 2-2, the Poisson's ratio can be easily evaluated, i.e.

$$\frac{V_p}{V_s} = \sqrt{\frac{2(1-\nu)}{(1-2\nu)}} \qquad (2\text{-}3)$$

It is clear that the ratio V_p/V_s depends only on Poisson's ratio. Equation 2.3 shows that the P-wave velocity can exceed the S-wave velocity by an amount that depends on the compressibility of the body or medium. In other words, when Poisson's ratio approaches 0.5, as in the case of saturated cohesive soils, $V_p \Rightarrow \infty$ and the ratio $V_p/V_s \Rightarrow \infty$ as well. This is so because $\nu = 0.5$ implies an incompressible medium. Furthermore, Equation 2-3 can be used to establish the Poisson's ratio from tests in which wave velocities V_p and V_s are measured.

2.1.2 Surface Waves

For near-surface earthquake engineering problems, the ground is often idealized as a half-space. When the two body wave systems reach the ground surface, an interesting change occurs in the behaviour of wave motion resulting in producing different surface wave systems. Some of the important surface waves are: Rayleigh waves and Love waves. Surface waves are concentrated in a shallow zone near the free surface of the half-space. The focus of this study will be on the ground-borne vibrations due to machine foundations. Since most of these foundations are located on or near the ground surface,

Rayleigh waves generated by surface sources are of primary interest in vibration isolation studies.

The Rayleigh wave (R-wave) was first studied by Rayleigh (1885) and later was described by Lamb (1904). The Rayleigh wave is confined to the neighbourhood of the surface of a half-space. The influence of Rayleigh waves decreases rapidly with depth. The Rayleigh wave motion has two components: horizontal translation and vertical translation. Their vector sum determines the trajectory of the motion, which is a retrograde ellipse with the vertical axis larger than the horizontal axis as shown in Figure 2-3. The motion occurs in the vertical plane and the horizontal axis of the ellipse is parallel to the direction of wave propagation.

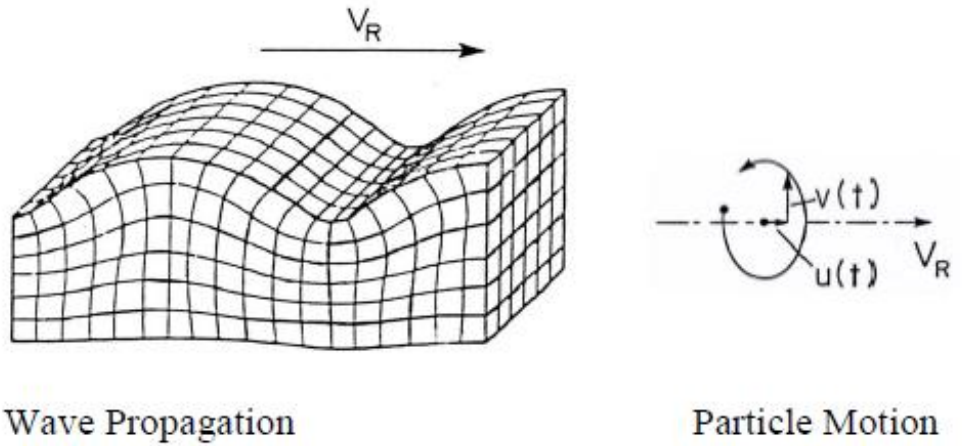

Figure 2- 3: Rayleigh wave (R-wave)

The Rayleigh wave propagates along the surface of the half-space with a phase velocity, V_R, which is related to the shear wave velocity, V_s, and the Poisson's ratio, ν. The Rayleigh wave velocity can be calculated accurately by:

$$K^6 - 8K^4 + (24 - 16\alpha^2)K^2 + 16(\alpha^2 - 1) = 0 \qquad (2\text{-}4)$$

where $K = V_R/V_s$ and $\alpha = V_s/V_p$, or approximately by:

$$V_R = \frac{0.862 + 1.14\nu}{1 + \nu} V_s \qquad (2\text{-}5)$$

As ν varies from 0 to 0.5, the Rayleigh wave velocity increases monotonically from 0.862 to 0.955 V_s. The variation of velocities V_P, V_s and V_R with the Poisson's ratio is shown in Figure 2-4.

Rayleigh waves are important because their amplitudes attenuate with distance at a much lower rate than those of other waves. Consequently, at larger distances from the source, Rayleigh waves contain more energy than other waves and their amplitudes dominate the tremors even when the shape of ground motion may deviate from the theoretically suggested ellipse. The horizontal amplitude is usually larger than the vertical one and trajectories other than ellipses are often observed. This is so because the properties and geometry of the ground differ from the ideal assumptions of the theory.

The variation of the Rayleigh wave components with depth is shown in Figure 2-5. The variation depends on the Rayleigh wave frequency and its wavelength.

Also, the vertical component reaches its maximum when the horizontal component is zero while the motion diminishes to about 0.1 of the surface motion at a depth of about 1.5 λ_R, Rayleigh wavelength.

For vertically oscillating circular energy source on the surface of homogeneous, isotropic, elastic half-space with Poisson's ratio equals to 0.25, the distribution of the total input energy among the three elastic waves is found to be: 67% R-wave, 26% S-wave, and 7% P-wave (Miller and Pursey, 1955) as presented in Figure 2-6. Furthermore, as seismic waves propagate away from the source, they encounter an increasingly larger volume of soil medium; thus, the energy density in each wave decreases with distance from the source. This decrease in energy density or decrease in displacement amplitude is called geometrical damping. The geometrical damping leads to attenuation of body waves a rate equal to 1/r (except along the surface where it is $1/r^2$), where r is the distance from the source, but the rate will be $1/r^{0.5}$ for Rayleigh waves. Accordingly, Rayleigh waves attenuate at a much slower rate than body waves. The geometric damping is a function of the excitation frequency and that as the frequency of the excitation increases, the geometric damping increases, which results in further attenuation of the generated waves at higher frequencies. Given that 67% of the total input energy is transmitted away from a surface energy source in the form of Rayleigh waves that decay with distance much slower than waves, it is obvious that the Rayleigh wave is of primary concern for vibration isolation problems.

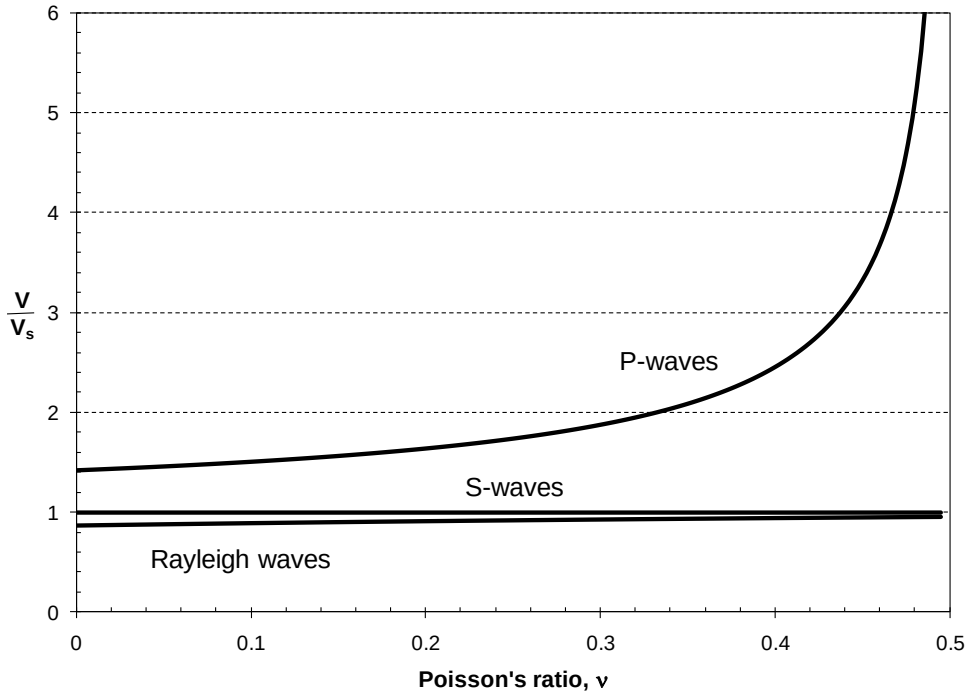

Figure 2- 4: Variation of R-wave P-wave, and S-wave velocities with Poisson's ratio

For foundations supporting rotary machines with constant low or high operating frequency, a steady-state response given by constant wave amplitude is expected. In this case, the Rayleigh wavelength can be calculated using the following equation

$$\lambda_R = \frac{V_R}{f} = \frac{2\pi V_R}{\omega} \tag{2-6}$$

where λ_R is the Rayleigh wavelength (m), V_R is the Rayleigh wave velocity (m/sec), f is the exciting frequency (Hz), and ω is the exciting angular frequency (rad/sec).

2.2 WAVES DISPERSION AROUND THE IN-FILLED TRENCH BARRIERS

The mechanisms that occur when elastic surface waves encounter an interface of impedance difference (i.e. shear wave velocity and density difference) such as reflection, scattering and diffraction of the wave energy are extensively examined in the available literature (Richart et al. 1970; deBremaecker 1958; Haupt 1977, 1978; Fuyuki and Matsumoto 1980). The understanding of these phenomena is exploited in wave screening by creating a finite material discontinuity (i.e. the concept of vibration isolation by wave barriers). The vibration screening is achieved by impeding the wave traveling field resulting in wave energy degradation. The most effective barrier transmits minimum wave energy. In general, wave barriers may consist of solid, fluid, or air (open) zones situated in the ground. For instance, open trenches are considered to be the most efficient wave barriers because no waves are transmitted and, therefore, wave reflection plays the governing role. Thau and Pao (1966) have shown theoretically that a thin crack is sufficient to screen vertically polarized SH-waves in an elastic medium.

A different phenomenon occurs in the case of in-filled trenches. When a Rayleigh wave hits a rectangular solid trench, it may be partitioned into: (1) a reflected Rayleigh wave that propagates to the right of the solid barrier, (2) a reflected body wave that radiates to the left of the solid barrier, (3) a transmitted Rayleigh wave that propagates to the right of the solid barrier, (4) a refracted body wave that radiates downward, and (5) a transmitted body wave that propagates to the right of the solid barrier. The energy distribution among these waves depends on the angle of the interface and the properties of the soil and barrier (Richart et al. 1970). The energy contained within the transmitted waves (Rayleigh and body waves) through the trench material causes the ground vibration

beyond the trench. The phenomenon of conversion of Rayleigh wave energy to other wave forms such as P- and S-wave due to the presence of solid trench (wave barrier) is known as mode conversion. With increasing barrier's proximity to the source of disturbance, transmitted body waves get partially transformed into Rayleigh waves. As in the case of open trenches, only wave reflection plays the governing role while both wave reflection and mode conversion play the governing role for the case of in-filled trenches.

2.3 TYPES OF MACHINE EXCITATIONS

The nature of ground-borne vibrations depends on the nature of the excitation force applied. The excitation can be periodic, transient or random (Figure 2-7). For example, typical machines that produce transient excitations are forging hammers, presses, crushers and mills. The excitation forces are quite short in duration and can be characterized as pulses or shocks. The ground-borne vibrations generated by the operation of these machines are often very powerful and can result in many undesirable effects such as large settlement of the foundation, cracking of the foundation, local crushing of concrete and vibration. This type of excitation is outside the scope of this study. The focus of this study is on the wave propagation due to periodic excitation produced by rotating or reciprocating machines. The simplest form of a periodic force is a harmonic force, e.g., the centrifugal forces associated with operation of rotating machines due to residual unbalances. Their magnitude can be estimated on the basis of balancing experiments or experience. In addition, reciprocating machines produce excitation forces that stem from inertial forces and centrifugal forces associated with the motion of pistons, the fly wheel

and the crank mechanism. Many of these forces can be balanced by counterweights but often, higher harmonic components and couples remain unbalanced.

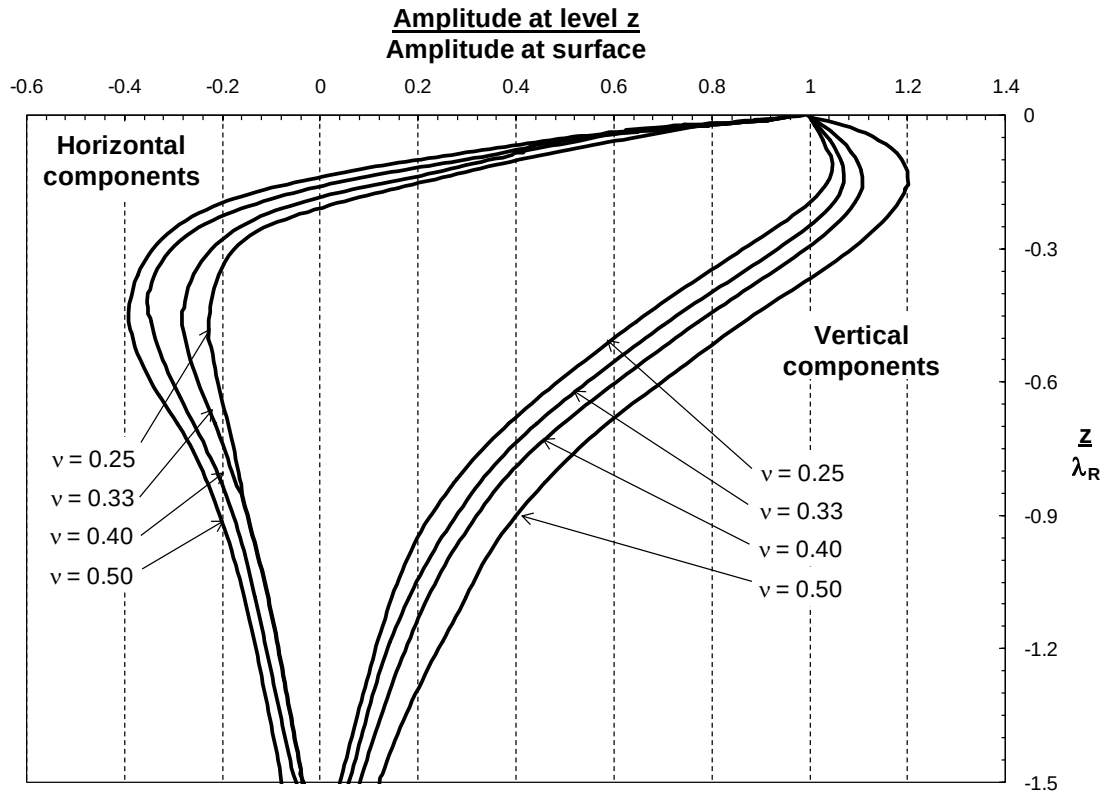

Figure 2- 5: Variation of Horizontal and vertical components of Rayleigh waves with depth.
A negative amplitude ratio indicates that the displacement is in the opposite direction of the surface displacement. (After Richart et al., 1970)

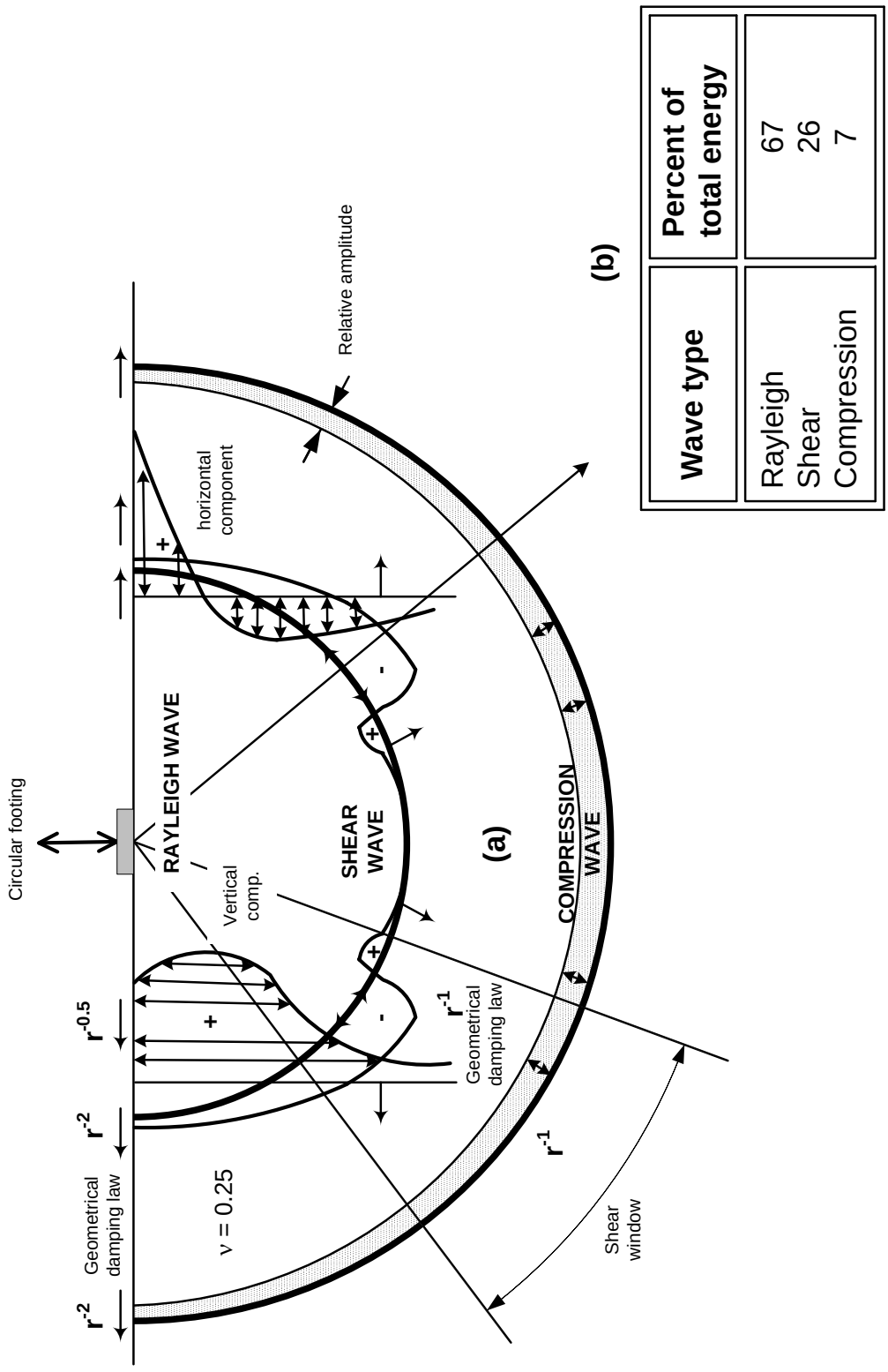

Figure 2- 6: Distribution of displacement waves from a circular footing on a homogeneous, isotropic, elastic half-space
(after Woods, 1968)

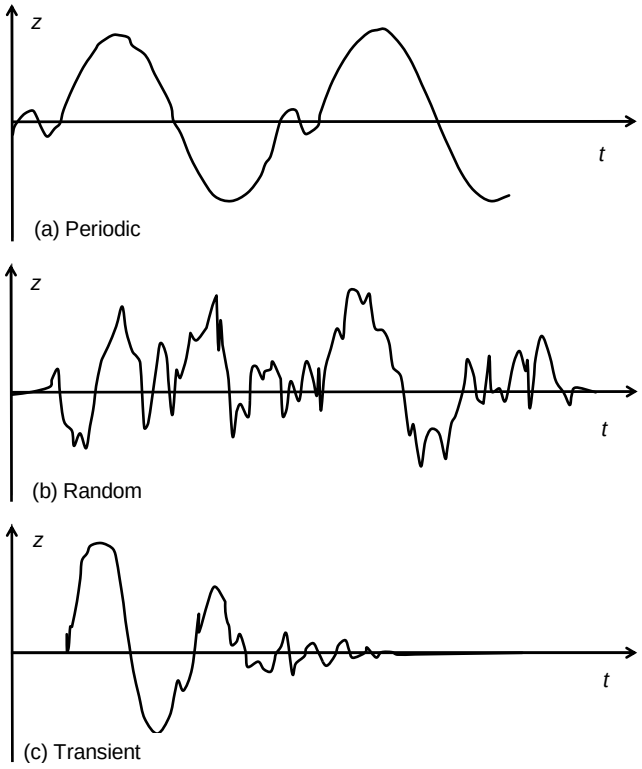

Figure 2- 7: Periodic, random and transient excitation.

2.4 VIBRATION ISOLATION USING WAVE BARRIERS

Isolation of structures and machine foundations from ground-borne vibration by the installation of wave barriers has been extensively investigated and met with various degrees of success. Several analytical and numerical studies as well as a few experimental studies investigated vibration isolation using wave barriers (also known as vibration screening) in the last few decades in order to improve the understanding of vibration scattering. The analytical approach is less used because closed-form solutions are extremely difficult to obtain except for very limited cases involving very simple

geometries and boundary conditions that hardly exist in practice. On the other hand, full-scale field experimentations are too expensive to be conducted while small-scale (i.e. field or laboratory models) ones are difficult to execute and inaccurate to extrapolate to prototype conditions. Numerical modeling represents an effective alternative and efficient tool to investigate wave propagation problems as well as the vibration scattering phenomenon. Therefore, a significant amount of work on this problem has been done using numerical techniques. A homogeneous half-space soil medium has been adopted in most of the studies that considered vibrations isolation by wave barriers.

Dolling (1965) performed a theoretical analysis of energy partitioning for Rayleigh waves across a trench. He proposed an isolation factor as a function of the normalized trench depth, given by trench depth divided by the Rayleigh wavelength. He concluded that soil Poisson's ratio does not appear to have a major influence on the isolation effect.

The wave-barrier problems for underground explosions have been numerically and theoretically investigated too. For example, Aviles and Sanchez-Sesma (1983, 1988) theoretically studied the foundation isolation from vibrations using solid piles as wave barriers. They proposed two closed-form analytical solutions for wave barriers formed with piles of finite length and circular cross section that were embedded in an elastic, homogeneous, and isotropic half-space: an exact solution for incident-plane SV waves on a two-dimensional barrier; and an approximate solution of incident-plane Rayleigh waves for a three- dimensional barrier. Closed-form solutions are ideal to use in design. However, they are usually difficult to develop and are typically limited to certain configurations/idealization.

Barkan (1962), Dolling (1965), Neumeuer (1963) and McNeill et al. (1965) were the first to report a number of practical case histories of vibration isolation. Barkan (1962) reported on an attempt to isolate a building from traffic induced vibration using open and sheet-wall barriers, as shown in Figure 2-8. This installation was unsuccessful and vibration from the sheet-wall continued to affect the building adversely. Moreover, he reported on several other cases where no positive results were achieved by the use of screening installations such as a trench filled with cinders and sheet-piling. The failure in meeting the screening criteria in his reported cases can be attributed to the improper understanding of the screening mechanism. However, he was first to recognize that the effectiveness of the barrier does not depend so much on its physical dimensions, but rather on the normalized dimensions with respect to the wavelength of incident wave. Therefore, Barkan (1962) and Dolling (1965) conducted some field tests and suggested some guidelines for barrier size and shape, which were considered very limited in their scope and cannot be generalized. Barkan (1962) concluded that a sheet-pile barrier with sufficiently large dimensions compared to the wavelength of the surface waves is required to achieve a suitable reduction in the vibration amplitude as a result of the presence of that barrier.

Dolling (1965) and Neumeuer (1963) reported on the isolation of a printing plant in Berlin from vibration induced by subway trains using a bentonite-slurry-filled trench. This application, as shown in Figure 2-9, was considered successful because only one-half of the vibration amplitude before trench installation was observed at the printing plant after the trench installation. Another successful application was reported by McNeill et al. (1965) in which a trench and sheet-wall barrier were used to isolate a sensitive

dimensional-standards laboratory, as shown in Figure 2-10. This isolation system effectively limited the acceleration of the slab to the owner's specifications.

Dolling (1970) conducted systematic field tests in large scale, using a 15m long and 6m deep trench that was filled with bentonite-slurry. He varied the wave length between 1.5 and 12m by changing the vibration frequency. Most tests were performed with a trench distance of 3m from the vibration source. Haupt (1978a) reviwed and analyzed Dolling's results and concluded that bentonite-slurry trenches could be used as efficient isolation barriers when the trench depth is at least $0.8\lambda_R$.

Woods (1968) conducted a series of scaled-field experiments to evaluate the screening effect of open trenches as wave barriers for both active and passive isolation cases. Based on the findings from these scaled-field experiments, Woods (1968) presented some guidelines for dimensioning open trenches to achieve a remarkable ground amplitude reduction. He suggested that the minimum trench depth should be $0.6\lambda_R$ for active isolation and $1.33\lambda_R$ for passive isolation to achieve an average reduction of 75% in vertical ground vibrations, where λ_R is the wavelength of Rayleigh waves. Woods et al. (1974) conducted some model tests utilizing the principle of holographic interferometry in order to study the effectiveness of rows of void cylindrical obstacles as passive isolation barriers. The applications were limited due to the wave reflections from the boundaries of the model.

Haupt (1981) carried out a series of scaled-model tests in uniform, artificially densified sand on the vibration isolation of various types of barriers in a laboratory setup. The barriers investigated include solid barriers (concrete walls), light weight barriers such

as rows of bore holes, and open trenches. The results showed that the screening performance of these barriers was a function of characteristic parameters in terms of wavelength-normalized dimensions. Therefore, all the results were presented as a function of characteristic parameters in terms of wavelength-normalized. He concluded that: for stiffer barriers, the ground amplitude reduction, in general, is related to the cross-sectional area normalized with respect to the square of Rayleigh wavelength rather than the actual shape of the barrier. On the other hand, for softer barriers, it depends on the shape, however, a satisfactory screening is not achieved except for some specific dimensions.

Massarsch (1991) introduced an innovative gas-cushion screen system installed in a deep trench, which is then filled with a self-hardening cement–bentonite grout. He conducted full-scale tests in different soil conditions to examine the effectiveness of gas-cushions and open trenches in vibration isolation. It was concluded that the efficiency of the gas-cushion screen is comparable to that of open trenches, as determined from model tests performed in the field and in the laboratory.

Baker (1994) conducted a series of field model tests to investigate the effectiveness of barriers made of bentonite (i.e. soft barrier) and concrete (i.e. stiff barrier) installed near and far from the source of disturbance, which are known as active and passive vibration screening, respectively. He compared the experimental findings with the available numerical results in the literature obtained using the boundary element method (BEM) and the empirical design equations developed by Al-Hussaini (1992).

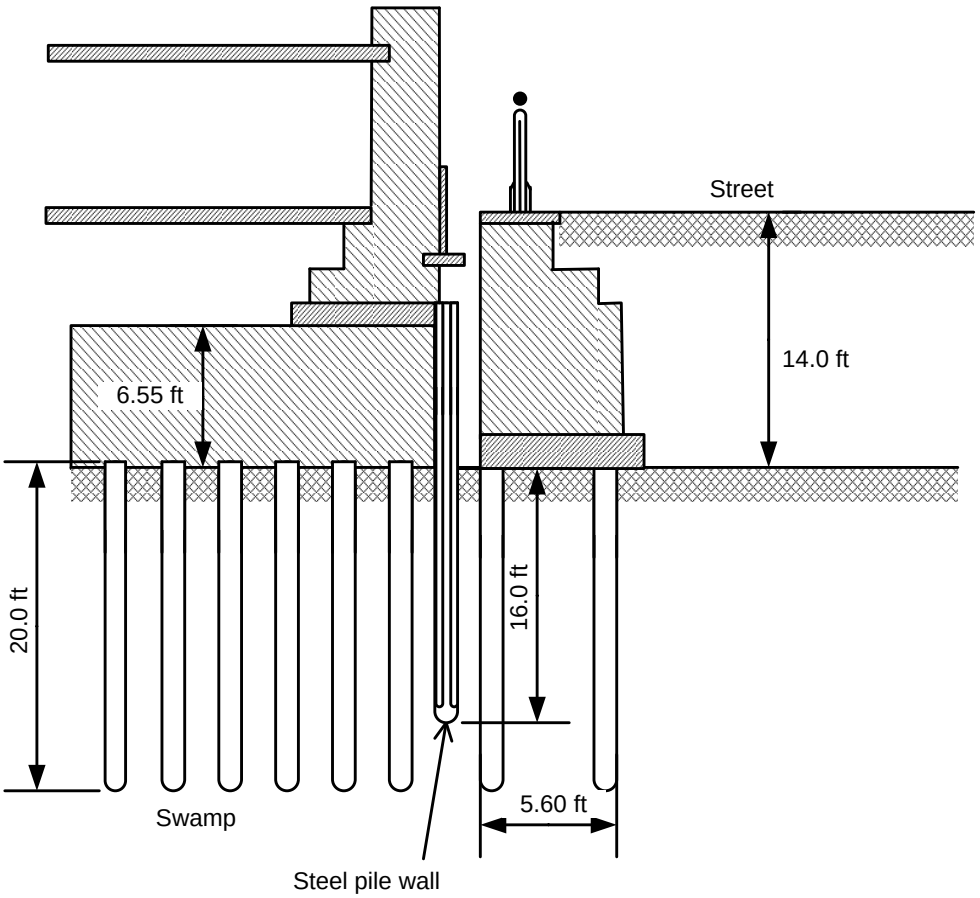

Figure 2- 8: Isolation of building from traffic induced vibration (after Barkan, 1962).

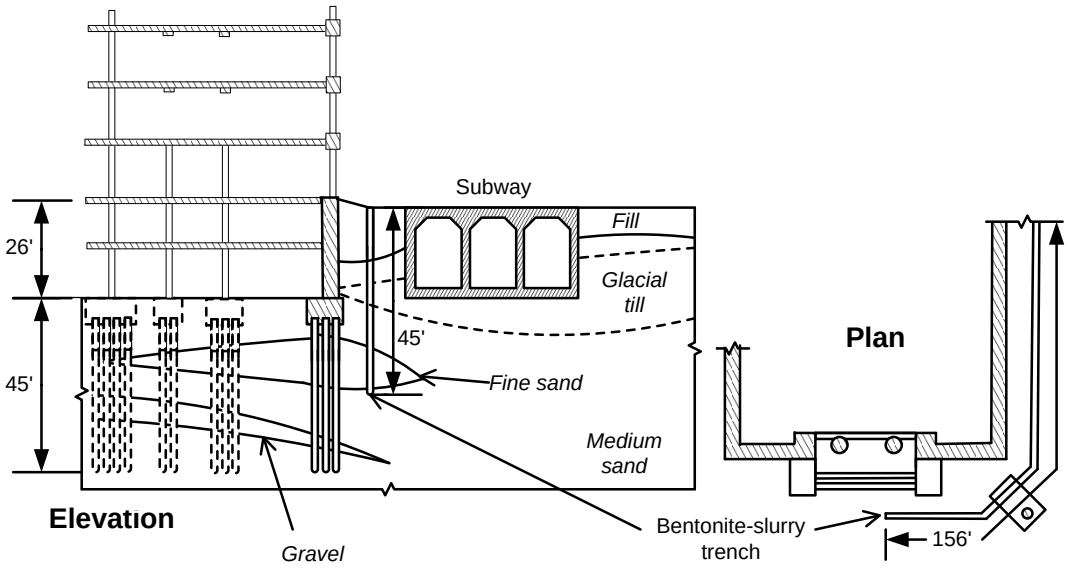

Figure 2- 9: Building isolation using bentonite-slurry-filled trench (after Neumeuer, 1963).

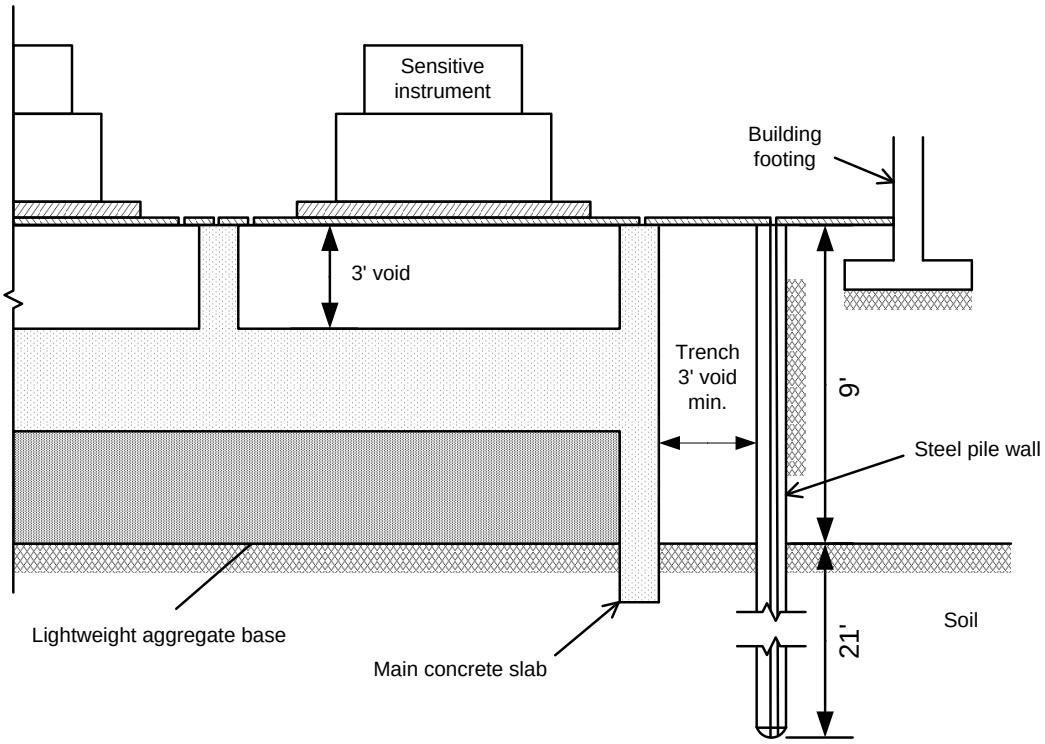

Figure 2- 10: Isolation of standards laboratory (after McNeill et al., 1965).

Numerical modeling is an efficient tool to investigate wave propagation problems. Various numerical techniques have been used by researchers to study the vibration isolation problem. The Finite Element Method (FEM) and BEM have been widely used in simulating the problem of vibration isolation by wave barriers.

Waas (1972) utilized the frequency domain finite element method to study the screening of horizontal shear waves (SH) by trenches. He used transmitting element to account for the radiation conditions at the boundaries. Haupt (1977, 1978) employed FEM, utilizing the influence-matrix boundary concept for computational efficiency, to investigate the effectiveness of using solid trenches (concrete walls) as well as the influence of their geometrical configurations and material characteristics in isolating harmonic vibrations. He studied both active and passive isolation cases and verified his numerical results with those obtained from small-scale laboratory tests (Haupt, 1981). His experimental data were in good agreement with the results from calculations using a finite element code.

El Naggar and Chehab (2005) have examined, numerically, the effectiveness of both soft (gas cushions, empty trenches, soil-bentonite trenches) and stiff (concrete-infilled trenches) wave barriers in screening pulse-induce waves produced by shock producing equipment foundation resting. A 2-dimensional time domain finite element model was developed for this purpose. It was concluded that both soft and stiff barriers are not effective in scattering pulse-induced waves by hammer foundations founded on half-space soil. However, for limited thickness soil layer underlain by rigid strata, soft barriers are more effective than stiff barriers in scattering pulse-induced waves if the barrier depth is more than one half the thickness of the soil layer.

Andersen and Nielsen (2005) developed a coupled FEM–BEM model to investigate the reduction of ground vibrations by means of barriers or soil improvement along a railway track. Beskos (1985, 1986a, 1986b) developed a BEM algorithm in the frequency domain to investigate the vibration isolation of surface waves using open and in-filled trenches in both homogeneous and layered soils.

Al-Hussaini and Ahmad (1991, 1996) and Ahmad and Al-Hussaini (1991) conducted an extensive numerical parametric study on the screening efficiency of a rectangular barrier by using a higher-order BEM algorithm. The results agree reasonably well with numerical and experimental results by others (Haupt 1981; Woods 1968). Moreover, they reported that open trenches, in-filled (concrete or bentonite) barriers, sheet pile walls, or even rows of piles could be effective wave barriers. Al-Hussaini et al. (2000) compared the BEM results with experimental data available in the public literature and reported a reasonable agreement between the predicted values for the average amplitude reduction ratio.

Yang and Hung (1997) developed a finite element model with infinite elements at the boundaries to allow for wave radiation to investigate the effectiveness of open trenches, in-filled trenches and elastic foundation in screening ground-borne vibrations due to the passage of trains. They examined the efficiency of the barriers for a range of frequencies and it was found that the performance is largely wavelength dependent. Hence, they concluded that all the trenches investigated are not suitable for low frequencies, however, all the three barriers are suitable for isolating vibrations associated with waves of higher frequencies. Kattis et al. (1999a, 1999b) compared the effectiveness of open trenches, in-filled trenches and row of pile barriers (concrete and hollow piles) in

scattering vertical vibrations using a BEM model in the frequency domain. It was found that trenches are more effective than pile barriers, except for vibrations with large wavelengths where deep barriers are needed and, thus, pile barriers are more practical.

A few studies examined vibration barriers in layered soil profiles. Segol et al. (1978) used a 2D, plane-strain, finite element model with non-reflecting boundaries to study vibration screening by open and in-filled trenches in layered soils. They found that the barriers are more effective in isolating the vertical component of the motion than the horizontal component. May and Bolt (1982) used a 2D finite element model to study the effectiveness of vibration screening using single and twin open trenches in a two-layered soil medium.

From the above review, research efforts of vibration isolation were mainly focused on open trenches, in-filled concrete or bentonite trenches, sheet-pile walls, and rows of solid or hollow concrete or steel piles. However, a few studies have been performed to explore vibration isolation using geofoam material as wave barriers.

Davies (1994) carried out a series of 20-g centrifuge tests to investigate the screening effectiveness of expanded polystyrene EPS barrier, concrete wall and their composites on the nearby buried structures. The results from this centrifuge testing program indicated that barriers containing low acoustic materials were highly effective in the attenuation of stress wave propagation and that a well-designed wave barrier could largely reduce the magnitude of ground shock loading on buried structures.

Wang (2008) has numerically investigated the performance of the expanded polystyrene geofoam (also called a soft porous layer) to protect buried structures against

the effect of blast-induced ground shock. An open trench, an inundated water trench, three in-filled geofoam walls with different densities, and a concrete wall have been included in the numerical simulation. The numerical model was developed based on the prototype dimensions of the centrifuge tests carried out by Davies (1994). The results from the numerical model demonstrated that geofoam barriers performed well in reducing the blast-induced stress waves and that the geofoam barrier can be designed to perform as a permanent protection barrier. Moreover, Wang (2008) noted that the geofoam barrier is considered to provide flexibility in design that can be easily and efficiently implemented in the field. However, vibration sources in the above-mentioned two studies were blast-induced ground shock.

Itoh et al. (2005) have examined the efficiency of low acoustic impedance materials (expanded polystyrene EPS) as wave barrier in decreasing the transmission of traffic vibrations. A series of 50-g centrifuge tests, in which vertical vibration similar to that generated by high-speed trains, have been conducted. It was found that such barriers made of expanded polystyrene EPS materials are very effective in preventing the propagation of vibratory forces and reducing the soil particles vibratory amplitude.

More recently, Murillo et al. (2009) performed centrifuge tests to simulate the traffic vibration and to investigate the efficiency of expanded polystyrene EPS barriers in scattering such type of ground-borne vibrations. As part of these centrifuge tests, a parametric study was conducted to examine the expanded polystyrene EPS barriers effectiveness based on the dimensionless geometry of the barrier and its location from the source of disturbance. The results showed that the barrier effectiveness is mainly dependent on the barrier depth and its location from vibratory source. Also, the barrier

width had a minor influence in the case of deeper barriers and higher frequencies. On the other hand, a remarkable influence of the barrier width was observed for the case of shallow barriers and lower frequencies.

It can be concluded that in-filled trenches can be used as an effective wave barriers to screen ground-borne harmonic vibrations, and that expanded polystyrene EPS provides an attractive construction material for these barriers.

2.5 GEOFOAM MATERIAL

Geofoam term was proposed by Horvarth (1995) to describe all plastic foams used in geotechnical applications. Expanded polystyrene EPS foam belongs to the geofoam group (Negussey, 1998). Over the past few years, expanded polystyrene EPS has been used in many geotechnical applications due to its mechanical behaviour, energy dissipation characteristics, low density, low permeability and ease of use. EPS use extends to light weight embankments construction, slope stabilization, lateral and vertical pressures reduction, vibration dampening and sub-base fill material.

The geofoam material used in this research is a two-component Polyurethane lightweight material supplied by URETEK Canada (currently known as POLY-MOR Canada). The properties of this material are presented in Appendix A. It is worth mentioning that this is the first attempt to employ the Uretek polymeric material in vibration isolation applications. Hence, Uretek polymer has been chosen because of the following reasons:

- Uretek polymer is a lightweight polymeric material (has a density of about 3% to 4% of soil), and when a trench is filled with this soft material, it creates a finite material discontinuity for the wave field, leading to a better screening (impedance difference).

- Uretek polymer has considerable compressive and shear strength, which makes it able to maintain the soil's lateral pressure.

- Uretek polymer does not have any detrimental effect on the environment due to decomposition or degradation.

Uretek polymer has been used for a long time in a wide range of applications in the industrial, commercial, residential, public works and institutional markets, examples of which are listed below:

- Slab lifting: lifting any non-structural slab-on-grade structures, driveways, warehouse floors, highways, bridge approaches, etc.

- Soils stabilization: densifying weak soils through chemical grouting using an array of expanding hydro-insensitive polymer resin systems.

- Foundation lifting: slab-on- grade, footed or rafted foundations lifted and aligned.

- Leak sealing: catch basins, manholes, culverts, electrical vaults, cracked walls, tailings ponds, dams, etc.

- Reinforced polymer base: providing a contiguous and continuous base over weak base soils such as permafrost, peat, muskeg, hog fuel, active soils, etc. to prevent settlement and movement. a structural base, with very high thermal characteristics as well as a vapour barrier

- Polymer piles: a unique gravel-lock pile fill system that sets up in minutes even in northern permafrost laden soils, shoring system, anchoring system, liquefaction prevention

- Hollow core block wall retrofit: a system to reinforce and fill cindercrete and other hollow core block wall cavities to strengthen them against seismic activity.

Machine foundation problems are classified as low strain level problems. Thus, the resonant column test, commonly used for measuring shear modulus (G) and damping ratio, is used to evaluate the properties of the geofoam. The test specimens were cylindrical samples with a diameter 7.0 cm and height 15cm trimmed from a big geofoam block that has a density of 61kg/m^3 when it is installed in the trench under no pressure, i.e., free to expand. The test was conducted at the University of Waterloo. Resonant column tests were executed by vibrating samples within a range of frequencies to determine their resonant conditions. The results obtained from the Resonant Column test are presented in Figure 2-11. The Resonant Column test results (shear wave velocity) were confirmed with Bender Elements test shear wave velocity with very small difference. Therefore, the adopted dynamic properties for geofoam material are to be: shear wave velocity of 312 m/sec, and a Poisson's ratio close to zero.

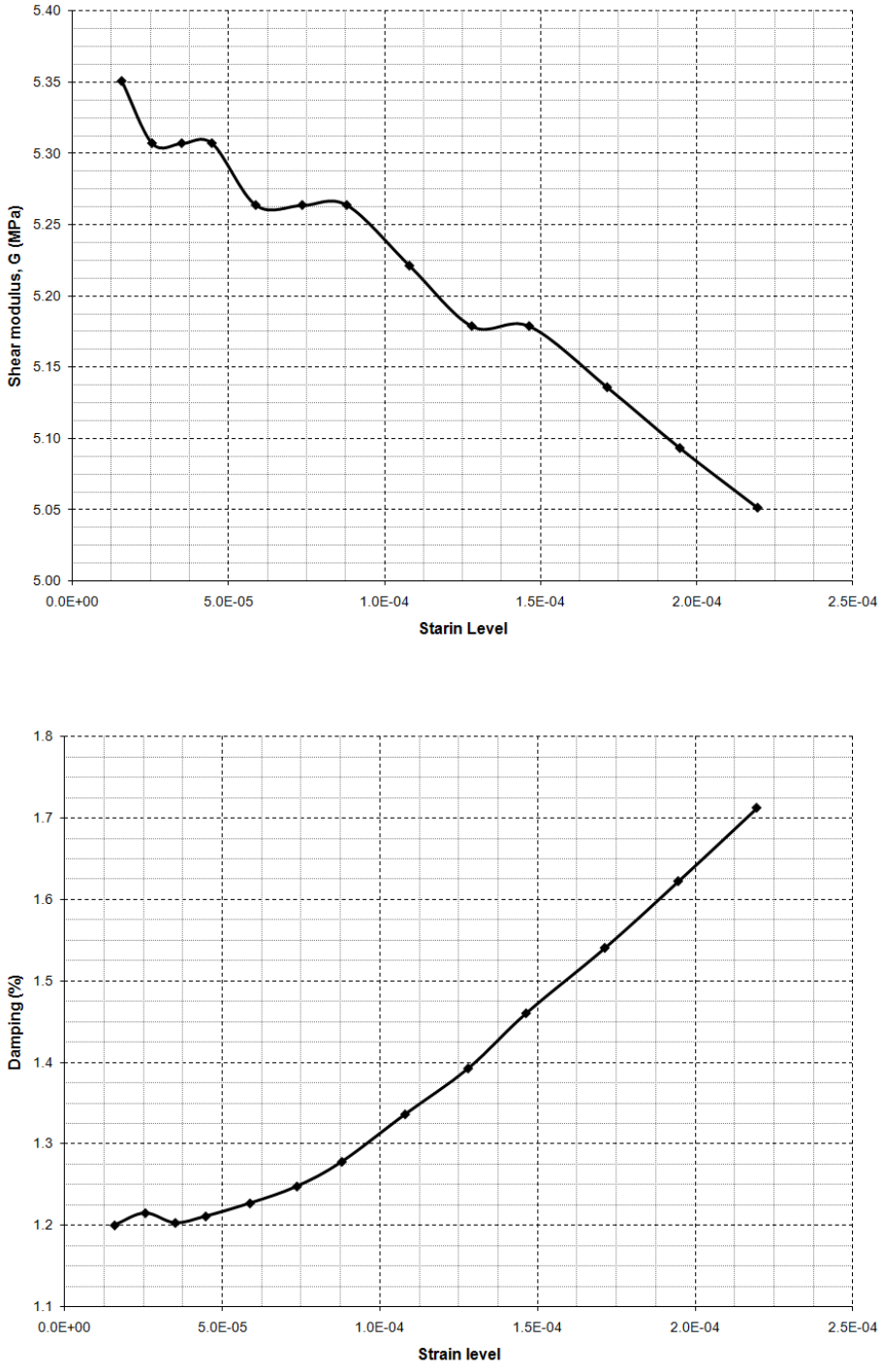

Figure 2- 11: Shear modulus (G) and damping ratio versus shear strain (γ) for geofoam material used in this study.

2.6 ARTIFICIAL NEURAL NETWORK

The artificial Neural Networks (ANNs) method pertains to artificial intelligence techniques, which attempts to mimic the behaviour of the human brain and nervous system. The ANNs simulate, in a very simplified way, the activities of the human brain in order to perform highly complex, nonlinear, and parallel computing operations. In ANN analysis, the networks self-learn from provided input data and use the data to adjust their weights in an attempt to capture the relationship between the model input parameters and the corresponding desired outputs. Consequently, ANNs do not need any prior knowledge about the nature of the relationship between input and output parameters, which differentiates this method from most empirical and statistical methods.

Over the last few years, ANNs have been widely applied in several areas of civil engineering applications including geotechnical engineering (Adeli, 2001). The method is capable and well suited to model complex problems where the relationship between the model variables is unknown (Hubick 1992). The literature reveals that ANNs have been used successfully in pile capacity prediction, site characterisation, earth retaining structures, estimating the bearing capacity of shallow foundations and settlement prediction, slope stability, design of tunnels and underground openings, liquefaction during earthquakes, soil compaction and permeability (Shahin et al., 2001).

2.6.1 Theoretical Background

The theoretical background for ANNs has been widely published (Wasserman 1989; Bishop 1995; Nielsen 1998; Haykin 1999). A typical structure of ANNs consists of three

processing layers: an input layer, an output layer and one or more hidden layers. The input and output layers consist of a number of processing elements (PEs) or nodes (neurons) equal in number to the input and output parameters, respectively. The number of hidden neurons is optimized, using trial and error, to minimise the mean squared error as well as to avoid under-fitting (i.e. large training and validating errors) and prevent over-fitting (i.e. low training error but high validating error). Each connection between neurons is assigned a numerical value, known as a weight, which can be changed during neural network training. Therefore, the input from each node in the previous layer (x_i) is multiplied by an adjustable connection weight. At each node, the weighted input signals are summed and a threshold (bias) value is added. This combined input is then passed through a non-linear transfer function to produce the output of the node. The output of one node provides the input to the nodes in the next layer. This process is summarised and illustrated in Figure 2-12.

An advantage of ANNs over physically based models is their ability to learn complex relationships among data sets. Once this knowledge is acquired, they may be applied in instances where new data do not completely define the system. When modeling a system, an ANN is independent of that system's physical laws. The objective in ANN modeling is to minimize the error with respect to the connection weights. This process is known as learning, and several learning algorithms exist in the literature (Poulton 2001). The performance of an ANN can be assessed by keeping the difference between actual and predicted or output values minimum.

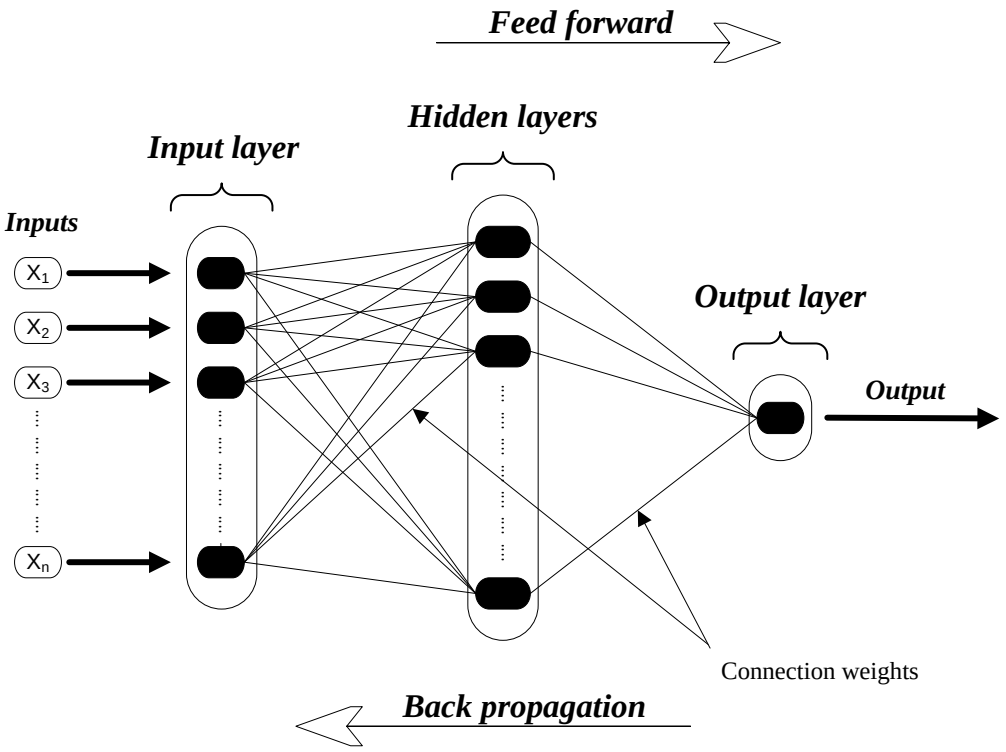

Figure 2- 12: Typical three-layer, feed forward back propagation neural network architecture showing input, hidden, and output layers

CHAPTER THREE

PRELIMINARY NUMERICAL INVESTIGATIONS

This chapter presents the preliminary numerical investigation, which is conducted to examine the behaviour and efficiency of in-filled geofoam trenches as wave barriers in mitigating the ground-borne vibrations due to periodic harmonic loadings in the vertical direction. The numerical models are verified and excellent agreement with previously published results was observed. A comprehensive parametric study has been carried out to investigate the effectiveness of different configurations of in-filled geofoam trench barriers in screening ground-borne vibrations with emphasize on excitations due to machine operation. Both 2D and 3D numerical models in the time domain were developed for this purpose utilizing the finite element package, ABAQUS (2007). The results of the parametric study are analyzed and interpreted to provide preliminary recommendations for the implementation in wave barriers design.

3.1 METHODOLOGY

Well-calibrated 3D finite element models have been established in order to investigate both active and passive isolation problems. The calibration process of the models was conducted using three well-documented reference studies. As an example for active vibration isolation case, the case simulated a 3D wave-diffraction open-trench analyzed

by Kattis et al. (1999). For passive isolation case, the model was calibrated based on a 3D boundary element analysis developed by Ahmad and Al-Hussaini (1991) and Beskos et al. (1986). In order to limit the computational effort and time, 2D plane -strain conditions were adopted for the passive isolation case. The accuracy of the 2D plane-strain model was verified by comparing the obtained results with those from the reference study. A staged mesh refinement has been carried out to obtain an optimized meshing configuration.

Different configurations of the in-filled geofoam trench were adopted based on the verified models. A comprehensive parametric study has been carried out to investigate the performance of the proposed in-filled geofoam trenches as active and passive wave barriers in the form of box-wall, single-continuous wall, double-continuous and double-staggered wall systems. It is worth mentioning that all four systems can be used as active or passive isolation systems, except the box wall system which is only applicable for the active isolation case. The simulated model results are analyzed and interpreted and the results are used to for the design of the wave barrier system considered in the experimental study. All geometric parameters are normalized by the Rayleigh wavelength, λ_R.

3.2 FINITE ELEMENT MODELS

Both 2D and 3D finite element analyses were performed employing the finite element package, ABAQUS. The explicit dynamics analysis procedure has been adopted in performing the numerical modelling using direct integration solution. The 3D model was mainly used for studying the active box-wall system and the active and passive double-

staggered wall systems. The soil was modeled as a homogeneous, isotropic, elastic, half-space. In these models, the soil and the wave barriers were modeled using 8-noded first-order hexahedron elements with relevant properties, Figure 3-1-(a). The 2D model was adopted for single-continuous and double-continuous passive wall systems. The soil and wave barriers were modeled using 4-noded bilinear, reduced integration, plane-strain rectangular elements with relevant properties, Figure 3-1-(a). To assure accurate model results, the maximum element size was kept less than one-eighth the shortest possible Rayleigh wavelength λ_R (Kramer 1996).

To ensure complete energy dissipation, non-reflecting semi-infinite boundaries have been imposed to simulate the half-space soil conditions. First-order 8-noded solid continuum, one-way semi-infinite elements were assigned to represent the non-reflecting boundaries in the 3D model while first-order plane-strain 4-noded solid continuum, one-way semi-infinite elements were used to represent the artificial non-reflecting boundaries in the case of the 2D model, Figure 3-1-(b).

Exploiting the symmetrical nature of the considered 3D problems, a reduced quarter model was adopted in the case of the box-wall active system, Figure 3-2. Similarly, a reduced half model was utilized in the case of active and passive double-staggered wall systems. Thus, symmetry boundary conditions were applied by restraining the displacement in the perpendicular direction to the symmetry surfaces. However, for the 2D models the axis of symmetry was placed across the point of load application, Figure 3-3.

The surface waves have been generated by applying vertical harmonic dynamic loading represented by a sine function. The load was applied at varying distances from the barriers and pointed directly on the ground surface. For modelling purposes, the footing carrying the dynamic load was eliminated as it did not practically affect the vibration results (Kattis 1999).

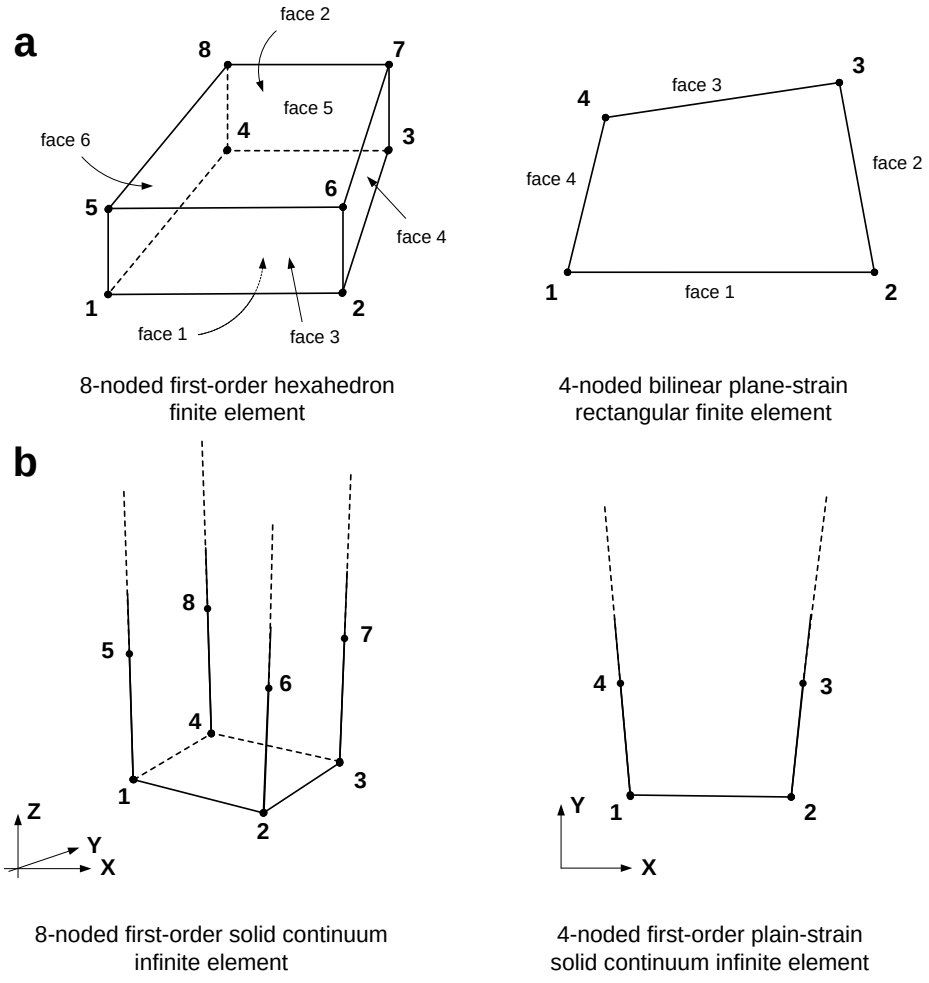

Figure 3- 1: Nodes order for 2D and 3D solid elements used in the numerical model: (a) finite elements (b) infinite elements

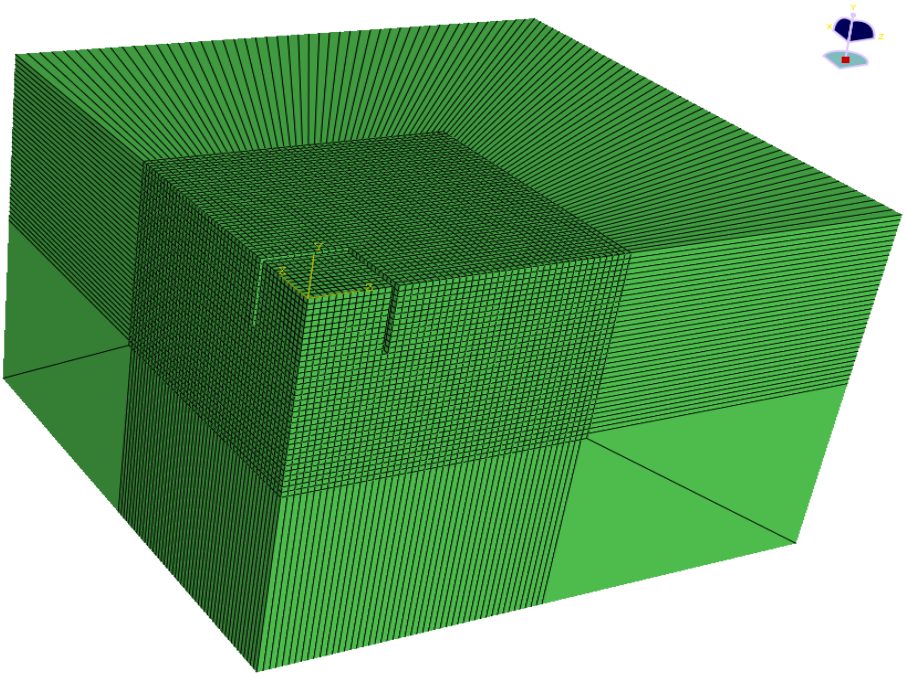

Figure 3- 2: 3D finite element model mesh for the case of active isolation by open trench

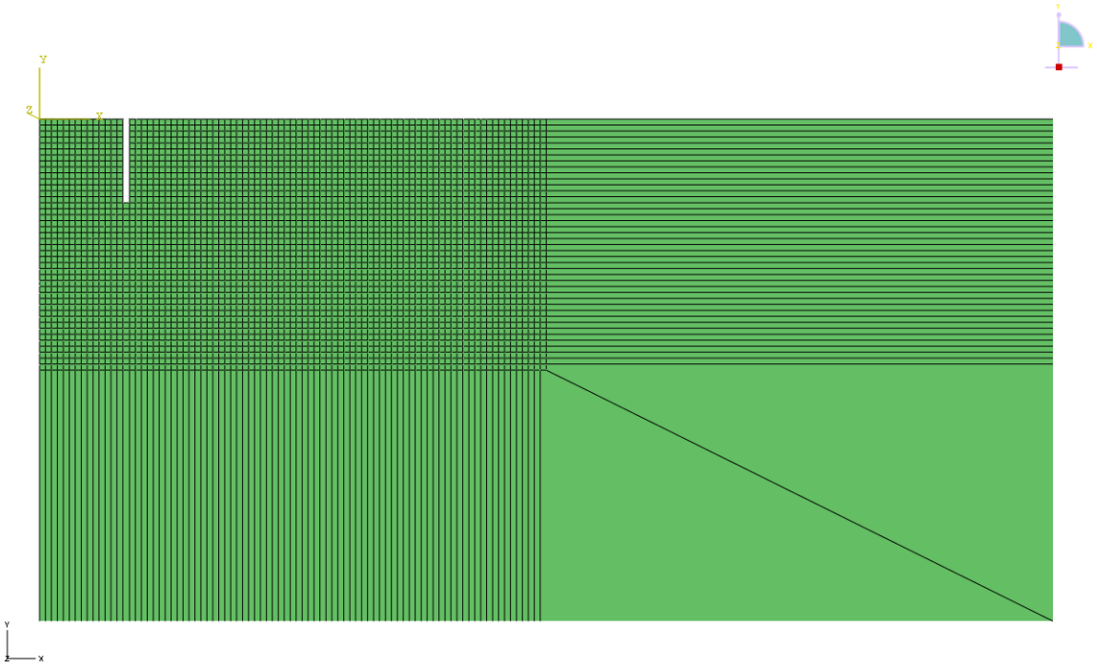

Figure 3- 3: 2D finite element model mesh for the case of passive isolation by open trench

3.3 FINITE ELEMENT MODELS VERIFICATION

The developed numerical models were verified by analyzing both the active and passive isolation problems using open trenches to simulate the conditions described in the referenced studies. The simulated results were presented in terms of the vertical response amplitude reduction factor, A_r. The amplitude reduction factor is defined as the normalized post-trench installation maximum vertical response amplitude, $(U_v)_{After}$, to the maximum vertical response amplitude before trench installation, $(U_v)_{Before}$, as given in Equation 3-1. The maximum vertical response amplitudes were obtained at specified monitoring nodes from the simulated time histories. Woods (1968) considered the averaged vertical response amplitude reduction ratio to be smaller or equal to 0.25 for an effective isolation system.

$$A_r = \frac{(U_v)_{After}}{(U_v)_{Before}} \tag{3-1}$$

For active isolation, an open trench of depth $d=0.5\lambda_R$, and width $w=0.06\lambda_R$ located at a distance $x=0.4\lambda_R$ from the source of vibration in an elastic half-space soil was considered. The material properties of the soil medium were in accordance to Kattis *et al*. (1999): shear wave velocity Vs=275 m/sec, Poisson's ratio ν=0.25, Rayleigh wave velocity V_R=253 m/sec, Rayleigh wave length λ_R =5.0 m, mass density ρ=17.5 kN/m^3 and Rayleigh damping ξ=5%. The source of vibration is modeled as a vertical harmonic load of magnitude of 1.0 kN and frequency of 50 Hz, Figure 3-4-a. Figure 3-4-b

illustrates that results from the present study in terms of A_r coincide favourably with those obtained by Kattis *at al*. (1999).

(a)

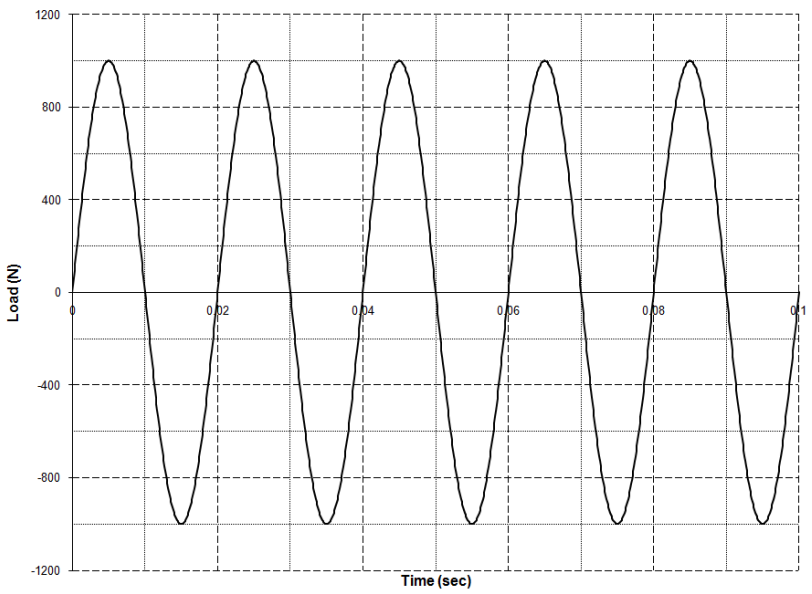

(b)

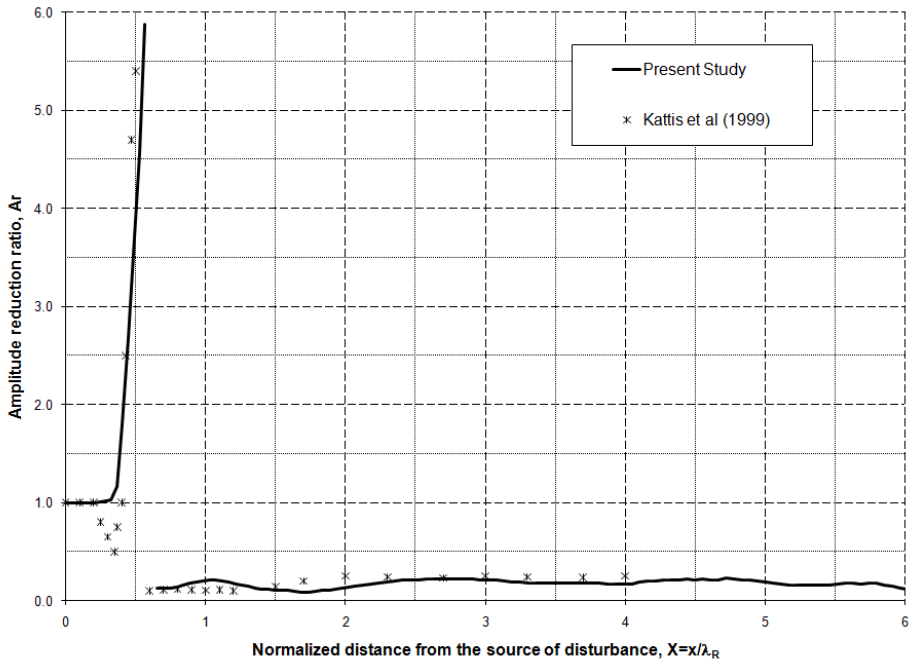

Figure 3- 4: Active isolation case:
a) Source of disturbance, vertical harmonic load (P=1000N & f=50Hz)
b) Finite element model verification, comparative study with Kettis *et al.* (1999) for open trench (W=0.06, D=0.5, X=0.4)

For the passive isolation, an open trench of depth $d=1.0\lambda_R$ and width $w=0.1\lambda_R$ located at a distance $x = 5.0\lambda_R$ from the source of vibration, which was a periodic harmonic load of magnitude of 1.0 kN frequency of 31 Hz, Figure 3-5-a, in an elastic half-space soil. The material properties of the soil medium were in accordance to Yang and Hung (1997): shear wave velocity Vs=101 m/sec, Poisson's ratio $\nu=0.25$, Rayleigh wave velocity $V_R=93$ m/sec, Rayleigh wave length $\lambda_R =3.0$ m, mass density $\rho=18$ kN/m^3 and Rayleigh damping $\xi=5\%$. Figure 3-5-b shows a good agreement between the simulated results and those reported by Ahmad and Al-Hussaini (1991) and Beskos *et al.* (1986).

3.4 COMPUTATIONAL CONFIGURATIONS

Four configurations of in-filled geofoam trench barriers were numerically investigated: box, single-continuous, double- continuous and double-staggered geofoam walls with a density of 80 kg/m^3. The dynamic properties of geofoam material were evaluated using Bender Element Tests: shear wave velocity of 330 m/sec. A summary of the adopted in-filled geofoam trench barriers configurations is demonstrated schematically in Figure 3-6. Top view of the proposed configurations layouts are shown in Figure 3-7. Figure 3-8 shows a typical vertical section, on which the barrier location, its geometrical dimensions, loading and corresponding induced Rayleigh wave and its direction are illustrated.

Unless stated otherwise, soil properties, magnitude and frequency of the applied load were considered the same as those used in the active verification case. Numerical results are presented in the subsequent text.

(a)

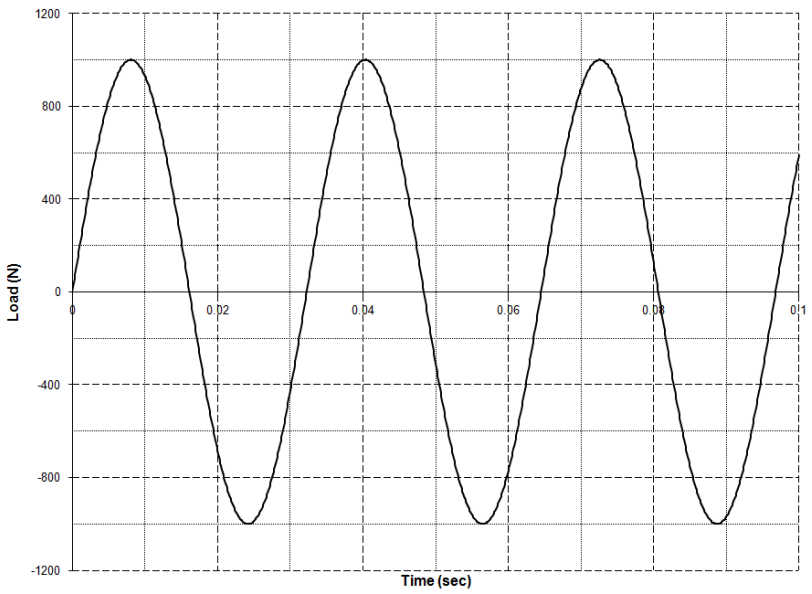

(b)

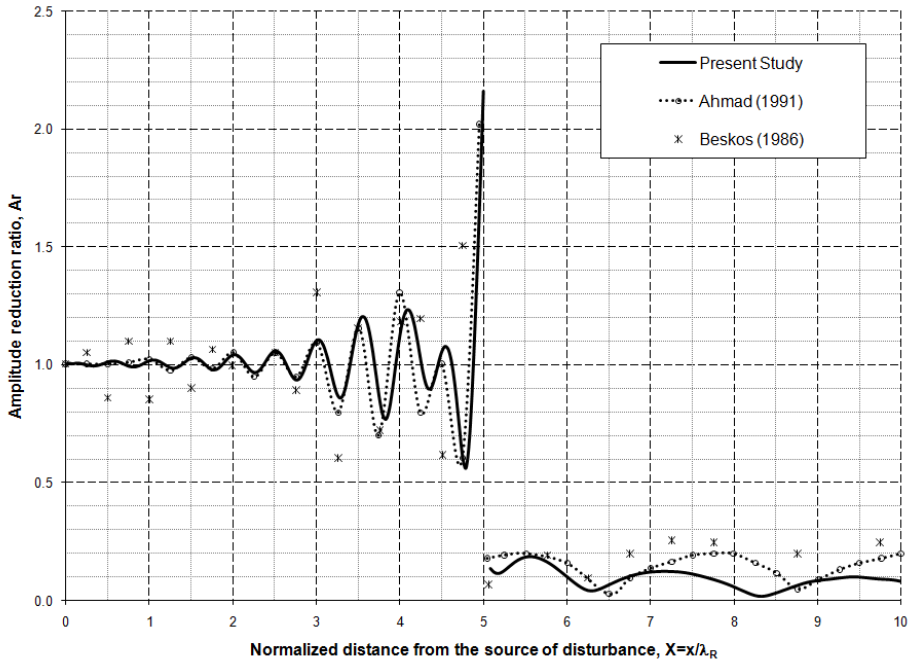

Figure 3- 5: Passive isolation case:
a) Source of disturbance, vertical harmonic load (P=1000N & f=31Hz)
b) 2D finite element model verification, comparative study with Ahmad and Al-Hussaini (1991) and Beskos *et al.* (1986) for open trench (W=0.1, D=1, X=5)

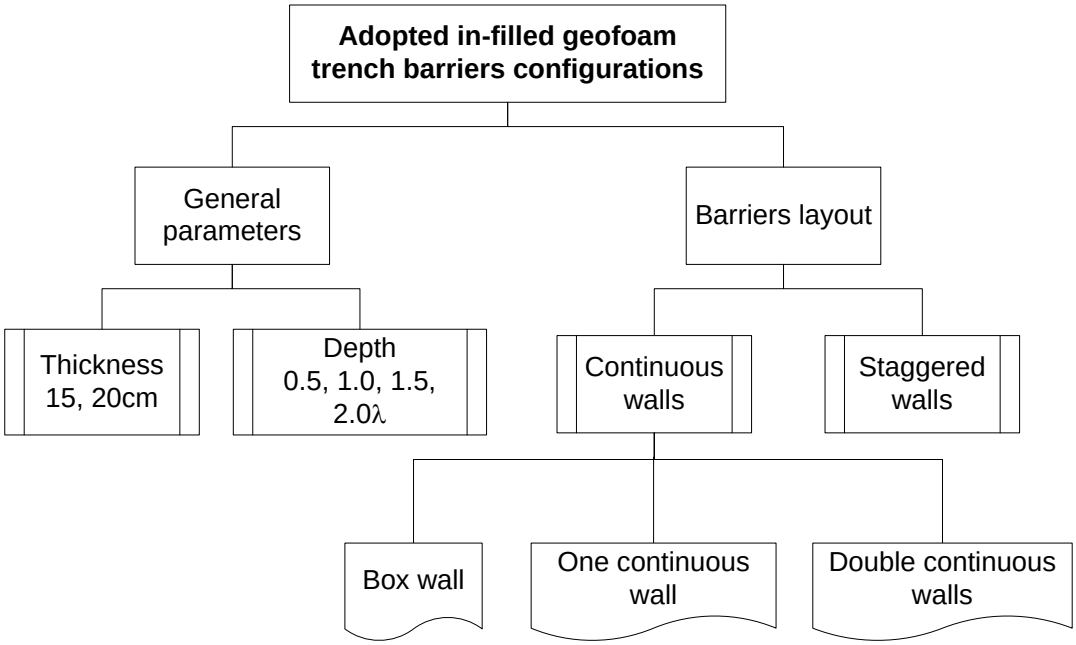

Figure 3- 6: Proposed in-filled geofoam trench barriers configurations

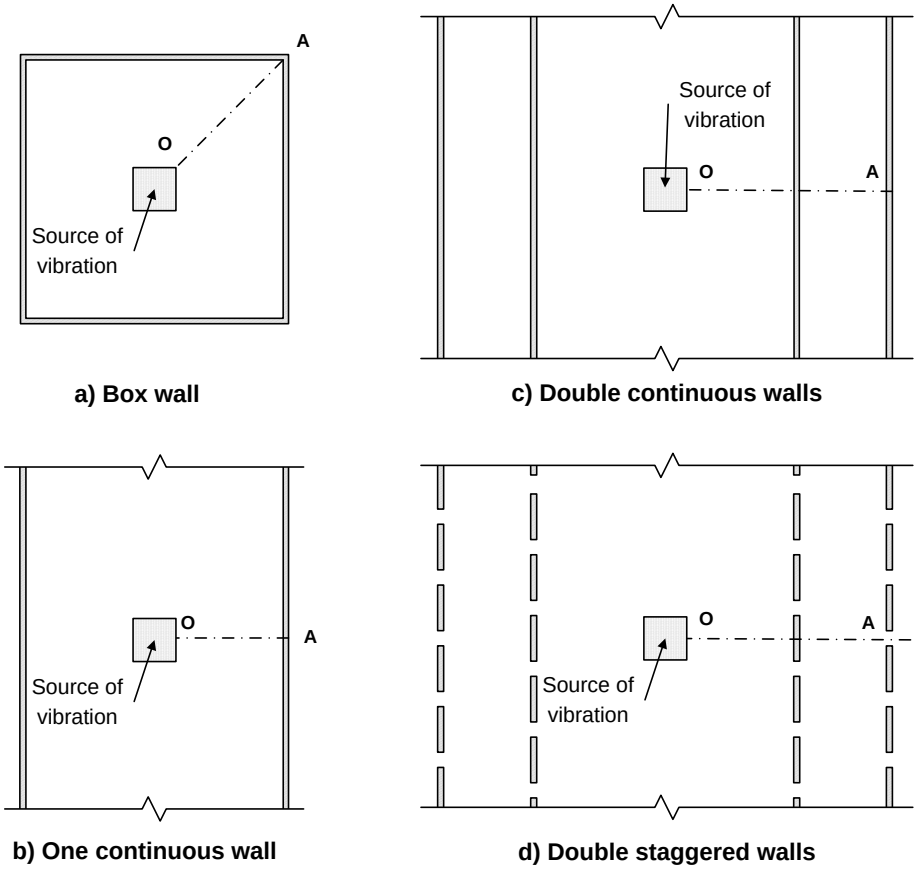

Figure 3- 7: Plan views of in-filled geofoam trench isolation systems

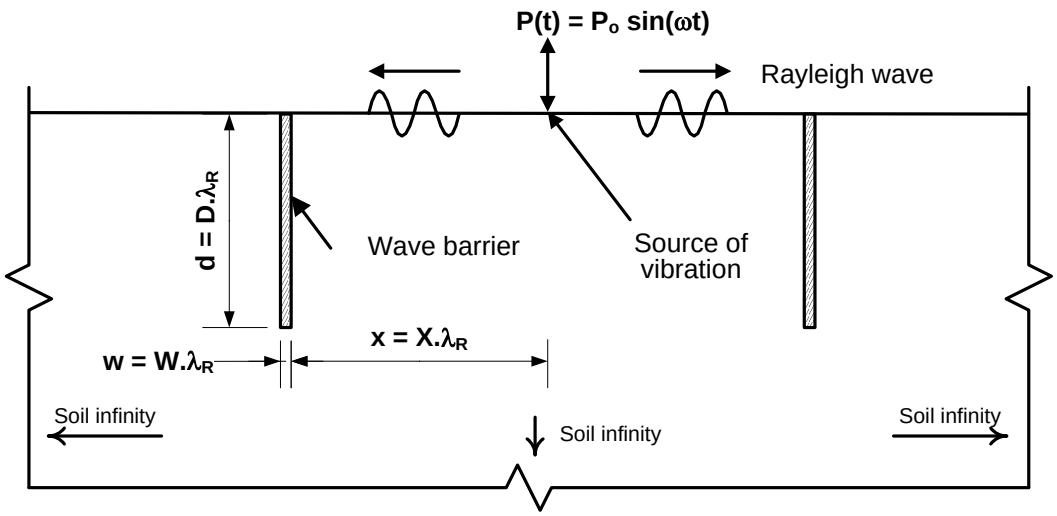

Figure 3- 8: Typical schematic of the vibration isolation system (active or passive) and geometric parameters.

3.5 PARAMETRIC STUDY AND RESULTS ANALYSIS

3.5.1 Introduction

The results of the parametric study will be presented in the form of system effectiveness. In all published literature, the system effectiveness is evaluated according to how much soil particle response amplitude reduction will be achieved. However, in practice, the effect of transmitted vibration is judged according to how much the soil particle velocities are at zones of interest. Thus, the velocity reduction factor, V_r, at a node on the assigned monitoring path (Figure 3-7) can be obtained by normalizing the post-trench installation maximum vertical velocity component amplitude, $(V_v)_{After}$, by the maximum vertical velocity component amplitude before trench installation, $(V_v)_{Before}$, measured on the

ground surface (Equation 3-2). The maximum vertical velocity component amplitudes are obtained at monitoring nodes from their time history.

$$V_r = \frac{(V_v)_{After}}{(V_v)_{Before}} \tag{3-2}$$

To evaluate the system effectiveness (screening effectiveness) of the wave barrier system on the ground surface behind the wave barrier, the averaged vertical velocity reduction factor, $\overline{V_r}$, was calculated by using the following equation:

$$\overline{V_r} = \frac{1}{x}\int V_r \, dx \tag{3-3}$$

where, $\overline{V_r}$, is the averaged vertical velocity reduction factor over a distance $x=5\lambda_R$ behind the in-filled geofoam trench barrier. Thus, the system effectiveness is calculated using Equation 3-4 as follows:

$$Eff_v = \left(1 - \overline{V_r}\right) \times 100 \tag{3-4}$$

A parametric study was performed to examine the proposed isolation systems effectiveness by investigating the influences of the in-filled geofoam trench barrier geometric dimensions (thickness and depth), location, barrier-system type and load frequency.

3.5.2 Box Wall Isolation System

The normalized distance between the box wall and the source of vibration X was varied from 0.4 to 2.0 and the normalized depth D was varied from 0.5 to 1.5 for the adopted two thicknesses, 15 and 20 cm, respectively. The particle vertical velocity was monitored along the path OA shown in Figure 3-7-a.

Figure 3-9 summarizes the obtained results. It is clear that increasing the wall thickness improved the system effectiveness. For example, the system effectiveness increased by about 11% as the wall thickness increased from 150 to 200 mm for the normalized wall depth D of 0.5 located at a normalized distance X of 0.4. Moreover, the system efficiency increased by about 22% as the wall thickness increased from 150 to 200 mm for D = 0.5 and X = 1.5. Furthermore, increasing the normalized wall depth D from 0.5 to 1.5 showed a slight improvement. For instance, increasing the wall depth D from 0.5 to 1.0 resulted in an improvement of about 7.5% with no significant improvement for walls deeper than $1.0\lambda_R$.

However, the system effectiveness decreased as the normalized distance between the box wall and the source of vibration X increased. For example, the system effectiveness decreased by about 35% as X increased from 0.4 to 2.0 for the wall thickness of 150 mm and D = 0.5. It is obvious that the system effectiveness values are the same for the same normalized distance and the same thickness regardless of the wall depth. In conclusion, the gained improvement from increasing the wall thickness was mainly affected by the wall thickness and system location rather than the wall depth.

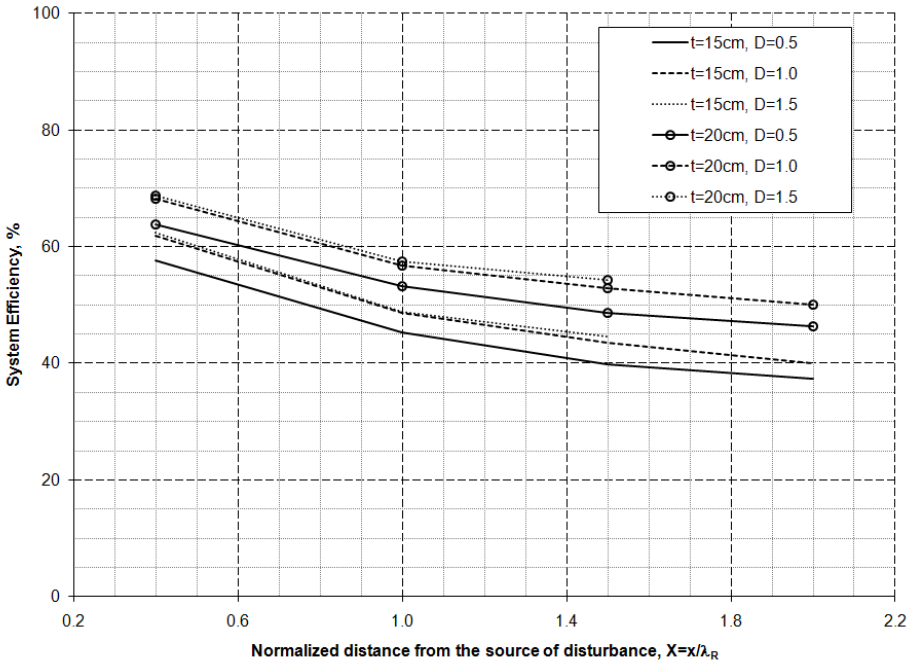

Figure 3- 9: Effect of wall dimensions and location on the box-wall system effectiveness

3.5.3 Single Continuous Wall Isolation System

Since this system can be used as an active or passive isolation system, the normalized distance X was varied from 0.4 to 5.0. The load frequency ranged from 20 to 50Hz and the normalized depth D varied from 0.5 to 2.0 for two barrier thickness values, 150 and 200 mm. The soil particle vertical velocity was monitored along the path OA shown in Figure 3-7-b.

Figure 3-10 summarizes all computed results for the load frequency 50Hz. By changing the normalized distance X of the wall for the same normalized depth D, it is observed that the effectiveness declined for increased distances from the vibration source. For example, the system effectiveness decreased by about 22% as the normalized distance

increased from 0.4 to 5.0 for the wall thickness of 15cm and D = 0.5. Also, as the normalized wall depth D became greater than 1.0, no significant improvement was observed, Figure 3-11. Thus, the effectiveness values are the same for D = 1.5 and 2.0. In contrast, the system efficiency increased by about 13.5% as the wall thickness increased from 15cm to 20cm for D = 0.5 and X = 5.0.

Another important parameter that could affect the system performance, load frequency, was investigated to understand the performance of geofoam material used as wave barriers. The load frequency was varied between 20 and 50Hz. The effect of load frequency is plotted against the normalized distance in Figure 3-12 for wall thickness of 150 mm and D = 0.5. It is observed that system effectiveness decreased as the load frequency decreased. For example, at X = 5.0, the system effectiveness decreased by 46% and 49% as the load frequency decreased from 50 to 20Hz, respectively, for D = 0.5 and 1.0.

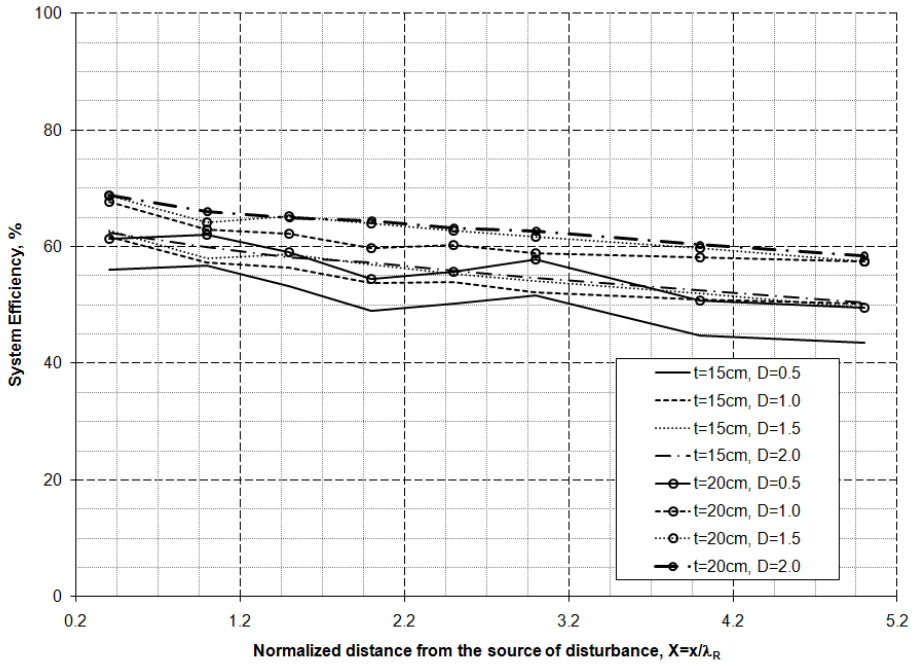

Figure 3- 10: Effect of wall dimensions and location on the single-wall system effectiveness

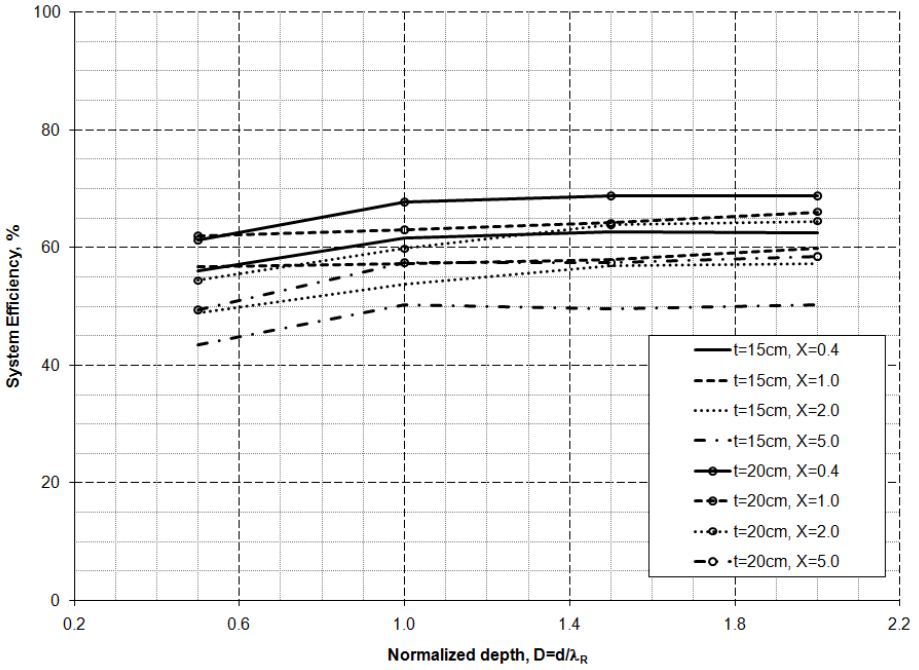

Figure 3- 11: Effect of wall dimensions and location on the single-wall system effectiveness

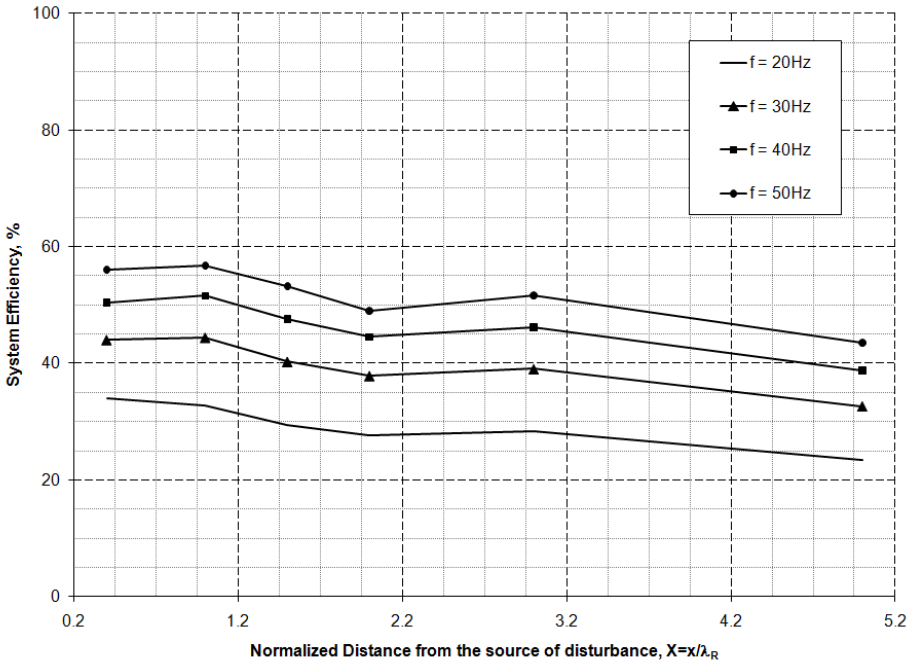

Figure 3- 12: Effect of load frequency on the single-wall system effectiveness (D=0.5, t=150 mm)

3.5.4 Double Continuous Walls Isolation System

Since this system can be used as either an active or passive isolation system, the normalized distance X was varied from 1.0 to 5.0. The load frequency was assigned as 50Hz and the normalized depth D ranged from 0.5 to 1.5 for wall thickness of 150 and 200 mm. The particle vertical velocity was monitored along the path OA shown in Figure 3-7-c.

A parametric study was carried out to find the optimum spacing between walls in order to reach the best isolation performance. The results showed that the optimum spacing is $0.5\lambda_R$, which provided the best system effectiveness.

The identified optimum spacing was used in further study to investigate the effects of changing the walls location, thickness and depth on the system effectiveness as demonstrated in Figure 3-13. It is noted that as the thickness and depth increased, the effectiveness increased regardless of the system location, X. In terms of walls depth, a small improvement could be gained from increasing D from 0.5 to 1.0 while no remarkable improvement was observed as a result of increasing D from 1.0 to 1.5. Moreover, the increase of the thickness from 150 to 200 mm resulted in an improvement of only 10%. In contrast, no improvement in effectiveness was monitored when varying the X value from 1.0 to 5.0. In other words, the system effectiveness was not affected by its location from the source of vibration.

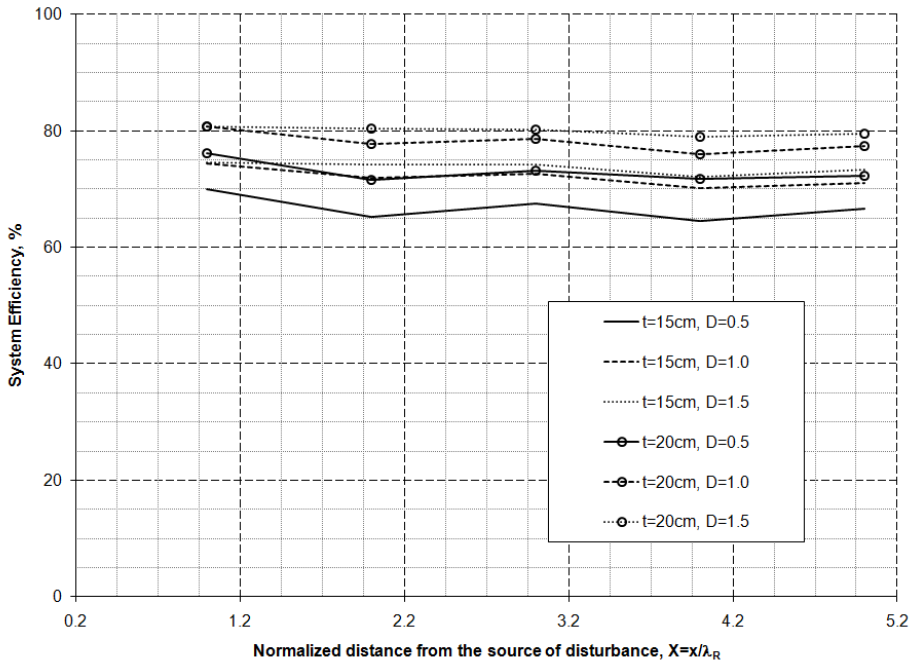

Figure 3- 13: Effect of changing walls dimensions and location on the double-continuous walls system efficiency

3.5.5 Double Staggered Walls Isolation System

Because of its geometrical configuration, a 3D finite element model was utilized to investigate the effectiveness of the double staggered walls isolation system. A parametric study was carried out to find the optimum configuration of the staggered walls that offered the best isolation effectiveness. Table 3-1 lists the adopted segments lengths and gaps that could be practically established between every two wall segments. The obtained results showed that the wall with configuration denoted as case 2 in Table 3-1 gave the best performance over the other two cases. Therefore, case 2 was adopted while performing the parametric study on this system. The spacing between walls was set to the obtained optimum spacing in the previous section which was $0.5\lambda_R$. The normalized distance X varied from 1.0 to 5.0. The load frequency was adopted as 50Hz and the normalized depth D ranged from 0.5 to 1.0 for two wall thicknesses, 150 and 200 mm. Different values of the wall depth and its location relative to the source of disturbance were considered in the analysis. The particle vertical velocity was monitored along the path OA shown in Figure 3-7-d.

Figure 3-14 shows that increasing the wall thickness improved the system effectiveness. It increased by about 21.5% as the wall thickness increased from 150 to 200 mm for the normalized wall depth, D = 0.5, located at a normalized distance, X = 4.0. However, no significant improvement (only 5.8%) was observed when increasing the walls thicknesses for the system located at X = 1.0. For systems located close to the source of vibration, increasing the walls thicknesses resulted in a negligible improvement. Furthermore, increasing the normalized wall depth D from 0.5 to 1.0 showed some gained improvement. For instance, increasing the wall depth D from 0.5 to 1.0 resulted in an

improvement of about 9.5% when the system was located at X = 1.0 with thickness of 150 mm. On the other hand, the system efficiency decreased as the normalized distance X was increased. For example, the system effectiveness decreased by about 19% as X increased from 1.0 to 5.0 for the wall thickness of 200 mm and D = 1.0. It can be concluded that the system effectiveness is mainly affected by the system location rather than the walls dimensions.

3.5.6 Evaluation of Different Isolation Systems

A comparison between the screening efficiency of all proposed isolation systems is carried out in this section. In general, for all proposed isolation systems, the system screening effectiveness increased as the thickness and depth of the wall increased. Moreover, the results revealed that for all systems, except for the double-continuous walls system, the effectiveness decreased as the system was placed far from the source of disturbance. For the case of double-continuous walls system, the normalized distance X had a minor effect on the system performance

Figures 3-15 and 3-16 compare the effectiveness of all systems considered in this study. It is clear that the double-continuous walls system, DCW, is the most effective barrier in reducing the induced waves regardless their location from the source of vibration. On the other hand, box-wall system, BW, has the lowest system effectiveness. However, for systems located at X = 1.0, the double-staggered walls system, DSW, effectiveness is almost the same as DCW system effectiveness, except for X value of 4.0, the DSW system effectiveness becomes close to that of the single-continuous wall system, SCW. In other words, for active isolation case, the DSW system screening

effectiveness is similar to that of the DCW system. For passive isolation case, however, its screening effectiveness is similar to the SCW system.

Table 3- 1: Proposed staggered wall configurations.

Case #	Segment length, λ_R	Gap length, λ_R	Spacing, λ_R
Case 1	0.24	0.08	0.5
Case 2	0.28	0.08	0.5
Case 3	0.30	0.10	0.5

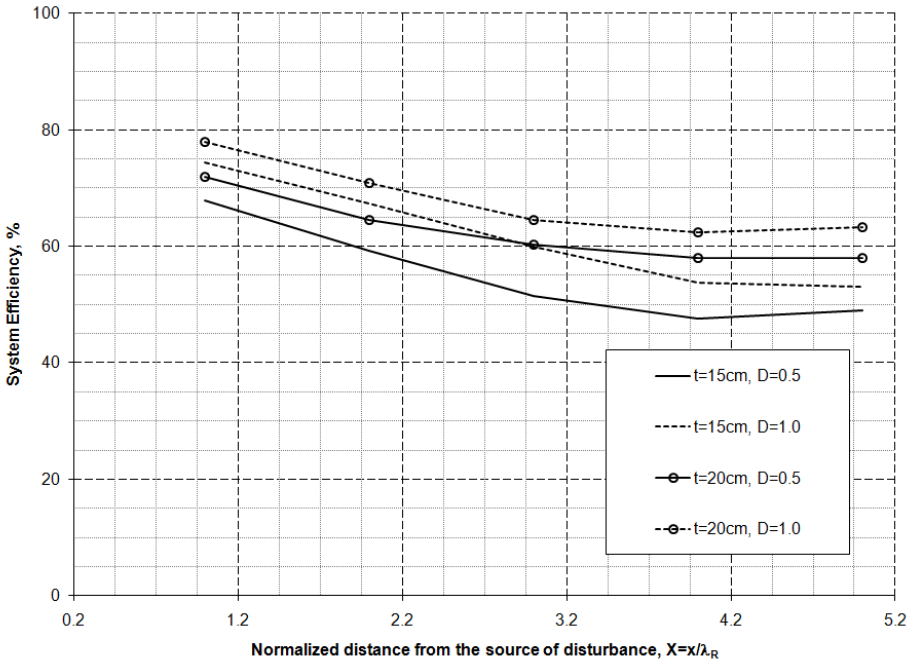

Figure 3- 14: Effect of wall dimensions and location on the double-staggered wall system effectiveness

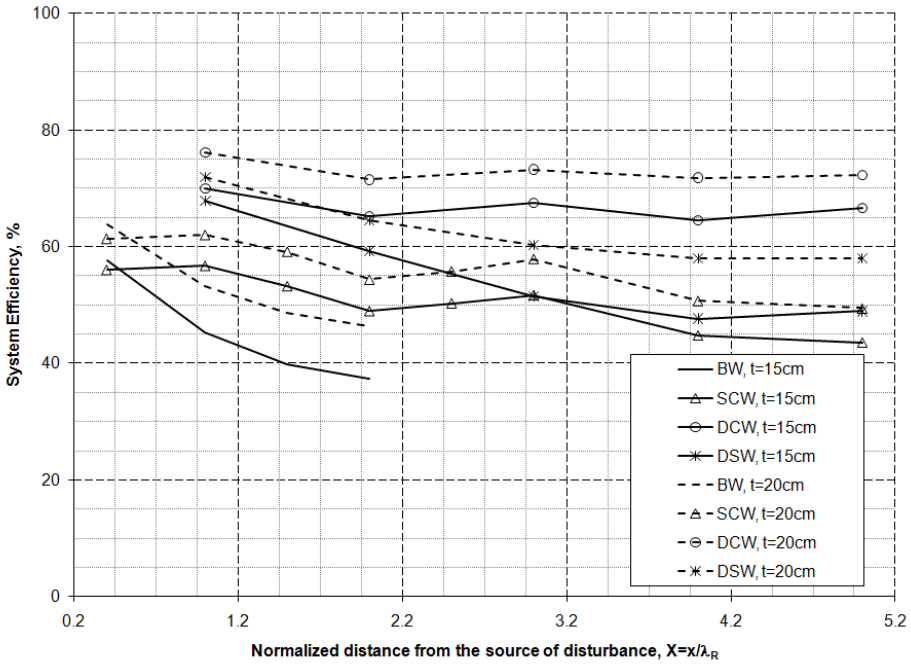

Figure 3- 15: Comparison between four isolation systems effectiveness (D=0.5)

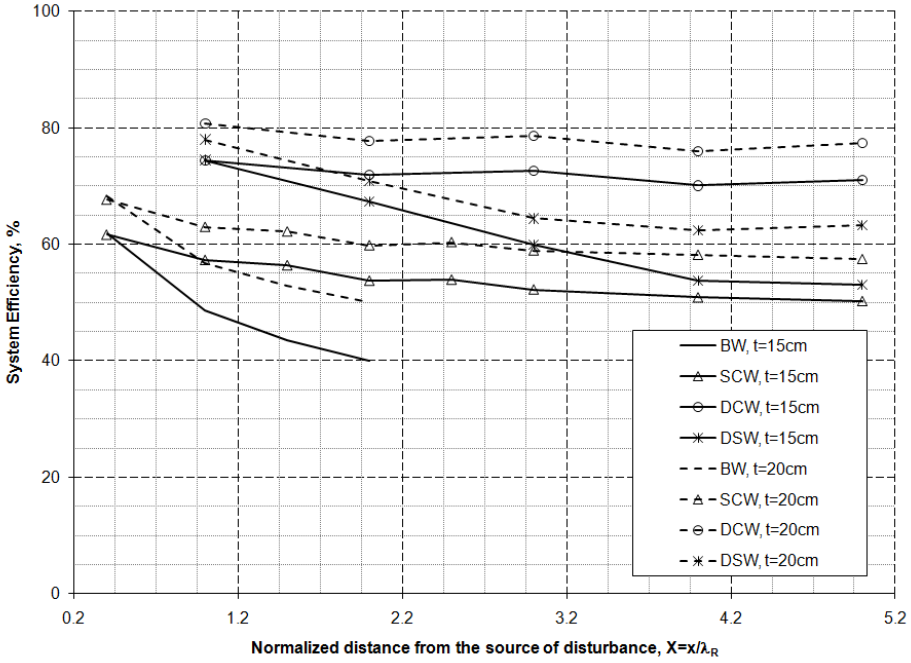

Figure 3- 16: Comparison between four isolation systems effectiveness (D=1.0)

3.6 SUMMARY AND CONCLUDING REMARKS

The analysis of active and passive vibration isolation problems was carried out to investigate the protective effectiveness of different configurations of in-filled geofoam trench barriers systems. The proposed systems were evaluated and compared based on the gained reduction in the soil particle velocities through an intensive parametric study. From the previous discussions and analyses of the results, the following understandings and conclusions can be made:

1. All the proposed geofoam barrier systems perform well in reducing the surface waves and the screening effectiveness varies between 38% and 80%. Furthermore, the geofoam barriers are of variable protection performances in low frequencies.

2. The most effective isolation system is the double-continuous walls system. However, this system protection effectiveness is not affected by its location from the source of disturbance.

3. The double-staggered walls system has capability to screen the vibration as the double-continuous walls system when used as an active isolation system. Thus, the double-staggered walls system is an economic solution as an active isolation system since less geofoam material will be used.

4. The single-continuous wall system and the double-staggered walls system perform almost the same as passive isolation systems. Thus, the single-continuous wall system is an economic solution as a passive isolation system since less geofoam material will be used.

CHAPTER FOUR

FIELD EXPERIMENTAL WORK AND ITS NUMERICAL MODELING

This chapter presents in detail the field experimental work that has been conducted to investigate the protective performance of both open trench and in-filled trench with geofoam material as well as to examine the influences of wall geometry and location from the vibratory source on the isolation efficiency. Moreover, an experimental parametric study is conducted to investigate the influences of varying the ratio between the barrier depth and its location (i.e. to examine active and passive vibration isolation cases). An innovative approach to construct the open and in-filled geofoam trench is presented in this chapter as well. The results of the field experimental investigations are analyzed and interpreted to provide recommendations for implementation in design.

Furthermore, a finite element model is developed in order to simulate the field experimental work. The developed finite element model has been calibrated using the field experimental results to demonstrate its utility in conducting an extensive parametric study to further our understanding of the behaviour of in-filled geofoam trench barriers in different soil conditions.

4.1 SITE INVESTIGATION AND MATERIAL PROPERTIES

The test site is a flat area located 5km west of Ponoka, Alberta. The soil classification and soil profile were established based on the results of soil investigation that included boreholes and a Seismic Cone Penetration Test (SCPT), which were conducted at the site of this experimental study. Based on the boreholes data, the site soils are characterized as silty clays, calyey silt and sandy silt underlain by stiff fine grained and cemented sand layer.

The Multichannel Analysis of Surface Waves method (MASW) is adopted to investigate the soil layering and to establish the shear wave velocity profile. Multichannel Analysis of Surface Waves (MASW) was developed at Kansas Geological Survey (KGS) in 1995-1996 (Park et al. (1999a; 1999b). In the MASW procedure, seismic surface waves generated by a seismic source are measured using a series of geophones. The measurements are used to analyze the propagation velocities of the surface waves, and deduce the shear wave velocity. The data processing involves establishing dispersion curves of the generated surface waves by plotting the frequency versus phase velocity. By inverting the dispersion curves, the variation of shear wave velocity with depth is obtained. Further details and description of MASW can be found in Park et al. (1999a; 1999b). In this study, the MASW data were acquired using 24 vertical component velocity pickups (geophones), a seismic station, and a seismic source (20lb hammer). The 24 geophones were deployed on 2.5m interval as shown in Figure 4-1. The MASW test was performed in two directions: (1) the shot point at 2.5m from geophone #1 and (2) the shot point at 2.5m from geophone #1. Figure 4-2 presents the established shear wave velocity profile from the MASW investigation based on averaging the results from both

directions. All the MASW test measurements and the obtained dispersion curves are presented in appendix B.

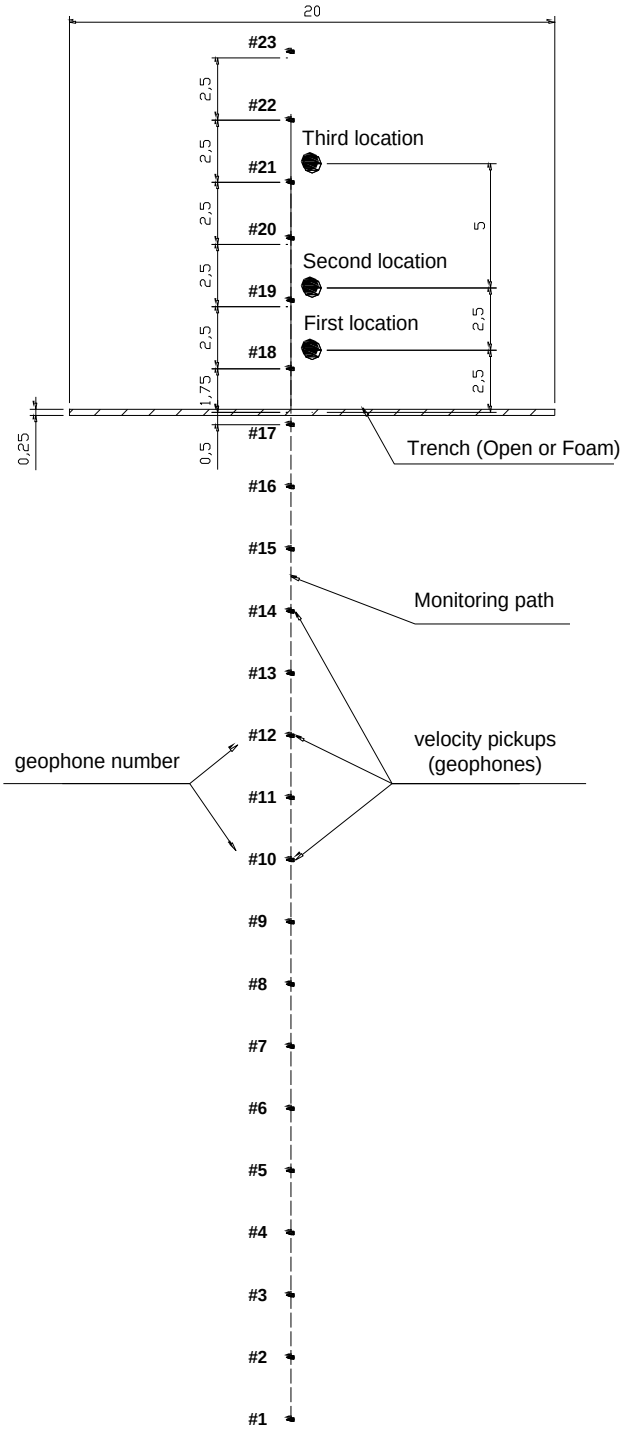

Figure 4- 1: Experimental layout and geophones numbering

The geofoam material is a two-component Polyurethane lightweight material supplied by URETEK Canada (currently known as POLY-MOR Canada). It is also known as URETEK expanded polymer (URETEK web site, 2010). The geofoam material has a density of 61kg/m^3 when it is installed in the trench under no pressure, i.e., free to expand. The dynamic properties of geofoam were evaluated using Bender Element tests and were found to be: shear wave velocity of 330 m/sec, and Poisson's ratio close to zero.

4.2 TEST PROCEDURE

A dynamic excitation comprising of a sinusoidal vertical harmonic load was induced using a mechanical oscillator. The excitation force was quadratic and characterised by harmonic forces proportional to the square of the driving frequency. This resulted in having surface waves with different wavelengths. The first stage of testing consisted of exciting the ground with loads at varying frequencies and recording measurements of ground motion at specified positions before digging the trench wall.

A hydro-dig technique was adopted in digging the trench wall, Figure 4-3. Stage two of testing consisted of exciting the ground after constructing the trench (i.e. open trench) and recording the measurements of ground motion for the same frequencies at the same previously selected locations in stage one. In stage three, the geofoam material was installed in the open trench and allowed sufficient time to cure. After the geofoam curing process was complete, the harmonic excitation was applied and ground motion measurements were recorded for the same frequencies and at the same specified locations. To assess the system effectiveness, the recorded time history of vertical soil

particles velocities at pickup points was converted to the frequency domain, analyzed and discussed in subsequent text.

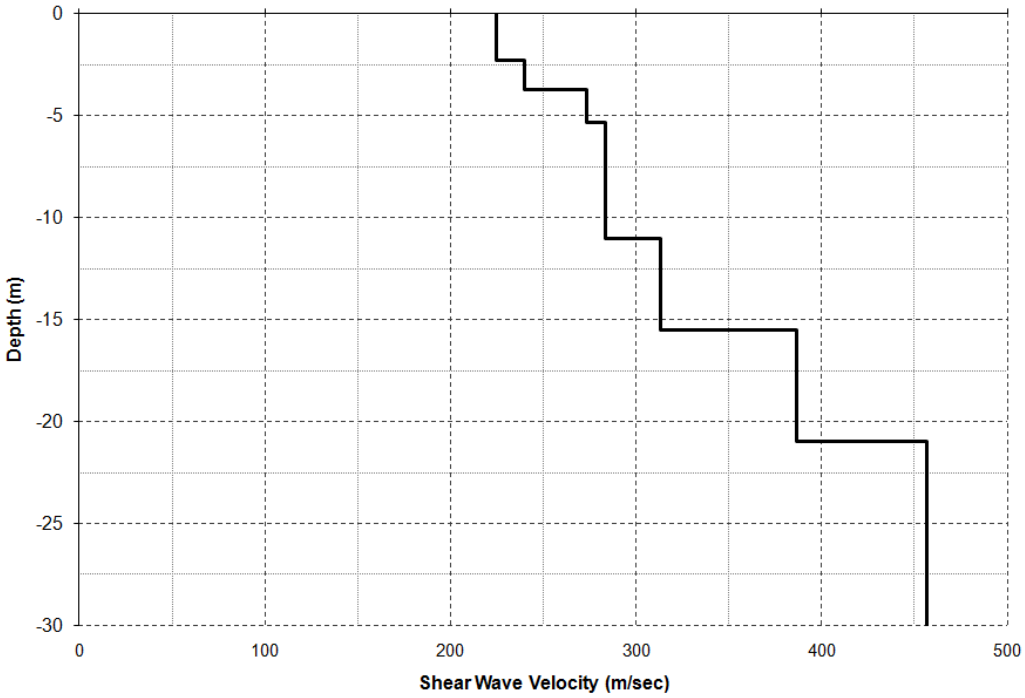

Figure 4- 2: Adopted shear wave velocity profile

(a)

(b)

Figure 4- 3: Digging the open trench using hydro-dig technique

4.3 INSTRUMENTATION AND TEST DESCRIPTION

This study investigates vibration scattering using open and in-filled geofoam trench wave barriers by conducting a parametric experimental study. Therefore, all test parameters and the results of the testing program are presented in dimensionless format.

A trench wall of 20m length, 0.25m width, and 3.0m depth was constructed. Since the ratio of the trench wall width to its depth is very small, it is impossible to dig such thin trenches using the classical techniques. In this situation, the hydro-dig technique was deemed to be the most efficient and practical way to dig such thin trench walls. Because the water table was well below the target depth and due to the nature of soil, stiff sandy silt to silty clay, the excavated trench can stay stable without collapse. That means the ground can be excited and measurements can be taken while the trench is open in order to compare the protective effectiveness of open and in-filled geofoam trench barriers for the same soil profile and testing conditions.

The source of excitation was a Lazan type (MO 2460) mechanical oscillator with eccentric masses. The oscillator comprised of two counteracting shafts each carried a set of eccentric masses to generate the harmonic excitation. The oscillator was driven by a 7.5 HP 220 V three phase motor capable of generating sinusoidal force of 23.5 kN peak-to-peak. The speed of the motor was controlled by a variable frequency AC speed drive, yielding stable operating speeds between 4 and 60 Hz.

The oscillator was welded on top of a circular steel plate with 0.72 m diameter. The maximum operating speed of the oscillator is 3600rpm with no loads. To simulate the machine foundation case and to keep the system acceleration during the excitation less

than 1g, the oscillator was placed centrically on top of twenty steel plates as shown in Figure 4-4. Thus, the center of gravity (CG) of the oscillator (where the dynamic force is applied) was above the geometric center of its base. The plates were bolted together using four threaded steel rods. The diameter of the steel plate was 0.72 m, its thickness was 2.5cm and its mass was 79kg. To ensure good contact between the oscillator and the ground, the excitation system was embedded about 0.25 m below the ground surface. Figure 4-5 shows the oscillator, motor, steel plates and the driving speed box.

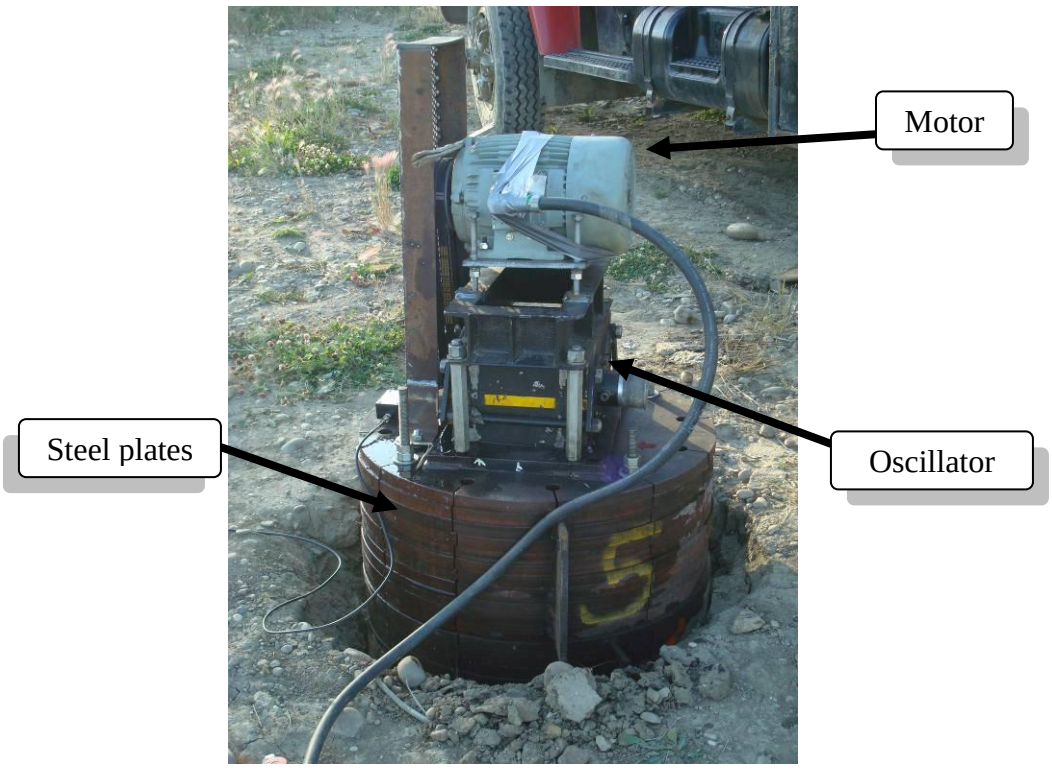

Figure 4- 4: The mechanical oscillator, steel plates and driving motor

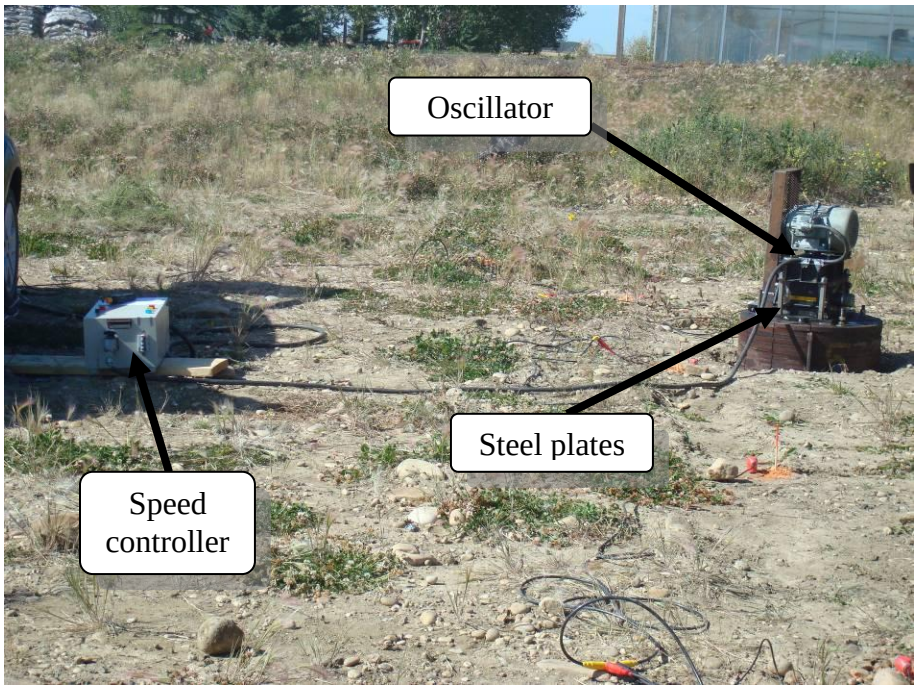

Figure 4- 5: The mechanical oscillator and the speed box controller

Ten loading events with different frequency were utilized in this experiment. The frequencies considered were 15, 20, 25, 30, 35, 40, 45, 50, 55, and 58.84 Hz. All geometrical parameters of the experiments are normalized by the Rayleigh wavelengths, (λ_R) which is a function of the excitation frequency. The resulting Rayleigh wavelengths, the barrier dimensionless geometry, and location were calculated and listed in Table 4-1 and they are also shown in Figure 4-6.

Table 4- 1: Dimensionless geometry of experiment

Frequency, Hz	Rayleigh wavelength	Barrier dimensionless depth	Dimensionless distance between vibration source and wave barrier		
			First location	Second location	Third location
	λ_R, m	$D=d/\lambda_R$	$X_1=x_1/\lambda_R$	$X_2=x_2/\lambda_R$	$X_3=x_3/\lambda_R$
15	14.09	0.21	0.17	0.35	0.70
20	10.57	0.28	0.22	0.46	0.93
25	8.46	0.35	0.28	0.58	1.17
30	7.05	0.43	0.34	0.69	1.40
35	6.04	0.50	0.39	0.81	1.64
40	5.28	0.57	0.45	0.92	1.87
45	4.70	0.64	0.51	1.04	2.10
50	4.23	0.71	0.56	1.15	2.34
55	3.84	0.78	0.62	1.27	2.57
58.84	3.59	0.84	0.66	1.36	2.75

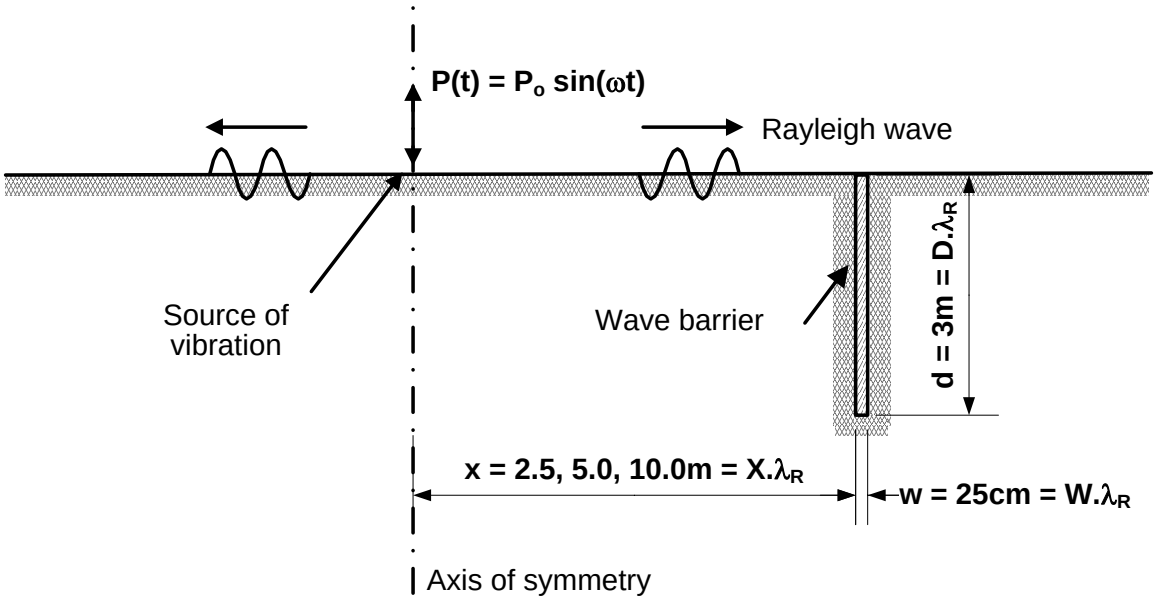

Figure 4- 6: Typical schematic of the vibration isolation system and geometric parameters

Geophones were deployed along a line perpendicular to the centre of the barrier with 2.5m intervals. The experimental layout and geophones numbering are illustrated in Figure 4-1. Also, Figure 4-7 shows the geophones deployment in the file. The geophones were connected to a 24-channel Geode/ES-3000 seismic station. A laptop computer equipped with PCMCIA card was used to control the seismic station through Seismodule Control Software. For every selected frequency, a sample of 8 seconds measurements of soil particles velocities was recorded using vertical component geophones with a 1 millisecond sample interval which results in have 8000 data points.

To study the influence of the proximity of the source of disturbance to the isolation system on its protective effectiveness, three locations were chosen to place the excitation system: 2.5, 5, and 10m from the center of the barrier. Measurements were taken for every location for the three stages (without trench, with open and with geofoam trench) at the ten excitation frequencies. Table 4-2 presents the experimental parameters, including: geometrical dimensions of barrier, its distance from source of disturbance, and loading frequencies considered. Figure 4-8 shows the trenches after construction completion.

Table 4- 2: Experimental parametric test

Barrier width (m)	w	0.25
Barrier depth (m)	d	3.0
Distance between the oscillator and the trench (m)	x	2.5, 5, 10
Exciting frequency (Hz)	f	15, 20, 25, 30, 35, 40, 45, 50, 55, 58.84

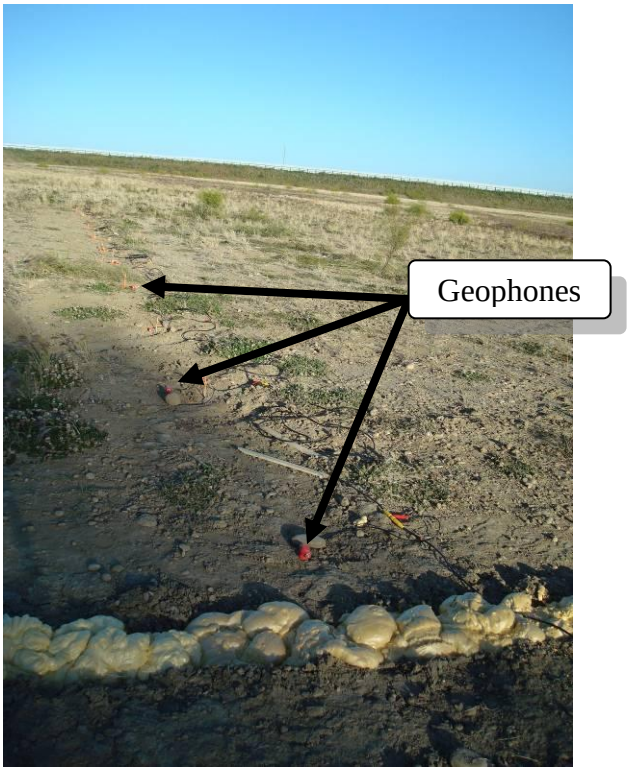

Figure 4- 7: Geophones deployment in the field

(a)

(b)

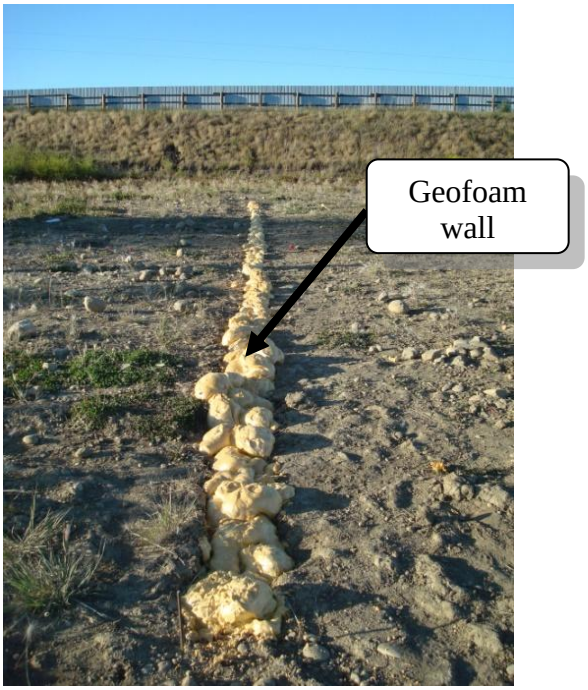

Figure 4- 8: Trench barriers after construction completion
(a) open trench and (b) in-filled geofoam trench

4.4 RESULTS ANALYSIS AND DISCUSSION

Because of the large number of conducted vibration tests, only a sample from the results will be presented in a compact format. A characterization of the source of disturbance is followed by a discussion on the influence of the barrier dimensionless geometry on its screening effectiveness as well as the influence of the barrier depth and its proximity to the source of disturbance. The results are presented in terms of the amplitude reduction ratio (A_r) as will be explained in the subsequent sections.

4.4.1 General Properties of the Responses

To assess the effects of the barrier geometry on the screening effectiveness, all vibration tests were conducted with the same initial conditions and the same vibrating frequencies. The vibratory system is controlled using a speed box. To ensure accurate and consistent vibration frequency at each testing frequency during the three stages, a tachometer is used to check real vibrating frequency with an accuracy of about ±0.25Hz before recording the responses.

Figures 4-9 to 4-11 show a typical time history and the Fast Fourier Transform (FFT) of the recorded signals that are measured on the ground along the monitoring path during stage one and the vibrating source is at first location. Channel #18 represents the vibrating source while the rest of channels represent the ground response at different locations. The obtained results displayed high quality signals for the harmonic excitations with different input frequencies. On the other hand, the Fourier spectrum indicates clearly

that the ground response has the same dominant frequency as the frequency of the applied dynamic load.

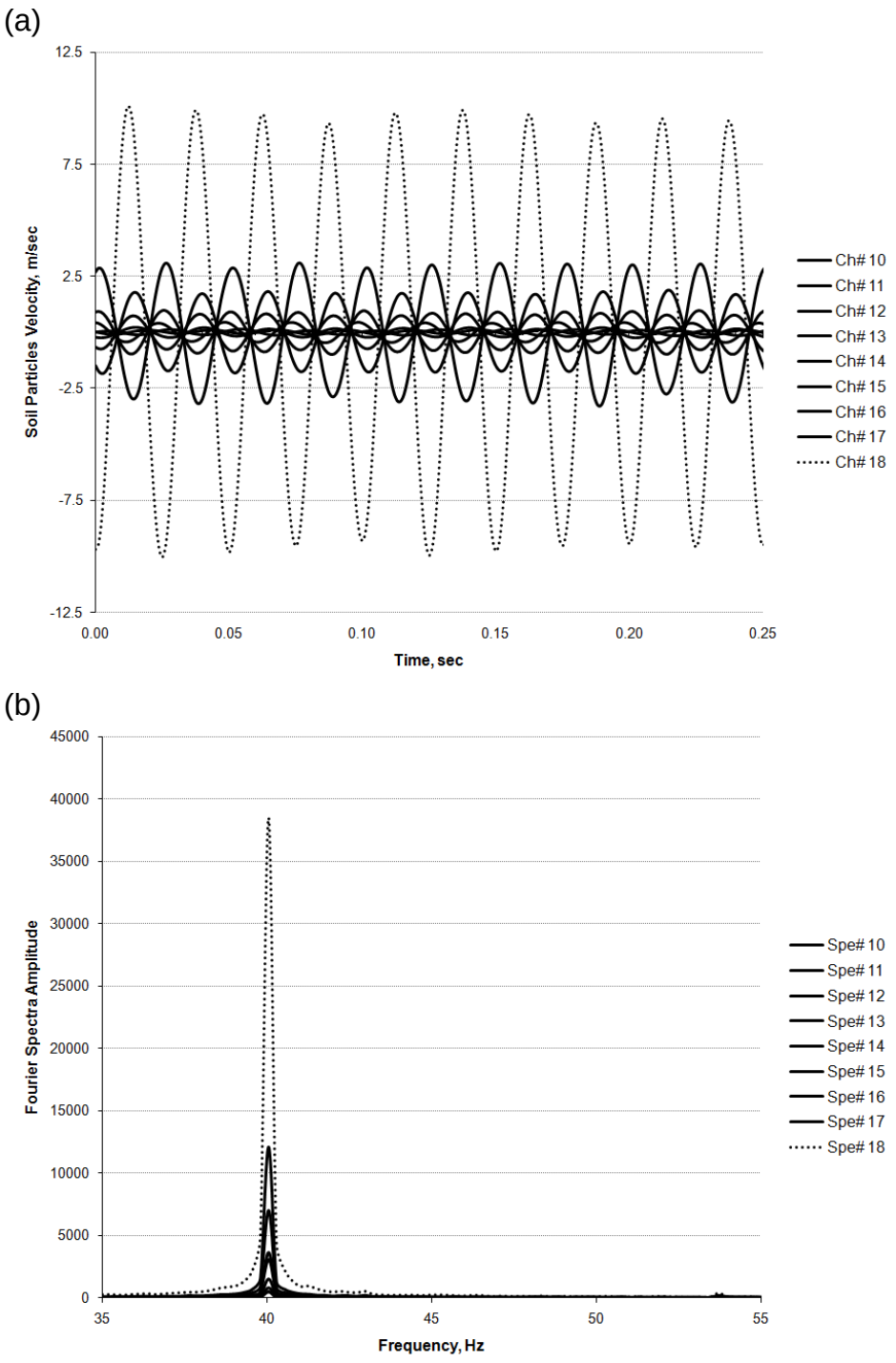

Figure 4- 9: Measured soil particles velocities during the first stage (f=40Hz) (a) in time domain, (b) corresponding FFT

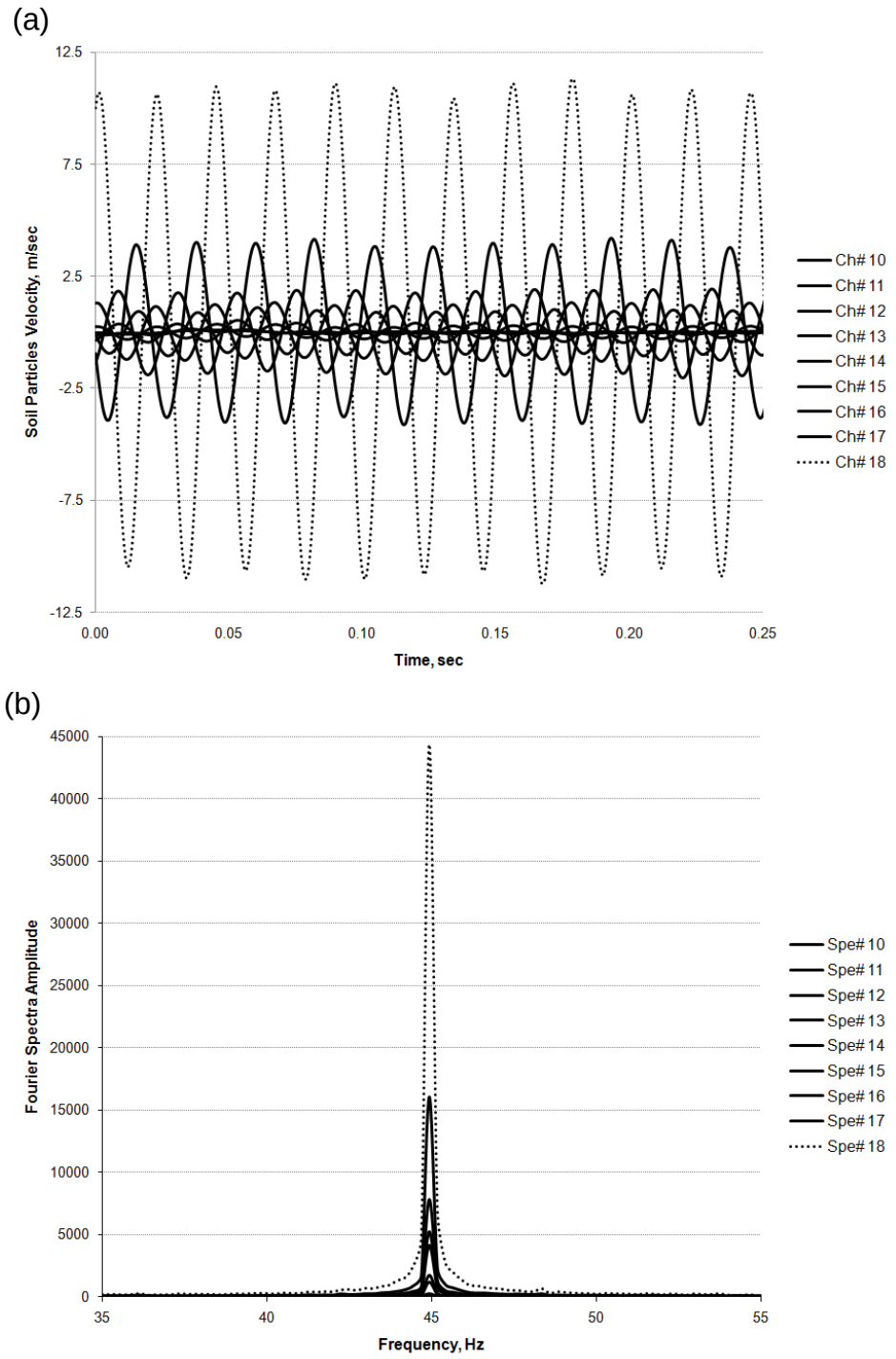

Figure 4- 10: Measured soil particles velocities during the first stage (f =45Hz) (a) in time domain, (b) corresponding FFT

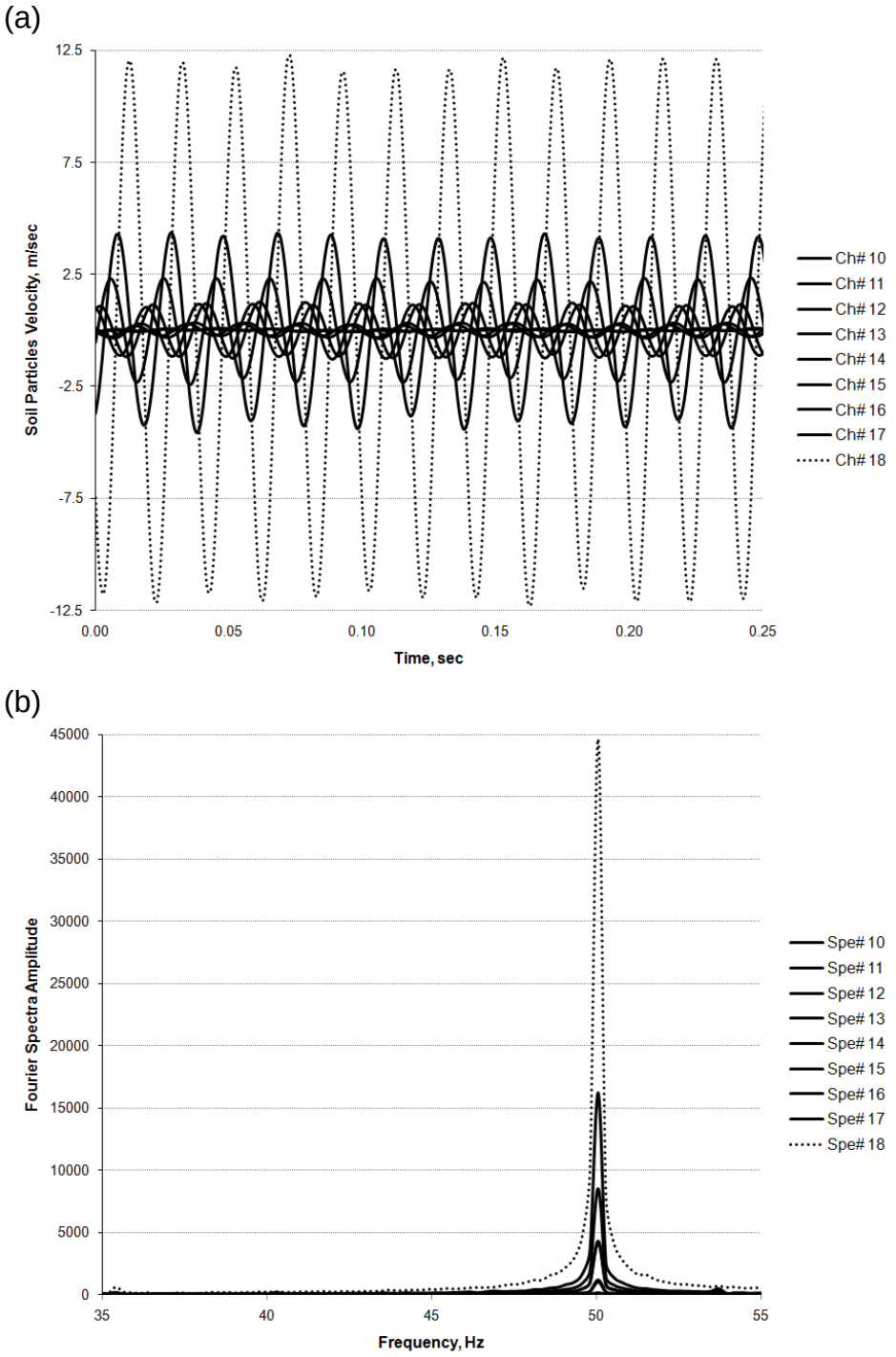

Figure 4- 11: Measured soil particles velocities during the first stage (f=50Hz) (a) in time domain, (b) corresponding FFT

4.4.2 Amplitude Reduction Ratio

The source of vibration simulates the case of machine foundation vibration, which results in a steady state response. The system effectiveness can be evaluated based on the observed displacement, velocity or acceleration with and without the vibration barrier. In most of the published literature, the system effectiveness was evaluated in terms of the achieved reduction in response amplitude of soil particle. In practice, the effect of transmitted vibration is usually evaluated in terms of soil particles velocity at points of interest. Since velocity pickups were used to measure the soil particles velocity, the system effectiveness can be presented in terms of reduction in soil particle velocity. Therefore, the results are presented in the form of amplitude reduction ratio, A_r, which is calculated by normalizing the post-trench installation maximum spectral velocity amplitude, $(A_r)_{After}$, by the maximum spectral velocity amplitude before trench installation, $(A_r)_{Before}$, measured on the ground surface. The maximum spectral velocity amplitude can be obtained from Fourier curves, which are established from applying FFT on the time history records at the points of interest. The amplitude reduction ratio is then given by:

$$A_r = \frac{(A_r)_{After}}{(A_r)_{Before}} \tag{4-1}$$

To evaluate the system effectiveness (screening effectiveness) of the wave barrier system, the averaged amplitude reduction ratio ($\overline{A_r}$) over a distance of interest x measured behind the wave barrier can be calculated using the following equation:

$$\overline{A_r} = \frac{1}{x}\int A_r \, dx \tag{4-2}$$

Thus, the system effectiveness is calculated using Equation 3-4 as follows:

$$Eff_A = \left(1 - \overline{A_r}\right) \times 100 \tag{4-3}$$

4.4.3 Attenuation Due to the Presence of Barriers

Figures 4-12 to 4-15 show the measured soil particle velocities normalized by the soil particle velocity at the source of disturbance (i.e. attenuation curves for vertical soil particles velocities) for the cases of open, geofoam and without barrier for frequencies 30Hz, 40Hz, 50Hz and 58.84Hz. The recorded measurements follow the expected trends in terms of amplitude versus distance for all frequencies. The results show a very steep decay, which indicates that the soil damping is relatively high. This means that the ground motion is damped both geometrically and materially. It is worth mentioning that as the frequency of the excitation increases, the geometric damping increases as well, which results in further attenuation of the generated surface waves. It is noted from Figures 4-12 to 4-15 that at the measuring point located 20.0 m from source of disturbance, the attenuated velocity amplitude is less than 2% of that at the source for the ground conditions at this site. Therefore, the analysis of A_r and barrier effectiveness will be limited to a distance 18.0 m from the source, as the amplitudes at larger distances are negligible, even without any wave barrier. Hence, the measured responses will not allow reliable and meaningful evaluation of the barrier effectiveness at distant points.

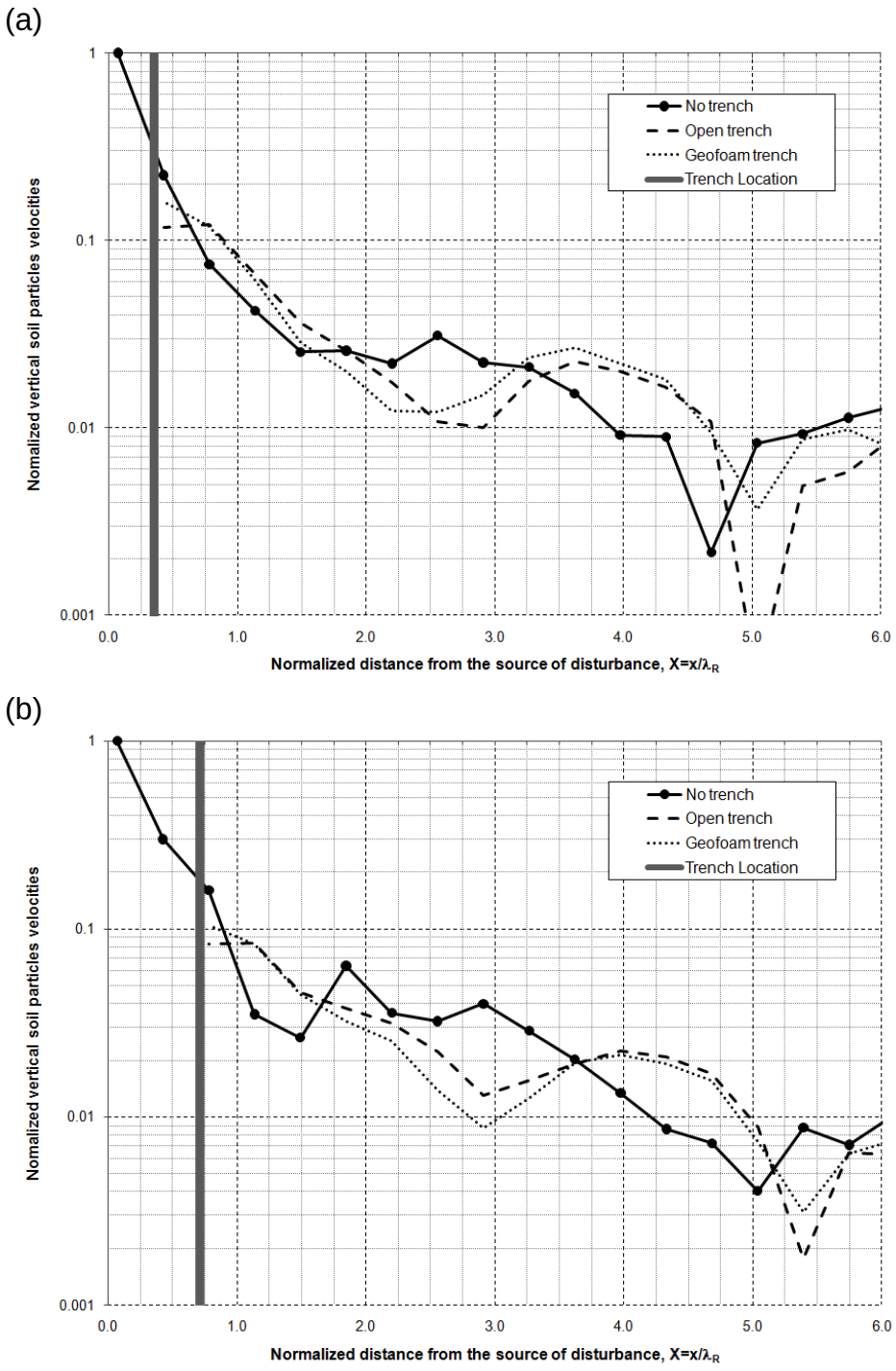

Figure 4- 12: Normalized ground motion for exciting frequency of f=30Hz
(a) trench at first location, 2.5m, (b) trench at second location, 5.0m

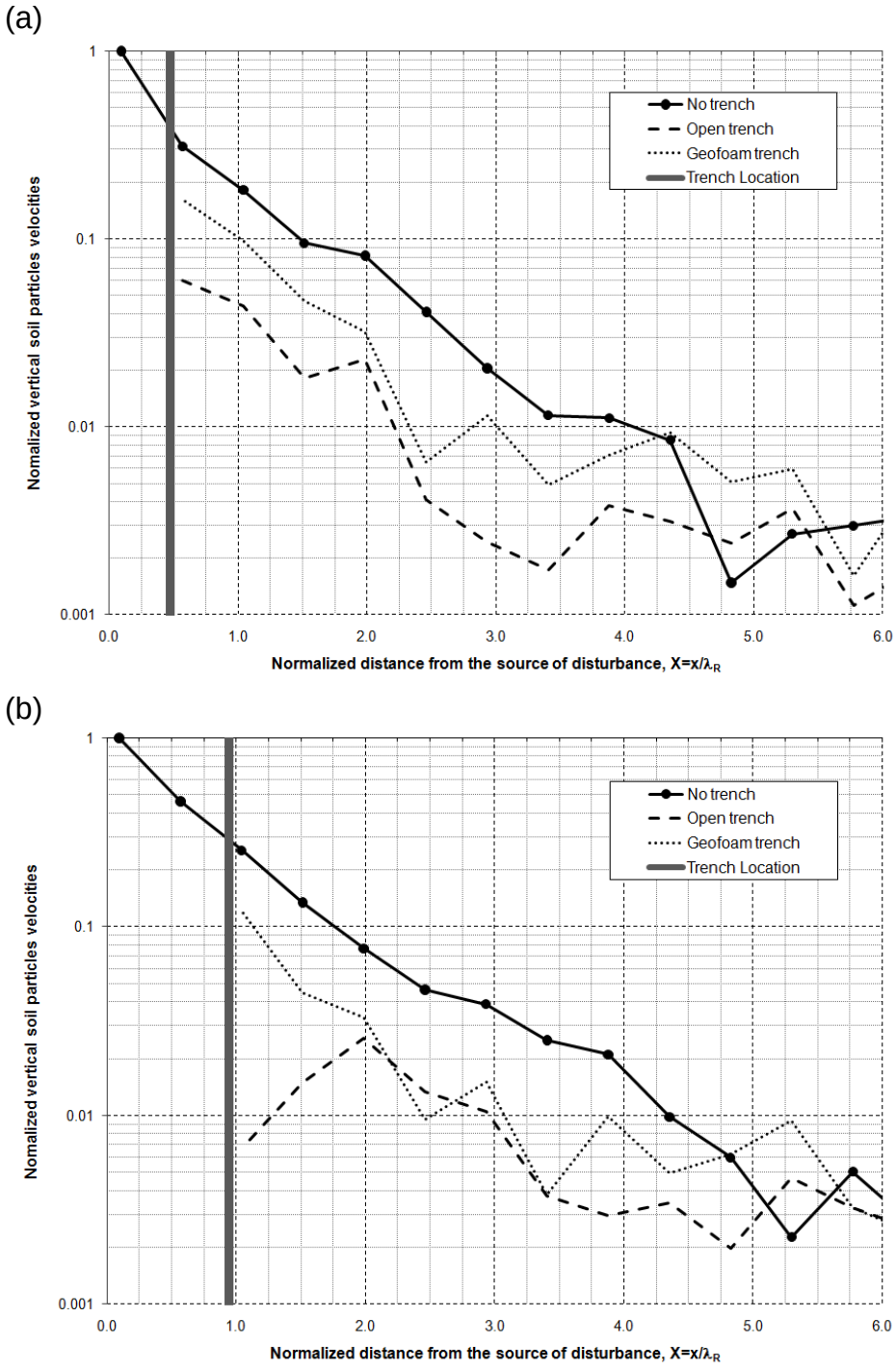

Figure 4- 13: Normalized ground motion for exciting frequency of f=40Hz (a) trench at first location, 2.5m, (b) trench at second location, 5.0m

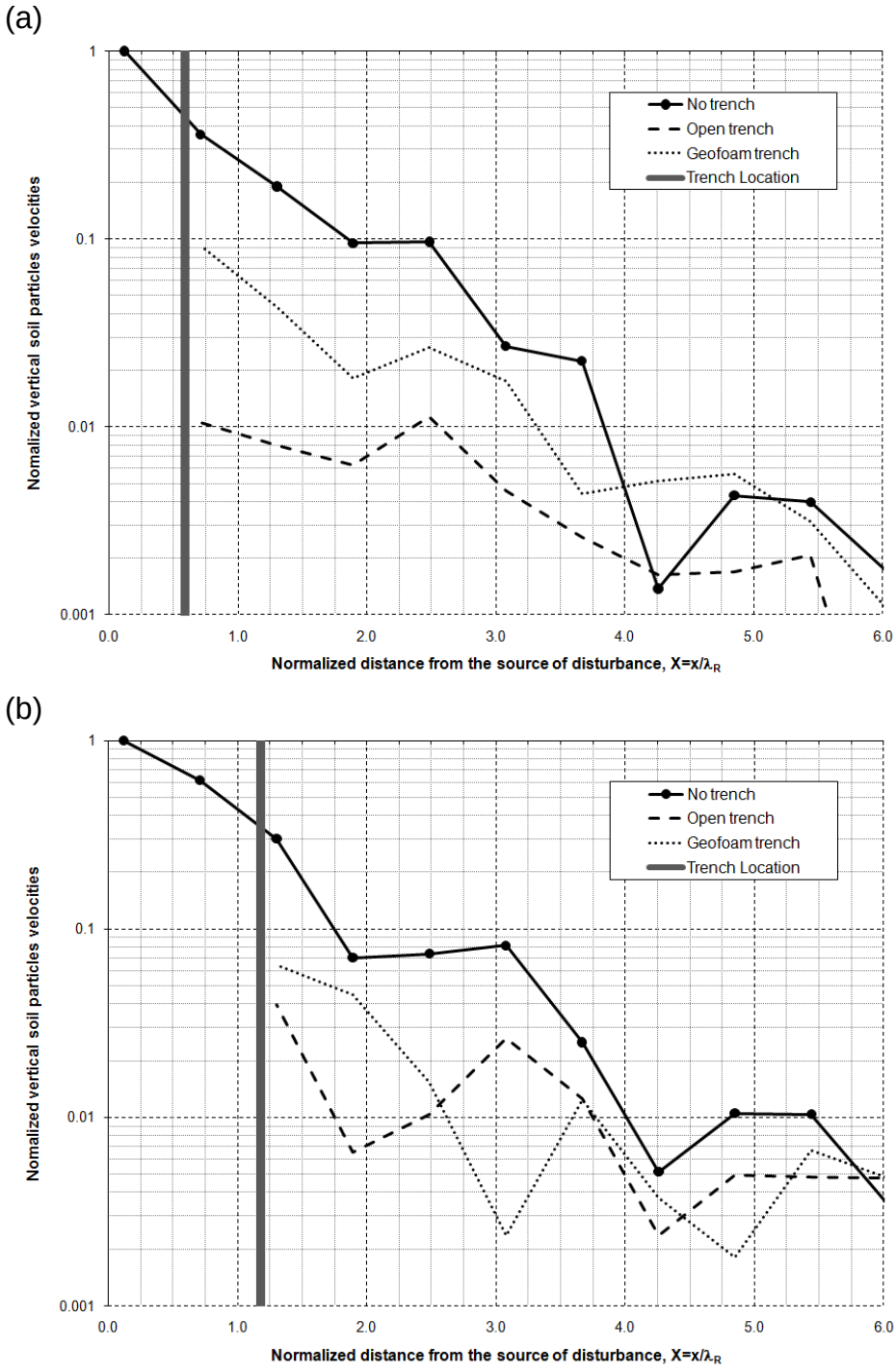

Figure 4- 14: Normalized ground motion for exciting frequency of f=50Hz (a) trench at first location, 2.5m, (b) trench at second location, 5.0m

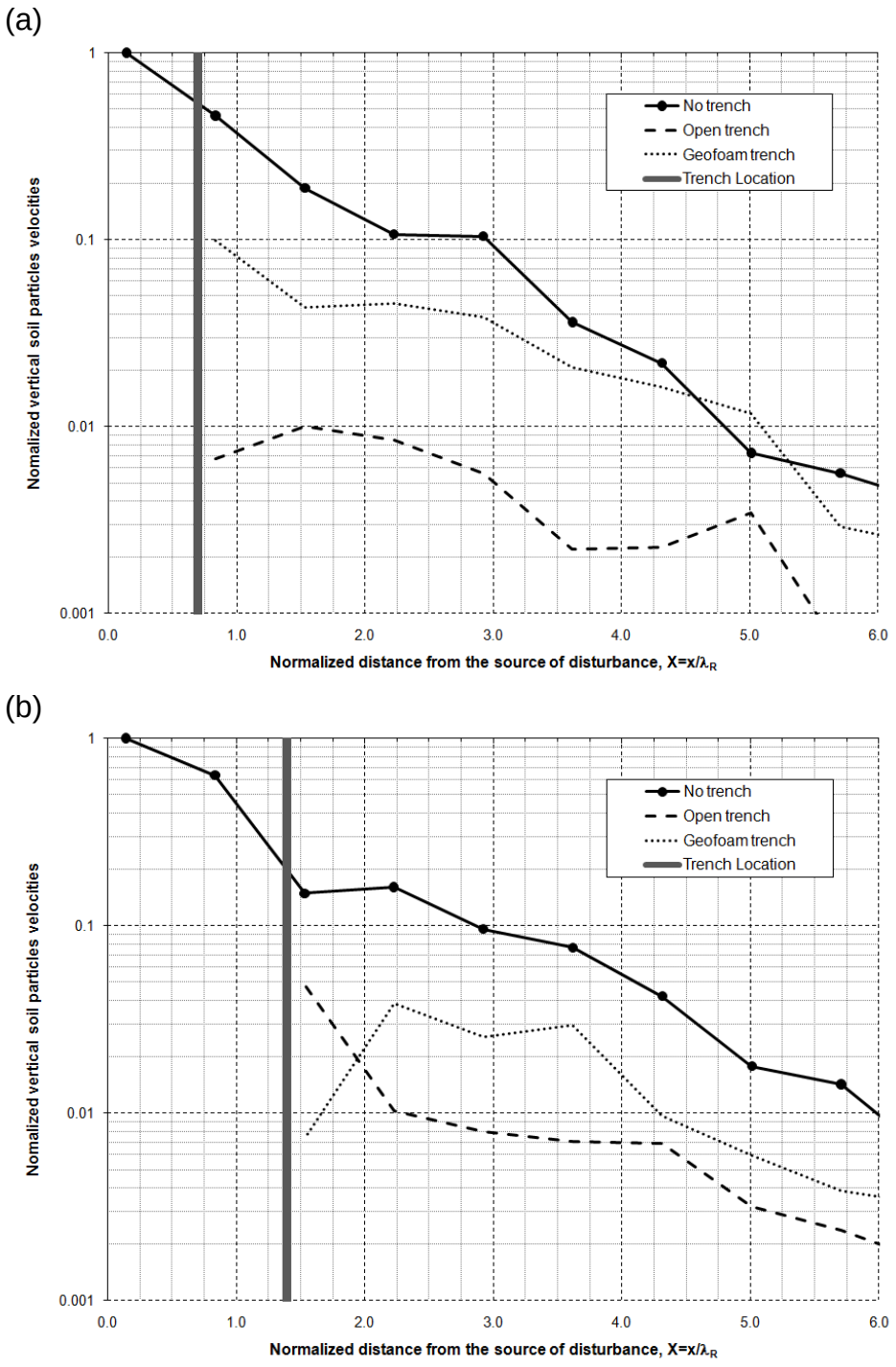

Figure 4- 15: Normalized ground motion for exciting frequency of f=58.84Hz
(a) trench at first location, 2.5m, (b) trench at second location, 5.0m

Figures 4-16 to 4-18 show the calculated amplitude reduction ratios for the three locations of the disturbance source for the exciting frequencies of 40Hz, 45Hz, 50Hz, 55Hz, and 58.84Hz during the presence of open and in-filled geofoam trench barriers. As it can be noted from the figures, the amplitude reduction ratio changes randomly as the distance from the trench exceeds about 15.0 m (3.9λ to 5.7λ). This may be attributed to two reasons: first, the reflected waves at the soil layers interfaces, which pass beneath the barrier are in-phase or out-of-phase; second, the vibration amplitudes are very negligible even without the barrier, and any variation in the response represents a large change in the ratio. The in-phase and out-of-phase behaviour arises from the phenomena of minima and maxima. In other words, these are the points where waves are closest to exactly in-phase and out-of-phase with each other causing maximum and minimum A_r. This behaviour was documented by Woods (1968) in his experimental study on open trenches, Baker (1994) in his experimental on in-filled trenches and by Beskos (1986) in his study of sheet pile barriers as vibration isolators. They noted that the distance to the principal minima decreases as the barrier depth increases, i.e. by increasing the exciting frequency. A similar behaviour is observed in this study. For example, Figure 4-16 shows clear minima immediately behind the barrier resulting in having a quiet area.

Local soil inhomogeneity and high soil damping can be considered the reasons of having many maxima as we move away from the barrier resulting in the random nature of the calculated A_r. For instance, one of the observations during digging the trench is that a large stone was found at depth of about 1.8m and because of its size, it cannot be taken out. On the other hand, as the distance away from the barrier increased, the vibration amplitudes were much smaller and thus the distant geophones measured negligible

velocity values, which were possibly mixed with ground noise. When these small values are used to evaluate the amplitude reduction ratio, significant numerical errors are likely to occur. As a result, the large A_r values are suspect and are considered misleading and unreliable. Therefore, the readings of channels located within a distance of about 18m from the source will be included only when calculating the averaged amplitude reduction ratio, $\overline{A_r}$.

4.4.4 Influence of Barriers Dimensions and Location on Screening Effectiveness

The Rayleigh wavelength, λ_R, decreases as the excitation frequency increases. Consequently, an increase in the frequency leads to an increase in the normalized barrier dimensions and the normalized distance, X, because all dimensions are normalized by λ_R. However, the distance x is constant for every location but varied as the source of disturbance was moved from one location to another. Accordingly, the influence of the barrier normalized depth as well as the coupled effect of the barrier location to its depth will be discussed. All previously published experimental studies have been conducted on constant distance to depth ratios, which means the coupled effect of barrier location and depth together has not been taken into consideration. The influence of barrier normalized width will be ignored in this study since the proposed practical width to construct this type of in-filled geofoam trench barrier system is 0.25 m, which was found to provide excellent performance in scattering the induced ground vibration as described in chapter three. Therefore, the barrier performance will be assessed according to its normalized depth and the ratio of barrier-source distance to barrier depth. The normalized barrier dimensions and barrier-source distances are listed in Table 4-1.

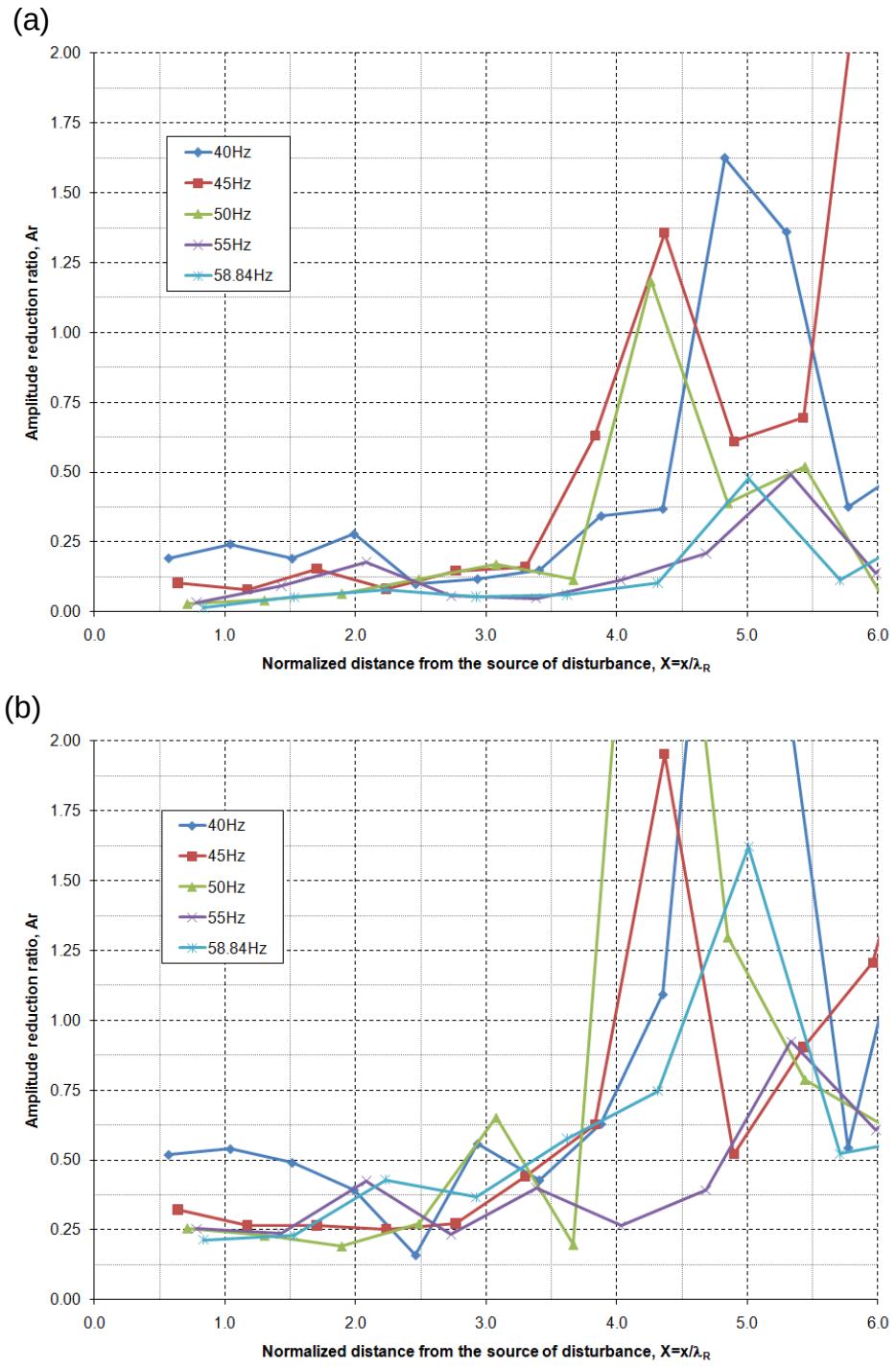

Figure 4- 16: Calculated amplitude reduction ratio for a trench located at the first location (x=2.5m)
(a) open trench, (b) in-filled geofoam trench

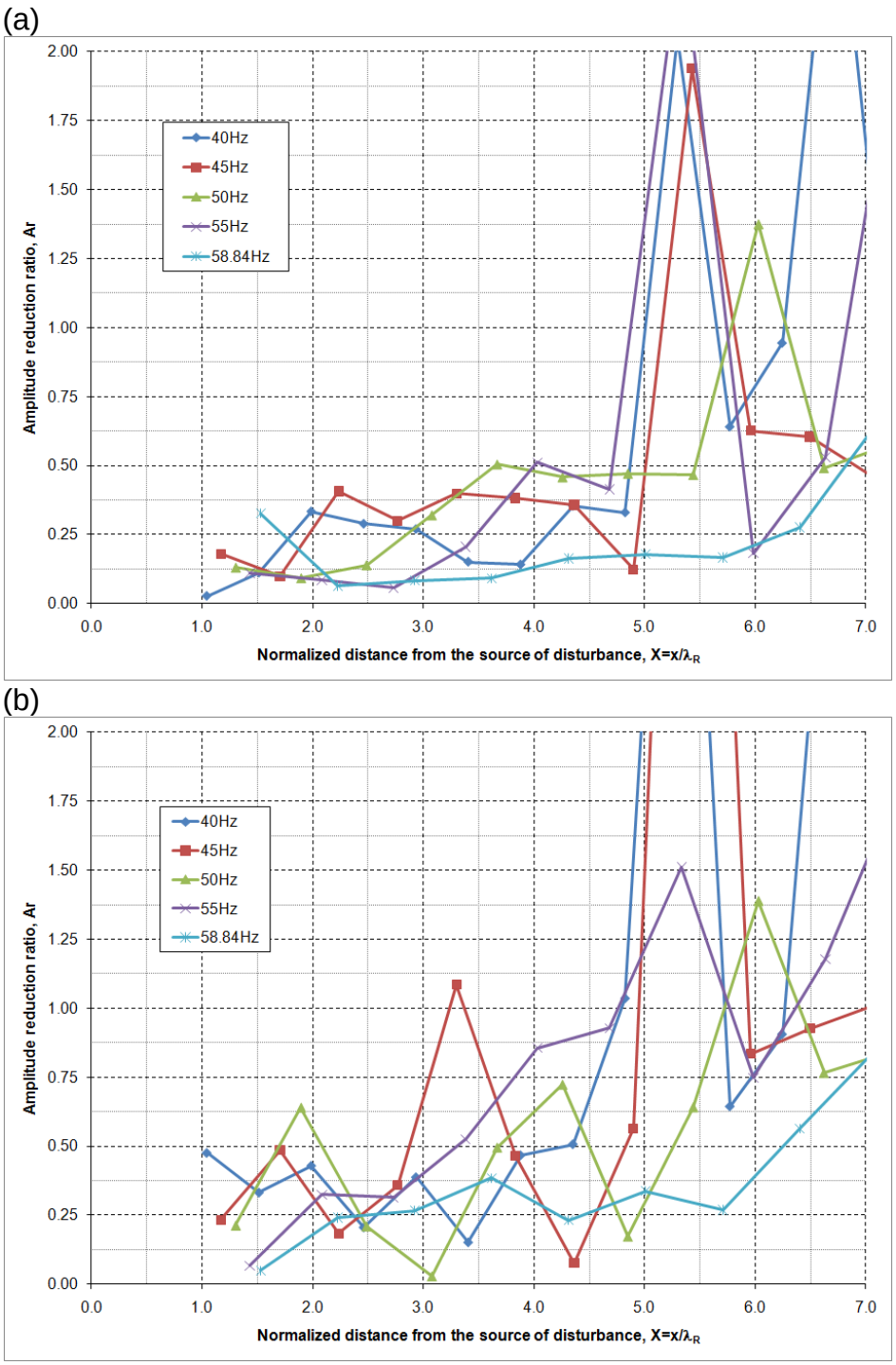

Figure 4- 17: Calculated amplitude reduction ratio for a trench located at the second location (x=5.0m)
(a) open trench, (b) in-filled geofoam trench

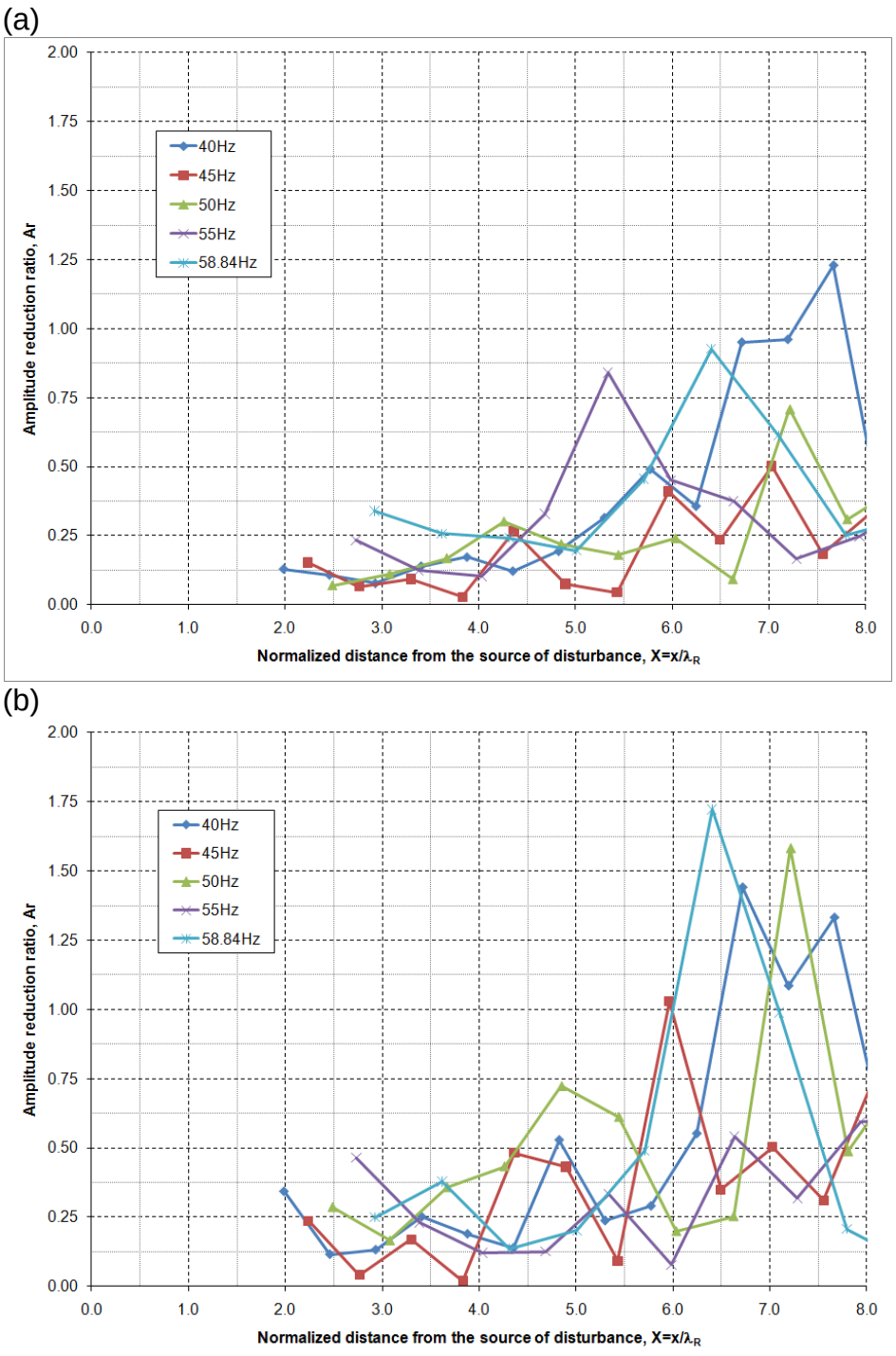

Figure 4- 18: Calculated amplitude reduction ratio for a trench located at the third location (x=10.0m)
(a) open trench, (b) in-filled geofoam trench

The influence of barrier normalized depth, D, is demonstrated in Figure 4-19 for both open and in-filled geofoam trench barriers. It is noted that as the normalized depth, D, increased, the averaged amplitude reduction ratio decreased, which means the system protective effectiveness improved. The results show that a significant improvement can be achieved when the normalized depth is greater than or equal to 0.57 for both open and in-filled geofoam trench barriers. Hence, the normalized depth D = 0.57 can be considered as an optimum depth for both open and in-filled geofoam trench barriers. For example, an overall average amplitude reduction ratio of about 0.16 and 0.31 are achieved for the open and in-filled geofoam trench barriers systems, respectively. That means the vibration amplitudes are decreased (i.e. barrier effectiveness) by 84% and 69% for the open and in-filled geofoam trench barriers, respectively.

Figure 4-20 demonstrates the influence of the barrier location normalized by its depth on the effectiveness of open and in-filled geofoam trench barrier systems. The adopted ratios of x/d are 0.79, 1.63, and 3.29 for the first, second, and third locations, respectively. It can be observed that as the distance between the barrier and the vibration source increases, a deeper trench is required in order to achieve a significant improvement in the system effectiveness. For example, in the case of an open barrier system, when x/d = 0.79 (first location), a significant improvement can be gained by placing the barrier at a normalized distance, $X \geq 0.45$ with $D \geq 0.57$. Meanwhile, for x/d = 3.29 (third location), similar improvement can be achieved by placing the barrier at $X \geq 1.64$ with $D \geq 0.57$. The same trend is observed in the case of in-filled geofoam trench barrier. This means average system effectiveness of 79% and 64% can be achieved by placing the barriers at X = 0.92-1.36 for the cases of open and in-filled geofoam trench barriers,

respectively, with x/d = 1.63 and D = 0.57-0.84. Furthermore, average system effectiveness of 84% and 78% can be achieved by placing the barriers at X = 1.64-2.75 for the cases of open and in-filled geofoam trench barriers, respectively, with x/d = 3.29 and D = 0.50-0.84. It can be concluded that as x/d decreases, a shallower barrier can be used to achieve the same improvement in system effectiveness.

4.5 COMPARISONS WITH PUBLISHED RESULTS FOR OPEN TRENCH CASE

The ground motions were monitored along a center line perpendicular to the trench (Figure 4-1) which have been used to calculate the amplitude reduction ratio, $\overline{A_r}$, instead of the area behind the trench as done by Woods (1968), and Baker (1994). The reason of choosing the present methodology in calculating $\overline{A_r}$ is that the trench had sufficient length (20m) and was narrow, which means the edge effects can be ignored, especially at higher frequencies. On the other hand, published literature revealed that all the experimental studies were performed using small scale models while the experiments conducted in this thesis involves a large (full) scale setup in which the soil layering effects is expected to influence the results. Therefore, no strict and direct comparisons can be made between the present and previously published results.

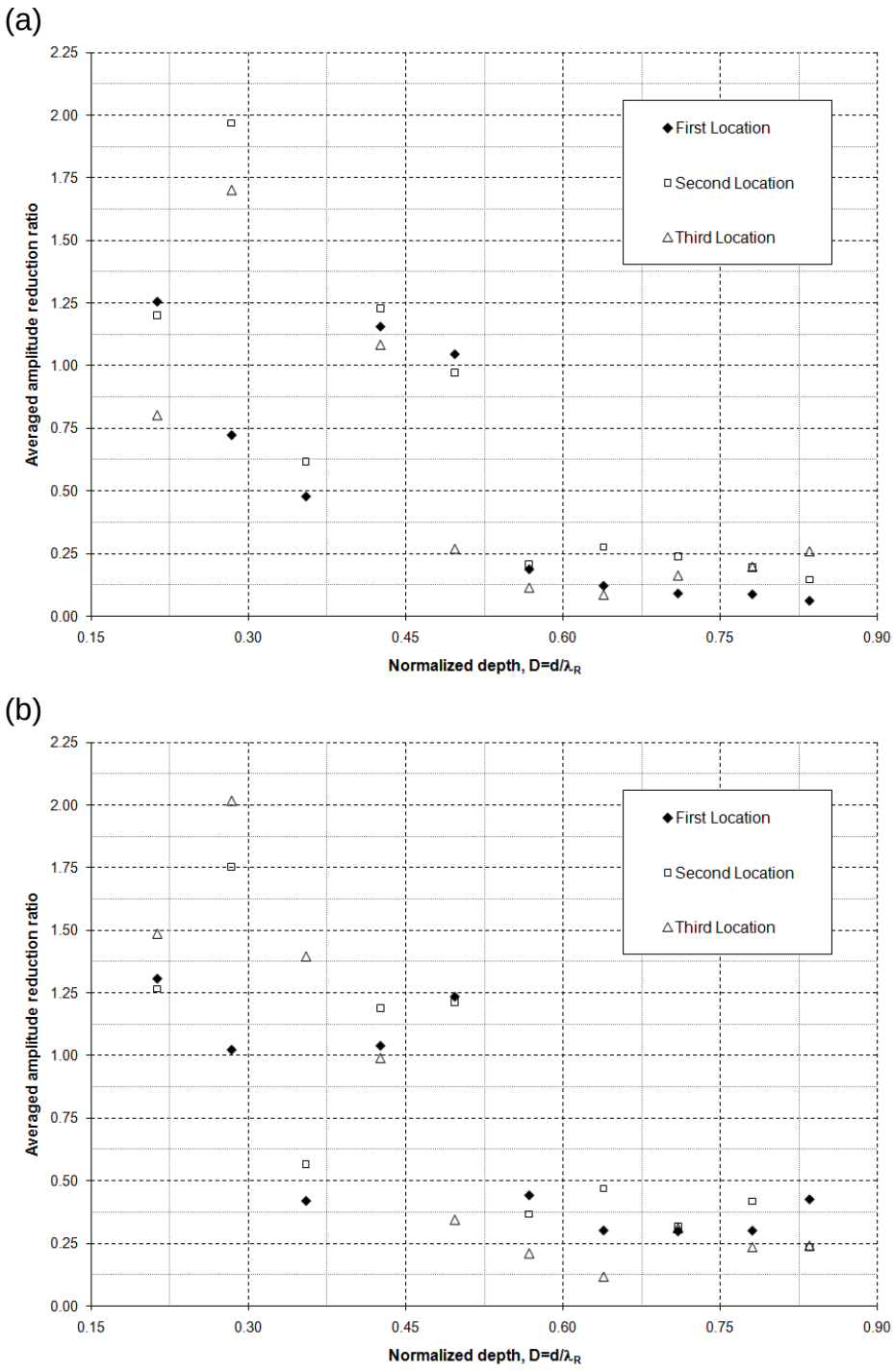

Figure 4- 19: Influence of the normalized depth for barrier placed at different locations (a) open trench, (b) in-filled geofoam trench

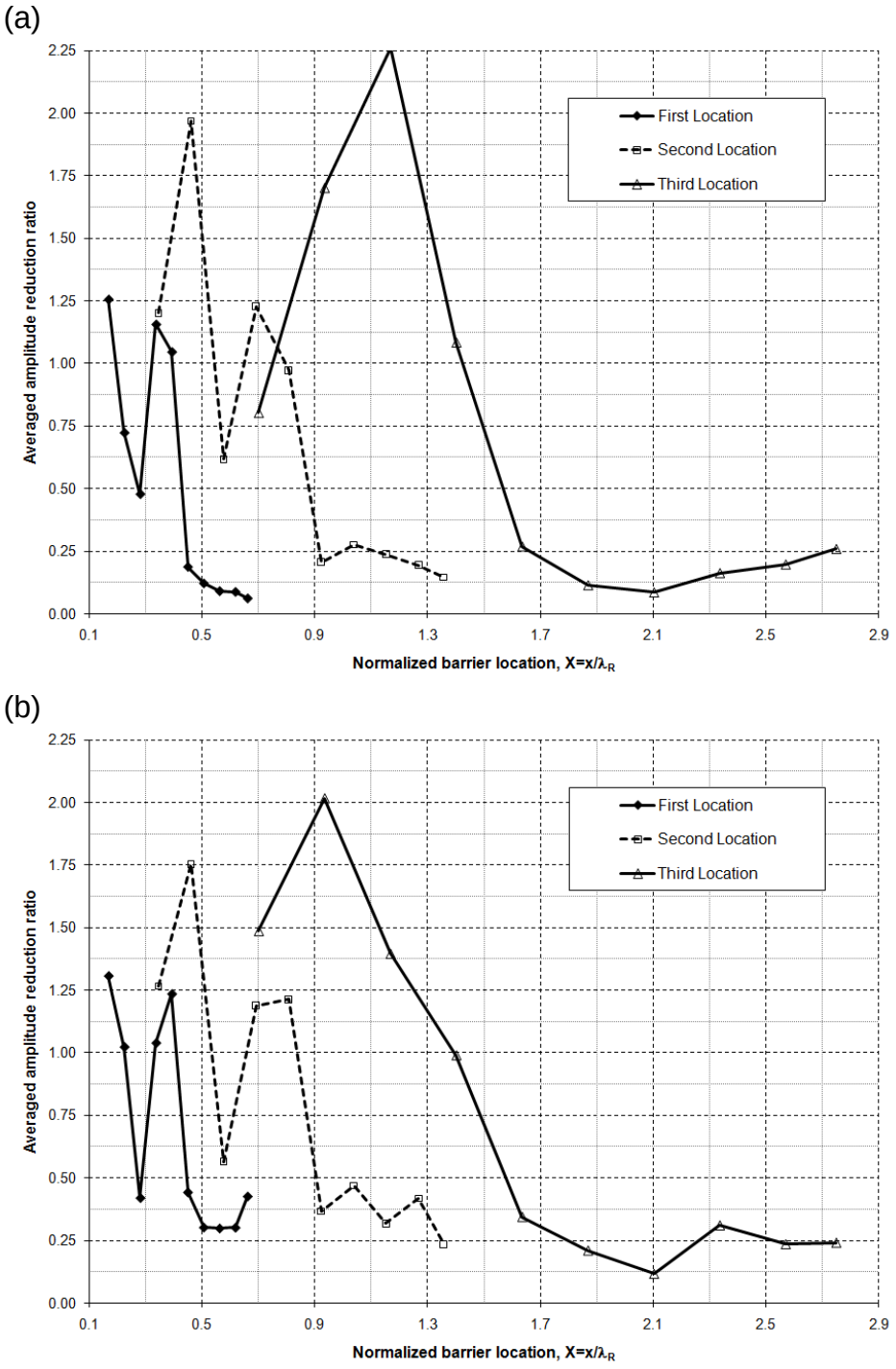

Figure 4- 20: Influence of the normalized distance for barriers placed at different locations
(a) open trench, (b) in-filled geofoam trench

The laboratory model test results of Haupt (1981) and the empirical formula derived by Ahmad and Al-Hussaini (1991) are compared in Table 4-3 against the present experimental results. The present experimental results are lower of about half of the published results. That is probably because of the true nature of full scale experiment in which a real wave propagation problem can be simulated taking into consideration a real soil conditions in terms of soil non-homogeneity and layering as well as the applied frequencies are the same as what soil will experience in practice. Besides, the difference in defining $\overline{A_r}$ could be another source of having some discrepancy even though its influence will be minor. However, the results follow the same general trend which is as the trench normalized depth increased, a better screening efficiency is achieved. In terms of optimum normalized depth, the recommended optimum normalized depth in the study agrees with the minimum normalized depth recommended by Woods (1968) D=0.6 for the case of active isolation to achieve a remarkable level of screening.

Table 4- 3: Comparison of the present experimental results with published results

Barrier dimensionless depth $D=d/\lambda_R$	Amplitude reduction ratio						
	Haupt (1981)		Empirical formula, Ahmad and Al-Hussaini (1991)	Present experiment			
	$\overline{A_r}$, values	$\overline{A_r}$, average	$\overline{A_r}$	$\overline{A_r}$, X_1	$\overline{A_r}$, X_2	$\overline{A_r}$, X_3	$\overline{A_r}$, average
0.57	0.34, 0.41	0.375	0.305	0.187	0.114	0.206	0.169
0.71	0.27, 0.30, 0.40	0.323	0.241	0.090	0.162	0.238	0.163
0.84	0.19,0.28,0.30,0.37	0.285	0.202	0.061	0.259	0.146	0.155

4.6 FINITE ELEMENT MODELS

2D and 3D finite element models were developed utilizing the finite element package, ABAQUS (2007) following the same methodology adopted in Chapter 3 in terms of choosing the finite elements and analysis type. The soil was modeled as a homogeneous, isotropic, layered soil profile. As aforementioned in chapter four, the soil profile was evaluated by conducting MASW and based on previously conducted SCPT at testing site. The bedrock was assumed to be at 30.0m below the ground surface, Figure 4-21. The adopted soil shear wave profile is shown in Figure 4-2. The soil density varies between 1812.5 and 1955.3kg/m^3, Poisson's ratio of 0.4, and Rayleigh damping of about 5%, which is defined by mass and stiffness coefficients calculated according to the applied exciting frequency. The geofoam material used in this verification is a two-component Polyurethane lightweight material supplied by URETEK Canada. The geofoam material has a density of 61kg/m^3 when it is installed in the trench under no pressure, i.e., free to expand. The dynamic properties of geofoam were evaluated using the Bender Elements and Resonant Column tests and were found to be: shear wave velocity of 312 m/sec, and Poisson's ratio close to zero.

For modelling purposes, the footing carrying the dynamic load was eliminated as it did not practically affect the vibration results, Kattis *et al.* (1999). Therefore, the source of disturbance was modeled as a vertical harmonic dynamic load represented by a sinusoidal function. The load was applied at a distance of 2.5, 5.0 and 10.0m from the center of the barrier (first, second and third location, respectively) and pointed directly on the ground surface. Based on the symmetrical nature of the considered 3D test configuration, a reduced half model was adopted which means only half of the trench

wall was considered, Figure 4-22. Similarly, a reduced half model was utilized in the case of the 2D model, Figure 4-23. Thus, symmetry boundary conditions were applied by restraining the displacement in the perpendicular direction to the symmetry surfaces. For the 2D model the axis of symmetry was placed across the point of load application. The analysis has been extended until the conditions of steady state response conditions were reached.

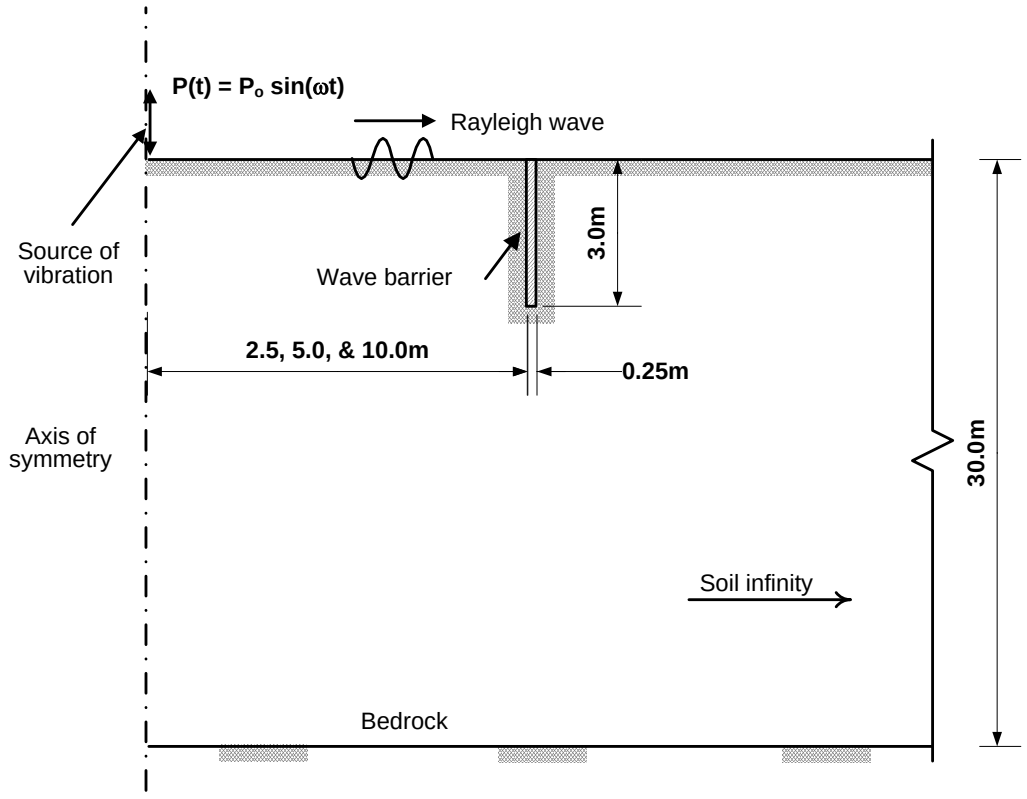

Figure 4- 21: Typical schematic showing the adopted dimensions for the 2D model

For every frequency, a time history of only 0.5 second of vertical steady state response was considered with a 0.5 millisecond sample interval, which results in collecting 1000 data points. The amplitude reduction ratio, A_r, at the nodes where

geophones were located in the experimental program, can be obtained by normalizing the post-trench installation maximum vertical response amplitude, $(A_r)_{After}$, by the maximum vertical response amplitude before trench installation, $(A_r)_{Before}$, measured on the ground surface using Equation 4-1.

4.7 2D VERSUS 3D MODEL

The adequacy of using the 2D instead of the 3D finite element model was assessed by solving a problem of vibration isolation using in-filled geofoam trench barrier. Therefore, an in-filled geofoam trench of depth $d=1.0\lambda_R$, and width w=0.25m located at a distance $x=1.0\lambda_R$ from the source of vibration in a homogeneous, isotropic, elastic half-space soil was considered. The material properties of the soil medium were in accordance to Kattis *et al*. (1999): shear wave velocity V_s=272 m/sec, Poisson's ratio ν=0.25, Rayleigh wave velocity V_R=250 m/sec, Rayleigh wave length λ_R =5.0 m, unit weight γ=17.5 kN/m^3 and Rayleigh damping ξ=5%. The source of vibration is modeled as a vertical harmonic load of magnitude of 1.0 kN and frequency of 50Hz.

As documented by Al-Hussaini and Ahmad (2000), it is expected to have this discrepancy because of the 3D nature of the field tests in which the waves were generated by a circular source. They concluded that a 3D analysis is more appropriate. However, Figure 4-24 illustrates that the results obtained from 2D and 3D finite element models are in excellent agreement. Thus, it is concluded that the 2D finite element model can be used, with confidence, in modeling the field experimental tests as well as in conducting a parametric study.

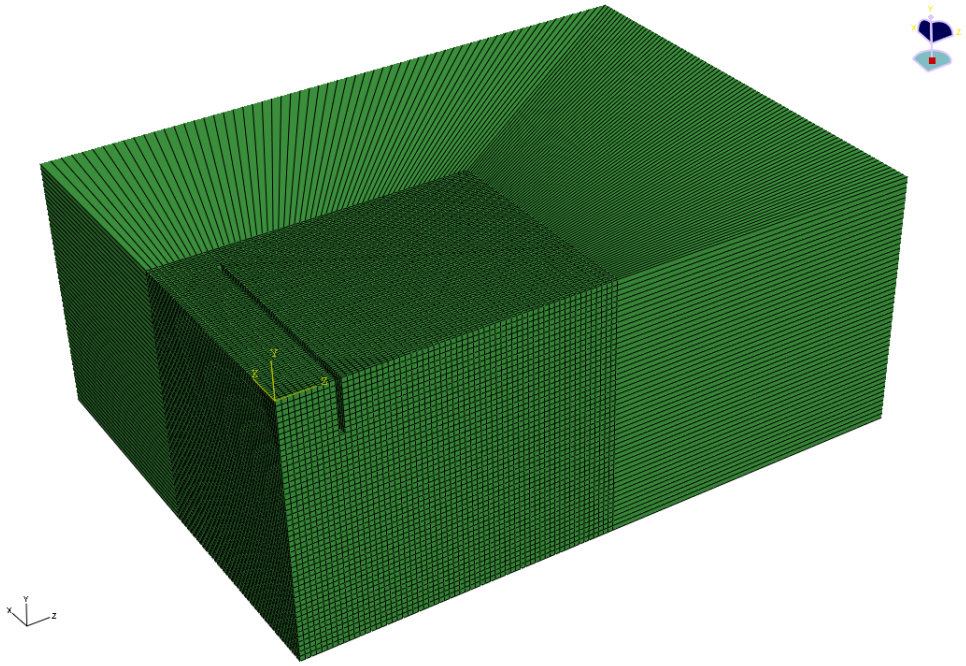

Figure 4- 22: 3D finite element model mesh for the case of open trench

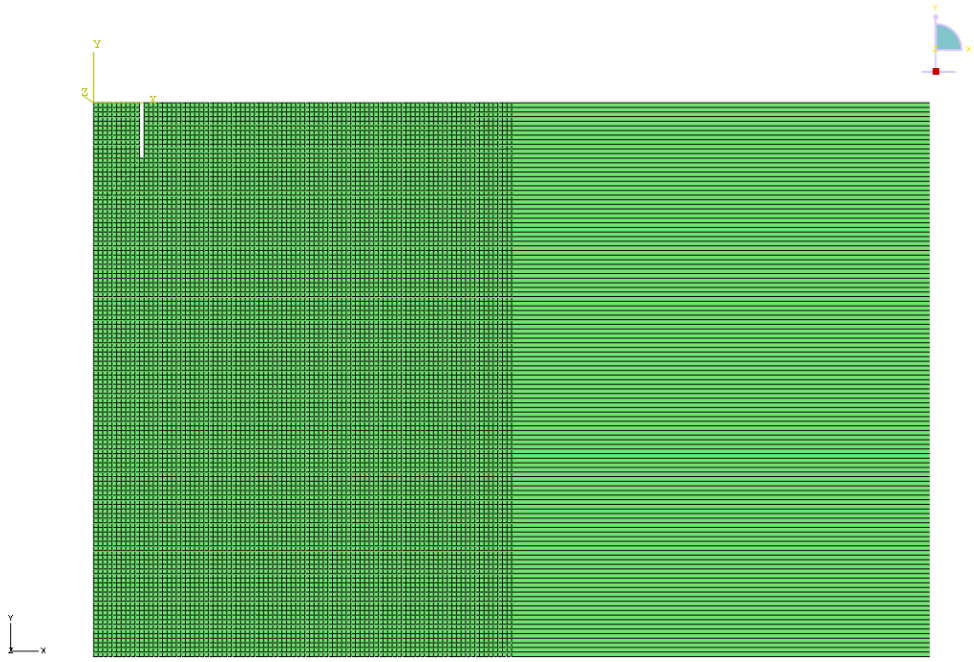

Figure 4- 23: 2D finite element model mesh for the case of open trench

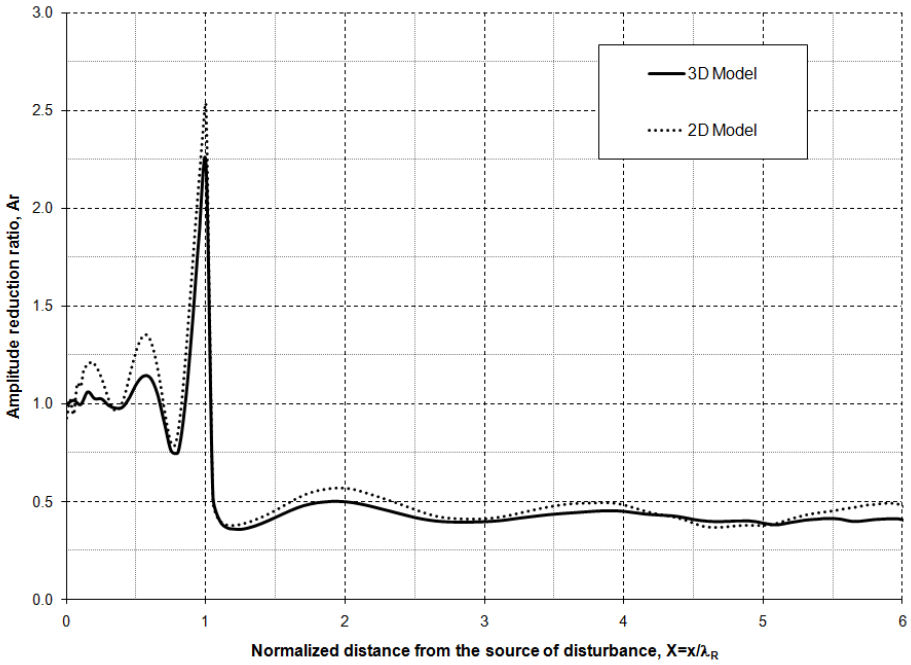

Figure 4- 24: 2D verses 3D finite element model, in-filled geofoam trench (w=0.25m, D=1.0, X=1.0)

Boundary element (BEM) studies were conducted by Beskos (1986) and Al-Hussaini (1992) for passive isolation cases demonstrated a certain amount of amplitude magnification ($A_r > 1.0$) in the incident zone. Both studies modelled open trench barriers considering plane strain conditions similar to the conditions adopted in this study: Beskos (1986) calculated a maximum A_r value of between 1.5 and 2.0, while Al-Hussaini (1992) obtained a maximum A_r value close to 2.0. It was observed that this behaviour would peak relatively close to the open barrier and have a pattern of peaks and values $0.5\lambda_R$ apart as can be noted from Figure 4-5-b. Similar amplitude magnification was also observed by Woods (1968) and Haupt (1981) with different values. This is due to reflected waves having multiple angles of incidence and reflection at the barrier interface

causing a complicated pattern of constructive and destructive interference in the incident zone.

The current study considers an in-filled geofoam trench barrier, and as explained in Chapter two, Section 2.2, a more complicated wave phenomena is expected to occur in the incident zone for the case of in-filled barrier than for an open trench barrier. However, slightly higher amplitude magnification values are observed. According to Figure 4-24, maximum A_r values of 2.25 and 2.5 are obtained from 3D and 2D finite element models, respectively.

The validity and accuracy of the results of 2D finite element model in comparison with a 3D one in simulating the field experimental tests was also assessed by modeling a sample case from experimental tests. The 3D finite element model was mainly developed because of the 3D nature of the experimental tests. Moreover, due to the high computational cost of the 3D model, it was used only for modeling open and in-filled trench barriers located at 2.5m from the source of disturbance (referred to as the source at first location). The same case was modeled using the 2D model, and the results were compared with those of the 3D finite element model. As it can be noted from Figures 4-25 and 4-26, the results obtained from the 2D finite element model agree favourably with those obtained from the 3D finite element model. Accordingly, it was concluded that the adopted 2D finite element model is adequate to predict the barrier protective efficiency. Hence, the 2D finite element model was adopted in modeling all the field experimental tests and later to make a comparison with those obtained experimentally.

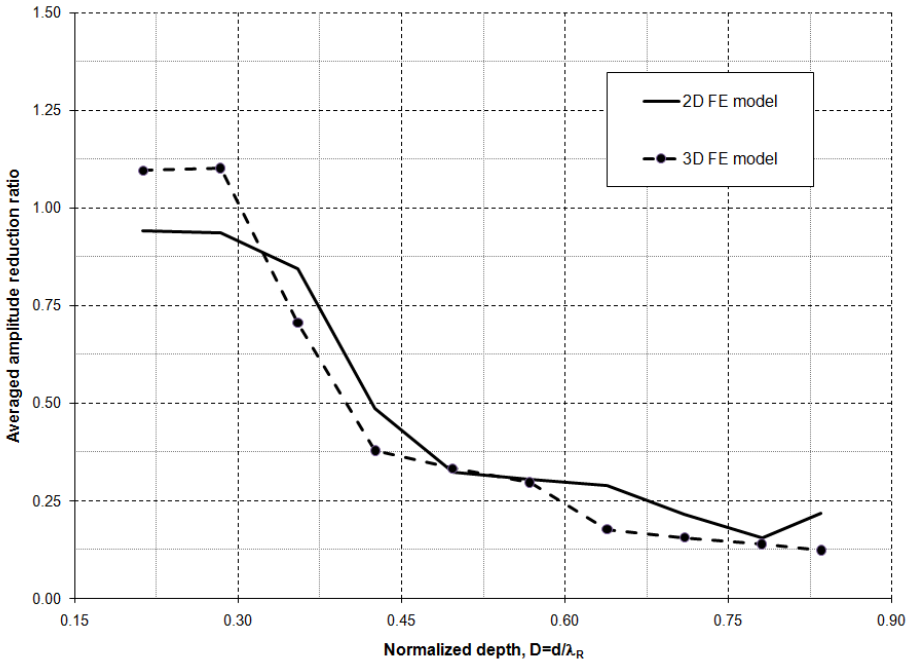

Figure 4- 25: 2D verses 3D FE model, open trench
(first location, x = 2.5m)

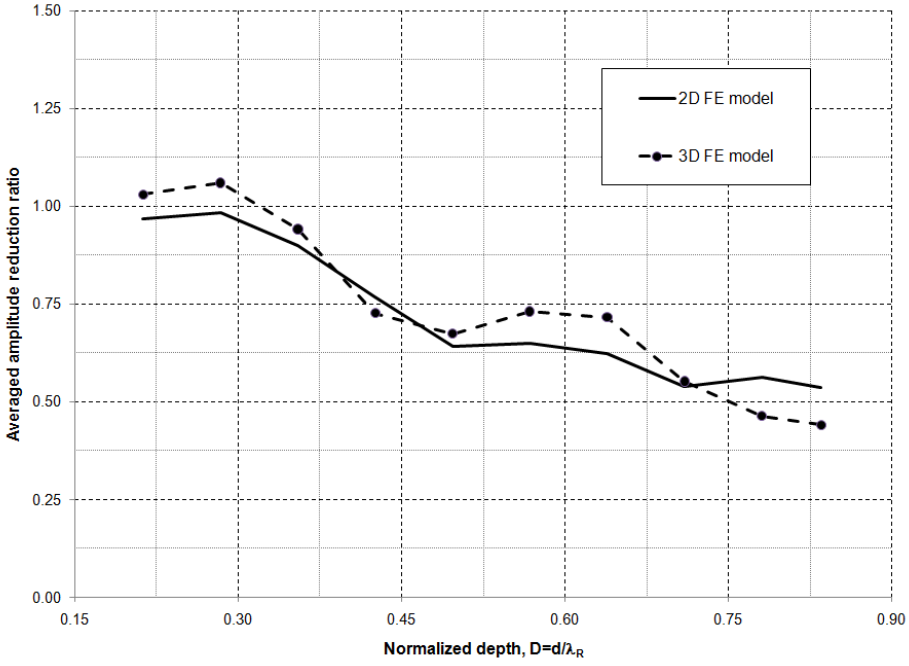

Figure 4- 26: 2D verses 3D FE model, in-filled geofoam trench
(first location, x = 2.5m)

4.8 EXPERIMENTAL VERIFICATION OF FINITE ELEMENT MODELS

The developed models were verified by comparing the results from the field and finite element model in terms of wave attenuation curves to ensure that the numerical model simulates the same field wave propagation. Figures 4-27 to 4-29 show the measured and calculated decay curves, in logarithmic scale, of the ground motion during the three testing stages for two exciting frequencies, 40Hz and 50Hz.

As it can be observed from Figures 4-27 to 4-29, the finite element model results follow the trend of the experimental results, but with slightly higher values at some points and lower values at others. This may be attributed to considering horizontal homogeneous soil layers in the finite element model, which may or may not be the case in the field. Another source for the discrepancy between the experimental and the finite element model results is that large cobbles were observed while digging the trench, which induce local soil inhomogeneities. Nonetheless, it can be concluded that the finite element model can adequately represent the vibration scattering problem for the case of open and in-filled geofoam trench barriers. Thus, the model can be reliably used to extrapolate the results and conduct an extensive parametric study to better understand the in-filled geofoam trench barrier behaviour.

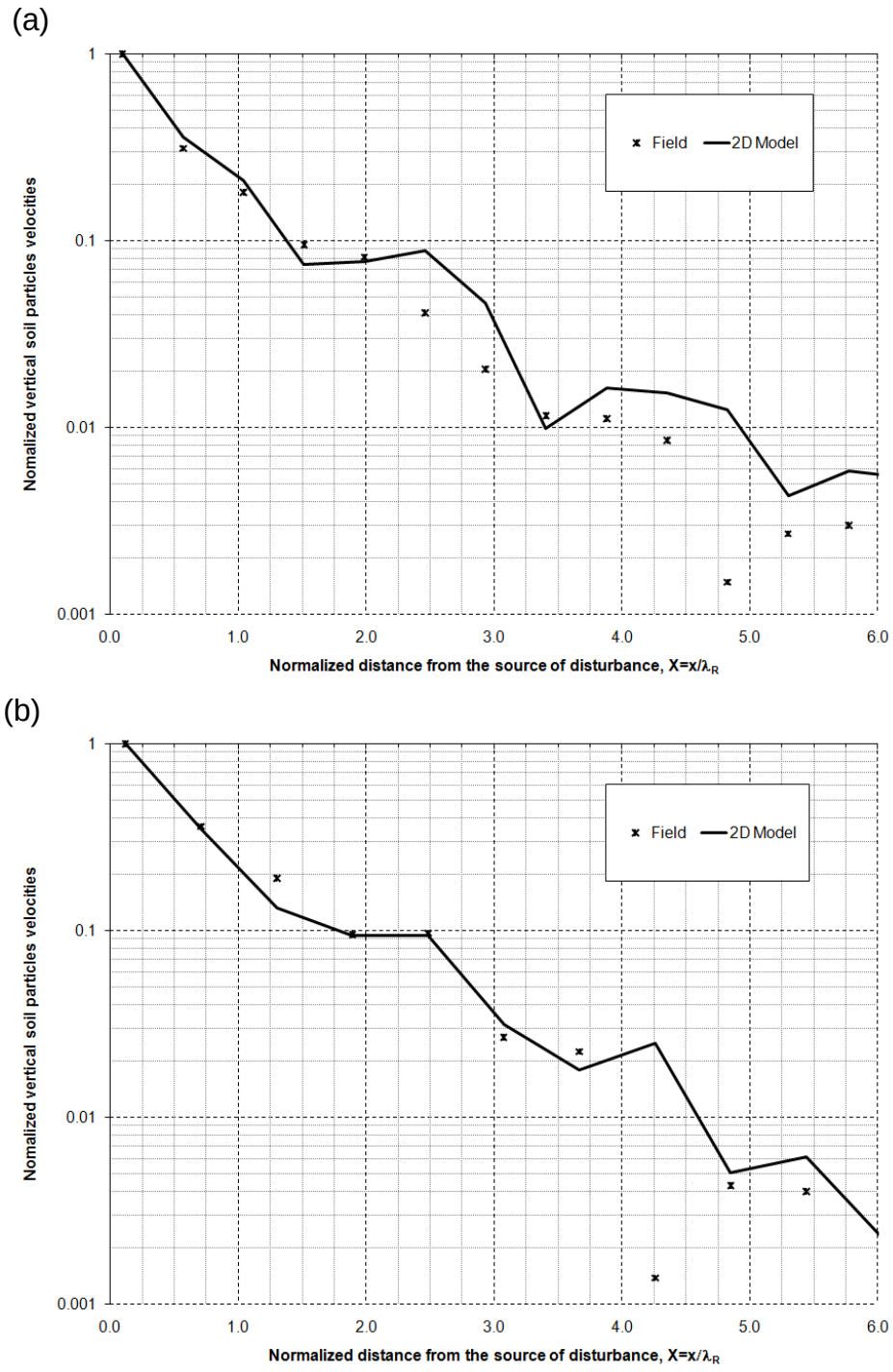

Figure 4- 27: Comparison of field and finite element model attenuation curves (1st location, no trench)
(a) 40Hz, (b) 50Hz

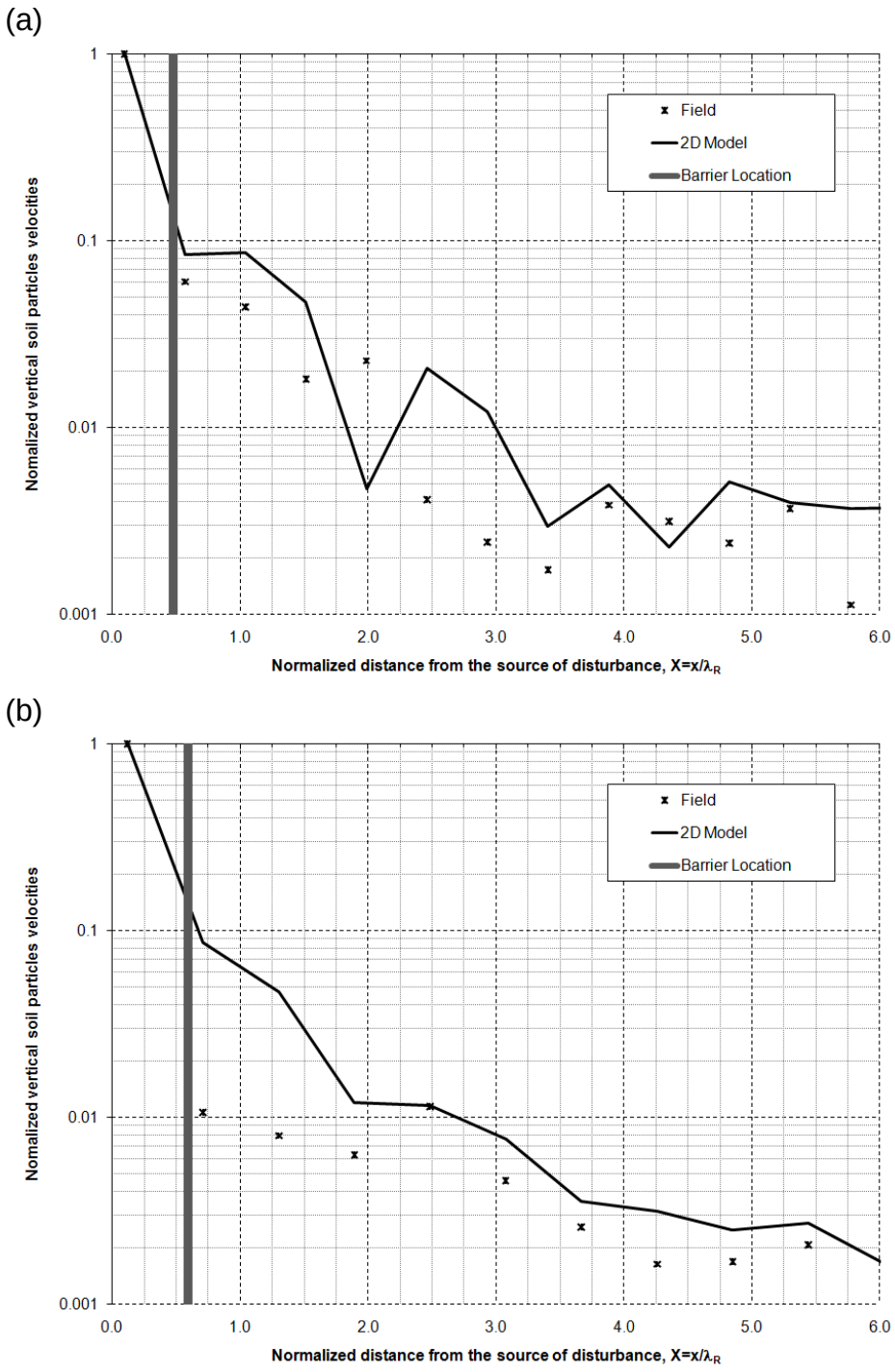

Figure 4- 28: Comparison of field and finite element model attenuation curves (1st location, open trench)
(a) 40Hz, (b) 50Hz

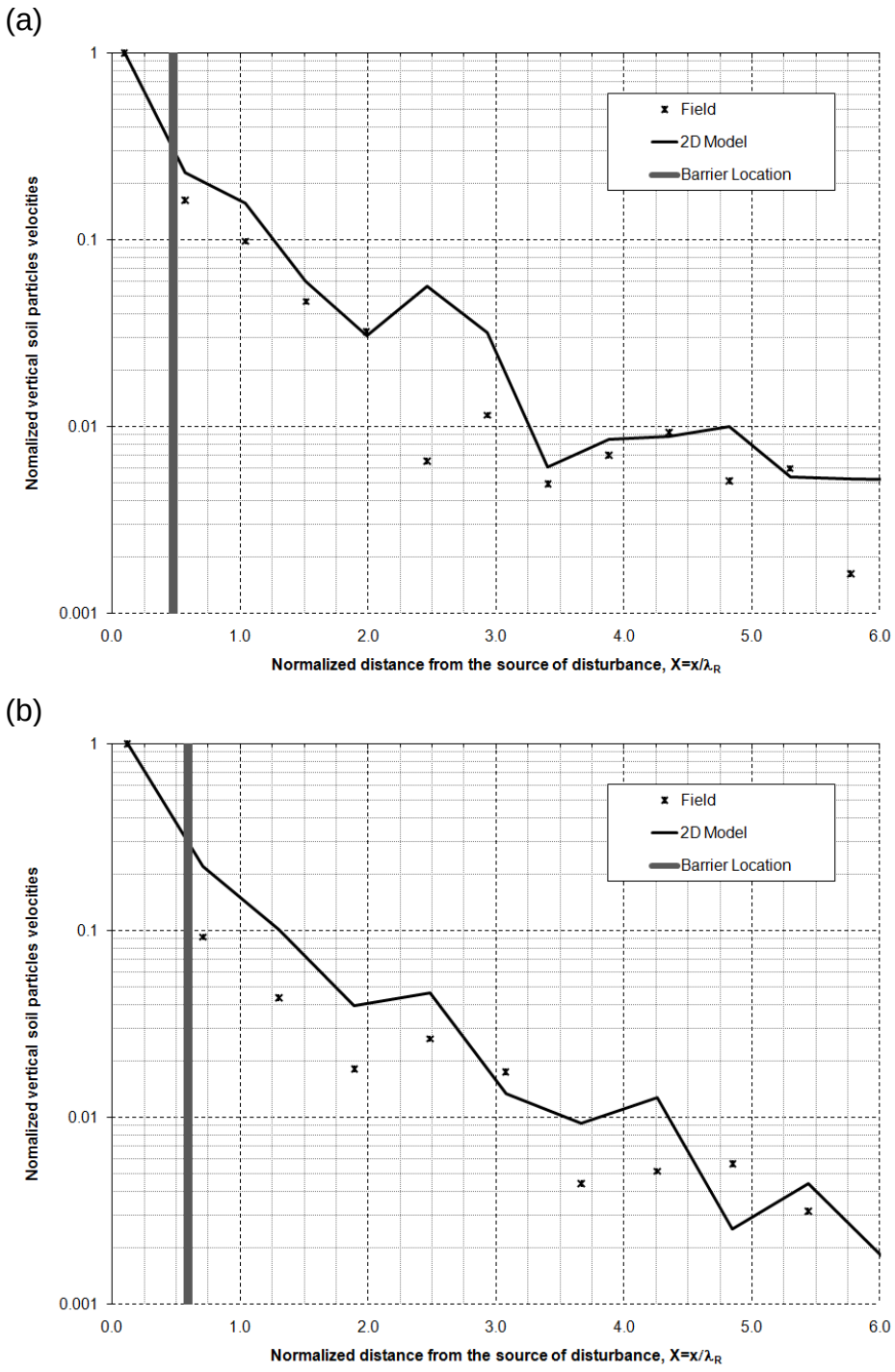

Figure 4- 29: Comparison of field and finite element model attenuation curves (1st location, in-filled geofoam trench)
(a) 40Hz, (b) 50Hz

4.9 RESULTS ANALYSIS AND DISCUSSION

Figures 4-30 to 4-32 represent the averaged amplitude reduction ratio for both open and in-filled geofaom trench barriers with respect to the barrier normalized depth obtained from field measurements and finite element models for the adopted three locations for the oscillator. Even though finite element model results follow the trend of field results, it is clear that finite element model results are slightly higher than those obtained from the measured values in the field. In other words, the averaged amplitude reduction ratios obtained by the finite element model fall in the conservative side, i.e., underestimating the protective efficiencies compared with the field results.

By considering only the results obtained from the exciting frequencies greater than or equal to 40Hz, which are equivalent to normalized depth greater than or equal to 0.57, the following observations can be made. For the case of an open trench barrier at a distance of 2.5m from the source (first location), the average system effectiveness is 89.08% and 76.35% for the field and finite element model results, respectively. For the case of in-filled geofaom trench barrier at the first location, the average system effectiveness is 64.53% and 41.79% for the field and finite element model results, respectively. The discrepancy between the results of finite element model and field tests are 14.29% and 35.24% for open and in-filled geofaom trench barriers, respectively. As it can be noted, the finite element model is more efficient in predicating the open trench barrier protective effectiveness rather than the case of in-filled geofaom trench barrier. In addition to the reasons explained in the previous section, the reason of having a discrepancy of about 35.19% for the case of in-filled geofoam trench barrier can be attributed to the fact that a full bond between the geofaom wall and soil was assumed in

the finite element model, which may not be the case in the real experiment. Generally speaking, finite element model results fall in the conservative side by underestimating the protective effectiveness of the wave barrier system. Hence, it can be concluded that the predicted protective effectiveness provided by the finite element model is in good agreement with that obtained from the field measurements.

Tables 4-4 and 4-5 summarize the average protective efficiencies (Eff_A) by considering only the efficiencies obtained by exciting frequencies greater than or equal to 40Hz which are equivalent to $D \geq 0.57$ for open trench and in-filled geofoam trench barriers.

Table 4- 4: Open trench barrier protective efficiency

Trench location	1st location	2nd location	3rd location
Field (%)	89.08	78.82	83.68
2D Model (%)	76.35	78.08	69.69
Difference (%)	14.29	0.94	16.72

Table 4- 5: In-filled geofoam trench barrier protective efficiency

Trench location	1st location	2nd location	3rd location
Field (%)	64.53	63.92	77.73
2D Model (%)	41.79	45.11	45.93
Difference (%)	35.24	29.44	40.91

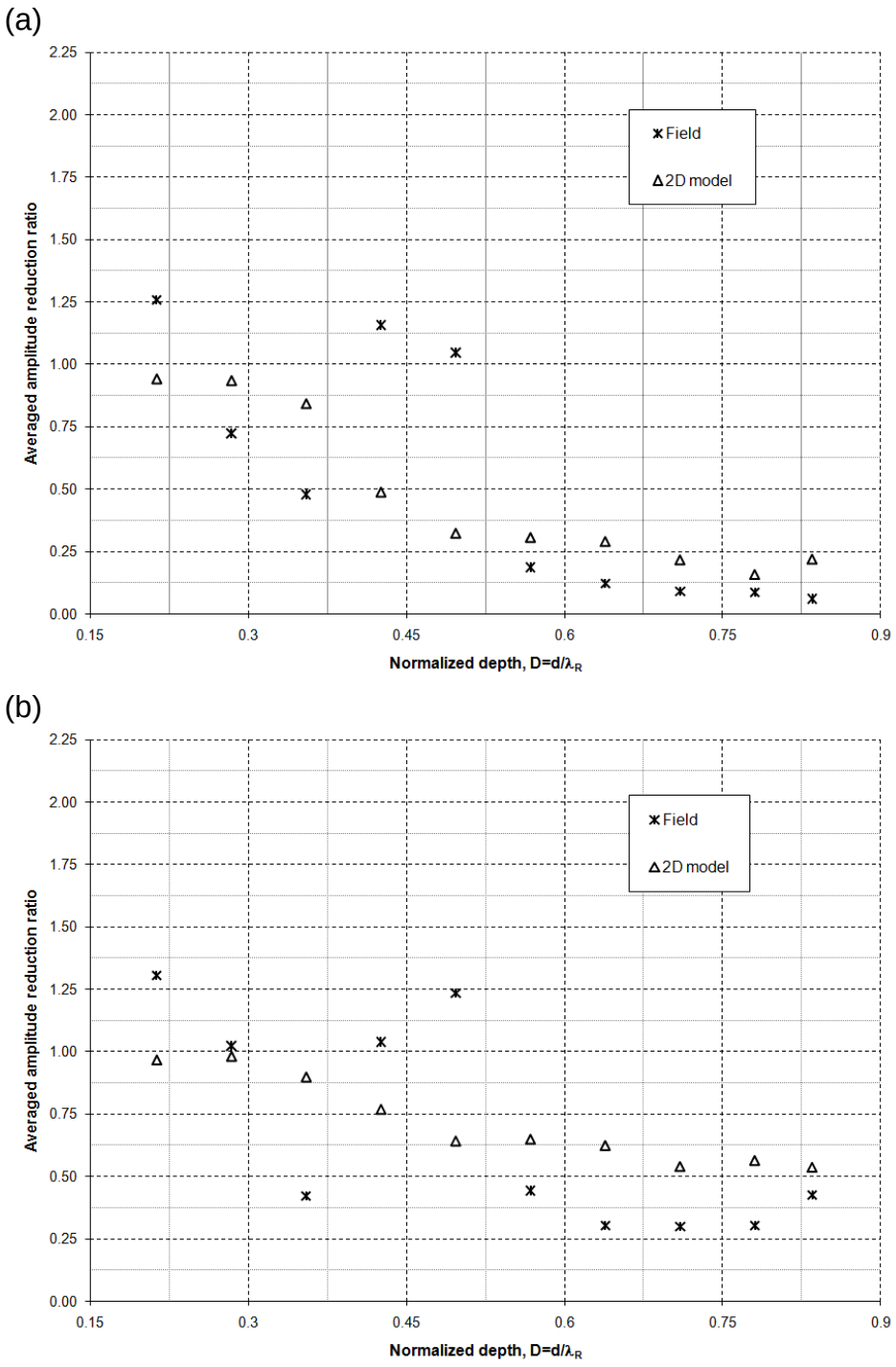

Figure 4- 30: Comparison of field and finite element model results (1st location, x=2.5m) (a) open trench, (b) in-filled geofoam trench

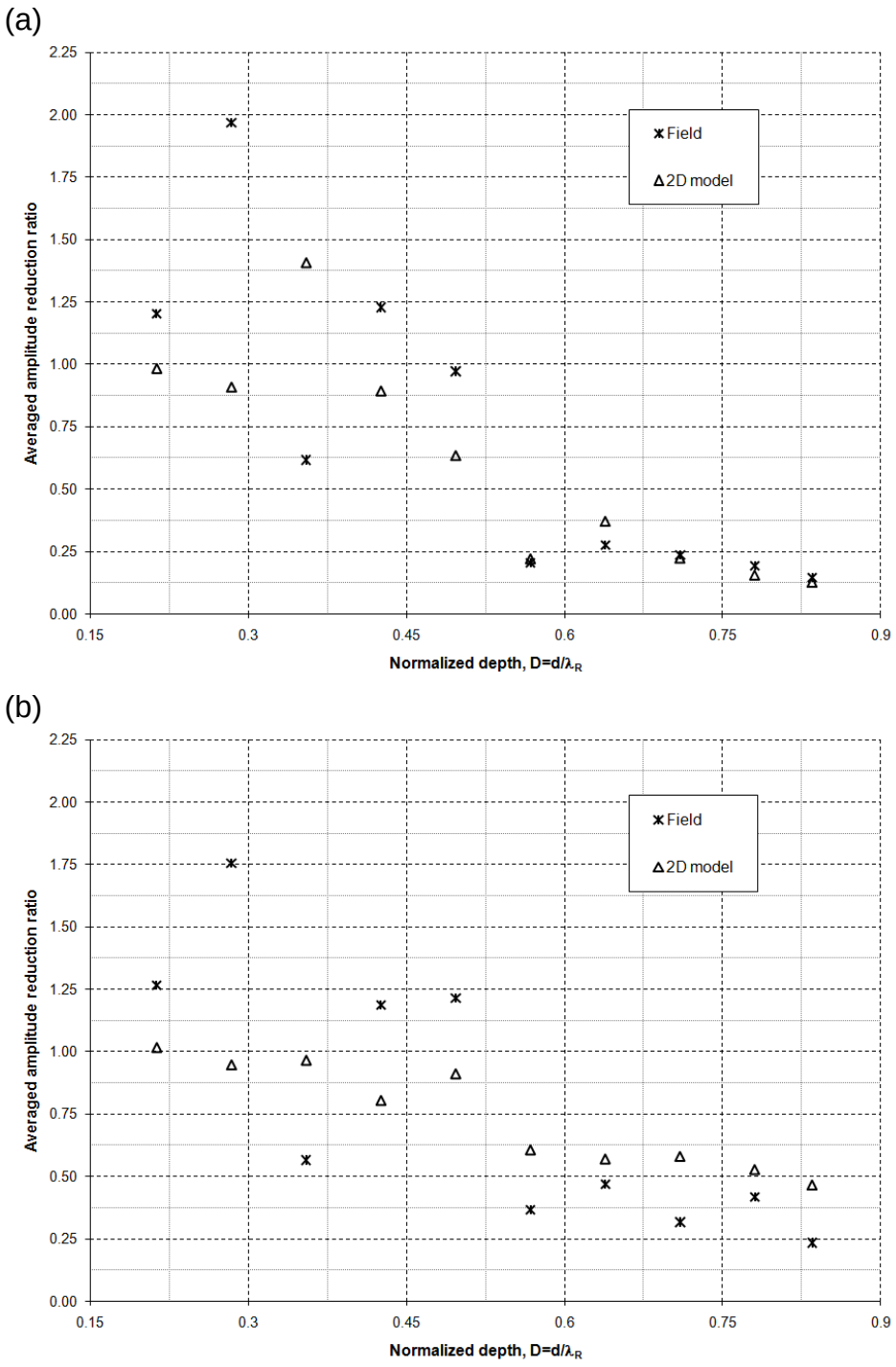

Figure 4- 31: Comparison of field and finite element model results (2nd location, x=5.0m) (a) open trench, (b) in-filled geofoam trench

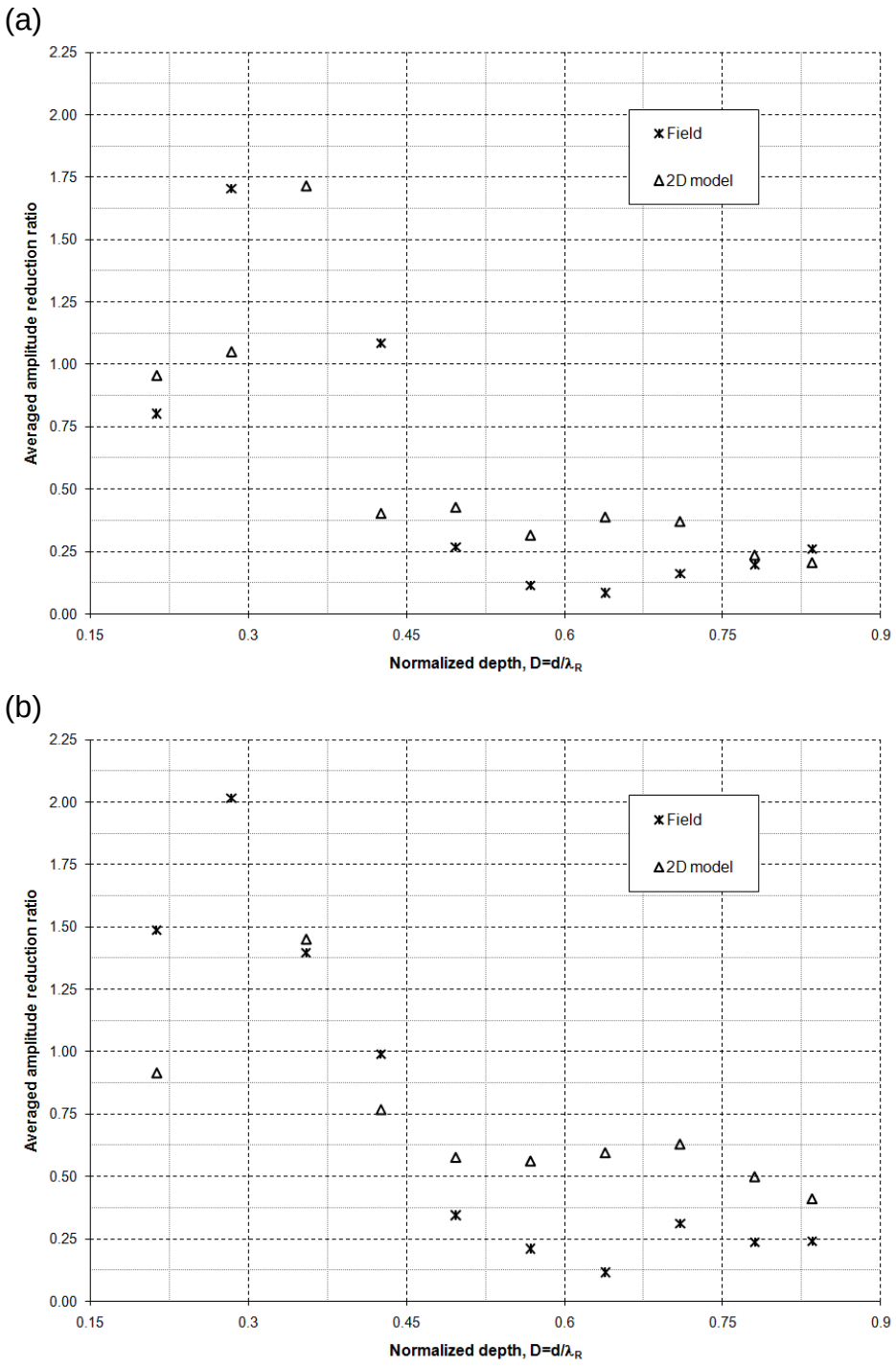

Figure 4- 32: Comparison of field and finite element model results (3rd location, x=10m) (a) open trench, (b) in-filled geofoam trench

4.10 SUMMARY AND CONCLUDING REMARKS

A full scale experimental test program was carried out to investigate the protective effectiveness of open and in-filled geofoam trenches as wave barriers to scatter the steady state vibration induced by machine foundations. In order to simulate the machine foundations vibration, a mechanical oscillator was used. The wave barriers protective effectiveness was evaluated based on the achieved reduction in soil particle velocities through a parametric study by changing the exciting frequency and the location of the wave barriers. Considering the same experimental work conditions, 2D and 3D finite element models have been developed to simulate, numerically, the open and in-filled trench barriers behaviour in scattering surface steady state waves. The field experimental results were used to calibrate the developed finite element models. The validity and accuracy of the 2D finite element model results has been assessed by comparing with those obtained by the 3D finite element model. Based on the obtained results and their analysis, the following conclusions can be made:

1. The field results show that the in-filled geofoam trench barrier can be considered as a practical alternative for wave scattering; and the observed protective effectiveness was up to 68% or higher.

2. The wave barriers protective effectiveness is influenced by the barriers normalized depth and the barrier's proximity to the source of disturbance. The barriers are found to be generally more effective when $D \geq 0.60$ (i.e. an optimum barrier normalized depth) for both open and in-filled geofoam trench barriers. For x/d of about 0.79, 1.63 and 3.29, the normalized distance X of 0.45, 0.92 and 1.64 are the

optimum barrier locations corresponding to the optimum normalized depth D of about 0.60.

3. The results show that a deeper trench is required as the ratio x/d increases to achieve the same improvement in the system's effectiveness. As the ratio x/d increased, the open trench barrier effectiveness decreased while no significant change was observed in the case of in-filled geofoam trench barrier effectiveness.

4. The experimental observations made in this study are valid for the soil profile considered in this study.

5. The results obtained from 2D and 3D finite element models are in excellent agreement. Thus, 2D finite element model can be used instead of 3D finite element model, with confidence, in modeling the field experimental tests as well as in conducting a parametric study.

6. Wave attenuation curves obtained numerically utilizing the 2D finite element model follow the same trend of the experimental measurements and they are in good agreement, but with slightly higher values at some points and lower values at others.

7. The results obtained from the finite element models are comparable to those obtained experimentally with a difference of about 10.65% and 35.19% for open and in-filled geofoam trench barriers, respectively. The discrepancy can be attributed to the soil non-homogeny as well as imperfect bonding between the soil and the geofoam wall.

8. The developed finite element models can be used to extrapolate the results and conduct a parametric study on the in-filled geofoam trench barrier performance with different dimensions and in different soil profiles.

CHAPTER FIVE

PARAMETRIC STUDY AND DEVELEOPMENT OF DESIGN MODEL

This chapter presents the results of the comprehensive parametric study that examined the influence of various geometrical and material parameters of in-filled geofoam trenches on their protective effectiveness as wave barriers. The key parameters considered include: barrier geometric dimensions, location, and soil dynamic properties. A 2D finite element model, which was verified using experimental results as shown in Chapter 4, has been employed to conduct the parametric study. The results are analyzed, interpreted and some guidelines regarding the importance of the investigated parameters are outlined. The key geometrical and material parameters that govern the performance have been identified and a design model using multiple linear regression analysis has been developed for estimating the vibration screening effectiveness of in-filled geofoam trench barriers.

5.1 METHODOLOGY

The 2D finite element model was employed to conduct an extensive parametric study in order to better understand the behaviour of in-filled geofoam trench barriers with different dimensions, locations and different soil conditions. The accuracy of the 2D finite element plane-strain model was verified by comparing the obtained results with those obtained from a 3D finite element model, and the experimental results obtained in this research

program. A staged mesh refinement has been carried out to obtain an optimized meshing configuration.

The key parameters considered in this parametric study are: the barrier depth; the distance between the barrier and the source of disturbance; and the dynamic soil properties including shear wave velocity, density, Poisson's ratio, and material damping ratio. All geometric parameters are normalized by the Rayleigh wavelength, λ_R. The numerical model results are analyzed and interpreted to provide recommendations for design purposes. A typical schematic of the considered barrier geometric parameters are shown in Figure 5-1.

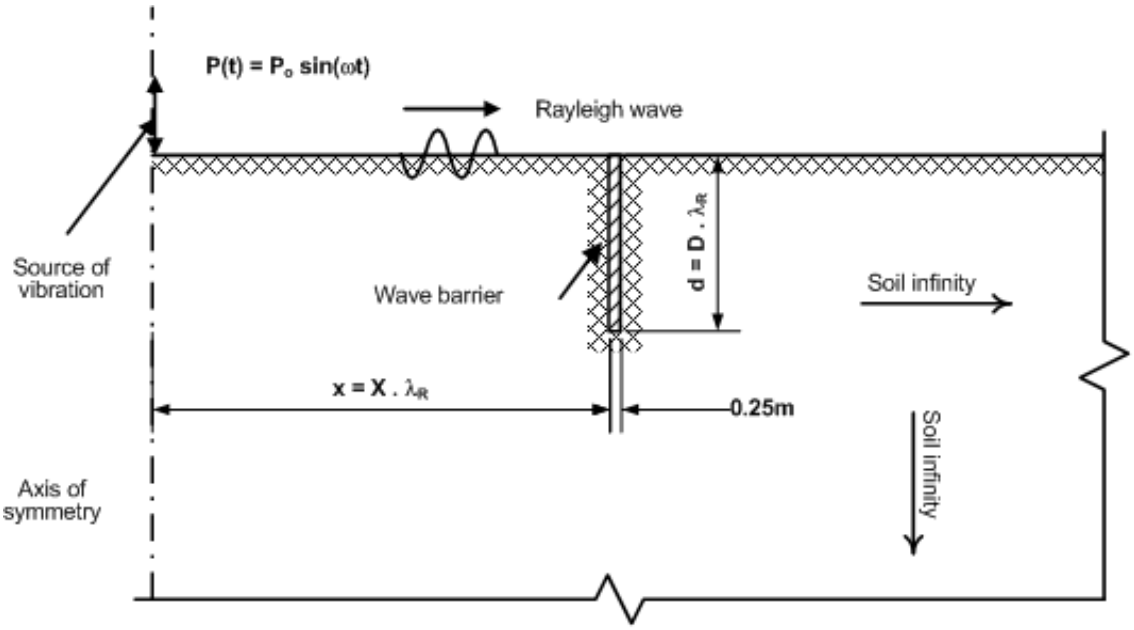

Figure 5- 1: Typical schematic presentation of the geometric parameters

5.2 PARAMETRIC STUDY AND RESULTS

The results of the parametric study are presented in the form of averaged amplitude reduction ratio, $\overline{A_r}$. As described in Section 4.4.2, Chapter 4, the amplitude reduction ratio, A_r, along the monitoring path is evaluated using Equation 4-1. The averaged amplitude reduction ratio, $\overline{A_r}$, over a distance of interest ($x=5\lambda_R$) measured behind the wave barrier is calculated using Equation 4-2. The system efficiency is then calculated using Equation 4-3.

5.2.1 Influence of Barrier Normalized Depth and Location from Source of Disturbance

The in-filled geofoam trench wall depth and its proximity to the vibration source have been varied independently. The normalized depth D is varied from 0.4 to 2.0 and the normalized distance X between the source of disturbance and barrier is varied from 0.3 to 4.0. It was reported by many researchers that the screening behaviour of an in-filled trench barrier is dependent upon the barrier's normalized width W in terms of the barrier absorption of energy and wave refraction from the bottom of the barrier (Ahmad and Al-Hussaini, 1991; Haupt, 1978; Fuyuki and Matsumoto, 1980; and others). However, the influence of normalized width W will not be considered in this parametric study as it was recommended in Chapter 4 that the practical width to construct such type of in-filled geofoam trench barrier system is 0.25 m. This width was found to provide excellent performance in scattering the induced ground vibration.

Figures 5-2 and 5-3 illustrate a 3D view and contours plot of the averaged amplitude reduction ratio $\overline{A_r}$ variation over the considered ranges for D and X values for an in-filled geofoam trench barrier installed in an elastic homogeneous half-space soil, which has the following dynamic properties: shear wave velocity V_s=250 m/sec, Poisson's ratio of ν=0.3, unit weight γ=19.5 kN/m^3, and Rayleigh damping ξ=5%. The screening performance of the in-filled geofoam trench barrier is found to be highly dependent on the normalized distance between the source and barrier, X. This is clearly depicted in Figures 5-2 to 5-4. Figures 5-2 and 5-3 also demonstrate the importance of the coupled influence of changing D and X on the barrier's performance.

Figures 5-4 and 5-5 provide a 2D presentation of the coupled influence of D and X (at specific values for D and X) on the averaged amplitude reduction ratio $\overline{A_r}$ for the same in-filled geofoam trench barrier considered above. It can be seen that changing the normalized distance between the barrier and the source of disturbance, X, from 0.3 to 1.5 has a significant influence on the barrier performance in a complex manner with the effect of the normalized depth D. The complexity of the influence of X can be attributed to the complex nature of wave propagation particularly in the vicinity of the barrier, as explained in Section 2.2. Figure 5-4 shows that X appears to govern the barrier's protective effectiveness for X ranging from 0.4 to 1.5. For X>1.5, the effectiveness remains almost constant regardless of the normalized depth. For the considered configuration, an optimum screening effectiveness can be achieved when the barrier is placed at X=0.4 and 1.2 (averaged amplitude reduction ratio $\overline{A_r}$ is minimum). For

deeper depths (D ≥1.2), placing the barrier at any distance X can result in acceptable screening effectiveness.

Another important observation is that it is apparent from Figure 5-5 that increasing the normalized depth D beyond 1.2 does not provide any remarkable improvement for in-filled geofoam trench barriers. Hence, it may be conservatively assumed D = 1.2 as an optimum depth for geofoam trench barriers. It is also concluded that as the geofoam barrier's proximity to the source of disturbance increases, a deeper trench is required to achieve significant improvement in the system effectiveness.

5.2.2 Influence of Soil Shear Wave Velocity

The soil shear wave velocity, V_s, and density, $\rho = \gamma/g$, are the most important soil dynamic properties in wave propagation problems, which govern the amount of reflection, refraction and mode conversion when a wave is incident at the interface between the in-filled geofoam trench barrier and the soil medium (impedance difference). Therefore, the effect of V_s on the vibration screening effectiveness of an in-filled geofoam trench barrier is demonstrated in this section while the influence of soil density will be discussed in the subsequent section.

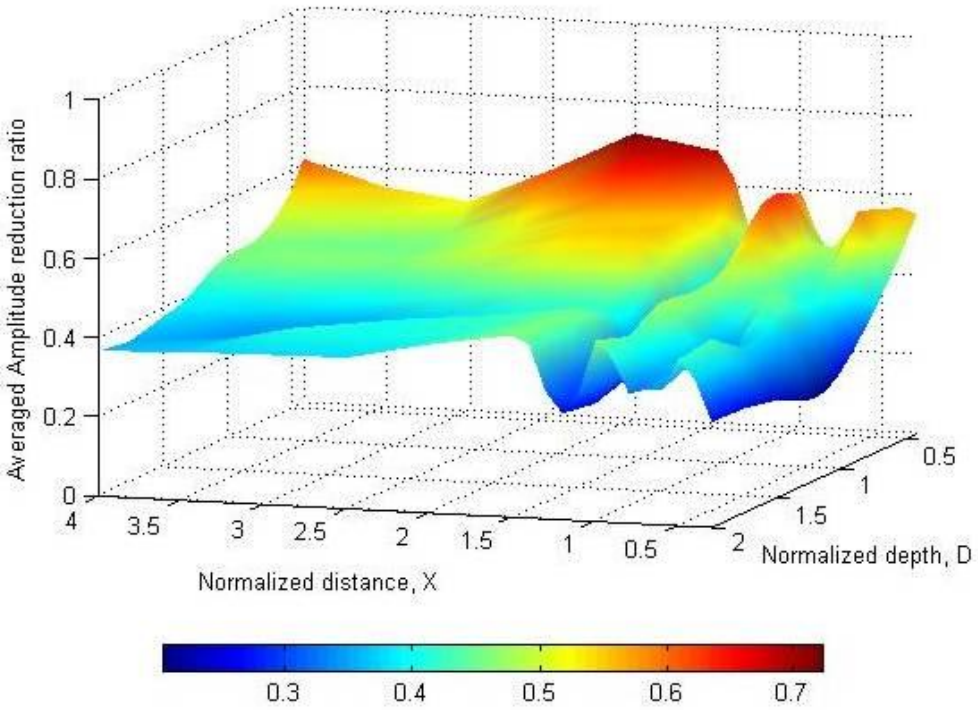

Figure 5- 2: 3D view of the averaged amplitude reduction ratio
(V_s=250 m/sec, ν=0.3, γ=19.5 kN/m^3, and ξ=5%.)

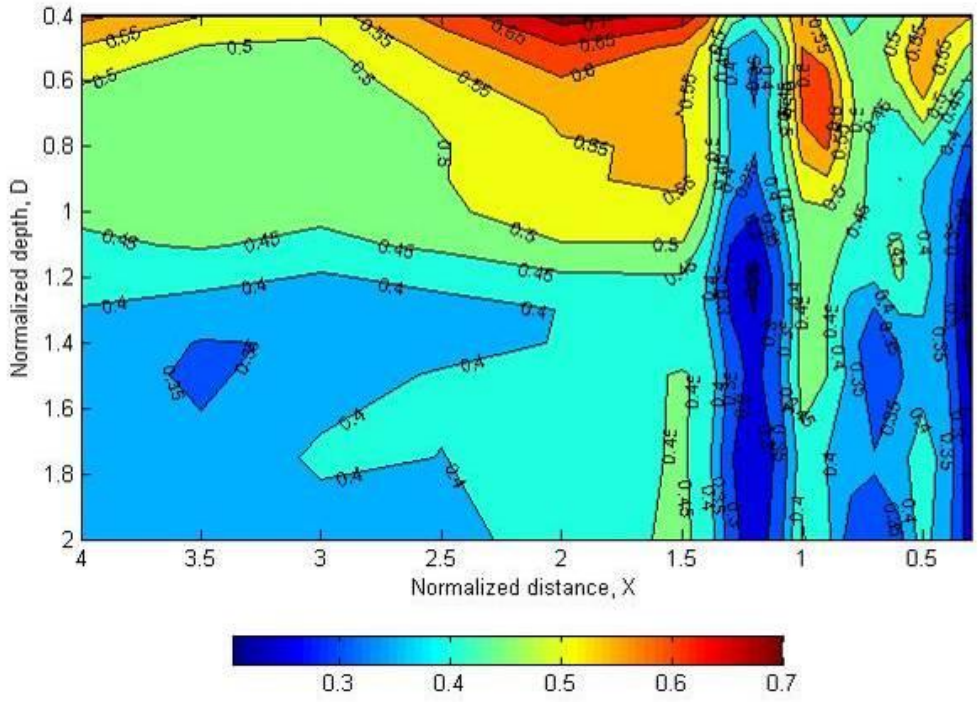

Figure 5- 3: Contour of the averaged amplitude reduction ratio
(V_s=250 m/sec, ν=0.3, γ=19.5 kN/m^3, and ξ=5%.)

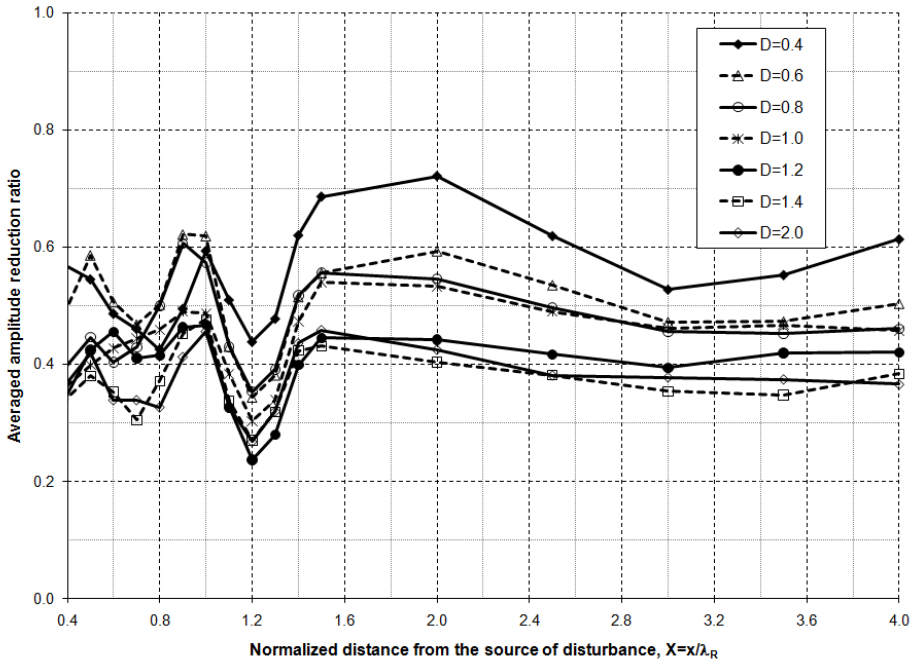

Figure 5- 4: Influence of normalized distance from the source of disturbance, X (V_s=250 m/sec, ν=0.3, γ=19.5 kN/m^3, and ξ=5%.)

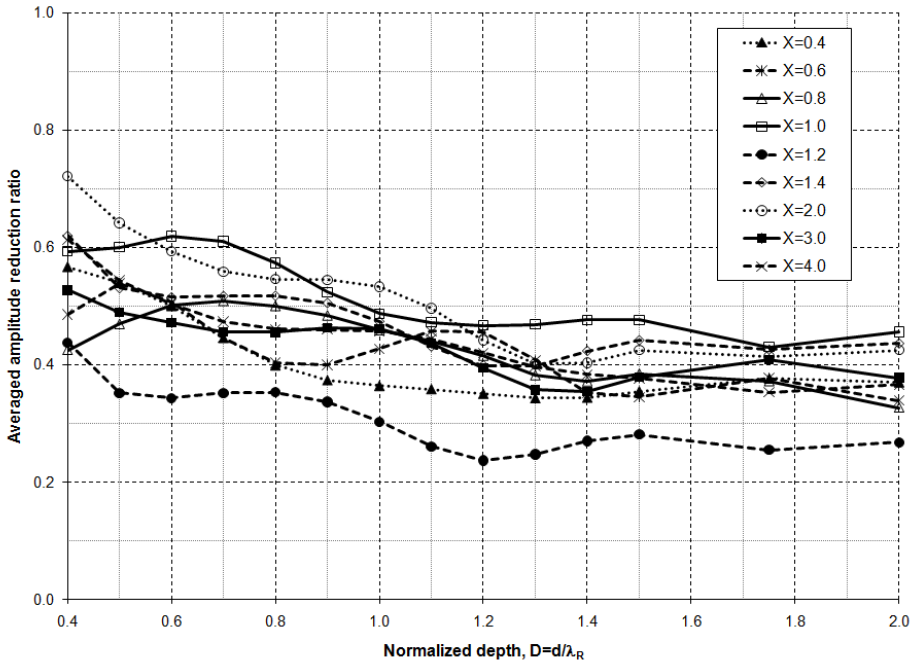

Figure 5- 5: Influence of normalized depth, D
(Vs=250 m/sec, ν=0.3, γ=19.5 kN/m3, and ξ=5%.)

The soil shear wave velocity is varied from 200 m/sec to 400 m/sec. The averaged amplitude reduction ratio results for a geofoam trench installed in an homogeneous elastic half-space soil and located at X=0.4 and 1.2 from the source of disturbance are presented in Figures 5-6 and 5-7, respectively. It is clear from Figures 5-6 and 5-7 that vibration screening using in-filled geofoam trenches is more effective in soils with higher V_s (i.e. stiffer soils).

By varying the normalized depth from 0.4 to 2.0 and the soil shear wave velocity from V_{s1} to V_{s4} (where $V_{s1}<V_{s2}<V_{s3}<V_{s4}$), Figures 5-8 and 5-9 clearly indicate that as the shear wave velocity increases, the averaged amplitude reduction ratio decreases. For example, the effectiveness of a geofoam trench barrier installed in a soil with V_s=380 m/sec will be greater than the same barrier installed in soil with V_s= 210 m/sec by about 45%. Hence, the soil shear wave velocity should be considered as the most important soil characteristic when designing in-filled geofoam trench barriers.

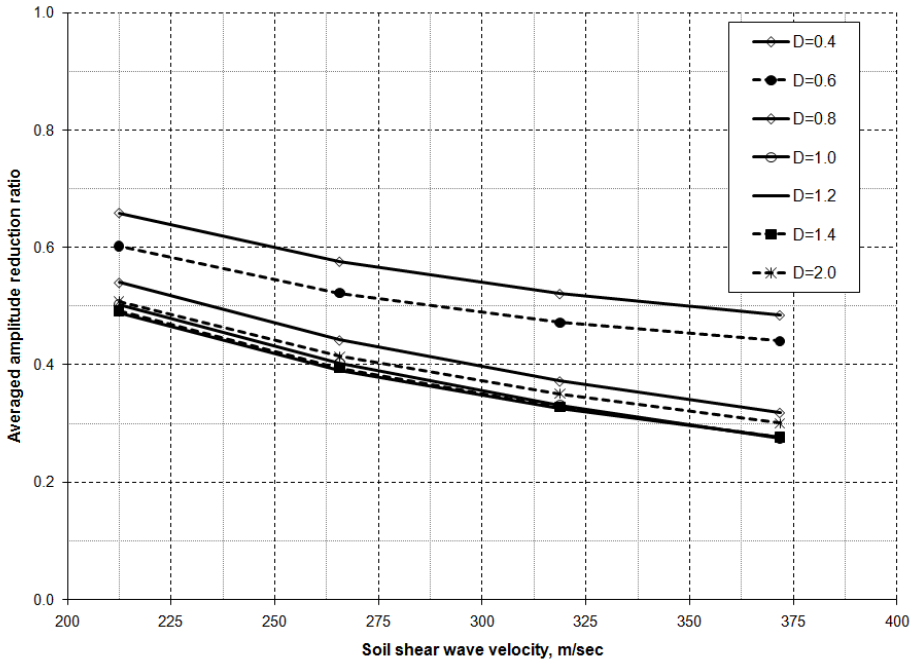

Figure 5- 6: Influence of soil shear wave velocity
(X=0.4, ν=0.25, γ=19.3kN/m^3, ξ=5%)

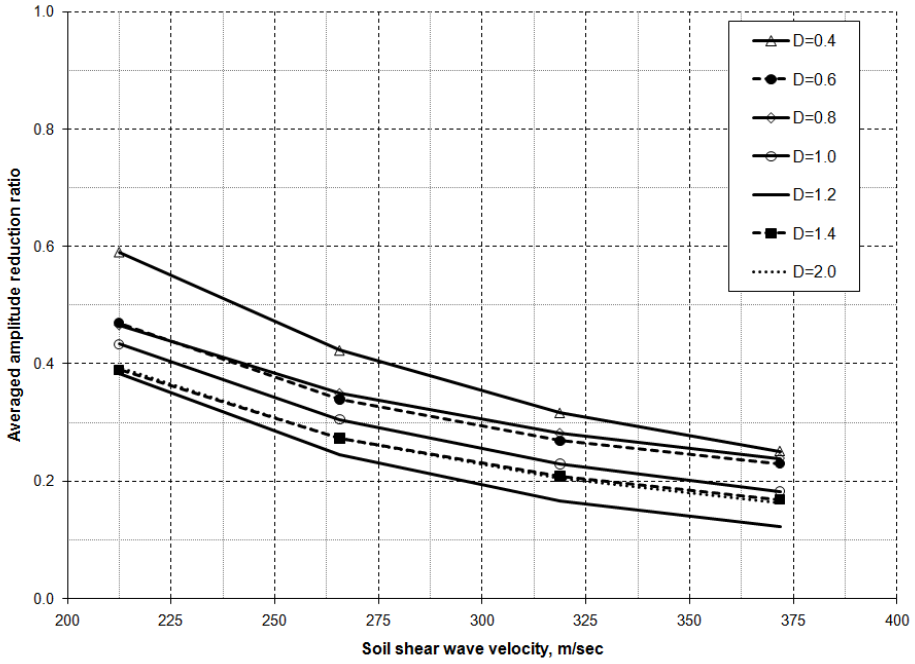

Figure 5- 7: Influence of soil shear wave velocity
(X=1.2, ν=0.25, γ=19.3kN/m^3, ξ=5%)

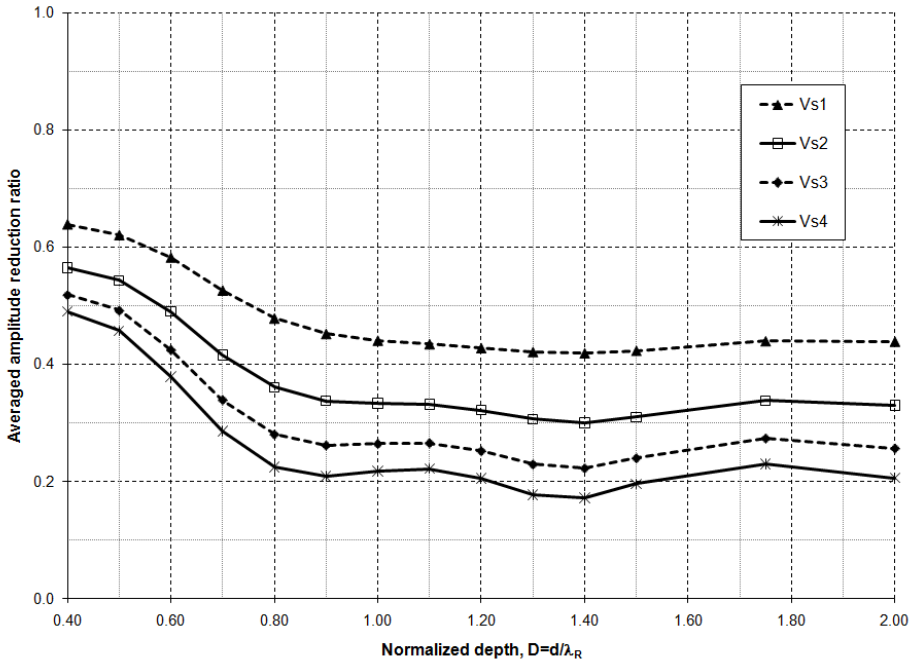

Figure 5- 8: Influence of soil shear wave velocity
(X=0.4, ν=0.35, γ=19.3kN/m3, ξ=5%)

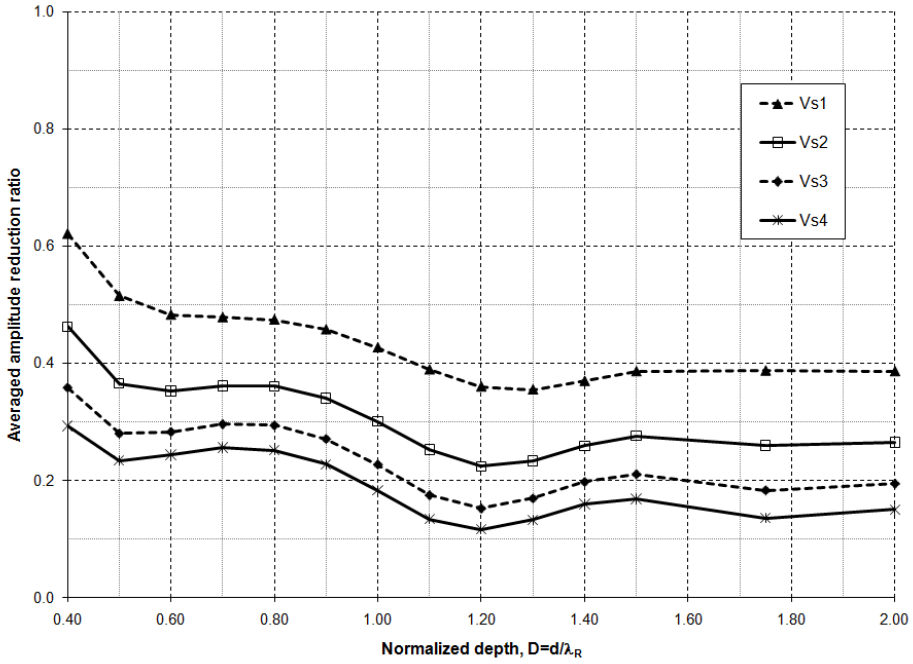

Figure 5- 9: Influence of soil shear wave velocity
(X=1.2, ν=0.35, γ=19.3kN/m3, ξ=5%)

5.2.3 Effect of Changing the Soil Density

To examine the effect of soil density on the vibration screening effectiveness of geofoam trench barriers, the soil unit weight is varied from 15.5 kN/m^3 to 19.5 kN/m^3 while the shear wave velocity is kept constant. A sample from the obtained results are presented in Figures 5-10 and 5-11 for barriers located at X=0.4 and 1.2, respectively. As it can be seen, the effect of soil density on screening effectiveness has the same trend as that of V_s. However, the effect of soil density on the screening effectiveness is less significant. For example, the vibration screening effectiveness is higher by about 9% for soil with unit weight of 19.5 kN/m^3 compared to that observed for soil with γ = 15.5 kN/m^3.

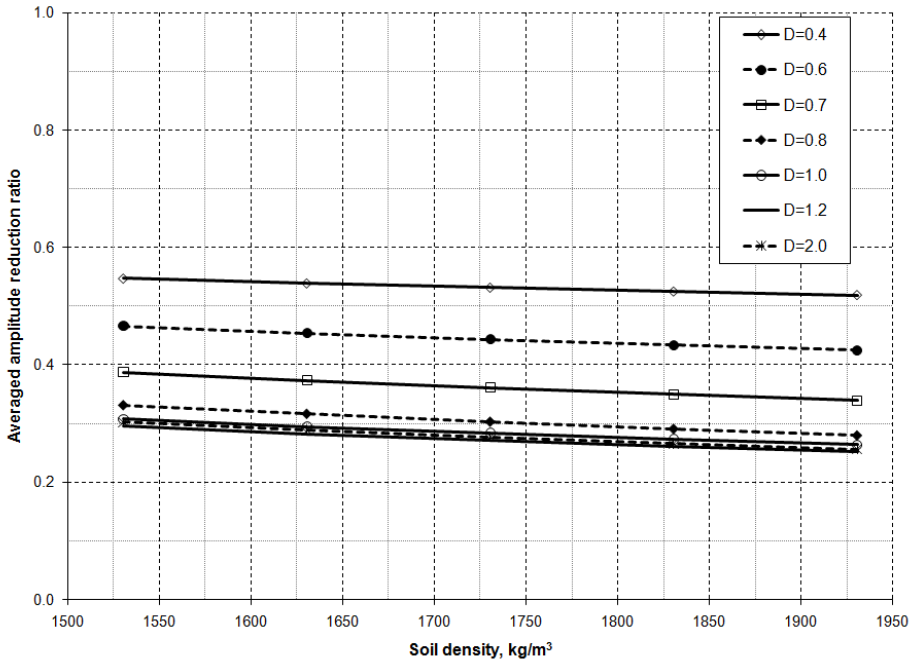

Figure 5- 10: Influence of soil density
(X=0.4, Vs=318m/sec, ν=0.35, ξ=5%)

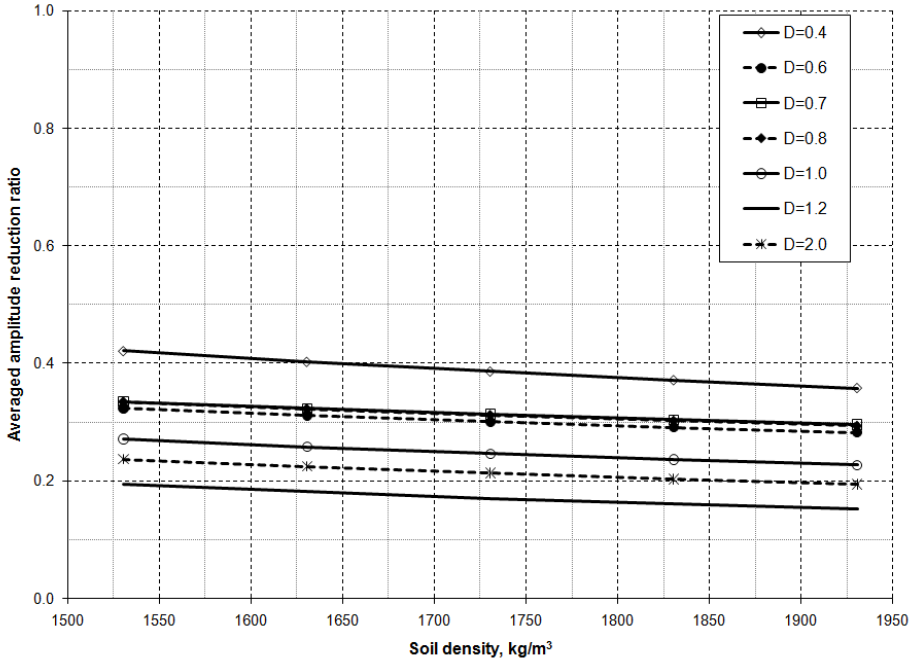

Figure 5- 11: Influence of soil density
(X=1.2, Vs=318m/sec, ν=0.35, ξ=5%)

5.2.4 Influence of Poisson's Ratio

The soil Poisson's ratio, ν, is varied from 0.25 to 0.4. Figures 5-12 and 5-13 demonstrate the influence of ν on the performance of an in-filled geofoam trench barrier. Figure 5-12 shows that the performance of an in-filled geofoam trench barrier with normalized depths ranging from D=0.6 to 1.2 and located at X=0.4 from the source installed in soil with ν = 0.4 is higher than the effectiveness of the same barrier installed in a soil with ν = 0.25 by about 15% or less. On the other hand, for barriers with proximity to the source X =1.2, Figure 5-13 shows that the effect of ν on screening effectiveness is unclear and insignificant. It can be concluded that the effect of the soil Poisson's ratio on the protective effectiveness of in-filled geofoam trench barriers is not important.

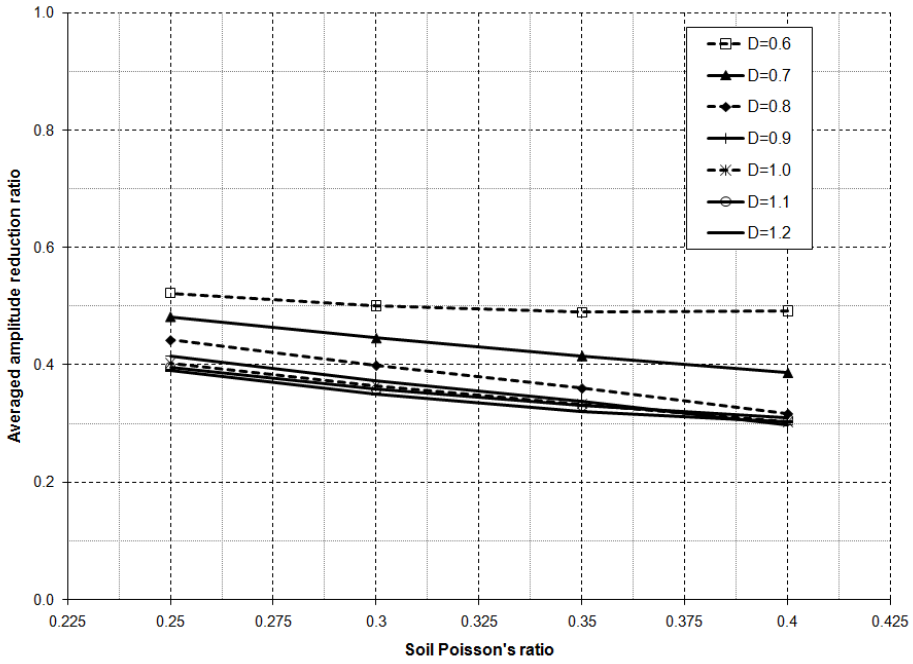

Figure 5- 12: Influence of soil Poisson's ratio
(X=0.4, V_s=265m/sec, γ=19.3kN/m^3, ξ=5%)

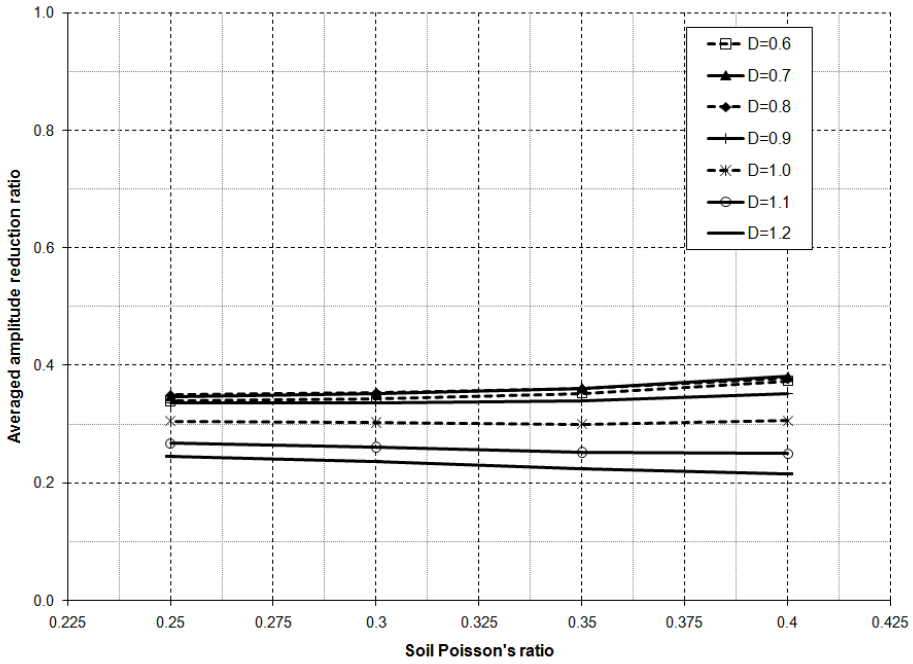

Figure 5- 13: Influence of soil Poisson's ratio
(X=1.2, Vs=265m/sec, γ=19.3kN/m3, ξ=5%)

5.2.5 Influence of Material Damping

The damping represents the system's ability to dissipate energy, which has to be accounted for when analyzing dynamic phenomena. In this parametric study, the soil material damping has been implemented in the finite element models in the form of Rayleigh damping. Rayleigh damping is defined by specifying two Rayleigh damping factors which are mass and stiffness proportional damping. The soil damping is varied from 1% to 10%. A sample from the obtained results is presented in Figure 5-14, which demonstrates the influence of changing the soil material damping on the performance of an in-filled geofoam trench barrier. Small differences in the average amplitude reduction are observed. Thus, it can be concluded that changing the soil material damping has a minor influence on the system screening performance.

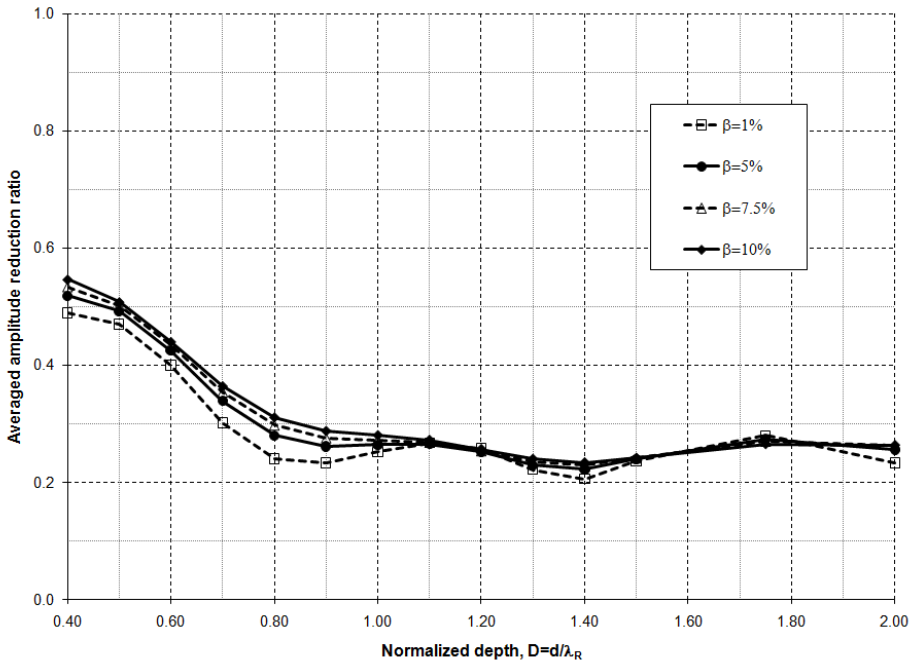

Figure 5- 14: Influence of material damping
(X=0.4, Vs=318m/sec, γ=19.3kN/m3, ν=0.35)

5.3 MLR MODEL TO PREDICT THE IN-FILLED GEOFOAM TRENCH BARRIER PERFORMANCE

Based on the results of the parametric investigation, a MLR model incorporating the effects of the key parameters governing the vertical vibration screening by in-filled geofoam trench wave barriers has been developed. As aforementioned, the adopted parameters in the parametric study have been varied independently, which results in having a database consisting of about 7056 data points. Only 6804 data points will be used in developing the MLR model while the remaining 252 data points will be used for verification purpose. The considered parameters and their limits are listed in Table 5-1.

Table 5- 1: Ranges of parameters considered in parametric study

Input parameters	**Minimum**	**Maximum**
Barrier normalized depth, D	0.4	2.0
Barrier's proximity to the source of disturbance, X	0.3	4.0
Soil shear wave velocity, Vs (m/sec)	210	380
Soil unit weight, γ (kN/m^3)	15.5	19.5
Soil Poisson's ratio, ν	0.25	0.40
Soil material damping, ξ (%)	1%	10%

The coupled effects of the adopted parameters on the screening effectiveness of in-filled geofoam are complex and not easy to model. Moreover, it was concluded that some parameters have significant influence on the system performance while other

parameters have less significant influence. The barrier depth, barrier's proximity to the source of disturbance, and the shear wave velocity of soil medium appear to have significant influence on the system screening efficiency; while the soil density, Poisson's ratio, and material damping have less significant influence on the screening efficiency.

Regression analysis is employed for fitting a model to data. Six parameters were considered in the parametric study, which requires a regression technique that is capable of dealing with an arbitrarily large number of explanatory variables. Thus, a multiple linear regression (MLR) analysis approach has been utilized in developing a MLR design model that can predict, efficiently, the performance of an in-filled geofoam trench as a wave barrier. The general purpose of multiple linear regression is to learn more about the relationship between several independent or predictor variables (in this case: barrier's geometry, location and soil dynamic properties) and a dependent or criterion variable (in this case: averaged amplitude reduction ratio). According to Rawlings et. *al* (1998), the linear additive model for relating a dependent variable to p independent variables can be presented as:

$$Y_i = \beta_0 + \beta_1 X_{i1} + \beta_2 X_{i2} + \ldots\ldots + \beta_p X_{ip} + \varepsilon_i \qquad (5\text{-}1)$$

where Y is the dependent variable, X_{i1}, X_{i2}, ... X_{ip} are the independent variables, and ε is random error. The subscript i denotes the observational unit from which the observations on Y_i and the p independent variables (X_{i1}, X_{i2}, ... X_{ip}) were taken. The second subscript designates the independent variable. The sample size is denoted with n (i =1, . . . , n), and p denotes the number of independent variables. There are (p + 1) regression coefficients

β_j, (j = 0, . . . , p) to be estimated when the linear model includes the intercept β_0. It is assumed that n > (p+1). The linear model is expressed in matrix notation as follows:

$$\underset{n\times 1}{\begin{pmatrix} Y_1 \\ Y_2 \\ \vdots \\ Y_n \end{pmatrix}} = \underset{n\times(p+1)}{\begin{bmatrix} 1 & X_{11} & X_{12} & X_{13} & \cdots & X_{1p} \\ 1 & X_{21} & X_{22} & X_{23} & \cdots & X_{2p} \\ \vdots & \vdots & \vdots & \vdots & & \vdots \\ 1 & X_{n1} & X_{n2} & X_{23} & \cdots & X_{np} \end{bmatrix}} \underset{(p+1)\times 1}{\begin{pmatrix} \beta_0 \\ \beta_1 \\ \vdots \\ \beta_p \end{pmatrix}} + \underset{n\times 1}{\begin{pmatrix} \varepsilon_1 \\ \varepsilon_2 \\ \vdots \\ \varepsilon_n \end{pmatrix}} \qquad \text{(5-2a)}$$

or

$$Y = X\beta + \varepsilon \qquad \text{(5-2-b)}$$

Where: Y : the n×1 column vector of observations on the dependent variable Y_i;

X: the n×(p+1) matrix consisting of a column of ones, which is labelled 1, followed by the p column vectors of the observations on the independent variables;

β: the (p+1)×1 vector of regression coefficients to be estimated; and

ε: the n×1 vector of random errors.

Each element β_j is a partial regression coefficient reflecting the change in the dependent variable per unit change in the j^{th} independent variable, assuming all other independent variables are held constant. The definition of each partial regression coefficient is dependent on the set of independent variables in the model.

The regression model is established assuming: (1) linear stochastic relationship (Equation 5-1) for i=1, 2, ..., n; (2) the error term ε is a random variable distributed with zero mean and constant variance σ^2 for all i; (3) the error terms ε_i are independent of each other; (4) the error terms ε_i and the independent variables (X_{i1}, X_{i2}, ... X_{ip}) are independent; (5) the error term ε has a normal distribution; and finally, (6) there is no exact linear relationship among the independent variables (uncorrelated).

5.3.1 Methodology

Before running the multiple linear regression analysis, it is important to determine if a relationship exists between the independent wave barrier parameters with each other, and between each of them and the barrier performance. Linear correlation analysis is used to quantify the strength of a linear relationship between the parameters of the wave barrier and its effectiveness through calculating the correlation coefficient. The correlation coefficient represents the normalized measure of the strength of linear relationship between variables. When there is no correlation between the two variables, then there is no tendency for the values of one variable to increase or decrease with the values of the second variable. The correlation coefficients range from -1 to 1. Values close to 1 suggest that there is a positive linear relationship between the data columns, values close to -1 suggest a negative linear relationship, while values close to or equal to 0 suggest that there is no linear relationship between the data columns.

After ensuring that there is a relationship between the specific barrier parameters and its performance, it is appropriate to run the multiple linear regression analysis. The

first criterion to measure the model goodness is by calculating the coefficient of determination (R^2) and adjusted coefficient of determination (R^2_{adj}). The coefficient of determination, (R^2), is a commonly used statistic to evaluate model fit and is given by the following equation:

$$R^2 = 1 - \frac{RSS}{TSS} \qquad (5\text{-}3)$$

where:

RSS is the residual sum of squared errors for the fitted model.

TSS is the total sum of squares.

When the variability of residual values around the regression line relative to the overall variability is small (i.e. R^2 close to 1.0), the predictions from the regression equation are good, and indicates that it has accounted for almost all variability of variables specified in the model (Rawlings et al., 1998). However, the value of R^2 increases as more independent variables are included. Thus, the use of the R^2 criterion for model building requires a judgment as to whether the increase in R^2 from additional variables justifies the increased complexity of the model. On the other hand, R^2_{adj}, is a modification of R^2 that adjusts for the number of explanatory terms in a model. In other words, R^2_{adj} is a rescaling of R^2 by degrees of freedom so that it involves a ratio of mean squares (MS) rather than sums of squares (SS), i.e.

$$R^2_{adj} = 1 - \frac{RMS}{TMS} \tag{5-4a}$$

$$R^2_{adj} = 1 - \frac{\left(1 - R^2\right)(n-1)}{(n-m-1)} \tag{5-4b}$$

where:

RMS is the residual mean squared errors for the fitted model.

TMS is the total mean of squares.

n is the sample size (observations).

m is the number of independent variables.

The expressions given in Equation 5-4 remove the impact of number of degrees of freedom and give a quantity that is more comparable than R^2 over models involving different numbers of variables. Unlike R^2, R^2_{adj} need not always increase as variables are added to the model and tend to stabilize around some upper limit as variables are added. The adjusted R^2 can be negative, and will always be less than or equal to R^2.

Another indicator to measure the model quality is the p-value. If the p-value is very small, (i.e. p-value ≤ 0.05) the model is good and the results are statically significant and the overall model is a good model to predict the value of $\overline{A_r}$.

The validity of the regression assumptions and the fitted model goodness are checked by drawing the diagnostic plots. The diagnostic plots are: (1) Residuals versus

Predictor plot, to assess the normality of residuals as well as to check if there is any pattern, (2) Quantile-Quantile plot or Q-Q Plot in which the estimated values of the barrier performance are plotted against the measured ones, and (3) Histogram plot which is a useful plot for exploring the shape of the distribution of the values of the residuals and should reveal a bell shaped curve. Figure 5-15 summarizes the above mentioned steps for developing the MLR model.

Given that the relationships between the wave barrier parameters and its performance is complex and that there is no prior knowledge regarding the model form, a linear combination between variables was assumed first. Subsequently, a more sophisticated combination to simplify the relationship between the barrier parameters and its performance is assumed using the variables transformation technique, which will be added to the first linear combination. However, the model is still to be linear in terms of the parameters (β_0 to β_p); only the form in which the independent variables are expressed is being considered non-linear.

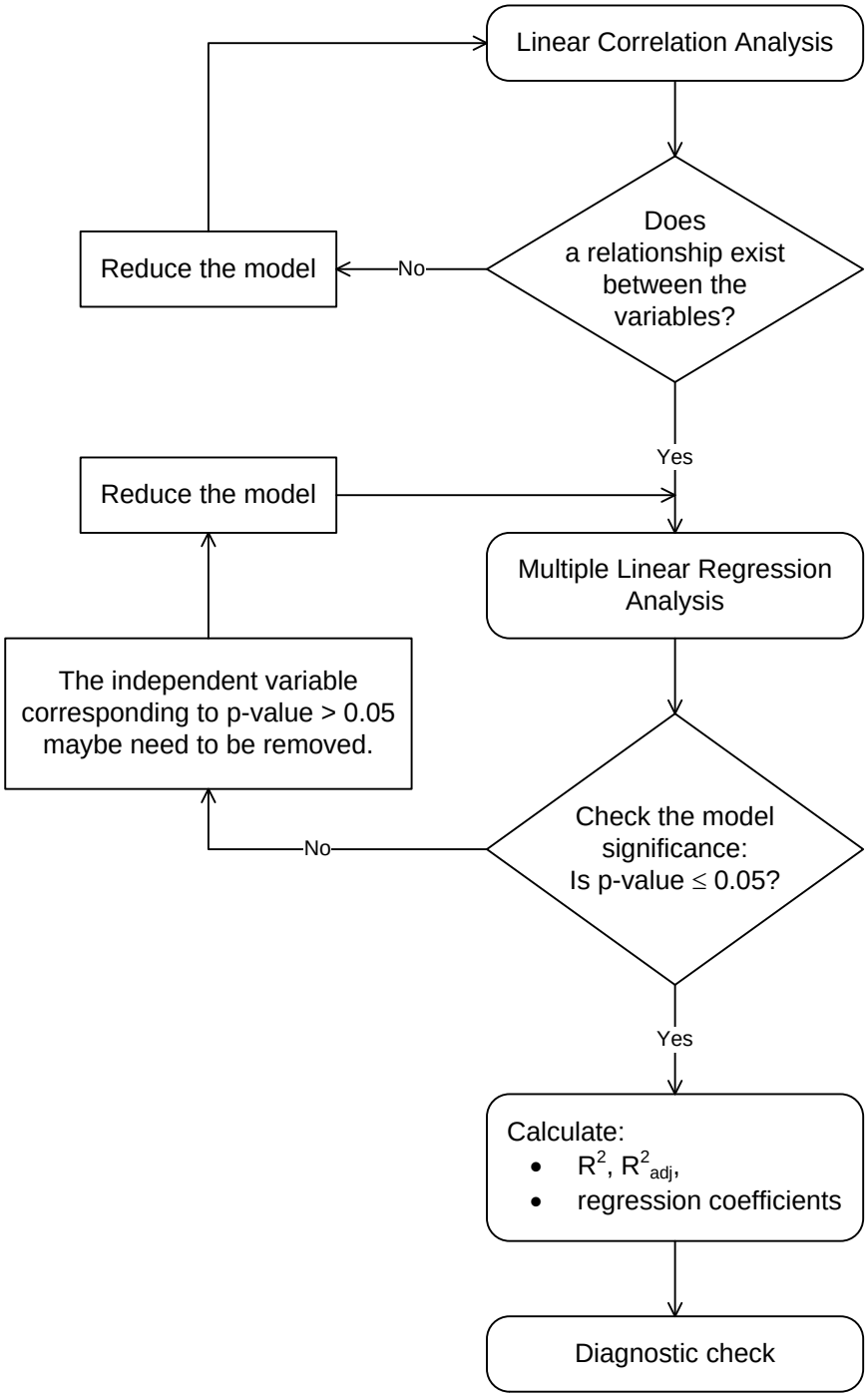

Figure 5- 15: Flowchart explains the MLR design model developing methodology.

5.3.2 Developing the MLR Design Model Utilizing MATLAB

MATLAB (R2009b) is a high-level numerical computing and interactive environment for algorithm development, data visualization, data analysis, and numeric computation. A short program is coded utilizing MATLAB statistic functions to perform the steps listed in Section 5.3.1. First, linear correlation analysis that involves calculating the correlation coefficients is performed using *corrcoef* function, which also returns a matrix of p-values for testing the hypothesis of no correlation. Second, two functions (*regress* and *regstats*) have been used in running the multiple linear regression analysis as follows:

- *regress* function computes the following statistics assuming that the model contains a constant term, and are incorrect otherwise:

    1. β_0 to β_i regression coefficients.

    2. the confidence intervals (lower and upper confidence bounds) for the regression coefficient estimates, using a 100*(1-α)% confidence level, where α is a number between 0 and 1 to specify a confidence level. The default value, 0.05, is adopted for 95% confidence intervals.

    3. The residuals that can be used later as a diagnostic check.

    4. The coefficient of determination R^2, the F statistic and its p-value, and an estimate of the error variance.

- *regstats* function also performs a multiple linear regression. *regstats* returns a structure stats, whose fields contain all of the diagnostic statistics for the regression analysis.

Finally, diagnostic plots have been plotted using *hist* and *qqplot* functions that are already implemented in MATLAB. The function *hist* creates a histogram for the residuals to inspect the distribution of the residual values while *qqplot* function creates a quantile-quantile plot of the estimated quantiles versus given observation quantiles. If the distribution is normal, the plot will be close to linear.

5.3.3 MLR Design Model Considering Linear Combination

A linear combination between the independent variables (X_{i1}, X_{i2}, ... X_{ip}) and the dependent variable ($\overline{A_r}$) is considered, as illustrated in Equation 5-5 and will be referred to as MLR Model-1.

$$\overline{A_r} = \beta_0 + \beta_1 X_1 + \beta_2 X_2 + \beta_3 X_3 + \beta_4 X_4 + \beta_5 X_5 + \beta_6 X_6 \qquad (5\text{-}5)$$

where :

$\overline{A_r}$, the averaged amplitude reduction ratio, is a dependent variable representing.

β_0 to β_6 are the regression coefficients which represent the independent contributions of each independent variable to the prediction of the dependent variable ($\overline{A_r}$).

X_1 is an independent variable represents the barrier normalized depth, D.

X_2 is an independent variable represents the barrier's proximity to the source of disturbance, X.

X_3 is an independent variable represents the soil shear wave velocity, Vs (m/sec).

X_4 is an independent variable represents the soil density, ρ (kg/m^3).

X_5 is an independent variable represents the soil Poisson's ratio, ν.

X_6 is an independent variable represents the soil material damping, ξ (%).

5.3.4 MLR Design Model Considering Variables Transformation

In addition to the linear combination considered in the previous section, new terms have been added based on an extensive trial and error in order to improve prediction efficiency of Equation 5-5 in estimating the averaged amplitude reduction ratio. The new terms are basically a transformation of the most important independent variables that are found to have a significant improvement when they are added to Equation 5-5. The final model is presented in Equation 5-6, and will be referred to as MLR Model-2, i.e.

$$\overline{A_r} = \beta_0 + \sum_{i=1}^{14} \beta_i X_i \qquad (5\text{-}6)$$

where :

$\overline{A_r}$, β_0 to β_{14} , and X_1 to X_6 are the same as listed in the previous section.

$X_7 = 1/X_1^2$,

$X_8 = 1/X_2^2$,

$X_9 = 1/\sqrt{X_2}$,

$X_{10} = \sqrt{X_1 + X_2}$,

$X_{11} = 1 \Big/ \sqrt{X_1^{\,2} + X_2^{\,2}}$,

$X_{12} = 1 \Big/ \sqrt{X_5}$,

$X_{13} = 1 \Big/ e^{X_6}$, and

$X_{14} = X_2 / X_1$.

5.3.5 Results Analysis and Discussion

A number of data combinations have been investigated for both models. Considering the whole data base, a sensitivity analysis has been conducted in order to identify the parameter that influences the most the ability of the model to accurately predict $\overline{A_r}$ for an in-filled geofoam trench barrier within the assigned limitations and conditions. The model's accuracy has been evaluated considering coefficients of determination (R^2, R^2_{adj}) as well as the diagnostic plots.

Through an extensive study of all considered combinations, it is found that dividing the range of normalized distance between the barrier and disturbance source (X) into sub-intervals has a huge influence on improving the model performance even when considering the whole range of normalized depth, ($0.4 \leq D \leq 2.0$). Moreover, narrowing the range of normalized depth (D) also helps in improving the model efficiency. Table 5-2 lists the obtained values of R^2_{adj} for all considered cases.

Tables 5-3 to 5-5 list the regression coefficients values (β_0 to β_6) for MLR Model-1 that were obtained by considering the whole and sub-interval X for ($0.4 \leq D \leq 2.0$), ($0.8 \leq D \leq 2.0$) and ($0.8 \leq D \leq 1.5$). Similarly, Tables 5-6 to 5-8 list the regression coefficients values (β_0 to β_{14}) for Model-2 that were obtained by considering the whole and sub-interval X for ($0.4 \leq D \leq 2.0$), ($0.8 \leq D \leq 2.0$) and ($0.8 \leq D \leq 1.5$).

Table 5- 2: Adjusted coefficients of determination (R^2_{adj})

Model	Normalized depth	Normalized distance				
		0.3≤X≤4.0	0.3≤X≤0.5	0.6≤X≤0.9	1.1≤X≤1.3	1.5≤X≤4.0
MLR Model-1	0.4≤D≤2.0	**0.6296**	0.6885	0.7301	0.7502	0.8323
	0.8≤D≤2.0	**0.6148**	0.7764	0.7614	0.7191	0.8354
	0.8≤D≤1.5	**0.7428**	0.7912	0.7726	0.7451	0.8663
MLR Model-2	0.4≤D≤2.0	**0.7442**	0.8864	0.8602	0.9226	0.9289
	0.8≤D≤2.0	**0.7524**	0.8581	0.8989	0.9381	0.9446
	0.8≤D≤1.5	**0.7512**	0.8634	0.9259	0.9503	0.9511

Table 5- 3: Regression coefficients for MLR Model-1 ($0.4 \leq D \leq 2.0$)

	Normalized distance, X				
	1	2	3	4	5
	$0.3 \leq X \leq 4.0$	$0.3 \leq X \leq 0.5$	$0.6 \leq X \leq 0.9$	$1.1 \leq X \leq 1.3$	$1.5 \leq X \leq 4.0$
β_0	**1.424537**	1.119084	1.185351	1.448602	1.659988
β_1	**0.015223**	0.705139	0.201804	-0.167135	-0.034463
β_2	**-0.141048**	-0.152372	-0.134748	-0.110526	-0.157724
β_3	**-0.000225**	-0.000217	-0.000189	-0.000210	-0.000245
β_4	**0.160772**	0.006338	-0.002247	0.058853	0.372202
β_5	**-0.001610**	-0.001556	-0.001359	-0.001483	-0.001783
β_6	**-0.006448**	0.000741	-0.001952	0.003060	-0.014861

Table 5- 4: Regression coefficients for MLR Model-1 ($0.8 \leq D \leq 2.0$)

	Normalized distance, X				
	1	2	3	4	5
	$0.3 \leq X \leq 4.0$	$0.3 \leq X \leq 0.5$	$0.6 \leq X \leq 0.9$	$1.1 \leq X \leq 1.3$	$1.5 \leq X \leq 4.0$
β_0	**1.433630**	0.957487	1.304087	1.388490	1.674236
β_1	**0.017751**	0.802176	0.209546	-0.144177	-0.030163
β_2	**-0.084733**	-0.017546	-0.102680	-0.069407	-0.116183
β_3	**-0.000238**	-0.000220	-0.000224	-0.000208	-0.000253
β_4	**0.016939**	-0.151587	-0.151149	-0.049727	0.217797
β_5	**-0.001685**	-0.001593	-0.001543	-0.001459	-0.001845
β_6	**-0.006376**	0.000156	-0.002445	0.002888	-0.014600

Table 5- 5: Regression coefficients for MLR Model-1 ($0.8 \leq D \leq 1.5$)

	Normalized distance, X				
	1	2	3	4	5
	$0.3 \leq X \leq 4.0$	$0.3 \leq X \leq 0.5$	$0.6 \leq X \leq 0.9$	$1.1 \leq X \leq 1.3$	$1.5 \leq X \leq 4.0$
β_0	**0.014317**	1.022406	1.381144	1.502752	1.752979
β_1	**0.025354**	0.798816	0.221132	-0.172776	-0.028858
β_2	**-0.085226**	-0.086437	-0.175036	-0.145064	-0.213859
β_3	**0.000265**	-0.000217	-0.000220	-0.000206	-0.000250
β_4	**0.859787**	-0.151198	-0.219493	-0.052531	0.252833
β_5	**-0.001190**	-0.001589	-0.001516	-0.001455	-0.001825
β_6	**0.000132**	0.000819	-0.002527	0.002526	-0.014688

As it can be noted that when the whole database is considered, the adjusted coefficients of determination (R^2_{adj}) are about 0.62 and 0.75 which means that 62% and 75% of the variability in the values of the averaged amplitude reduction ratio ($\overline{A_r}$) can be explained by MLR Model-1 and Model-2, respectively. On the other hand, dividing the considered range of normalized distance (X) into sub-intervals increased the models efficiency. For example, dividing X into four sub-intervals significantly improved the model prediction of $\overline{A_r}$, i.e., 86% to 95% of its variability can be explained by MLR Model-2, compared to only 75% when considering the whole database. However, eliminating some D values that were found to yield poor barrier performance, has minor influence on R^2_{adj} values. It can be concluded that MLR Model-2 with ($0.8 \leq D \leq 1.5$) and X in the form of sub-intervals can provide the best prediction for $\overline{A_r}$ over the assigned limits for independent variables. Figures 5-16 to 5-19 present the diagnostic plots for the

recommended MLR Model-2 for sub-interval cases in terms of X and D ranges from 0.8 to 1.5. All plots confirm that the assumptions are satisfied: (1) The residual plots show no pattern; (2) Q-Q plots confirm the normality of estimated dependent variable; and (3) Histogram plots confirm the shape of the distribution of residuals values and they clearly have a bell shaped curve.

Table 5- 6: Regression coefficients for MLR Model-2 ($0.4 \leq D \leq 2.0$)

	Normalized distance, X				
	1	2	3	4	5
	$0.3 \leq X \leq 4.0$	$0.3 \leq X \leq 0.5$	$0.6 \leq X \leq 0.9$	$1.1 \leq X \leq 1.3$	$1.5 \leq X \leq 4.0$
β_0	**-4.420924**	-17.106137	-6.917174	25.059260	0.406364
β_1	**-0.209616**	-4.053935	1.054275	12.920244	0.826408
β_2	**-0.072054**	-2.732386	-0.478808	6.697397	0.462767
β_3	**-0.000244**	-0.000222	-0.000203	-0.000214	-0.000281
β_4	**0.153695**	0.026130	-0.001833	0.080209	0.334553
β_5	**0.002302**	0.002390	0.002021	0.002304	0.002454
β_6	**-0.000364**	0.002014	0.002126	0.003855	-0.002856
β_7	**-0.018471**	0.030864	0.222482	2.882723	-1.586397
β_8	**-0.059646**	-0.222541	-0.083953	0.142264	-0.004204
β_9	**0.975413**	3.890705	1.039582	-3.801766	0.233960
β_{10}	**0.976706**	12.457876	2.103830	-30.908491	-3.179969
β_{11}	**0.325699**	1.020939	0.630730	-4.364819	0.881439
β_{12}	**38.887589**	39.069316	33.561598	37.476990	42.292518
β_{13}	**0.124409**	-0.018239	0.072655	-0.030115	0.294784
β_{14}	0.035731	-0.153409	0.109085	0.943681	0.895257

Table 5- 7: Regression coefficients for MLR Model-2 ($0.8 \leq D \leq 2.0$)

	Normalized distance, X				
	1	2	3	4	5
	$0.3 \leq X \leq 4.0$	$0.3 \leq X \leq 0.5$	$0.6 \leq X \leq 0.9$	$1.1 \leq X \leq 1.3$	$1.5 \leq X \leq 4.0$
β_0	**-4.136067**	-28.572311	15.771031	-132.399067	-5.639481
β_1	**0.018600**	-7.279822	6.688266	-24.417010	0.446715
β_2	**0.343397**	-5.387194	4.600117	-18.285920	1.142537
β_3	**-0.000258**	-0.000227	-0.000238	-0.000214	-0.000290
β_4	**0.010311**	-0.134075	-0.150220	-0.031831	0.181963
β_5	**0.002397**	0.002500	0.002144	0.002299	0.002551
β_6	**-0.000164**	0.002020	0.001916	0.004272	-0.002727
β_7	**-0.023085**	0.039112	0.102389	7.997081	-0.656486
β_8	**-0.161347**	-0.748221	0.098404	-1.574993	-0.700359
β_9	**1.846533**	4.712897	-0.753579	23.211870	4.955478
β_{10}	**-0.065452**	22.865807	-18.381770	99.557078	-1.821328
β_{11}	**-0.049962**	3.960911	-3.412202	11.107205	0.233012
β_{12}	**40.570427**	40.531195	36.601155	37.210459	43.858678
β_{13}	**0.125778**	-0.002839	0.076688	-0.012287	0.288615
β_{14}	**0.033156**	-0.165319	0.161230	-5.029879	0.415200

Table 5- 8: Regression coefficients for MLR Model-2 ($0.8 \leq D \leq 1.5$)

	Normalized distance, X				
	1	2	3	4	5
	$0.3 \leq X \leq 4.0$	$0.3 \leq X \leq 0.5$	$0.6 \leq X \leq 0.9$	$1.1 \leq X \leq 1.3$	$1.5 \leq X \leq 4.0$
β_0	**-11.586991**	-47.012339	101.709390	-75.684249	-13.033122
β_1	**-0.035634**	-15.273915	32.501545	-10.461661	0.755141
β_2	**1.691636**	-11.885130	25.212106	-4.387515	3.393052
β_3	**-0.000255**	-0.000224	-0.000235	-0.000212	-0.000287
β_4	**0.006041**	-0.132783	-0.220342	-0.035264	0.215687
β_5	**0.002385**	0.002564	0.002120	0.002274	0.002527
β_6	**-0.000057**	0.002595	0.002093	0.003988	-0.002632
β_7	**-0.026850**	0.075871	-0.578681	6.850153	-0.599578
β_8	**-1.066689**	-0.755349	0.516900	-2.292814	-1.922868
β_9	**8.467075**	4.806988	-10.214733	23.830042	13.780740
β_{10}	**0.202807**	44.522589	-100.838147	45.464585	-3.373126
β_{11}	**0.045719**	6.687791	-13.420393	0.794679	-0.548138
β_{12}	**40.320294**	41.129616	36.110613	36.924705	43.438626
β_{13}	**0.129331**	-0.006313	0.085061	-0.009577	0.294654
β_{14}	**0.051984**	-0.326137	1.275529	-4.549011	0.359790

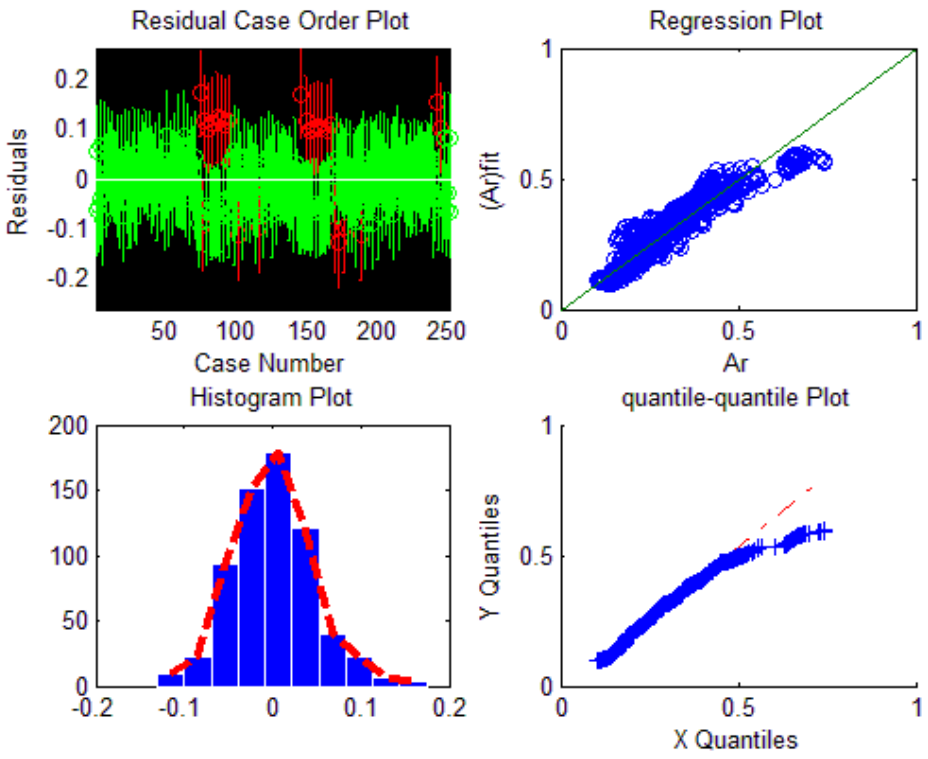

Figure 5- 16: Diagnostic plots for MLR Model-2 with ($0.3 \leq X \leq 0.5$) and ($0.8 \leq D \leq 1.5$)

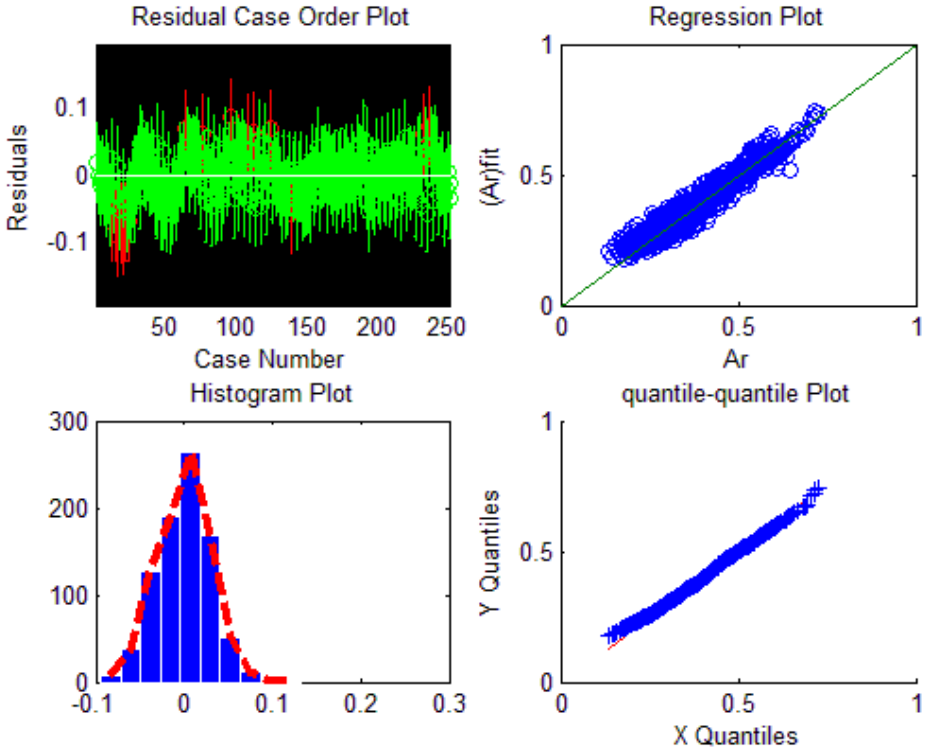

Figure 5- 17: Diagnostic plots for MLR Model-2 with ($0.6 \leq X \leq 0.9$) and ($0.8 \leq D \leq 1.5$)

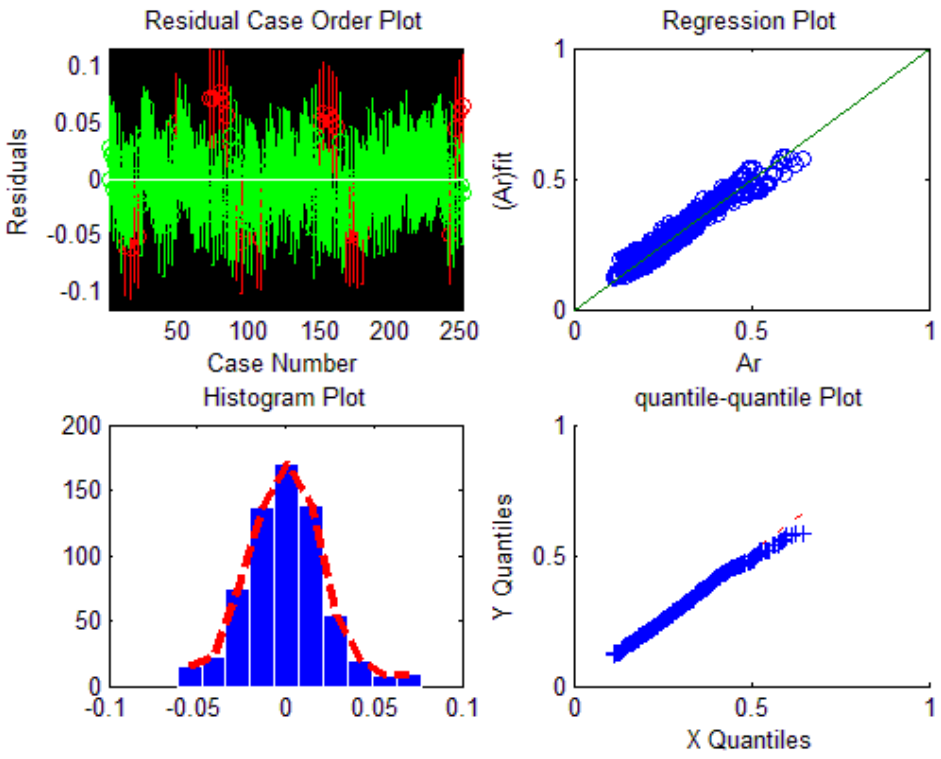

Figure 5- 18: Diagnostic plots for MLR Model-2 with ($1.1 \leq X \leq 1.3$) and ($0.8 \leq D \leq 1.5$)

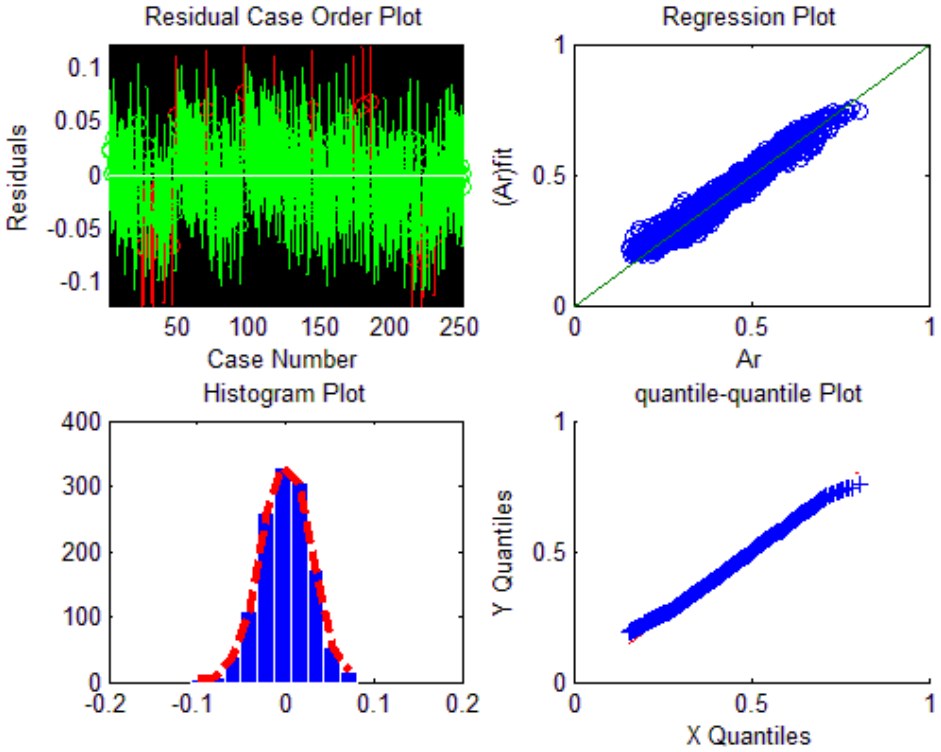

Figure 5- 19: Diagnostic plots for MLR Model-2 with ($1.5 \leq X \leq 4.0$) and ($0.8 \leq D \leq 1.5$)

5.4 EVALUATION OF MLR DESIGN MODEL PREDICTIONS

The developed MLR design models are used here to estimate the averaged amplitude reduction ratio $\overline{A_r}$ for several in-filled geofoam trench barrier geometric dimensions and its validity is established through comparison with finite element results. The material properties of the soil medium are chosen to be within the database range and have not been used in developing the MLR design model. A homogeneous half-space soil deposit is considered. The dynamic soil properties used in this example are as follows: shear wave velocity V_s=265 m/sec, Poisson's ratio of ν=0.35, unit weight γ=19.3 kN/m^3, and Rayleigh damping ξ=5%. Barrier geometric dimensions are: barrier thickness w=25 cm, barrier normalized depths D =1.0 and 1.2, and the normalized distance between the barrier and the source of disturbance X=0.4, 0.8, 1.2 and 2.0.

The averaged amplitude reduction ratio $\overline{A_r}$ can be estimated using MLR Model-1 by applying the appropriate regression coefficients (β_i) from Tables 5-3 to 5-5 to Equation 5-5. Similarly, MLR Model-2 can also be used to estimate the averaged amplitude reduction ratio $\overline{A_r}$ by applying the appropriate regression coefficients (β_i) from Tables 5-6 to 5-8 to Equation 5-6. According to the above considered configurations, $\overline{A_r}$ needs to be evaluated eight times and referred to as Ex1 to Ex8. The corresponding numerical values for the independent variables (X_1 to X_{14}) are listed in Table 5-9.

As previously mentioned in section 5.3.5, the developed MLR design model can be used to predict $\overline{A_r}$ considering the normalized distance (X) as one interval (column 1

in Tables 5-3 to 5-8) or by dividing the adopted range for normalized distance ($0.3 \leq X \leq 4.0$) into sub-intervals (columns 2 to 5 in Tables 5-3 to 5-8). Hence, Tables 5-10 and 5-11 list a sample from the performed numerical calculations on an Excel spreadsheet to estimate $\overline{A_r}$ utilizing MLR Model-1 and MLR Model-2, respectively. Tables 5-12 and 5-13 present finite element results against the final predicted $\overline{A_r}$ for all considered cases. Moreover, Figures 5-20 to 5-21 illustrate a visual presentation of MLR design model predictions (D1 for $0.4 \leq D \leq 2.0$, D2 for $0.8 \leq D \leq 2.0$ and D3 for $0.8 \leq D \leq 1.5$). It is clear that dividing the adopted range of normalized distance (X) between the trench and the source of disturbance into small intervals and then obtaining an equation for every sub-interval resulted in a significant improving in the performance of MLR models to capture the change in the $\overline{A_r}$ as X changes. Moreover, as reflected in Figures 5-20 and 5-21, another observation can be made: MLR Model-2 (which was developed based on variables transformation) gives better predictions than MLR Model-1.

Furthermore, it was observed that both models overestimate the averaged amplitude reduction ratio $\overline{A_r}$ which means underestimating the in-filled geofoam trench barrier protective efficiency. Hence, it can be concluded that the MLR design model predictions fall on the conservative side. Finally, it is worth mentioning that the obtained results for normalized depth D = 1.2 follow the same trend discussed above and, hence, they confirm that the MLR design Model-2 based on sub-interval is recommended to be used in estimating the preliminarily geofoam wall optimum dimension and location.

Table 5- 9: Calculations for the independent variables, X_i

		Ex1	**Ex2**	**Ex3**	**Ex4**	**Ex5**	**Ex6**	**Ex7**	**Ex8**
X_1	X	0.4	0.8	1.2	2.0	0.4	0.8	1.2	2.0
X_2	D	1.0	1.0	1.0	1.0	1.2	1.2	1.2	1.2
X_3	ρ	1930	1930	1930	1930	1930	1930	1930	1930
X_4	ν	0.35	0.35	0.35	0.35	0.35	0.35	0.35	0.35
X_5	V_s	265.0	265.0	265.0	265.0	265.0	265.0	265.0	265.0
X_6	ζ	5.0	5.0	5.0	5.0	5.0	5.0	5.0	5.0
X_7	$1/X_1^2$	6.250	1.563	0.694	0.250	6.250	1.563	0.694	0.250
X_8	$1/X_2^2$	1.000	1.000	1.000	1.000	0.694	0.694	0.694	0.694
X_9	$1/\sqrt{X_2}$	1.000	1.000	1.000	1.000	0.913	0.913	0.913	0.913
X_{10}	$\sqrt{X_1 + X_2}$	1.183	1.342	1.483	1.732	1.265	1.414	1.549	1.789
X_{11}	$1/\sqrt{X_1^2 + X_2^2}$	0.928	0.781	0.640	0.447	0.791	0.693	0.589	0.429
X_{12}	$1/\sqrt{X_5}$	0.061	0.061	0.061	0.061	0.061	0.061	0.061	0.061
X_{13}	$1/e^{X_6}$	0.007	0.007	0.007	0.007	0.007	0.007	0.007	0.007
X_{14}	X_2/X_1	2.500	1.250	0.833	0.500	3.000	1.500	1.000	0.600

Table 5- 10: Numerical calculations for Ex1 case using MLR Model-1

		$0.4 \leq \mathbf{D} \leq 2.0$		$0.8 \leq \mathbf{D} \leq 2.0$		$0.8 \leq \mathbf{D} \leq 1.5$	
		One interval	Sub-intervals	One interval	Sub-intervals	One interval	Sub-intervals
	X_i	$\beta_i X_i$	$\beta_i X_i$	$\beta_i X_i$	$\beta_i X_i$	$\beta_i X_i$	$\beta_i X_i$
β_0		1.42454	1.11908	1.43363	0.95749	0.01432	1.02241
X	0.4	0.00609	0.28206	0.00710	0.32087	0.01014	0.31953
D	1.0	-0.14105	-0.15237	-0.08473	-0.01755	-0.08523	-0.08644
ρ	1930	-0.43448	-0.41800	-0.45983	-0.42499	0.51214	-0.41892
ν	0.35	0.05627	0.00222	0.00593	-0.05306	0.30093	-0.05292
V_s	265.0	-0.42666	-0.41237	-0.44660	-0.42209	-0.31534	-0.42111
ζ	5.0	-0.03224	0.00371	-0.03188	0.00078	0.00066	0.00410
$\overline{A_r}$	$\boldsymbol{\Sigma}$	**0.45248**	**0.42432**	**0.42362**	**0.36145**	**0.43761**	**0.36663**

Table 5- 11: Calculations sample (MLR Model-2)

		$0.4 \leq \mathbf{D} \leq 2.0$		$0.8 \leq \mathbf{D} \leq 2.0$		$0.8 \leq \mathbf{D} \leq 1.5$	
		One interval	Sub-intervals	One interval	Sub-intervals	One interval	Sub-intervals
	X_i	$\beta_i X_i$	$\beta_i X_i$	$\beta_i X_i$	$\beta_i X_i$	$\beta_i X_i$	$\beta_i X_i$
β_0		-4.42092	-17.10614	-4.13607	-28.57231	-11.58699	-47.01234
X	0.4	-0.08385	-1.62157	0.00744	-2.91193	-0.01425	-6.10957
D	1.0	-0.07205	-2.73239	0.34340	-5.38719	1.69164	-11.88513
ρ	1930	-0.47145	-0.42817	-0.49765	-0.43857	-0.49279	-0.43205
ν	0.35	0.05379	0.00915	0.00361	-0.04693	0.00211	-0.04647
V_s	265.0	0.61004	0.63348	0.63508	0.66240	0.63214	0.67950
ζ	5.0	-0.00182	0.01007	-0.00082	0.01010	-0.00029	0.01297
	6.25	-0.11544	0.19290	-0.14428	0.24445	-0.16782	0.47420
	1.00	-0.05965	-0.22254	-0.16135	-0.74822	-1.06669	-0.75535
	1.00	0.97541	3.89071	1.84653	4.71290	8.46708	4.80699
	1.183	1.15565	14.74036	-0.07744	27.05519	0.23996	52.67984
	0.928	0.30240	0.94792	-0.04639	3.67761	0.04245	6.20946
	0.061	2.38885	2.40001	2.49222	2.48981	2.47686	2.52657
	0.007	0.00084	-0.00012	0.00085	-0.00002	0.00087	-0.00004
	2.500	0.08933	-0.38352	0.08289	-0.41330	0.12996	-0.81534
$\overline{A_r}$	Σ	**0.35113**	**0.33013**	**0.34802**	**0.33400**	**0.35424**	**0.33322**

Table 5- 12: Averaged amplitude reduction ratio by FE and MLR Model-1

	FE results	$0.4 \leq \mathbf{D} \leq 2.0$		$0.8 \leq \mathbf{D} \leq 2.0$		$0.8 \leq \mathbf{D} \leq 1.5$	
		One interval	Sub-intervals	One interval	Sub-intervals	One interval	Sub-intervals
Ex1	**0.3331**	0.4525	0.4243	0.4236	0.3615	0.4376	0.3666
Ex2	**0.4084**	0.4586	0.4756	0.4307	0.4621	0.4477	0.4664
Ex3	**0.3001**	0.4647	0.3754	0.4378	0.3545	0.4579	0.3609
Ex4	**0.5359**	0.4768	0.5448	0.4520	0.5229	0.4782	0.5302
Ex5	**0.3212**	0.4243	0.3938	0.4067	0.3579	0.4206	0.3493
Ex6	**0.3712**	0.4304	0.4487	0.4138	0.4415	0.4307	0.4314
Ex7	**0.2239**	0.4364	0.3533	0.4209	0.3406	0.4408	0.3319
Ex8	**0.4425**	0.4486	0.5132	0.4351	0.4996	0.4611	0.4874

Table 5- 13: Averaged amplitude reduction ratio by FE and MLR Model-2

	FE results	$0.4 \leq \mathbf{D} \leq 2.0$		$0.8 \leq \mathbf{D} \leq 2.0$		$0.8 \leq \mathbf{D} \leq 1.5$	
		One interval	Sub-intervals	One interval	Sub-intervals	One interval	Sub-intervals
Ex1	**0.3331**	0.3511	0.3301	0.3480	0.3340	0.3542	0.3332
Ex2	**0.4084**	0.4159	0.4188	0.4192	0.4157	0.4262	0.4070
Ex3	**0.3001**	0.4256	0.2983	0.4307	0.2837	0.4359	0.2905
Ex4	**0.5359**	0.4344	0.4997	0.4381	0.5079	0.4437	0.5197
Ex5	**0.3212**	0.3227	0.3129	0.3232	0.3137	0.3170	0.3201
Ex6	**0.3712**	0.3860	0.3829	0.3842	0.3762	0.3765	0.3565
Ex7	**0.2239**	0.3983	0.2666	0.3915	0.2475	0.3822	0.2372
Ex8	**0.4425**	0.4063	0.4658	0.3957	0.4524	0.3861	0.4396

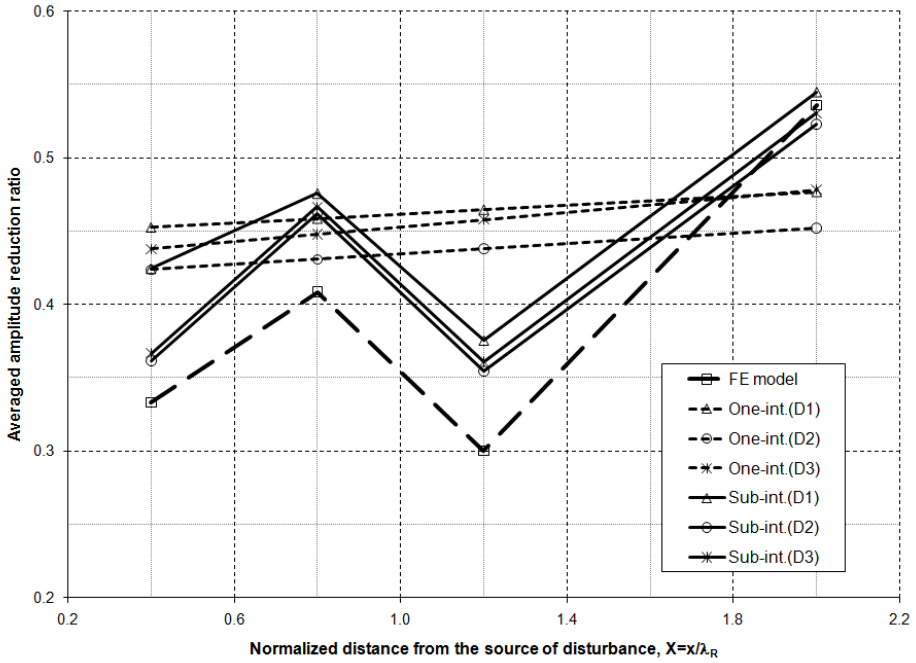

Figure 5- 20: Finite element verses MLR Model-1 predictions for averaged amplitude reduction ratio (D = 1.0)

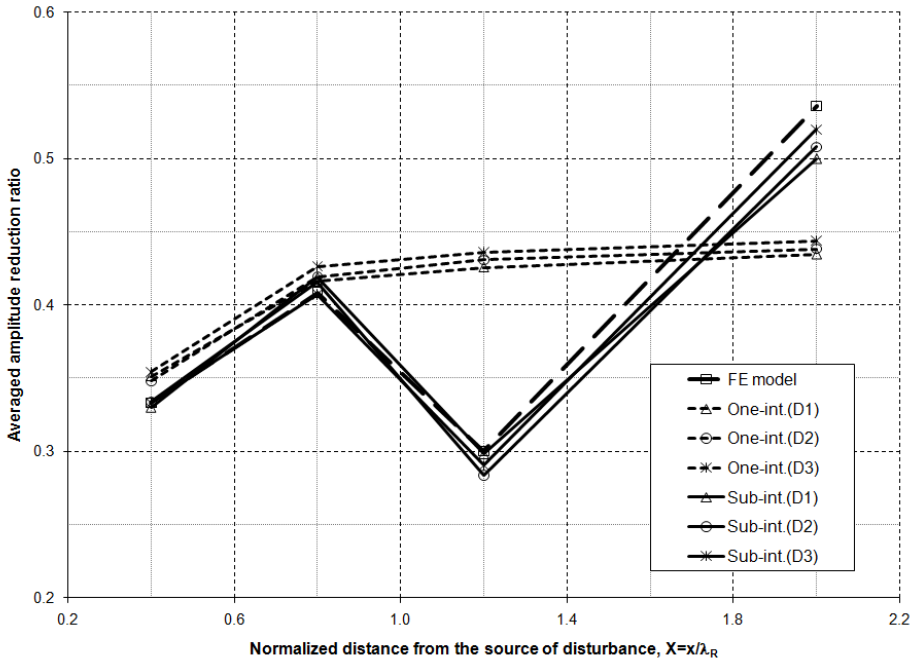

Figure 5- 21: Finite element verses MLR Model-2 predictions for averaged amplitude reduction ratio (D = 1.2)

5.6 WORKED EXAMPLE ON USE OF MLR MODEL-2

A foundation supporting a pump with an operating speed of 3000 rpm is causing unfavourable vibrations to adjacent structures. The pump foundation is located about 8m from the housing structure foundation. The structure experienced elevated vibration levels due to the vibration of the adjacent pump foundation. The objective is to design an in-filled geofoam trench barrier to reduce the induced vibrations by 60%. The proposed MLR Model-2 is adopted to design the vibration isolation system.

Based on the provided Seismic Cone Penetration Tests (SCPT) data, the soil profile is composed of a top layer of clay with silt underlain by sand with silt followed by a silt layer. Table 5-14 summaries the dynamic properties for each soil layer. Because the MLR Model-2 considers homogeneous halfspace, the weighted average of soil properties was calculated and the values are listed in Table 5-14 as well. These average soil properties are used in the preliminarily design of the in-filled geofoam trench.

The following procedure is used to establish the feasible barrier depth and location in order to achieve the specified reduction of 60% of the vibration amplitude:

- 60% reduction in the measured vibration amplitudes requires system efficiency of 60%. According to Equation 4-3, the targeted averaged amplitude reduction ratio: $\overline{A_r} = 0.4$.
- Equation 5-6 can be solved using an Excel spreadsheet employing the goal seek technique. By applying the regression coefficients (β_i) from Table 5-8 (columns 2 to 5) and starting with the normalized depth D = 0.8, the barrier feasible locations

(normalized distance between barrier and pump foundation, X) are calculated as listed in Table 5-15.

- The Rayleigh wavelength (λ_R) is calculated considering the Rayleigh wave velocity (V_R) and vibration frequency (*f*) (function of pump operating speed). Rayleigh wave velocity can be calculated using Equation 2-5, i.e.:

$$V_R = \frac{0.862 + 1.14\nu}{1+\nu} V_s = \frac{0.862 + 1.14 \times 0.355}{1+0.355} \times 256.27 = 241.08 \,\text{m/sec}$$

$$f = 3000 \,\text{rmp} = 50 \,\text{Hz}$$

$$\lambda_R = \frac{V_s}{f} = \frac{241.08}{50} = 4.82 \,\text{m}$$

- The actual depth and length of the barrier are calculated as:

  $d = \lambda_R \,.\, D$

  $x = \lambda_R \,.\, X$

  The calculated values are listed in Table 5-15.

Table 5- 14: Adopted soil profile

Property	**Soil layers**			
	Layer #1 Clay / Silt	Layer #2 Sand / Silt	Layer #3 Silt	Half-space
Layer thickness (m)	3	10	17	30
Shear wave velocity (m/sec)	181	247	275	256.27
Poisson's ratio	0.40	0.35	0.35	0.355
Bulk unit weight (kN/m^3)	18.0	19.0	19.5	19.18
Material damping (%)	4.0	3.0	3.0	3.1

Table 5- 15: Calculated depth and location of in-filled geofoam barrier

	D	X	$d = \lambda_R \cdot D$ (m)	$x = \lambda_R \cdot X$ (m)
Option 1	0.8	0.4140	3.86	2.00
Option 2	0.8	0.5845	3.86	2.82
Option 3	0.8	1.1356	3.86	5.48

5.7 SUMMARY AND CONCLUDING REMARKS

This chapter summarizes the results of a numerical investigation on the protective effectiveness of in-filled geofoam trenches as wave barriers to scatter the steady state vibration induced by machine foundations. The methodology used involved conducting a parametric study employing a 2D finite element numerical model for in-filled geofoam trench barriers installed in an homogeneous elastic half-space soil. The barrier depth and location were varied independently as well as the soil dynamic properties. The wave barriers protective effectiveness was evaluated based on the achieved reduction in soil particle response. A MLR Model-1 and Model-2 utilizing multiple linear regression analysis has been developed for estimating the vibration screening effectiveness of such type of barriers. Based on the results obtained and their analysis, the following conclusions can be made:

1 The key parameters that influence the barrier performance are its depth and proximity to the source of disturbance, and the shear wave velocity of soil medium. The soil density, Poisson's ratio, and material damping have some influence but are less significant.

2 Deeper trenches are required at greater distances from the source of disturbance to achieve the same level of performance.

3 The normalized depth D should be greater than 1.2 for maximum performance. However, D can be as low as 0.8 for X = 0.4. Also, for practical construction purposes, the width of geofoam barrier can be kept at 0.25m.

4 In-filled geofoam trench barrier performs more effectively in stiff soils (i.e. with relatively high Vs values) than in soft soils (i.e. with low Vs values). Accordingly, the soil shear wave velocity should be considered as the main soil characteristic when designing in-filled geofoam trench barriers.

5 Dividing the range of normalized distance between the barrier and disturbance source into sub-intervals significantly improved the MLR models performance. In addition, narrowing the range of normalized depth improved the model efficiency but not significantly.

6 The MLR Model-2 performed better than MLR Model-1 in predicting the averaged amplitude reduction ration.

CHAPTER SIX

EVALUATION OF IN-FILLED GEOFOAM TRENCH PERFORMANCE USING ARTIFICIAL NEURAL NETWORKS

In this chapter, an artificial intelligence-based method is proposed for predicting the effectiveness of in-filled geofoam trench barriers in screening harmonic ground vibration. An artificial Neural Network (ANN) model is developed using the feed forward back propagation neural networks. The model has been trained, validated and tested using the results of the parametric study conducted in Chapter 5. It is demonstrated that the ANN model can effectively and accurately predict the averaged amplitude reduction ratio of in-filled geofoam trench barriers. The feasibility of using the ANN model as a preliminary design tool is illustrated, and its predictions are compared with those obtained from the MLR model presented in Chapter 5.

6.1 INTRODUCTION

Artificial Intelligence (AI) techniques include expert systems, neural networks, genetic algorithms, fuzzy logic systems, cellular automata, chaotic systems, and anticipatory systems. Interestingly, most of these computational techniques simulate to some extent the biological or behavioural phenomena of humans. The artificial neural networks (ANN) approach has been employed successfully in a number of disciplines such as aerospace, automotives, banking, defense, electronics, entertainment, finance,

manufacturing, medicine, telecommunications, oil and gas, robotics, speech, securities, and transportation.

The ANN approach is a powerful modeling tool for problems where the rules that govern the results are either not defined properly or too complex (Adeli, 2001, Flood and Kartam, 1994). Neural networks simulate in a simplified way the activities of the human brain, which performs highly complex, nonlinear, and parallel computing operations at very high speeds. They are capable of learning from input data, which gives theANN diversified areas of application. ANNs have learning, self-organizing and auto-improving capabilities allowing it to capture complex interactions among variables without previous knowledge of the nature of these interactions. Consequently, an ANN does not require mathematical relationships between variables. A properly trained ANN also has the ability to recall full patterns from incomplete or noisy data (Rafiq et al., 2001).

The Basic working units of ANN are the connection weights, i.e., the variables that can be adjusted to map inputs to corresponding outputs. The inputs are applied to the neural network with some random values of connection weights. The neural network then gives out its output, which is compared with the target value corresponding to the input supplied. The connection weights are adjusted so that error is minimized. This type of learning is called supervised training. However, the learning can also be unsupervised (will be explained in detail in the subsequent section).

This chapter demonstrates the potential for using ANNs to predict the effectiveness of in-filled geofoam trench barriers in controlling harmonic ground vibration induced by machine foundations. In the current analysis of wave barrier

performance using ANN, The model inputs include the barrier depth and its proximity to the source of disturbance; and soil dynamic properties such as shear wave velocity, density, Poisson's ratio, and material damping. The averaged amplitude reduction ratio is the model output. The assembled database, model architecture and training and learning process of the ANN network are described. Moreover, a comparison between the ANN model and the proposed MLR model developed in Chapter 5 results has been conducted.

6.2 THE NEURAL NETWORK APPROACH

ANN has been used to estimate the averaged amplitude reduction ratio based on given key parameters such as barrier geometry, location and soil dynamic properties. ANN learns from input database information and has the capability of generalization, classification, pattern recognition, function approximation and simulation of sophisticated operations (Haykin, 1999). ANN structure consists of parallel multiple layers of linear and nonlinear processing elements (i.e. neurons) which can be classified into: an input layer, an output layer, and hidden layers, as shown in Figure 6-1. These neurons are linked by variable weights. The input layer receives original data (X_j), which is adjusted by connection weights (w_{ij}) and biases (w_{bi}). The bias unit is used to scale the input to a useful range to improve the convergence properties of the neural network (Shahin et *al.*, 2001). The adjusted inputs are subjected to a summation process to form a single input $(n)_i$ for all inputs received from the input layer.

$$(n)_i = \sum_{j=1}^{n} w_{ij} X_j + w_{bi} \qquad (6\text{-}1)$$

The result of this combined summation is passed through a transfer function (will be discussed in the subsequent section) to produce the output of the processing element. This single input is modified by an activation function to generate an output value of the processing unit through the hidden layers. The error between network outputs and desired targets is calculated and then propagated back to the network through a learning algorithm. The implementation of such an algorithm updates the network weights and biases in the direction in which the total network error decreases rapidly. ANN then synthesizes and memorizes the relationship between the inputs and outputs through a training process. The data used in the training process, however, should be sufficient and representative to allow the ANN to recognize the underlying correlations of the information involved. Once an ANN is established and well-trained, it will be capable of predicting outputs of any input set of data, and predicting the outcome of any unfamiliar set of inputs located within the range of the training data with an acceptable degree of accuracy. In civil engineering, feed-forward neural networks along with back-propagation algorithms are widely used and have shown good performance (Shahin *et al.*, 2001). Moreover, about 80% of neural network applications utilize back-propagation neural networks for prediction (Ahmad *et al.*, 2007) and it has been applied successfully to various problems of civil engineering. Hence, they are selected for constructing the proposed ANN model in this study.

6.2.1 Feed-Forward Neural Network

Feed-forward neural network model is widely used in engineering applications. In feed-forward neural networks, neurons are arranged in layers and all the neurons in each layer

are linked to all the neurons in the next layer. In general, the feed-forward neural network consists of an input layer, output layer and one or more hidden layers of neurons. The phrase "feed-forward" indicates that the data moves forward from one layer to the next during ANN modeling. The input layer receives input information and passes it forward to the neurons of the hidden layer, which in turn passes the information to the output layer. The output from the output layer is the corresponding prediction of the model for the data set supplied at the input layer. To construct a stable feed-forward neural network for a particular problem, the optimum number of neural units in each layer is selected using a trial and error approach as recommended by Rafiq *et al.*(2001).

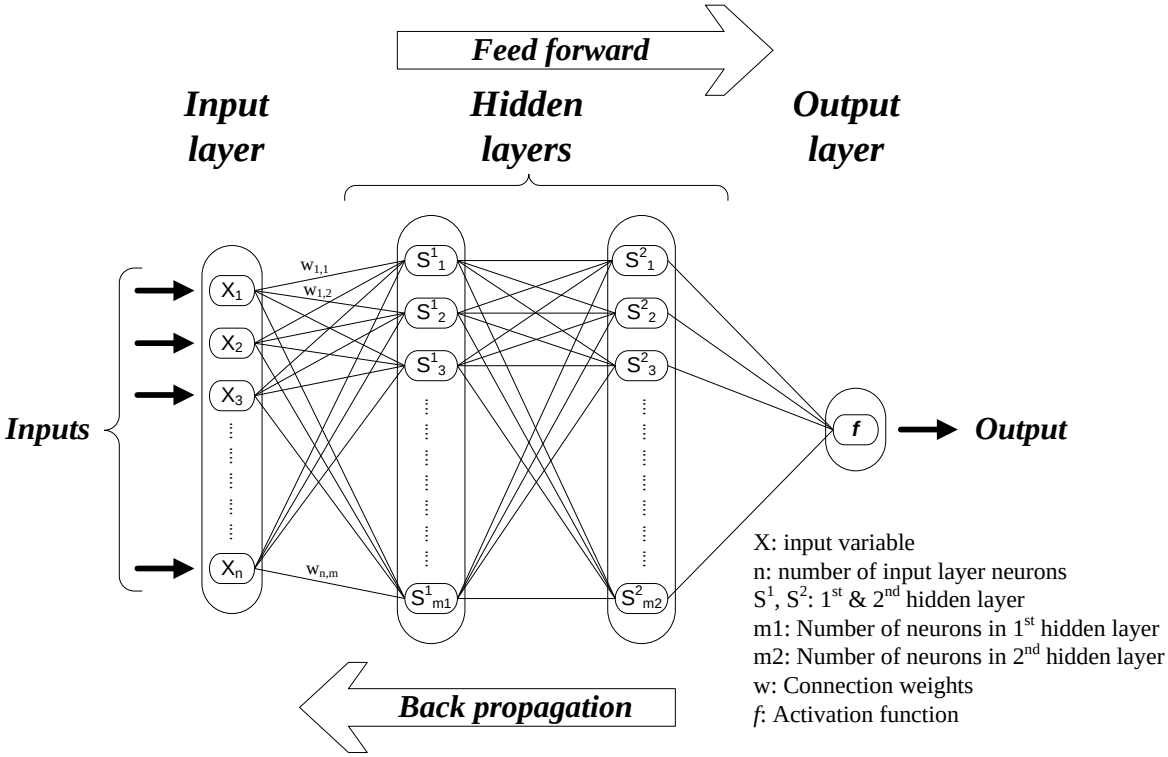

Figure 6- 1: The architecture of ANN model

6.2.2 Back-Propagation Learning Algorithm

Learning algorithms are techniques used to establish connections (i.e. weights and biases) between neurons forming the network structure and to adjust both weights and biases to obtain the desired values. There are two broad categories of algorithms: unsupervised (weights and biases are modified in response to network inputs only) and supervised (weights and biases are modified in order to move the network outputs closer to the targets) (Haykin, 1999). In the supervised learning process, the neural network is trained with the help of data that contains a set of inputs and corresponding target values. This basic training procedure is shown in Figure 6-2. However, the learning can be unsupervised where no targets are supplied to the network. In unsupervised learning there is no specific response required, but rather the response is based on the networks ability to organize itself. The vast majority of learning in engineering applications involves supervised learning.

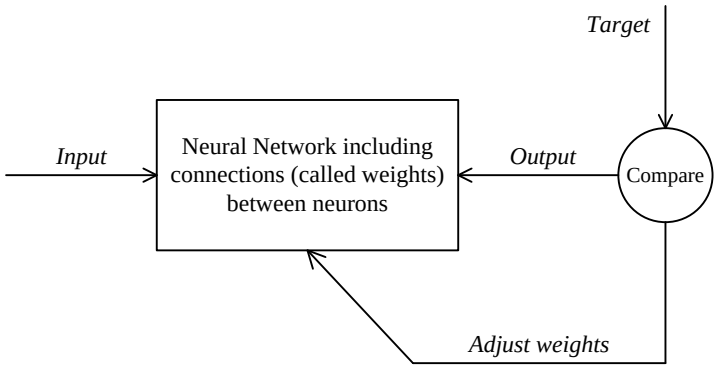

Figure 6- 2: Basic working of Supervised learning
(Adopted from MATLAB help)

One of the well-known supervised training algorithms for the feed-forward neural networks is the back-propagation algorithm. In this algorithm a gradient descent technique is applied to minimize the error for a particular training pattern in which it adjusts the weights by a small amount at a time. The learning error is calculated using the following equation (Equation 6-2):

$$\text{Error} = \tfrac{1}{2} \sum_{i} \left(t_i - o_i\right)^2 \qquad (6\text{-}2)$$

Where t_i is the target output and o_i is the predicted output at neuron (i), respectively. In the back-propagation phase, the error between the predicted and target output values is calculated and used to update the weights between neurons using Equation 6-3:

$$\Delta w_{i,j}(t) = \eta \delta_j o_i + \beta \Delta w_{i,j}(t-1) \qquad (6\text{-}3)$$

The advantage of these methods is that they have the ability to escape local minima in the error surface and, thus, produce optimal or near optimal solutions. However, they also have a slow convergence rate. If training speed is not a major concern, there is no reason why the back-propagation algorithm cannot be used successfully (Breiman 1994).

6.2.3 Data Preparation

The ability of the ANN model to predict the in-filled geofoam trench protective efficiency will largely depend on how comprehensive the database is. In other words, it will depend on the availability of sufficient data points to teach the ANN model the relationships between the adopted parameters and the averaged amplitude reduction ratio. Furthermore, the data points must cover the entire range over which the different input variables are expected to be. In this study, the database used in training the ANN model is obtained from the extensive parametric study conducted in Chapter 5 as there have not been any prior published results regarding the use of Uretek polymeric material as wave barriers.

Given the fact that ANNs are very sensitive to absolute magnitudes, the variables should be normalized in a way to produce a set of data values within the same order of magnitude. This is because when the variables are different in order of magnitude, fluctuations in the first input parameter will tend to swamp any importance given to the second input parameter, even if the second input is much more important in predicting the desired output. Thus, all data points should be scaled and normalized so that they correspond roughly to the same range of values. Scaling the data will avoid saturation of the hidden nodes and will ensure that all variables have a fair impact on the output. Therefore, the training data should be scaled such that the processed data lies in the range of [-1, 1]. The training, testing, and validating data sets are scaled according to:

$$\left(X_j\right)_n = 2\left(\frac{X_j - \min X_j}{\max X_j - \min X_j}\right) - 1 \qquad (6\text{-}4)$$

$$Y_n = 2\left(\frac{Y - \min Y}{\max Y - \min Y}\right) - 1 \qquad (6\text{-}5)$$

Where X_j is the input vector; Y is the target output vector; $(X_j)_n$ is the scaled input vector; Y_n is the scaled target output vector; $\min X_j$ and $\max X_j$ are the lower limit and upper limit of the input vector X_j, respectively; minY and maxY are the lower limit and upper limit of the target output vector Y, respectively.

The scaled data was then used to train the neural network. The data from the output neurons, $(Y_n)_{predicted}$, has to be converted back into its un-scaled format, $Y_{predicted}$, to get the actual predicted values according to the following equation.

$$Y_{predited} = \tfrac{1}{2}\left((Y_n)_{predited} + 1\right)(\max Y - \min Y) + \min Y \qquad (6\text{-}6)$$

6.3 PROPOSED ANN MODEL

A computer program has been developed in the MATLAB (R2009b) environment. A multilayer feed-forward network back-propagation algorithm was used to predict the averaged amplitude reduction ratio. This has been accomplished using *newff* feed-forward back-propagation network with *trainlm* as the back-propagation training function, *learngdm* as the back-propagation weight/bias learning function, *logsig* as the transfer function for hidden layers while a pure linear transfer function for the output layer (Equations 6-7 and 6-8), and mean squared error function *mse* as the performance function utilizing MATLAB software. The training function updates weight and bias

values according to Levenberg-Marquardt optimization and it is one of the fastest methods available for training moderate-sized feed-forward ANNs (Hagan *et al*., 1996).

$$f(n_{\mathrm{i}}) = a_{\mathrm{i}} = \frac{1}{1+\mathrm{e}^{-n_{\mathrm{i}}}} \tag{6-7}$$

$$f(n_{\mathrm{i}}) = a_{\mathrm{i}} = n_{\mathrm{i}} \tag{6-8}$$

where n_{i} is the weighted sum of all synaptic inputs plus the bias of neuron i, and a_{i} is the output of the neuron.

To simplify the learning process and reduce the required time for training, the back-propagation Levenberg-Marquardt Algorithm (LMA) was adopted as the learning algorithm. The LMA operates in a batch mode at which the weights and biases of the network are updated only after the entire training set has been applied to the network (Demuth and Beal, 1998). LMA propagates back the errors computed at the output layer to the network based on the Jacobian matrix J, which contains the first derivatives of the network errors with respect to weights and biases. An iteration of such algorithm can be written as follows (Equation 6-9)

$$\mathrm{w}_{\mathrm{j+1}} = \mathrm{w}_{\mathrm{j}} - \left[\mathrm{J}^{\mathrm{T}}\mathrm{J} + \mu\mathrm{I}\right]^{-1}\mathrm{J}^{\mathrm{T}}\mathrm{e} \tag{6-9}$$

where w_{j} is a vector of current weights and biases, μ is a learning rate, J is the Jacobian matrix, J^{T} is the transpose matrix of J, I is the identity matrix, and e is a vector of network errors.

The available set of data is divided randomly into three subsets: training, validation, and testing. The training data is used to train the model to recognize the patterns between input and output data. The validation data is used to evaluate the effectiveness of the designed model in generalizing the underlying relationships and achieving a good performance when new data are introduced. The final model is tested with the testing data set, not presented to the model before, to ensure that predictions are real and not artifacts of the training process (Demuth and Beal, 1998). Before training, all data (i.e. inputs and targets) were scaled so that they fall in the range [-1,1] using Equations 6-4 to 6-6. This pre-processing step increases the efficiency of the ANN training (Rafiq et al., 2001).

It is worth mentioning that the *newff* feed-forward back-propagation network randomly divides input and target vectors into three subsets as follows: training, validation, and testing using *dividerand* function. Therefore, the adopted criteria in this study is that 60% of the data is used for training, 20% for validating that the network is generalizing and to stop training before over-fitting, and the last 20% is used as a completely independent test of network generalization. Moreover, data scaling and un-scaling has been done in MATLAB using *mapminmax* function, which scales inputs and targets so that they fall in the range [-1,1].

The number of neurons in the hidden layer was determined by training several networks with different numbers of hidden neurons and comparing the predicted results with the desired output. In other words, the number of the hidden neurons was optimized, using trial and error, to minimise the mean squared error as well as to avoid under-fitting (i.e large training and validating errors) and prevent over-fitting (i.e. low training error

but high validating error). In this study, two hidden layers with different number of neurons were considered for ANN model. Parameters of the established ANN model are listed in Table 6-1.

Table 6- 1: The values of parameters used in the ANN model

Parameters	ANN
Number of input layer neurons	6
Number of hidden layers	2
Number of first hidden layer neurons	18
Number of second hidden layer neurons	24
Minimum gradient	1×10^{-10}
Goal	1×10^{-6}

6.4 RESULTS AND DISCUSSION

Table 6-1 lists the adopted inputs used in training the ANN model to predict the averaged amplitude reduction ratio as well as the upper and lower limits for all parameters (input variable). The database consists of 6804 data points. A successfully trained ANN model should give accurate output predictions, not only for input data used in the training process, but also for any new testing data that has not been seen by the model and of course within the range of the training database. Moreover, good ANN models normally have only slight difference between their validating and testing errors (Amegashie et al., 2006). Therefore, the performance of the ANN model was assessed at the training stage

statistically based on root-mean-squared (RMS) error, absolute fraction of variance (R^2), and mean absolute percentage error (MAPE) between the ANN model predictions and the finite element results (training database), which are expressed in Equations 6-10 to 6-12 (Sandemir, 2009).

$$\mathrm{RMS} = \sqrt{\frac{1}{n}\sum_{i=1}^{n}\left(t_i - o_i\right)^2} \tag{6-10}$$

$$R^2 = 1 - \left(\frac{\sum_{i=1}^{n}\left(t_i - o_i\right)^2}{\sum_{i=1}^{n}\left(o_i\right)^2} \right) \tag{6-11}$$

$$\mathrm{MAPE} = \frac{1}{n}\sum_{i=1}^{n}\left|\frac{t_i - o_i}{t_i}\right| \times 100 \tag{6-12}$$

Where t_i is the target output, o_i is the predicted output, and n is the number of data points.

Satisfactory performance of the training process was verified by requiring the ANN model to predict the averaged amplitude reduction ratio based on the whole training data using six input variables. Predictions of the ANN model are shown in Figure 6-3. The figure includes the equity line, as a reference, which represents the condition of equal values for the predicted and targeted values of averaged amplitude reduction ratio. It can be noted that the ANN model has captured the input-output relationships since the points are mostly located on and a very few are slightly under/above the equity line between the

finite element results (input data) and predicted values. The regression R-value is 0.99836 for the total response based on the trained network using the whole database. Statistically, the RMS, R^2 and MAPE values were 0.00813, 0.99965, and 0.00%, respectively, which indicates that the performance of ANN is excellent.

During the training stage, a linear regression analysis was performed on the network response. Figure 6-4 shows the linear regression results between the network outputs and the corresponding targets for the three subsets: training, testing, and validation as well as the overall case. The output tracks the targets very well for training, validation, test and overall total response, consequently, the regression R-values are 0.99897, 0.99734, 0.99770 and 0.99839, respectively.

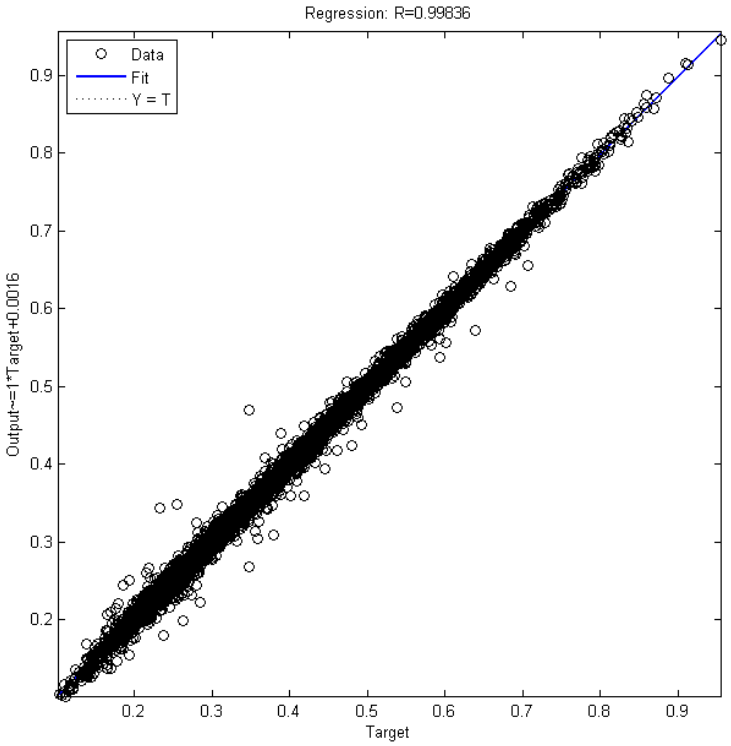

Figure 6- 3:Response of ANN model in predicting the averaged amplitude reduction ratio

To examine the generalization capacity of the ANN, it was tested using the testing data (20% of the original database, which was chosen randomly by *dividerand* function). Such testing points were not previously presented to the model, and thus the predictive capacity of the model for new data can be evaluated. The six input parameters of the testing data points were introduced to the ANN model and the response (predicted averaged amplitude reduction ratio) is shown in Figure 6-5. Similar to the case of the training data, the model predictions compare well with the actual provided data; testing data points were mostly located on and a few slightly diverted from the equity line. Hence, it can be deduced that the ANN can satisfactorily generalize the prediction of the averaged amplitude reduction ratio for the case of in-filled geofoam trench barrier installed in half-space soil. In addition, statistical parameters obtained from the validation data were comparable to that of the training and testing data indicating an excellent performance of the model.

A plot of the training, validation, and testing errors are shown in Figure 6-5. The results are considered to be good because of the following considerations: the final mean-square error is small; the test set and validation set errors have similar characteristics; and no over-fitting has occurred by iteration 412 (where the best validation performance occurs). The performance of the proposed ANN model was also evaluated by plotting the histogram of response errors (residuals). The plot confirms that the response errors follow normal distribution and clearly form a bell shaped curve, Figure 6-6.

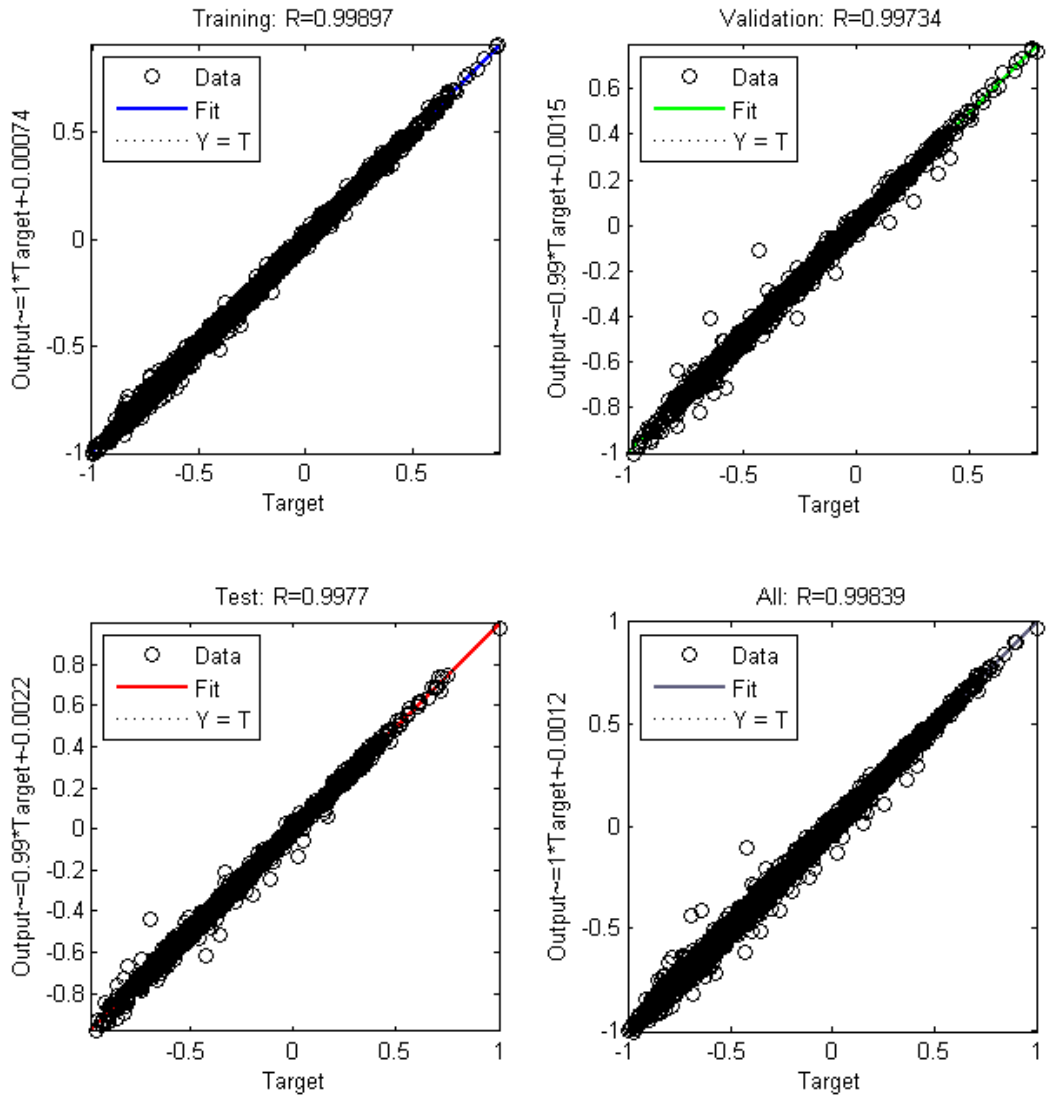

Figure 6- 4: Response of ANN model in predicting the averaged amplitude reduction ratio

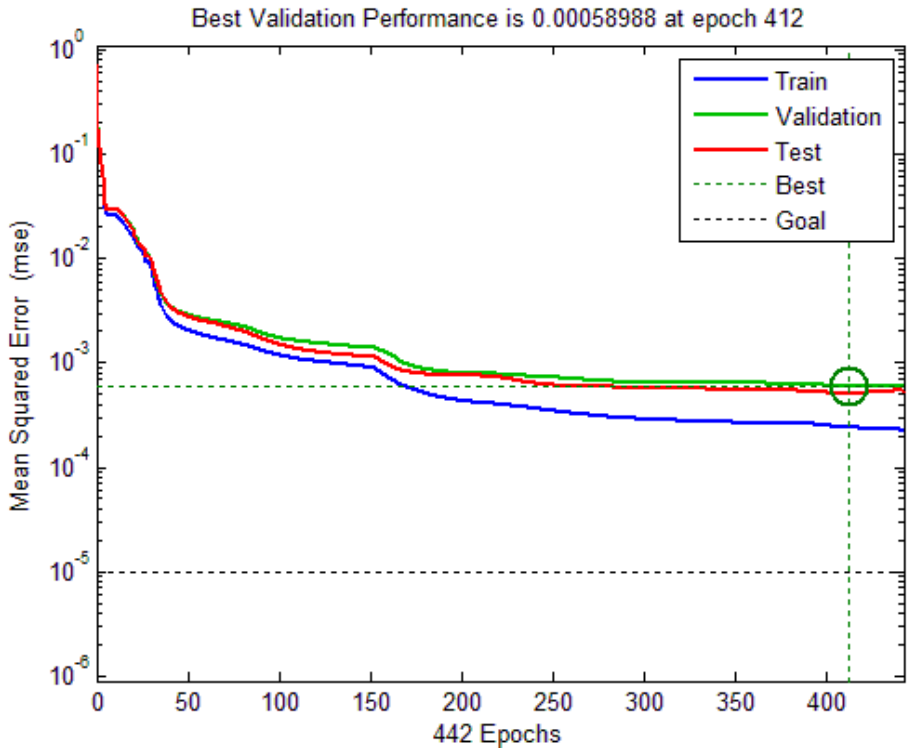

Figure 6- 5:Network Performance during the training, validation and testing stages

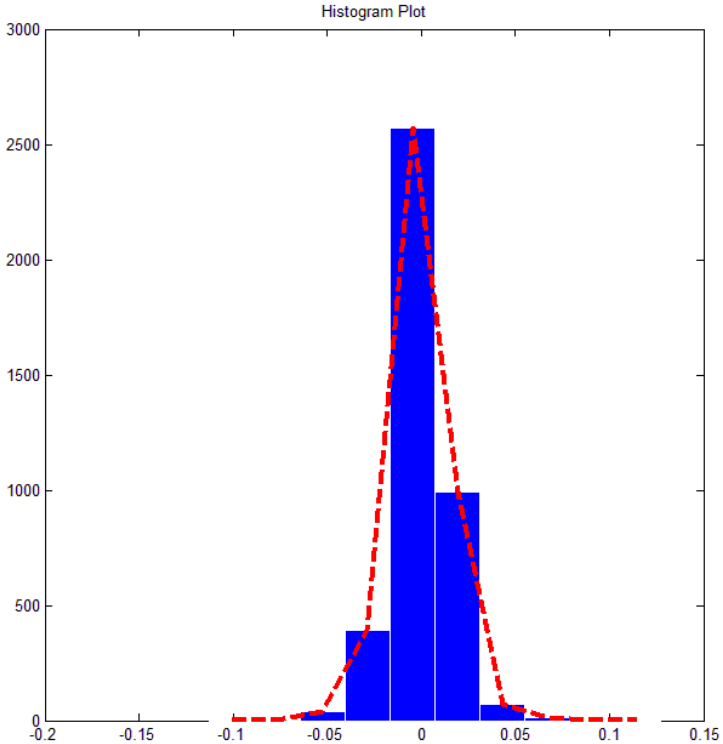

Figure 6- 6:Histogram of the network response over-all error

6.4.1 Validating ANN Model Using New Data Set

To independently demonstrate the utility of the proposed ANN model, a new set of input data (obtained from finite element analysis) that has not been included in the database used in training, validating and testing the network is compared to that predicted by the trained ANN model. A linear regression analysis between each element of the network response and the corresponding target has been performed and the results are illustrated in Figure 6-7. It is clear that the ANN model has captured the input-output relationships since the points are mostly located on and a very few points are slightly under/above the equity line between the finite element results (input data) and corresponding predicted values. The relationship between the predicted and targeted averaged amplitude reduction ratio can be represented by Equation 6-13. The results show that the regression R-value is 0.99885. Statistically, the RMS, R^2 and MAPE values were 0.00507, 0.99987, and 0.00022%, respectively, which indicates an excellent ANN model performance.

$$\overline{A}_{r\ predicted} = 0.0022 + 0.9947\overline{A}_{r\ given} \qquad (6\text{-}13)$$

A comprehensive comparison of the ANN model predictions with the corresponding finite element analysis results has been carried out. The barrier was assumed to be installed in an elastic half-space soil which has the following dynamic properties: shear wave velocity V_s=265 m/sec, Poisson's ratio of ν=0.35, unit weight γ=19.3 kN/m^3, and Rayleigh damping ξ=5%.

Figures 6-8 and 6-9 show the influence of changing normalized depth, D, on the averaged amplitude reduction ratio $\overline{A}_r$ for an in-filled geofoam trench barrier located at

normalized distances of 0.4 and 1.2. Figures 6-10 and 6-11 present a comparison between the predicted and targeted averaged amplitude reduction ratio in terms of changing the normalized distance, X for geofoam wall with normalized depths of 1.0 and 1.2. The ANN predictions were in excellent agreement with the finite element analysis results throughout the entire range of the assigned normalized barrier depths, D. Statistically, the RMS, R^2 and MAPE values for the whole new testing data were 0.00507, 0.99987, and 0.00022% while for X=0.4 were 0.00361, 0.99991, and 0.0349% and for X=1.2 were 0.00474, 0.99977, and 0.00769%, respectively, which indicating an excellent performance of the ANN model.

The excellent agreement between the predicted and targeted values indicates that the developed ANN model successfully captured the relationship the input parameters and the output (target). Hence, it can be used effectively as preliminarily design tool to predict the averaged amplitude reduction ratio for in-filled geofoam trench barriers in order to estimate the preliminarily geofoam wall optimum dimensions. Finally, it is worth mentioning that the results showed that the proposed ANN model is not capable of extrapolation beyond the domain of the training database.

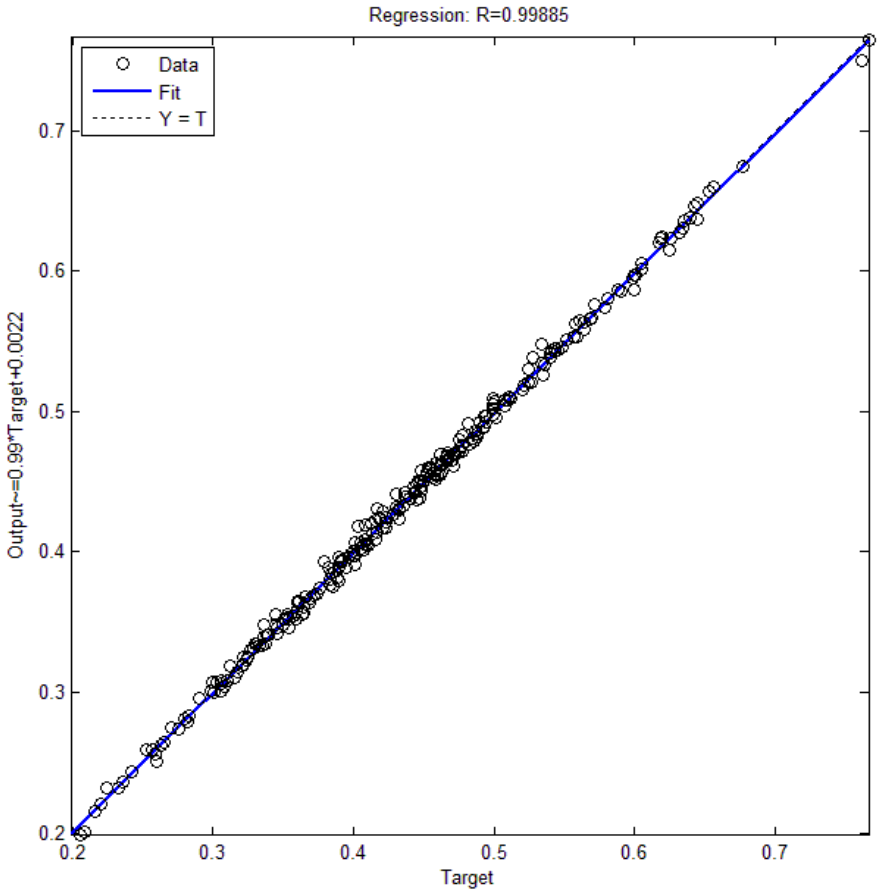

Figure 6- 7:Linear regression analysis on the response of ANN model in predicting the averaged amplitude reduction ratio

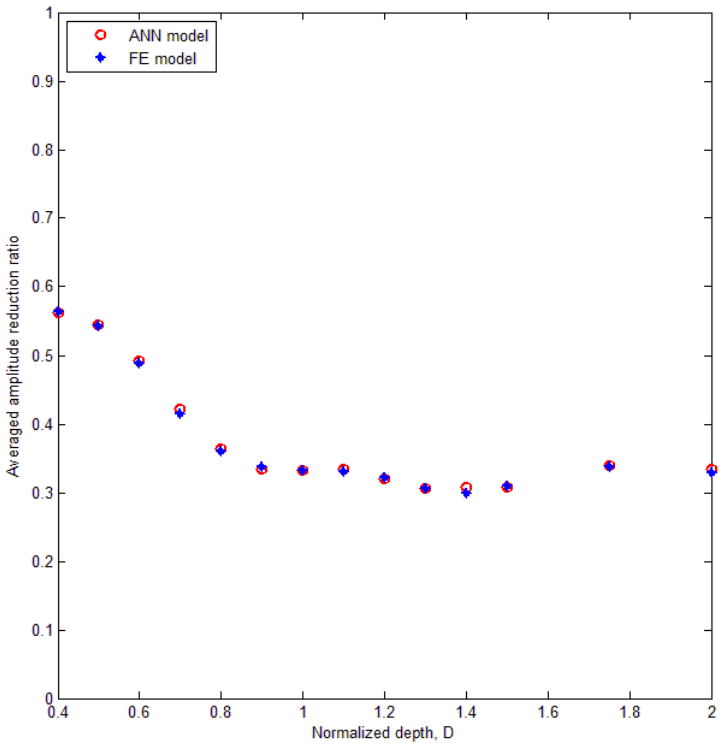

Figure 6- 8:Response of ANN model in predicting the averaged amplitude reduction ratio for normalized distance (X = 0.4)

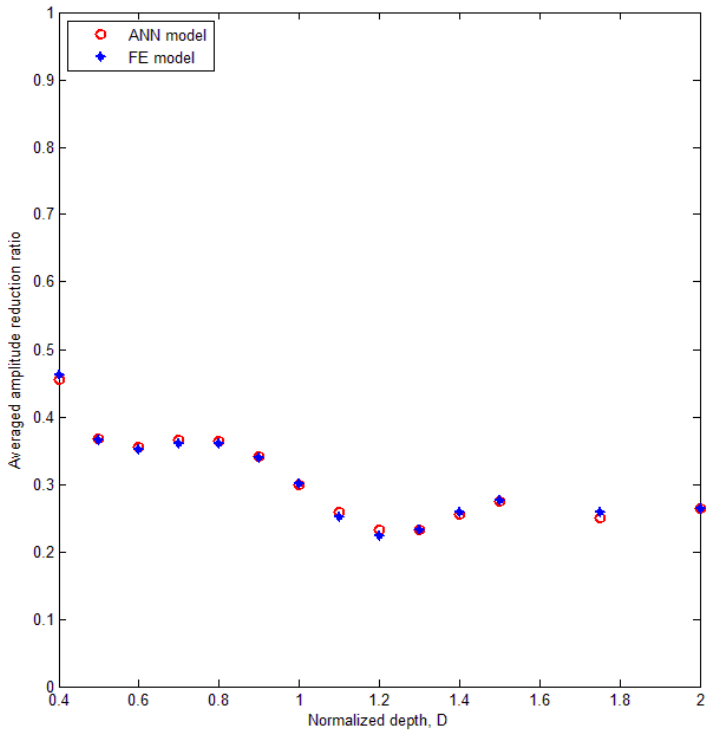

Figure 6- 9:Response of ANN model in predicting the averaged amplitude reduction ratio for normalized distance (X = 1.2)

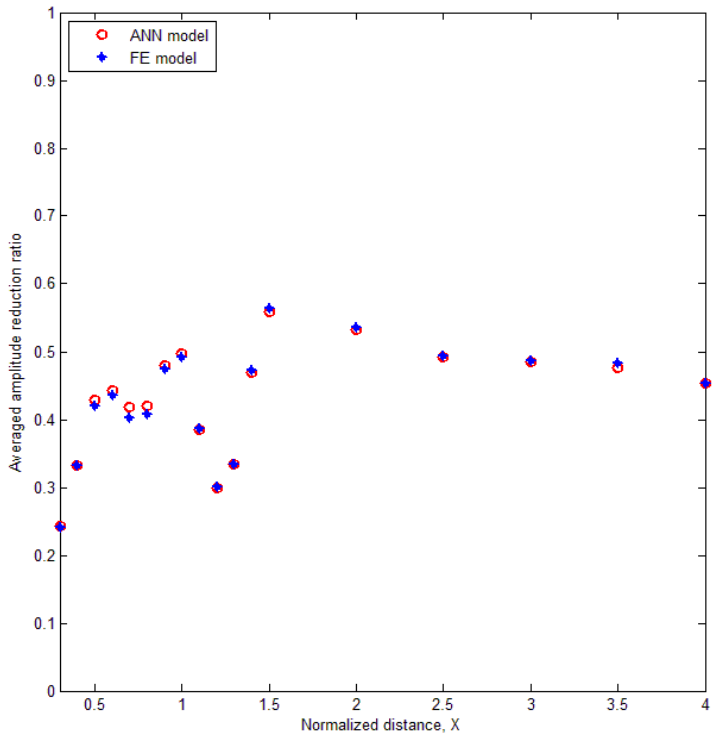

Figure 6- 10: Response of ANN model in predicting the averaged amplitude reduction ratio for normalized depth (D = 1.0)

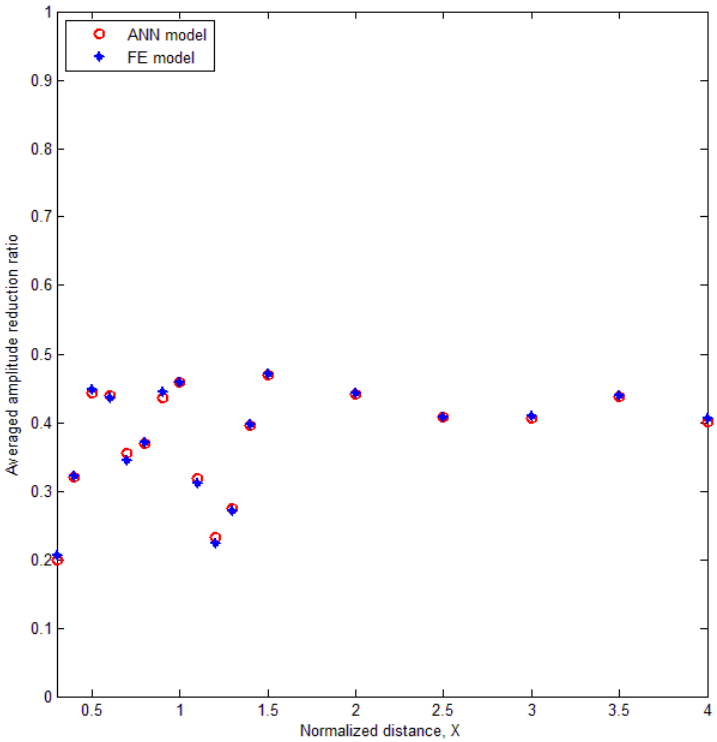

Figure 6- 11: Response of ANN model in predicting the averaged amplitude reduction ratio for normalized depth (D = 1.2)

6.5 TESTING THE ACCURACY OF BOTH REGRESSION ANALYSIS ANDANN-BASED APPROACH

The predictions of the MLR design model (developed in Chapter 5) are compared with those obtained from the proposed ANN model considering a new set of finite element results, which has never been utilized in developing either model. The same statistical methods of RMS, R^2, and MAPE values have been used for performing the comparison and the results are listed in Table 6-2.

The comparison shows that the averaged amplitude reduction ratio can be predicted by ANN with less error relative to that of the MLR models (Model-1 and Model-2). The mean absolute percentage error (MAPE) of the ANN model prediction is only 0.00022%, while that of the MLR model is 18.7%. However, the root-mean-squared (RMS) error and absolute fraction of variance (R^2) are very small for both models. Although the ANN model predictions seem to be more accurate than MLR models for averaged amplitude reduction ratio, both methods are appropriate for use in design because the difference in their predictions is small.

Table 6- 2: Comparison of accuracy values of models

Normalized distance	**Normalized depth**	**Model**	**RMS**	**R^2**	**MAPE (%)**
$0.4 \le D \le 2.0$	$0.3 \le X \le 4.0$	ANN model	0.00507	0.99987	0.00022
$0.4 \le D \le 2.0$	$0.3 \le X \le 4.0$	MLR model-1	0.083138	0.967492	17.56914
		MLR model-2	0.069495	0.974394	13.09228
	$0.3 \le X \le 0.5$	MLR model-1	0.070975	0.971522	18.73983
		MLR model-2	0.023595	0.996522	4.803234
	$0.6 \le X \le 0.9$	MLR model-1	0.052647	0.986801	10.59168
		MLR model-2	0.030554	0.995084	5.503215
	$1.1 \le X \le 1.3$	MLR model-1	0.050913	0.980969	13.06666
		MLR model-2	0.024342	0.995078	6.236023
	$1.5 \le X \le 4.0$	MLR model-1	0.050240	0.990324	8.879806
		MLR model-2	0.032000	0.995500	5.363264
$0.8 \le D \le 2.0$	$0.3 \le X \le 4.0$	MLR model-1	0.077759	0.965436	18.03679
		MLR model-2	0.063055	0.973885	13.118791
	$0.3 \le X \le 0.5$	MLR model-1	0.035785	0.990187	10.47068
		MLR model-2	0.020682	0.996195	3.977152
	$0.6 \le X \le 0.9$	MLR model-1	0.048112	0.987033	10.15090
		MLR model-2	0.028678	0.994800	5.432485
	$1.1 \le X \le 1.3$	MLR model-1	0.047265	0.97999	13.13484
		MLR model-2	0.015916	0.997398	4.203781
	$1.5 \le X \le 4.0$	MLR model-1	0.043214	0.991449	8.052857
		MLR model-2	0.024787	0.996713	4.524115

6.6 SUMMARY AND CONCLUDING REMARKS

Numerical modeling of the performance of in-filled geofoam trench barriers is highly complex and time consuming task. This study is aimed at demonstrating the possibility of adapting artificial neural networks to predict the averaged amplitude reduction ratio in using in-filled geofoam trenches as a wave barrier to mitigate the ground borne vibrations. A comprehensive database was assembled based on the finite element parametric study results and was used for training, validating and testing the ANN model. The accuracy of proposed ANN model and the MLR model (presented in Chapter 5) has been assessed by comparing their predictions with a new set of finite element results. Based on the results, the following conclusions can be drawn:

1. The ANN model is a viable method for predicating the averaged amplitude reduction ratio. It effectively captured the interrelationships amongst key system variables.

2. The proposed ANN model is not capable of extrapolation beyond the domain of the data used in its training. However, it can be extended beyond the current domain by including sufficient data points to the current database.

3. Statistical error analysis showed that the proposed ANN model and LR models can accurately predict the averaged amplitude reduction ratio, however, ANN model is shown to be more accurate.

4. The developed ANN model can be used as a design tool to predict the preliminary optimum dimensions for in-filled geofoam trench barrier in order to reduce the modeling cost and to save time and effort.

CHAPTER SEVEN

SUMMARY, CONCLUSIONS AND RECOMMENDATIONS

7.1 SUMMARY AND CONCLUSIONS

A good deal of numerical and experimental research has been carried out in the past few decades to study the vibration isolation using wave barriers and to improve the understanding of vibration isolation phenomena. Most of this body of research has mainly dealt with the development of numerical methodologies as a tool for analyzing vibration isolation problems, investigating open trenches, in-filled concrete or bentonite trenches, sheet-pile walls, and rows of solid or hollow concrete or steel piles.

On the other hand, a few studies have investigated the use of lightweight fill materials such as expanded polystyrene (EPS) geofoam material as wave barriers. These studies indicated that in-filled geofoam trench wave barriers can be used as an effective tool to screen blast-induced ground shocks and traffic activities, and that geofoam polymers can provide an attractive construction material for these barriers. However, no engineering design method based on a solid framework is available to date for the design of such type of wave barriers. Moreover, no information is available on the performance of in-filled geofoam trench barriers in reducing ground-borne vibrations due to machine foundations (i.e. steady state harmonic excitations).

This dissertation attempted to cover this gap in knowledge regarding this type of vibration isolation system through providing a series of extensive fundamental investigations, experimental and numerical, on the feasibility of using of geofoam polymers material as wave barriers taking into account all the parameters that adequately describe the vibration screening process. The study provides extensive evaluation of the performance of in-filled geofoam trench under steady state excitation in order to develop a preliminarily design tool to assess its protective efficiency.

The principles of wave propagation in an elastic half-space medium and their application to the problem of vibration isolation by wave barriers are reviewed. The comprehensive literature survey revealed that the reported research on vibration isolation using geofoam material is rather limited. The literature review also covered the geofoam material characterization principles and main methods of the artificial neural networks technique, which are later considered in the analysis.

The core themes of this research are to conduct numerical and experimental investigations on the vibration isolation by in-filled geofoam trench barrier. Prior to executing a costly experimental study, it was necessary to conduct a preliminary numerical investigations considering different configurations of in-filled geofoam trench barriers as active and passive isolation systems in order to examine their behaviour and effectiveness in mitigating harmonic vibrations. Therefore, 2D and 3D numerical models in the time domain utilizing the finite element package ABAQUS were developed for this purpose. The numerical models were first verified and excellent agreement with previously published results was observed. The proposed systems were then evaluated and compared based on the gained reduction in the soil particle velocities through an

intensive parametric study. From the results discussions and analyses, the following understandings and conclusions can be made:

1. All the proposed geofoam barrier systems perform well in reducing the surface waves and the screening effectiveness varies between 38% and 80%. However, the geofoam barriers are more effective in screening high-frequency vibrations.

2. The most effective isolation system is the double-continuous walls system, and its protection effectiveness is not affected by its distance from the source of disturbance.

3. The performance of double-staggered walls system in screening the vibration is similar to that of the double-continuous walls system when used as an active isolation system. Thus, the double-staggered walls system is recommended as an efficient solution for active isolation since is utilizes less geofoam material.

4. The single-continuous wall system and the double-staggered walls system perform almost the same as passive isolation systems. Thus, the single-continuous wall is recommended as an efficient passive isolation system.

One of the main core themes of this thesis is to conduct a full scale experimental work. The results of this part of the study serve two functions: first, it confirms the feasibility and effectiveness of the in-filled geofoam trenches as wave barriers; second, it provide valuable experimental measurements that can be used to verify/calibrate the finite element models used as part of the numerical investigation component of this study. A

field experimental program was designed and executed to investigate the protective effectiveness of open and in-filled geofoam trenches to scatter the steady state vibration induced by machine foundations. An innovative approach to construct the open and in-filled geofoam trench was proposed. The experimental study examined the influences of wall geometry and location from the vibratory source on the isolation effectiveness as active and passive vibration isolation cases). In order to simulate the machine foundations vibration, a mechanical oscillator was used. The wave barriers protective effectiveness was evaluated based on the achieved reduction in soil particle velocities through a parametric study by changing the exciting frequency and the location of the wave barriers. Based on the obtained results and their analysis, the following conclusions can be made:

1. The experimental results demonstrated the feasibility of using in-filled geofoam trench barrier for wave scattering and the observed protective effectiveness was up to 68% or higher.

2. The effectiveness of the wave barrier is governed by its normalized depth and proximity to the source of disturbance. The barriers are generally more effective when $D \geq 0.60$ (i.e. an optimum barrier normalized depth) for both open and in-filled geofoam trench barriers. For x/d of about 0.79, 1.63 and 3.29, the normalized distance X of 0.45, 0.92 and 1.22 are the optimum barrier locations corresponding to the optimum normalized depth D of about 0.60.

3. A deeper trench is required for larger x/d in order to achieve the same performance level. As the ratio x/d increased, the open trench barrier effectiveness decreased but the in-filled geofoam trench barrier performance was not affected.

   The experimental setup was simulated using 2D and 3D finite element models. The validity and accuracy of the 2D finite element model results have been compared with those obtained from the 3D finite element model. Based on the obtained results and their analysis, the following conclusions can be made:

4. The results obtained from 2D and 3D finite element models are in excellent agreement. Thus, 2D finite element model can be used with confidence in modeling the field experimental tests as well as in conducting a parametric study.

5. The numerical wave attenuation curves follow the same trend of the experimental measurements and are in good agreement, but with slightly higher values at some points and lower values at others. The maximum differences are about 10.65% and 35.19% for open and in-filled geofoam trench barriers, respectively.

6. The developed finite element models can be used to extrapolate the results and conduct a parametric study on the in-filled geofoam trench barrier performance with different dimensions as well as in different soil profiles.

A comprehensive numerical investigation of the performance of geofoam barriers was conducted using the verified/calibrated numerical model. The methodology used involved conducting a parametric study for in-filled geofoam trench barriers installed in

an homogeneous elastic half-space soil. The barrier depth and location were varied independently as well as the soil dynamic properties. The wave barriers protective effectiveness was evaluated based on the achieved reduction in soil particle response. Based on the results obtained and their analysis, the following conclusions can be made:

1. The key parameters that influence the barrier performance are its depth and proximity to the source of disturbance, and the shear wave velocity of soil medium. The soil density, Poisson's ratio, and material damping have some influence but are less significant.

2. Deeper trenches are required at greater distances from the source of disturbance to achieve the same level of performance.

3. The normalized depth D should be greater than 1.2 for maximum performance. However, D can be as low as 0.8 for X = 0.4. Also, for practical construction purposes, the width of geofoam barrier can be kept at 0.25m.

4. In-filled geofoam trench barrier performs more effectively in stiff soils (i.e. with relatively high Vs values) than in soft soils (i.e. with low Vs values). Accordingly, the soil shear wave velocity should be considered as the main soil characteristic when designing in-filled geofoam trench barriers.

Preliminarily design tool models are developed to estimate the in-filled geofoam trench barriers protective performance, which can be used to select the optimum barrier dimensions and location in order to maximize the system protective efficiency. Two

approaches have been adopted in developing two different predicting tools based on Multiple Linear Regression Analysis and Artificial Neural Networks.

After the key geometrical and material parameters that govern the performance of in-filled geofoam trench barriers have been identified, a multiple linear regression design model has been introduced. The multiple linear regression analysis identified the relationship between independent or predictor variables (barrier geometry and location, and soil dynamic properties) and a dependent or criterion variable (averaged amplitude reduction ratio). Two MLR design models were developed as follows: first, a linear combination between independent variables was assumed (Model-1); second, a more sophisticated combination between independent variables was assumed using the variables transformation technique (Model-2). Based on the results obtained and their analysis, the following conclusions can be made:

1. Model-2 performed better than model-1 in predicting the averaged amplitude reduction ration. The adjusted coefficients of determination (R^2_{adj}) were 62% and 75% of the variability in the averaged amplitude reduction ratio be explained by model-1 and model-2, respectively.

2. Dividing the range of normalized distance between the barrier and disturbance source into sub-intervals significantly improved the models performance..

3. Narrowing the range of normalized depth also helped in improving the model efficiency.

An original approach based on artificial neural networks (ANN) was proposed to assist engineers to explore feasibility of using the in-filled geofoam trench barrier in screening the ground-borne vibrations. This is particularly effective in selecting the optimum geofoam wall dimensions and location in order to achieve the desired vibration level. The ANN model inputs include the barrier depth, the distance between the barrier and the source of disturbance, and the dynamic soil properties including shear wave velocity, density, Poisson's ratio, and material damping ratio, while the averaged amplitude reduction ratio was the single model output. The ANN system combines the effects of barrier geometric dimensions, location in a dimensionless format with respect to the Rayleigh wavelength and the dynamic soil properties, which simplifies the decision-making process and improves the reliability of assessment.

The ANN model was trained using a database assembled from the comprehensive parametric study conducted in Chapter 5. The ANN model showed high capability to accurately predict the averaged amplitude reduction ratio which means predicting the in-filled geofoam trench barrier in scattering the steady state vibration induced by machine foundations. The ANN model also exhibited a good generalization capacity beyond the training stage as validated by new finite element results within the range of training database and have not been seen by the model before.

This model could be used as preliminarily design tool to estimate the optimum dimensions for in-filled geofoam trench barrier in order to reduce the modeling cost and to save time and effort. The developed ANN model is versatile and can be re-trained to encompass wider ranges of input variables and adding any new input variable that might influence the barrier performance when such data becomes available. However, the

results showed that the proposed ANN model is not capable of extrapolation beyond the domain of the training database. On the other hand, statistical error analysis showed that the proposed ANN model and MLR models can accurately predict the averaged amplitude reduction ratio with an advantage to use of ANN model because it gave slightly less errors.

7.2 RECOMMENDATIONS FOR FUTURE WORK

Further work to complement the current level of research on vibration isolation by in-filled geofoam trench barriers is suggested. A brief outline of areas which warrant future investigations is given below:

1. Since this was the first time to use geofoam material (Uretek polymer) in such application, further explorations need to be conducted to investigate the in-filled geofoam trench barrier behaviour with different soil conditions. This can be done by conducting similar full scale experimental work setup but in different soil profiles with different wall configurations.

2. The effectiveness of in-filled geofoam trench barriers in isolating transient disturbances (hammer machines, traffic vibrations, blasting activities) need to be studied.

3. Soils in the field may be anisotropic. The influence of anisotropy of soil on the screening effectiveness of wave barriers may be studied. Effects of soil layering on the in-filled geofoam trench barriers protective effectiveness need to be examined as well. It is also important to identify if these effects are due to the

dispersive behaviour of layered system, the characteristics of the vibration screening system becomes frequency dependent.

REFERENCES

Achenbach, J.D., 1973. Wave Propagation in Elastic Solids, North-Holland.

Adeli, H. 2001. Neural Networks in Civil Engineering: 1989-2000, Computer Aided Civil and Infrastructure Engineering, 16(2): 126–42.

Ahmad, S. and Al-Hussaini, T.M. 1991. Simplified Design for Vibration Screening by Open and In-Filled Trenches, Journal of Geotechnical Engineering, 117: 67-88.

Ahmad, S., Al-Hussaini, T.M. and Fishman, K.L. 1996. Investigation on Active Isolation of Machine Foundations by Open Trenches, Journal of Geotechnical Engineering, 122: 454-61.

Ahmad, S., Baker, JM. and Li, J. 1995. Experimental and Numerical Investigation on Vibration Screening by In-Filled Trenches, Proceedings of the third International Conference on Recent Advances in Geotechnical Earthquake Engineering and Soil Dynamics, Missouri, 2:757-62

Al-Hussaini, T.M. and Ahmad, S. 1991. Design of Wave Barriers for Reduction of Horizontal Ground Vibration, Journal of Geotechnical Engineering, 117: 616-36.

Al-Hussaini, T.M. and Ahmad, S. 1996. Active Isolation of Machine Foundations by In-Filled Trench Barriers, Journal of Geotechnical Engineering, 122: 288-94.

Al-Hussaini, T.M., Ahmad, S., and Baker, J.M. 2000. Numerical and Experimental Studies on Vibration Screening by Open and In-Filled Trench Barriers, in : S. Chouw(Ed.), Wave 2000, Balkema, Rotterdam, 241-50.

Al-Hussaini, T.M. 1992.Vibration Isolation by Wave Barriers, PhD Thesis, State University of New York at Buffalo, USA.

Alzawi, A. and El Naggar, M.H. 2009. Vibration Scattering Using GeoFoam Material as Vibration Wave Barriers, 62nd Canadian Geotechnical Conference, Halifax, NB, Canada, 997-1004.

Alzawi, A. and El Naggar, M.H. 2010. Experimental Investigations on Vibration Isolation Using Open and GeoFoam Wave Barriers: Comparative Study, 63rd Canadian Geotechnical Conference, Calgary, AB, Canada, 360-68.

Alzawi, A. and El Naggar, M.H. 2011. Full scale experimental study on vibration scattering using open and in-filled (geofoam) wave barriers, Soil Dynamics and Earthquake Engineering, 31: 306–17.

Alzawi, A. and El Naggar, M.H. 2011. Numerical Investigations on Vibration Screening by In-filled Geofoam Trenches, 64rd Canadian Geotechnical Conference, Toronto, ON, Canada, (Accepted).

Andersen, L. and Nielsen, SRK. 2005. Reduction of ground vibration by means of barriers or soil improvement along a railway track, Soil Dynamics and Earthquake Engineering. 25: 701–16.

Baker, J.M. 1994. An Experimental Study on Vibration Screening by in-filled trench barriers, M.Sc. Thesis, State University of New York at Buffalo, USA.

Barkan, D. D. 1962. Dynamics of Bases and Foundations, MacGraw-Hill Book Company Inc., 374-406.

Beskos, D.E., Dasgupta, G. and Vardoulakis, I.G. 1986. Vibration Isolation Using Open or Filled Trenches, Part1: 2-D Homogeneous Soil, Computational Mechanics 1: 43-63.

Bishop, C. 1995. Neural networks for pattern recognition, Oxford Press, New York

Dassault Systèmes. 2005. ABAQUS 6.6 User's Manual, Providence, RI, USA.

Dassault Systèmes. 2007. ABAQUS 6.7 User's Manual, Providence, RI, USA.

Davies, M.C.R. 1994. Dynamic Soil Structure Interaction Resulting from Blast Loading. Leung, Lee and Tan(Eds.), Centrifuge 94, Balkema, Rotterdam, 319-24.

deBremaecker, J. Cl. 1958. Transmission and reflection of Rayleigh waves at corners, Geophysics, 23(2): 253-66.

Dolling, H. J. 1965. Schwingungsisolierung von Bauwerken durch tiefe, auf geeignete Weise stabilisierte Schlitz (Vibration isolation of buildings by means of deep, suitably stabilized trenches). VDI Bericht Nr. 88.

Dolling, H. J., 1970. Abschirmung von Erschütterungen durch Bodenschlitze (Isolation of vibrations by trenches), Die Bautechnik, No. 6: 193-204.

El Naggar, M.H. and Chehab, A.G. 2005. Vibration Barriers for Shock-Producing Equipment, Canadian Geotechnical Journal, 42: 297–306.

Fuyuki, M., Matsumoto, Y., 1980. Finite difference analysis of Rayleigh wave scattering at a trench, Bulletin of the Seismological Society of America, 70: 2051–69.

Hagan, MT., Demuth, HB., and Beale M. 1996. Neural network design, Boston: PWS.

Haupt, W.A. 1977. Isolation of Vibrations by Concrete Core Walls, In Proceedings of the Ninth International Conference on Soil Mechanics and Foundation Engineering, vol. 2. Tokyo, Japan, 251-56.

Haupt, W. A. 1978. Surface-waves in non-homogeneous half-space. Proceedings of Dynamical Methods in Soil and Rock Mechanics, DMSR 77, vol. I, A.A. Balkema, Rotterdam, 335-67.

Haupt, W. A., 1981. Model tests on screening of surface waves. Proceedings of Xth International Conference on Soil Mechanics and Foundation Engineering. Stockholm, 3: 215-22.

Haykin S., 1999. Neural networks: a comprehensive foundation, 2nd ed., Prentice Hall, New Jersey

Horvath, J.S. 1995. Geofoam Geosynthetic, Horvath Engineering, P.C. Scarsdale, New York, USA, 217p.

Hubick, K. T. 1992. Artificial neural networks in Australia, Department of Industry, Technology and Commerce, Commonwealth of Australia, Canberra.

Juang CH, Chen CJ and Tien YM. 1999. Appraising Cone Penetration Test Based Liquefaction Resistance Evaluation Methods: Artificial Neural Network Approach, Canadian Geotechnical Journal, 36(3): 443–54.

Kattis, S.E., Polyzos, D. and Beskos, D.E. 1999. Vibration Isolation by a Row of Piles Using a 3-D Frequency Domain BEM, International Journal of Numerical Methods in Engineering, 46: 713-28.

Kattis, S.E., Polyzos, D. and Besko, D.E. 1999. Modeling of Pile Wave Barriers by Effective Trenches and Their Screening Effectiveness, Soil Dynamics and Earthquake Engineering, 18: 1–10.

Kolsky, H. 1963. Stress Waves in Solids, Dover Press.

Kramer, SL. 1996. Geotechnical Earthquake Engineering, Prentice-Hall Inc, Upper Saddle River, NJ, USA.

Lamb, H. 1904. On the Propagation of Tremors Over the Surface of an Elastic Solid. Philosophical Transactions of the Royal Society, London, Ser. A, 203: 1-42.

Murillo, C., Thorel, L. and Caicedo, B. 2009. Ground vibration isolation with geofoam barriers: Centrifuge modeling, Geotextiles and Geomembranes, 27:423–34.

Negussey, D. 1998. Putting Polystyrene to Work. Civil Engineering, ASCE, March, 65-67.

Nielsen, RH. 1998. Neurocomputing, picking the human brain. IEEE Spectr 25(3):36–41

Park, C.B., Miller, R.D., and Xia, J. 1999a. Multimodal analysis of high frequency surface waves, Proceedings of the symposium on the application of geophysics to engineering and environmental problems '99, 115-21.

Park, C.B., Miller, R.D., and Xia, J. 1999b. Multichannel analysis of surface waves, Geophysics, 64(3): 800-8.

Poulton, M. 2001. Computational neural networks for geophysical data processing, Paragons Press Ltd, Amsterdam, 335p.

Rayleigh, Lord, 1885. On Waves Propagated Along the Plane Surface of an Elastic Solid, London Mathematical Society Proceedings, 17: 4-11.

Rafiq, M., Bugmann, G. and Easterbrook, D. 2001. Neural network design for engineering applications, Computers and Structures, 79(17): 1541-52.

Rawlings, J.O., Pantula, S.G. and Dickey, D.A. 1998. Applied Regression Analysis: A Research Tool, 2nd ed., Springer Texts in Statistics.

Richart, F.E., Hall, J.R. and Woods, R.D. 1970. Vibrations of Solids and Foundations, Prentice-Hall.

Sarıdemir, M. 2009. Predicting the compressive strength of mortars containing metakaolin by artificial neural networks and fuzzy logic, Advances in Engineering Software, 40(9): 920-27.

Shahin, M. A., Jaksa, M. B., and Maier, H. R. 2001. Artificial neural network applications in geotechnical engineering, Australian Geomechanics, 36(1): 49-62.

Suhol, B. 1997. Infinite Boundary Elements for the Dynamic Analysis of Machine Foundations, International Journal for Numerical Methods in Engineering, 40: 3901-917.

Thau, S. A., and Pao, Y. 1966. Diffractions of Horizontal Shear Waves by a Parabolic Cylinder and Dynamic Stress Concentration, Applied Mechanics, Transactions of ASME, 785-92.

Technical Documentation. Retrieved July 5, 2011, from POLY-MOR (formally, URETEK Canada) official website: http://www.poly-mor.ca/VE/index.html

Wang, JG, Sun, W. and Anand, S. 2008. Numerical investigation on active isolation of ground shock by soft porous layers, Journal of Sound and Vibration, 321: 492–509.

Woods, R.D. 1968. Screening of Surface Waves in Soils, Journal of Soil Mechanics and Foundation Engineering Division, ASCE, 94(4): 951–79.

Wasserman, P. 1989. Neural computing: theory and practice, Van Nostrand Reinhold, New York.

Yang, Y.B., Kuo, S.R. and Hung, H.H. 1996. Frequency-Independent Infinite Elements Analyzing Semi-Infinite Problems, International Journal for Numerical Methods in Engineering, 39: 3553-69.

Yang, Y.B. and Hung, H.H. 1997. A Parametric Study of Wave Barriers for Reduction of Train Induced Vibrations, International Journal for Numerical Methods in Engineering, 40: 3729-47.

APPENDIX A

GEOFOAM MATERIAL PROPERTIES

Chemical Resistance of URETEK Polyurethane 486

CODE

E = excellent resistance
G = good resistance
F = fair resistance
P = poor resistance
S = severe solvent action or chemical attack, not recommended for use

Water	E	Styrene	E
Gasoline	E	Turpentine	E
Toluene	E	Benzene	E
Carbon Tetrachloride	E	Benzene Chloride	E
Methyl Ethyl Ketone	P	Formaldehyde	G
Brine Saturated	E	Kerosene	E
Brine 10%	E	Linseed Oil	E
Sulfuric Acid Concentrate	S	O. Chlorobenzene	G
Sulfuric Acid 10%	E	Methylene Chloride	F
Hydrochloric Acid Concentrate	G	Acetone	P
Hydrochloric Acid 10%	E	Nitric Acid Concentrate	S
Sodium Hydroxide Concentrate	E	Sulfuric Acid Concentrate	S
Sodium Hydroxide 10%	E	Diesel Oil	E
Isopropanol	E	Ethyl Alcohol	P
JP-4 Fuel	E	Methyl Alcohol	P
JP-5 Fuel	E	Orthodichlorobenzene	E
Trichloroethylene	G	Sulfuric Acid 10%	E
Diisobutylketone	E	NaO_2 25%	E
Acetic Acid 2%	G	HCI 25%	E
Potassium Hydroxide 1%	E	Butyral	E
Ammonium Sulfate e 2%	E	Ethylacetate	F
Potassium Chlorate 5%	E	Butylacetate	G
Ethylene Glycol 100%	G	Anylacetate	G
Hydrogen Sulfide 100% (wet)	E	Xylene	E
Hydrogen Sulfide 80% (wet)	E	Varsol	G
Ammonium Hydroxide Concentrate	G	Hexane	E
Ammonium Hydroxide 10%	E	Diisobutylene	E
Motor Oil	E	Mineral Spirits	E

Figure A- 1: Chemical Resistance of URETEK polyurethane material
(Retrieved July 5, 2011, from POLY-MOR (formally, URETEK Canada) official website: http://www.poly-mor.ca/VE/index.html)

Aging of Rigid Polyurethane Samples

Property	Control (aged indoors)	Buried in ground
Density, lb/ft3		
Original	4.0	4.0
After 10 years	3.8	3.8
Tensile Strength, psi (measured in buttons)		
Original	100	100
After 10 years	99	98
Elongation, %		
Original	5.1	6.5
After 10 years	5.1	6.0
Compression Strength, psi (at yield point)		
Original	90	89
After 10 years	88	82
K-Factor, BTU•in/hr•°F		
Original	0.123	0.123
After 10 years	0.144	0.168
Volume Change, % of original		
Original	0	0
After 10 years	0	-4.2%

Figure A- 2: Aging resistance for URETEK polyurethane material
(Retrieved July 5, 2011, from POLY-MOR (formally, URETEK Canada) official website: http://www.poly-mor.ca/VE/index.html)

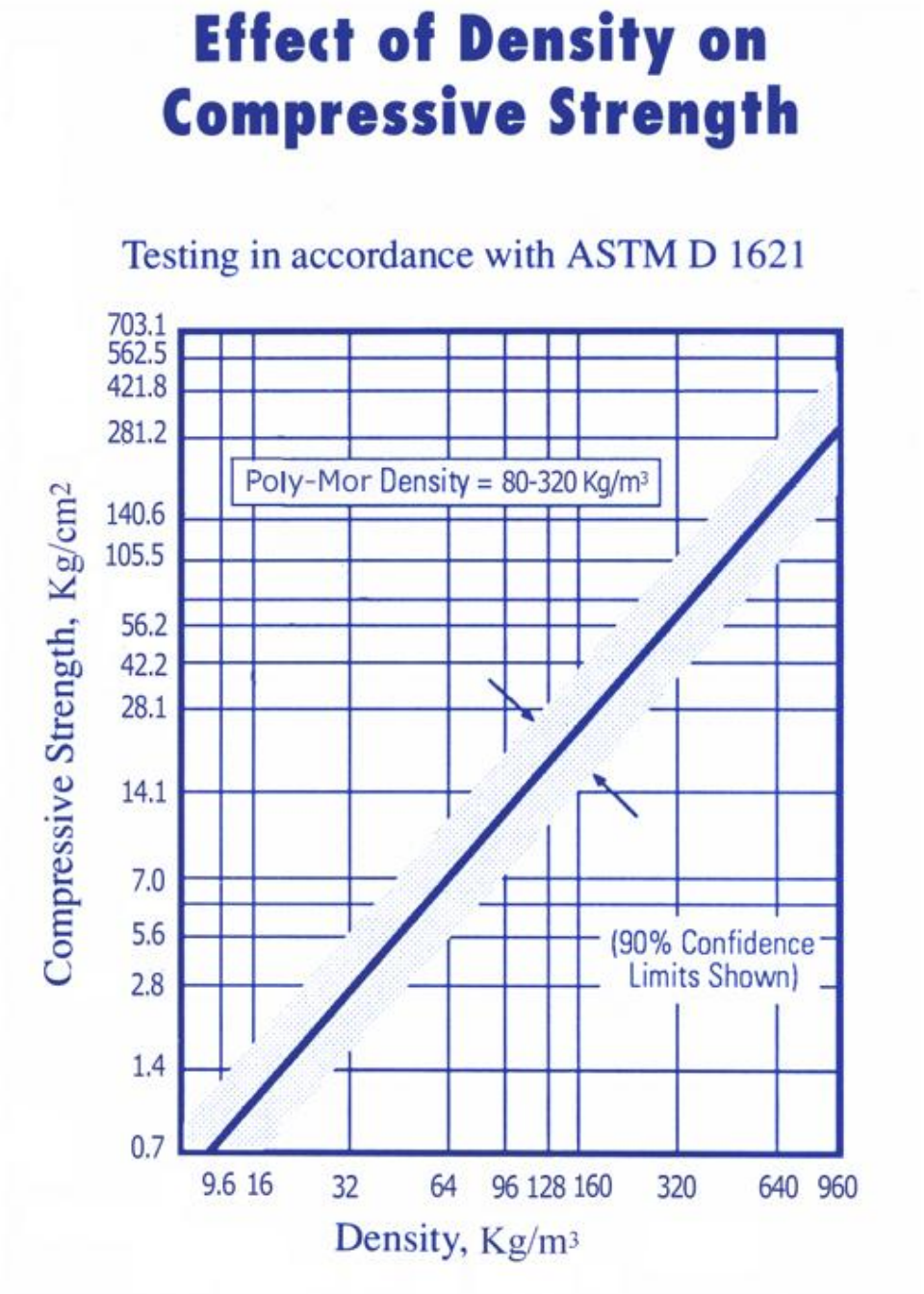

Figure A- 3: Effect of density on compressive strength for URETEK polyurethane (Retrieved July 5, 2011, from POLY-MOR (formally, URETEK Canada) official website: http://www.poly-mor.ca/VE/index.html)

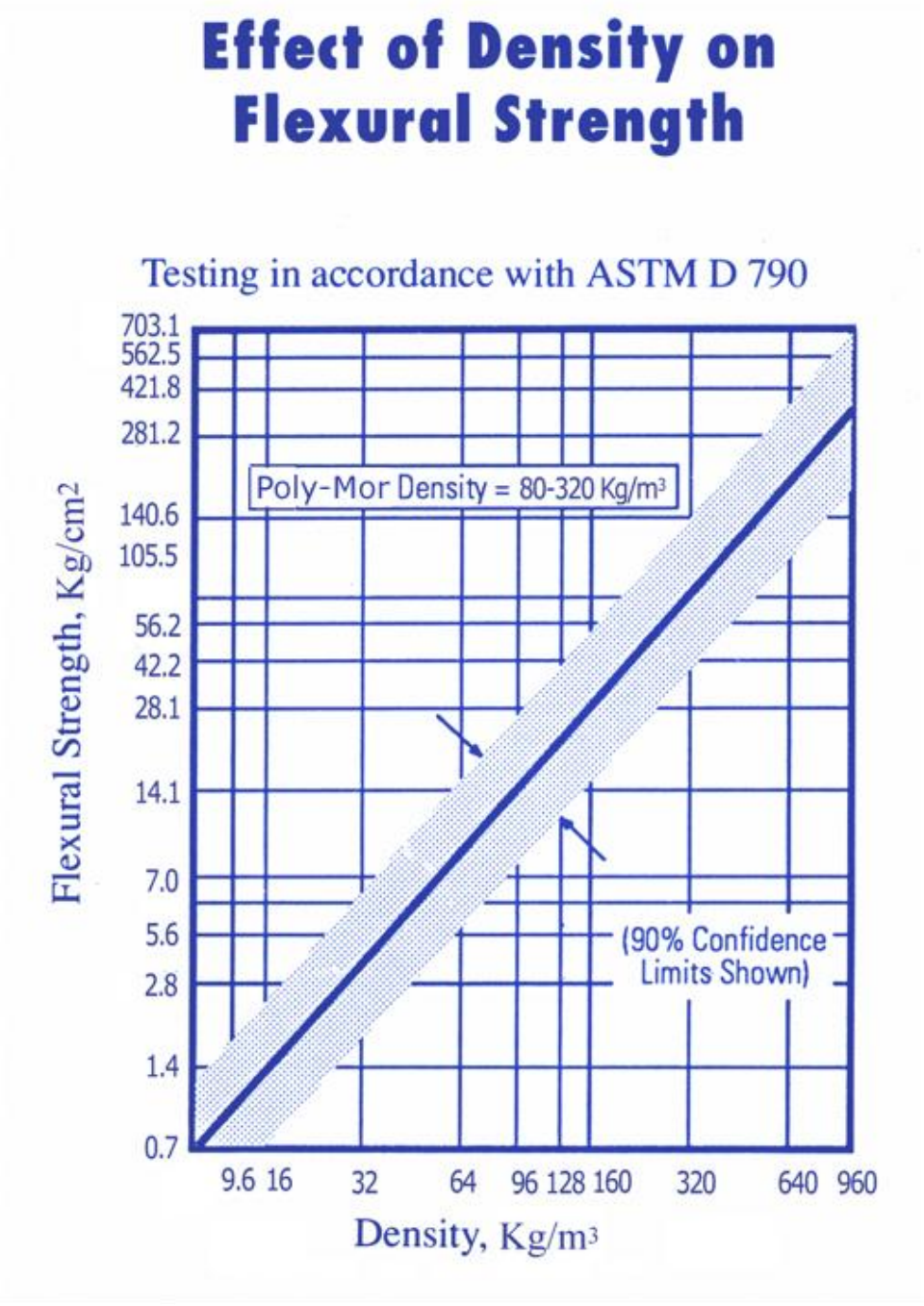

Figure A- 4: Effect of density on flexural strength for URETEK polyurethane (Retrieved July 5, 2011, from POLY-MOR (formally, URETEK Canada) official website: http://www.poly-mor.ca/VE/index.html)

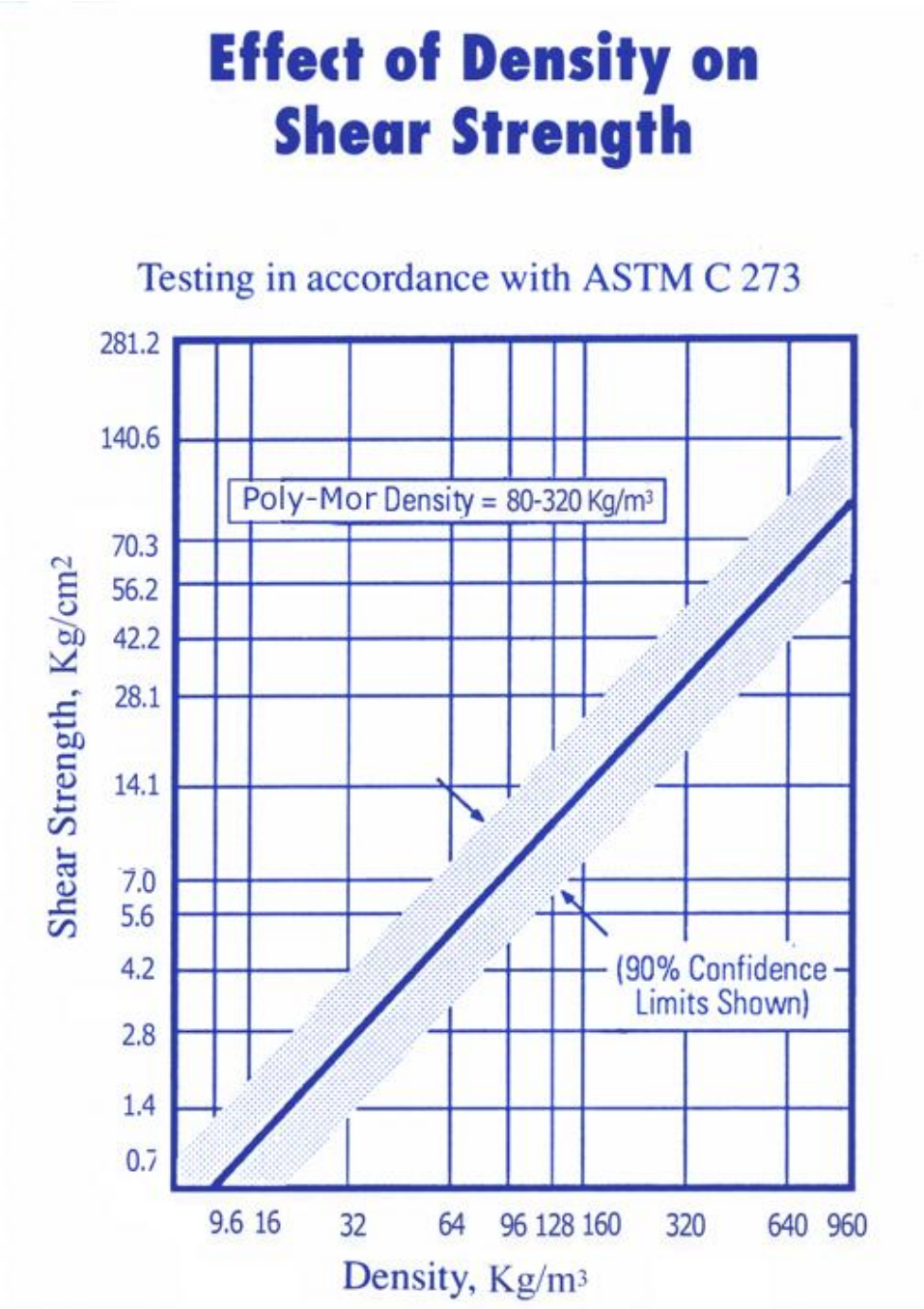

Figure A- 5: Effect of density on shear strength for URETEK polyurethane (Retrieved July 5, 2011, from POLY-MOR (formally, URETEK Canada) official website: http://www.poly-mor.ca/VE/index.html)

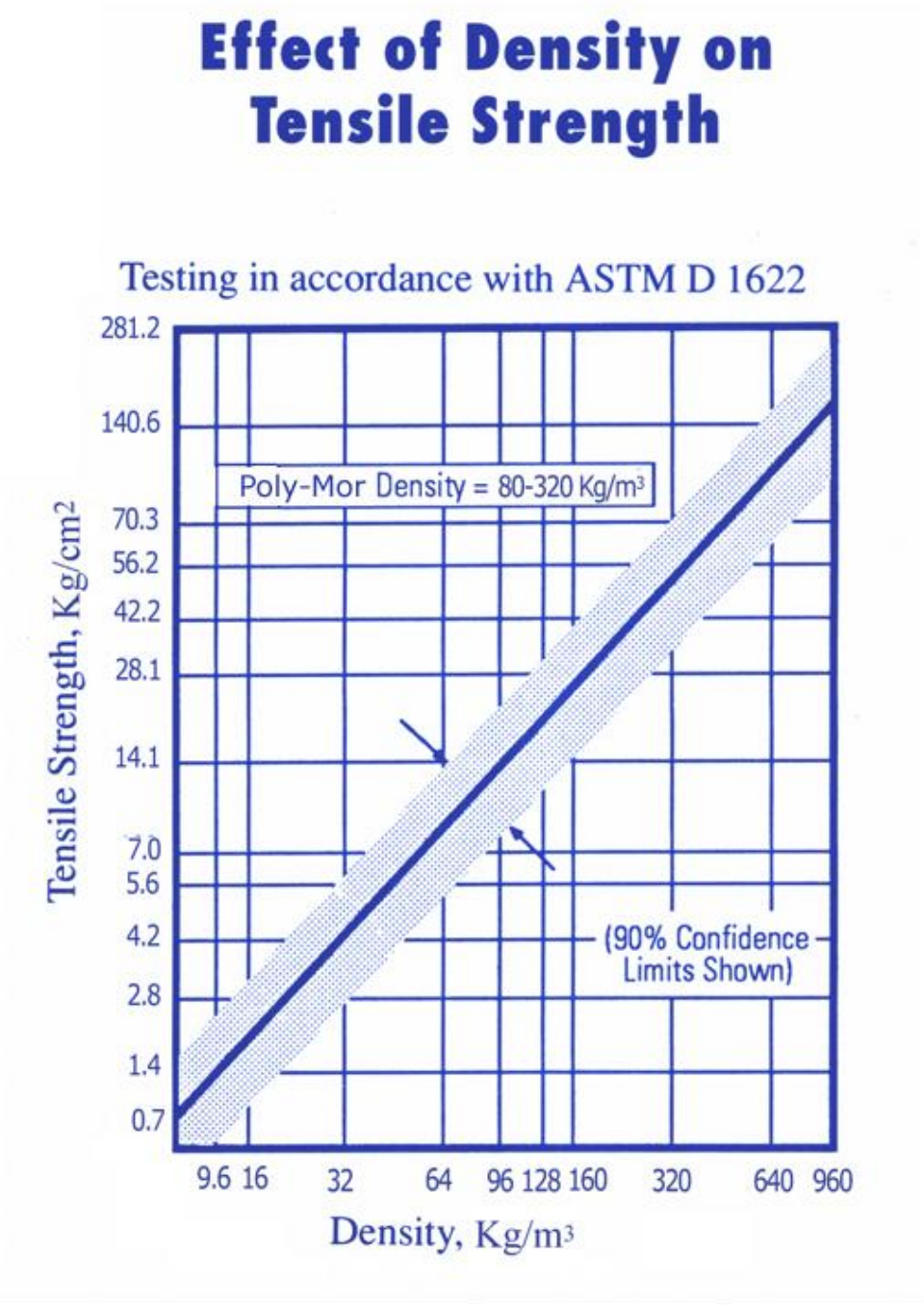

Figure A- 6: Effect of density on tensile strength for URETEK polyurethane (Retrieved July 5, 2011, from POLY-MOR (formally, URETEK Canada) official website: http://www.poly-mor.ca/VE/index.html)

APPENDIX B

MASW MEASUREMENTS

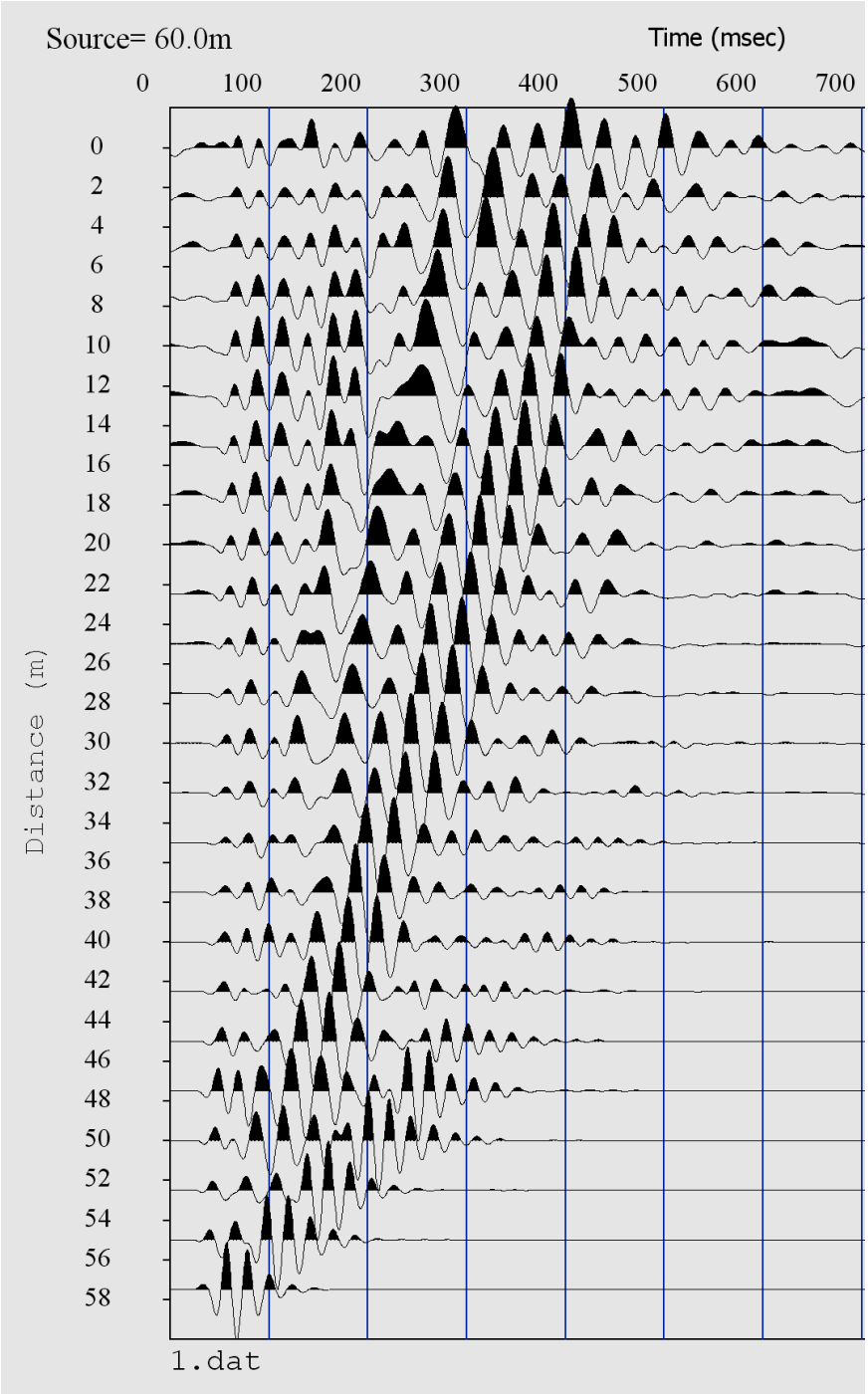

Figure B- 1: Field vibration measurements (source at 2.5 m from Channel #24)

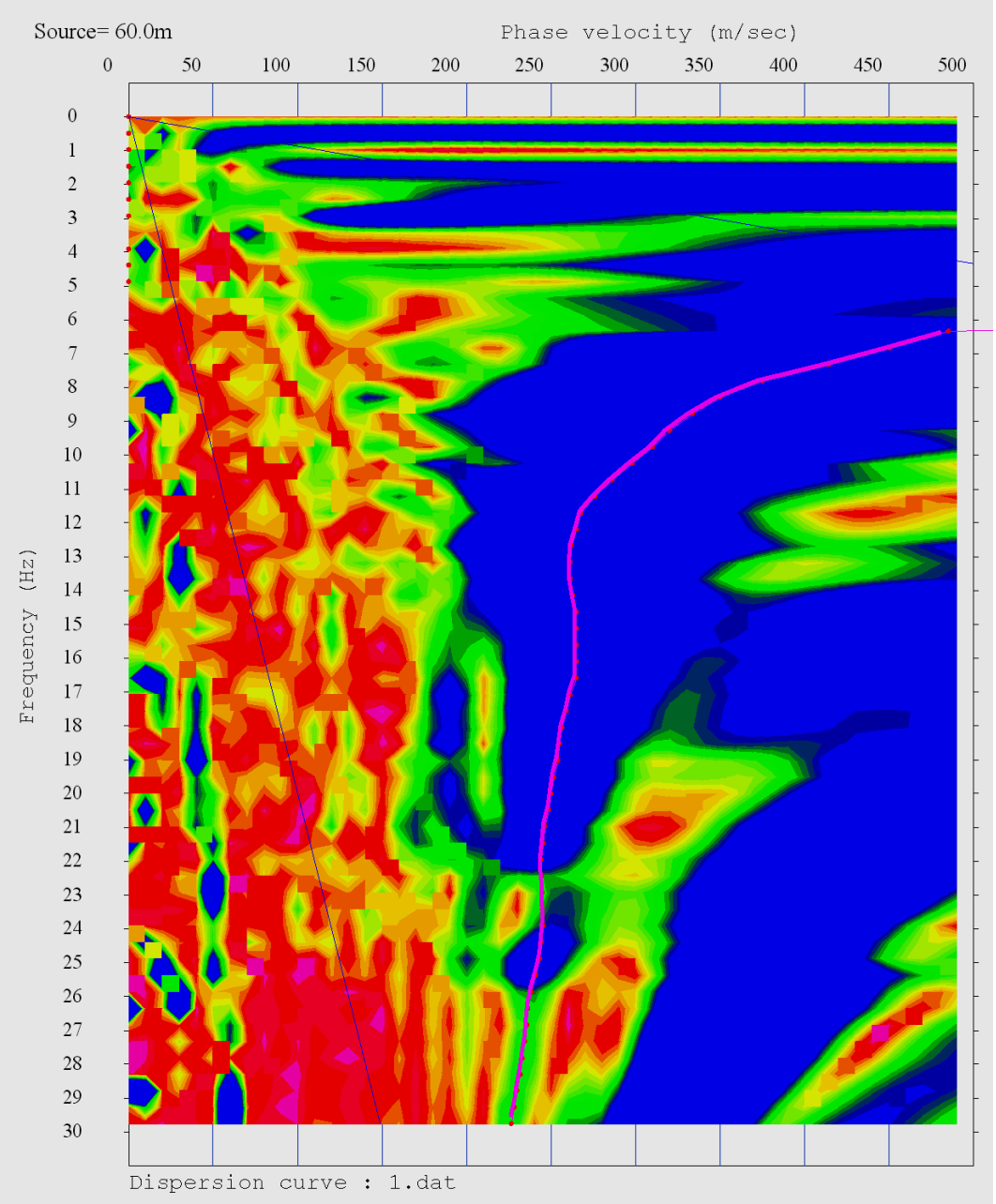

Figure B- 2: Dispersion image (source at 2.5 m from Channel #24)

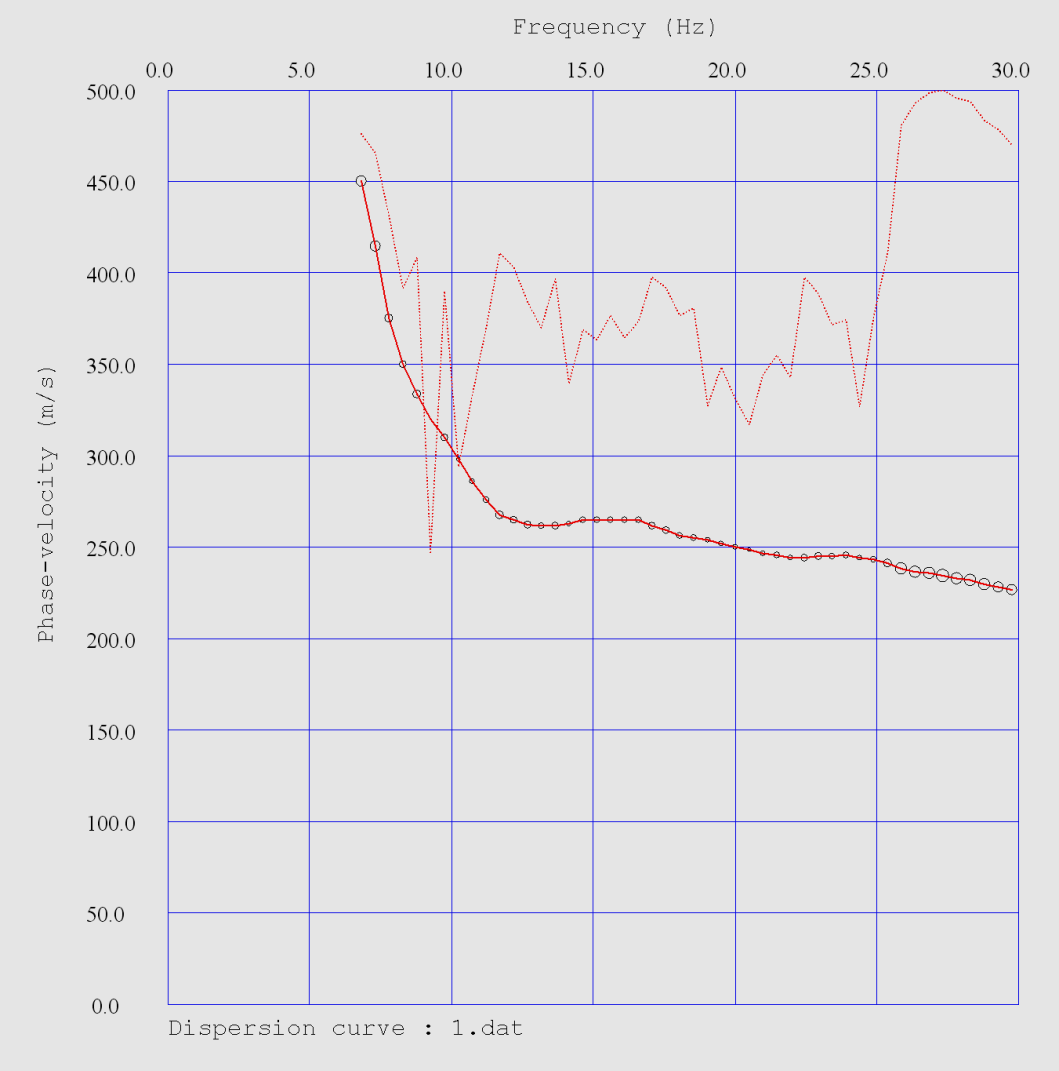

Figure B- 3: Dispersion curve (source at 2.5 m from Channel #24)

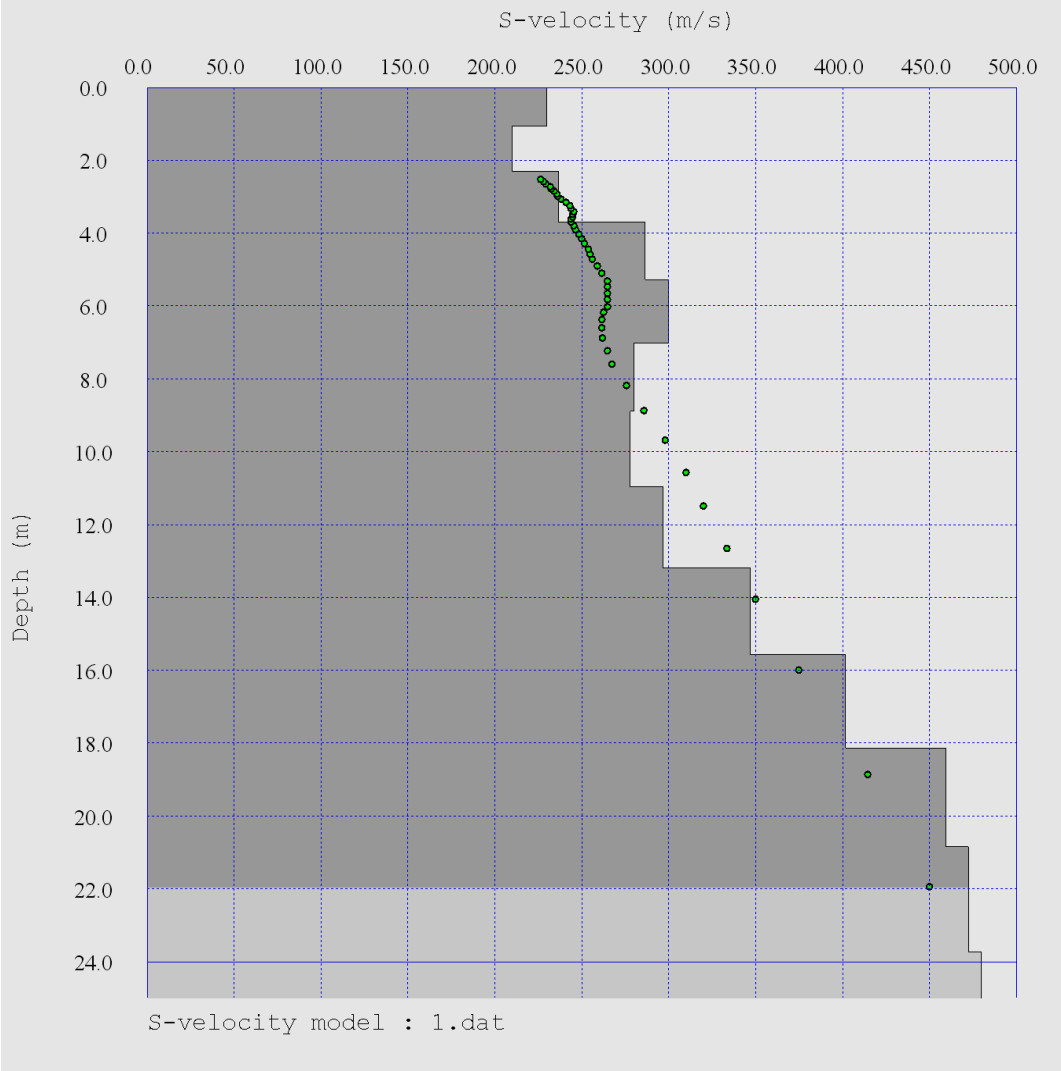

Figure B- 4: S-wave velocity model (source at 2.5 m from Channel #24)

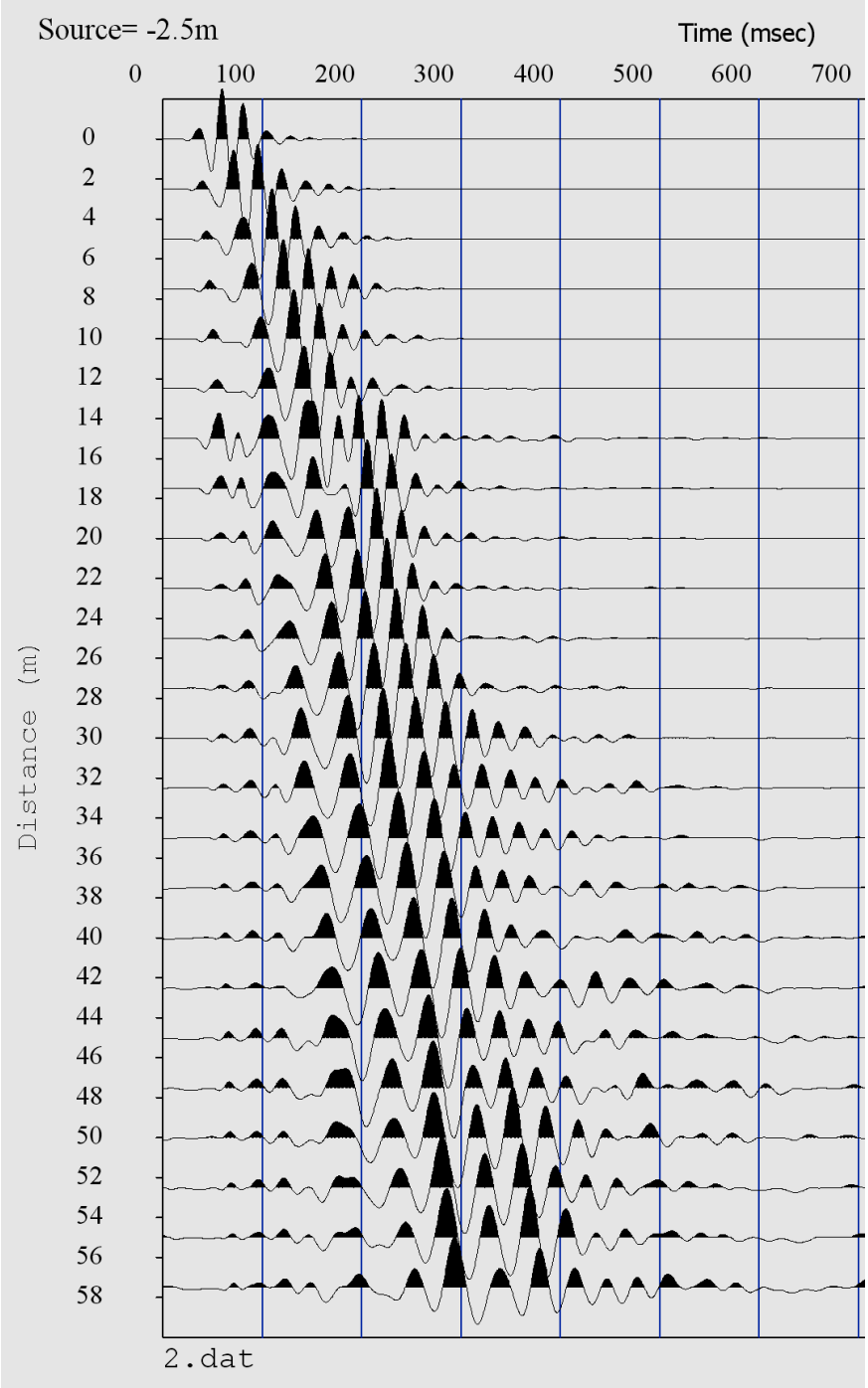

Figure B- 5: Field vibration measurements (source at 2.5 m from Channel #1)

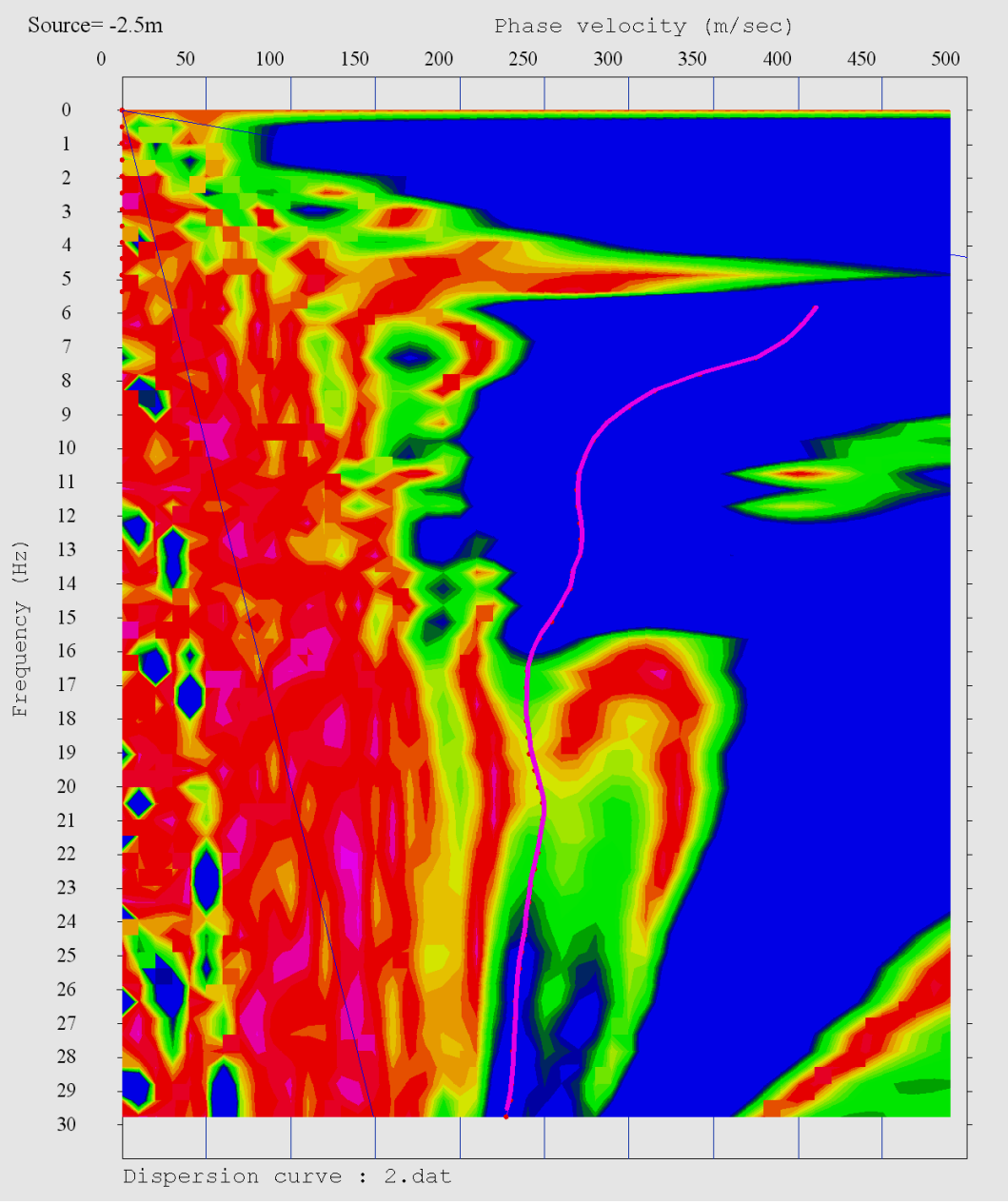

Figure B- 6: Dispersion image (source at 2.5 m from Channel #1)

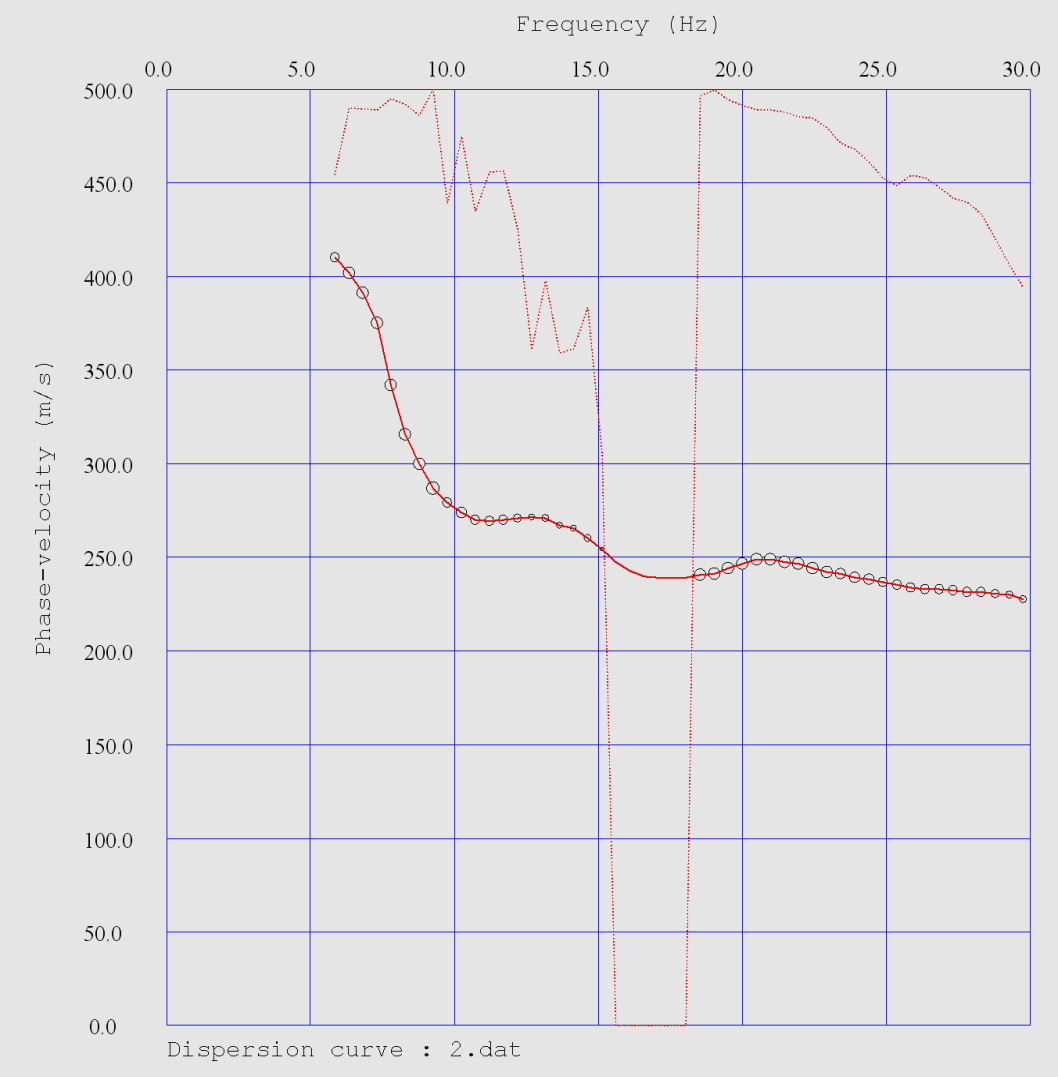

Figure B- 7: Dispersion curve (source at 2.5 m from Channel #1)

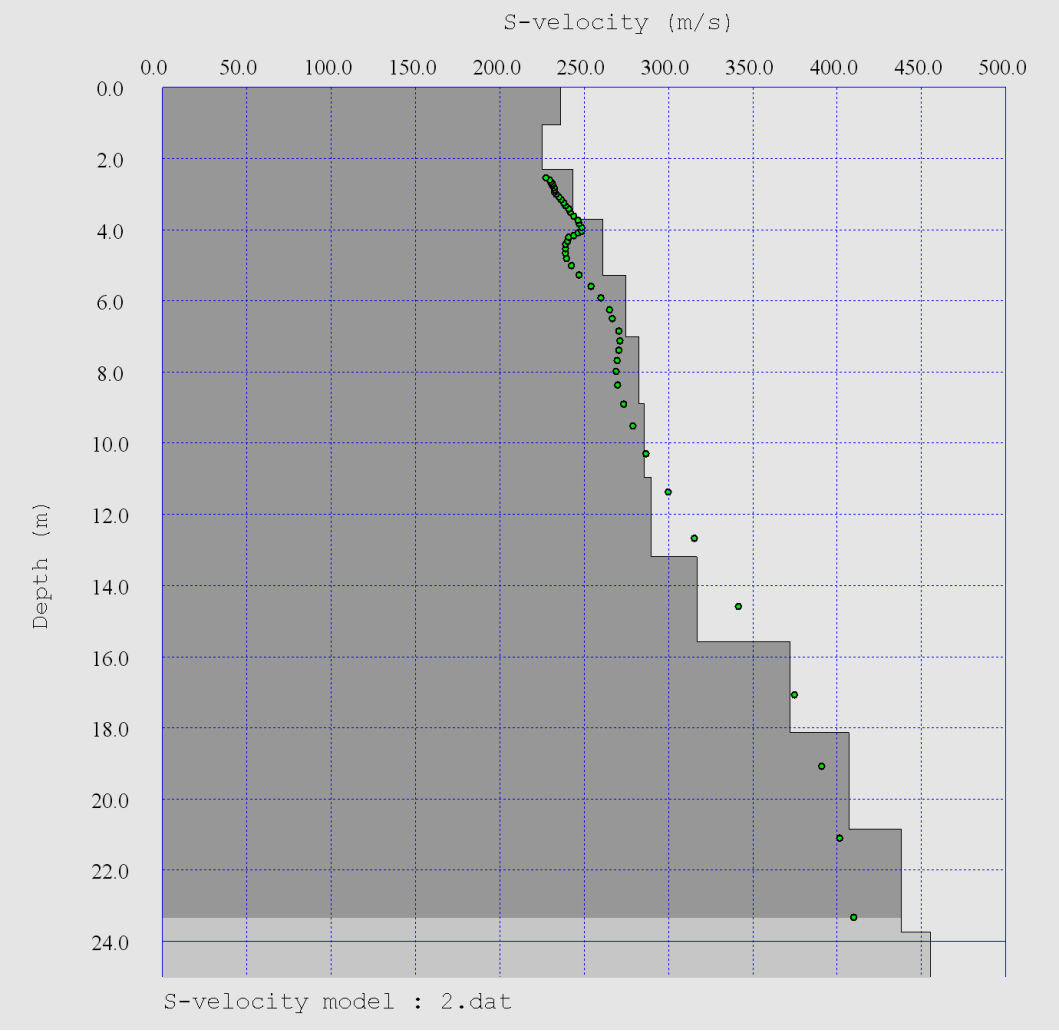

Figure B- 8: S-wave velocity model (source at 2.5 m from Channel #1)

VITA

Name:	Ashref Mohamed A. Alzawi
Post-secondary Education and Degrees:	Alfateh University of Windsor Tripoli, Libya 1992-1996 BSc. Alfateh University Tripoli Libya 1997-1999 MSc The University of Western Ontario London, Ontario, Canada 2007-2011 Ph.D.
Honours and Awards:	Milos Novak Memorial Award The University of Western Ontario 2009 Post-graduate Scholarship 2007-2011
Teaching Experience	Researcher/Teaching Assistant The University of Western Ontario 2007-2011 Lecturer Alfateh University 2000-2006 Teaching Assistant *(part time)* Alfateh University 1997-1999
Professional Experience	Structural Engineer Dar Traboulas for Engineering Work, Libya 2005-2006 Civil Engineer Tripoli's Office for Engineering Consultations, Libya 1996-2005

Publications:

Refereed Journal Publications

- Alzawi, A. and El Naggar, M.H., "Full scale experimental study on vibration scattering using open and in-filled (geofoam) wave barriers," Soil Dynamics and Earthquake Engineering, 31 (2011), pp. 306-317.

Refereed Conference Publications

- Y.M. El Mariamy, S.Y. Barony and Ashref Alzawi, "Accuracy and convergence of finite triangular elements in plane elasticity problems," Proceedings of 4th Alexandria International Conference on Structural and Geotechnical Engineering, Alexandria, Egypt, 2001.

- Alzawi, A. and El Naggar, M.H., "Vibration scattering using geofoam material as vibration wave barriers," Proceedings of 62nd Canadian Geotechnical Conference, Halifax, NB, Canada, 2009. p. 997-1004.

- Alzawi, A. and El Naggar, M.H., "Experimental investigations on vibration isolation using open and GeoFoam wave barriers: comparative study," Proceedings of 63rd Canadian Geotechnical Conference, Calgary, AB, Canada, 2010. p. 360-368.

- Alzawi, A. and El Naggar, M.H., "Numerical investigations on vibration screening by in-filled geofoam trenches," Proceedings of 64th Canadian Geotechnical Conference, Toronto, ON, Canada, 2011. (accepted)